Defining more rules of environmental and phenotypic buffering

Grace A. Mason

A dissertation

submitted in partial fulfillment of the

requirements for the degree of

Doctor of Philosophy

University of Washington

2018

Reading committee:

Christine Queitsch, Chair

Bonny Brewer

Ray Monnat

Program Authorized to Offer Degree:

Genome Sciences

University of Washington

Abstract

Defining more rules of environmental and phenotypic buffering

Grace A. Mason

Chair of the Supervisory Committee:
Associate Professor Christine Queitsch
Department of Genome Sciences

Phenotypes and organisms are robust, or 'buffered,' and thus able to withstand environmental and mutagenic disturbances to maintain wild-type functions. However, the specific mechanisms that ensure phenotypic buffering, and the degree to which these mechanisms overlap, remain poorly understood. The first mechanism I focused on was buffering of phenotype from both *de novo* and pre-existing genetic variation. The best characterized agent of buffering pre-existing 'cryptic' genetic variation is the molecular chaperone HEAT SHOCK PROTEIN 90 (HSP90). I found that when HSP90 was inhibited, the penetrance and heritability of *de novo* genetic variation increased. For pre-existing genetic variation, I characterized a novel phenotypic buffering factor, ARGONAUTE 1 (AGO1), a key player in microRNA-mediated gene regulation. When *AGO1* was genetically perturbed, phenotypes not only became unbuffered but also highly correlated traits became uncoupled. AGO1 is also a known client of HSP90. Despite this interaction, data in this dissertation support that AGO1's phenotypic buffering capabilities are largely independent of HSP90. For the second mechanism, I studied AGO1's capacity to buffer and integrate environmental stimuli. I identified in *ago1* mutants a novel, stress-induced phenotype and traced it to misinterpretation of environmental cues. The third mechanism I examined was whether redundancy within a gene family contributes significantly to buffering a developmental trait. In this particular case, phenotypic buffering comes from a single gene within the family. In sum, the data I generated indicates that organisms use several,

somewhat overlapping mechanisms to ensure stability of developmental traits and proper responses to the environment.

Table of Contents

Acknowledgements

This work was supported in part by the following grants: UW Genetic Approaches to Aging Training Grant (NIH-T32-AG00057), the National Science Foundation (graduate fellowship no. DGE–1256082), and the National Human Genome Research Institute (genome training grant no. T32 HG00035).

I would like to thank my advisor, Christine Queitsch, for being endlessly supportive of me, for giving me a chance to explore my ideas, and for always giving the sound of advice of "think mechanistically!" To this day, I continue to be inspired by her ideas and creativity.

I would like to thank Kerry Bubb. I would not have gotten through graduate school without her mentorship, both inside and outside of the lab. I will always be indebted to Kerry because she (patiently!) taught me about genetics, genomics, statistics, and computational science. She also gave tremendously helpful feedback on portions of this thesis.

I would like to thank Cris Alexandre. Without her vast knowledge and guidance, my experiments would have gotten too large and unwieldy and uninterpretable.

I would like to thank my co-authors Tzitziki Lemus, Jennifer Lachowiec, Keisha Carlson, Josh Cuperus, and Ken Jean-Baptiste. They were always patient with me and helped me to get my footing in the Queitsch lab.

I, of course, would like to thank all the Queitsch lab members, both past and present. If I actually listed all of the help I have received from them over the years, it would be about equal in length to this thesis.

I would like to thank my committee members Bonny Brewer, Ray Monnat, Jennifer Nemhauser and Steve Henikoff for their time, feedback, and encouragement.

I would like to thank my fellow classmates in the Department of Genome Sciences for sharing with me the trials and triumphs of being a graduate student.

I would like to thank my mother and her family for always driving home the importance of getting an education. I would like to thank my father for sharing his love of science and the natural world with me.

And Pat. Without him, none of this would have been possible.

Dedication

to Pat

Chapter 1: Introduction[1]

Abstract

Canalization, or phenotypic robustness in the face of environmental and genetic perturbation, is an emergent property of living systems. Although this phenomenon is well-recognized, its molecular underpinnings have remained enigmatic until recently. Here, I review the contributions of the molecular chaperone HSP90, a protein that facilitates the folding of many key regulators of growth and development, to canalization of phenotype – and de-canalization in times of stress – drawing on studies in eukaryotes as diverse as baker's yeast, mouse ear cress, and blind Mexican cavefish. HSP90 is a hub of hubs that interacts with many so-called 'client proteins' that affect virtually every aspect of cell signaling and physiology. As HSP90 facilitates client folding and stability, it can epistatically suppress or enable the expression of genetic variants in its clients and other proteins that acquire client status through mutation. HSP90's vast interaction network explains the breadth of its phenotypic reach, including HSP90-dependent *de novo* mutations. Intrinsic links between environmental stress and HSP90 function endow living systems with fundamental phenotypic plasticity in fluctuating environments. As environmental perturbations alter HSP90 function, they also alter HSP90's interaction with its client proteins, thereby re-wiring networks that determine the genotype-to-phenotype map. Ensuing de-canalization of phenotype creates phenotypic diversity that is not simply stochastic, but often has an underlying genetic basis. Thus, extreme phenotypes can be selected, and assimilated so that they no longer require environmental stress to manifest. In addition to acting on standing genetic

[1] Portions of this chapter are adapted from "It's not Magic - Hsp90 and its effects on genetic and epigenetic variation," Seminars in Cell and Developmental Biology: in review, by *R. Zabinsky, G. A. Mason, C. Queitsch, and **D. Jarosz. *First author. **Corresponding author. C.Q., D.J., R.Z. and G.A.M discussed and formulated the ideas presented in this review. G.A.M., D.J., R.Z., and C.Q. wrote the article. R.Z. created the figures.

variation, HSP90 perturbation has also been linked to increased frequency of *de novo* variation and several epigenetic phenomena, all with the potential to generate heritable phenotypic change. Here, I aim to clarify and discuss the multiple means by which HSP90 can affect phenotype and possibly evolutionary change, and identify their underlying common feature: at its core, HSP90 interacts epistatically through its chaperone function with many other genes and their gene products. Its influence on the phenotypic manifestation of genetic diversity is not magic but a fundamental property of genetics.

1.1. Introduction to Canalization and HSP90

1.1.1 The concept of canalization from theory to experiment

Across all kingdoms of life, a multitude of mechanisms ensure the fidelity of information transfer and its phenotypic manifestation. Indeed, when faced with ever changing environments, organisms must be robust to survive. Yet evolutionary success also requires adaptability, whether through phenotypic plasticity or the generation and selection of heritable biological novelty. Although genotype is the software that dictates development and expression of phenotype, selective forces ultimately operate on phenotypes. Mechanisms that influence the capacity of genetic variants to alter traits can thus have a fundamental impact on the adaptive landscape.

Some traits are more stable across environments and genetic backgrounds than others. A canalized, or phenotypically robust, trait is one that has a stable (*i.e.* buffered) phenotype in the face of genetic or environmental perturbation (**Figure 1.1A**). For example, many aspects of gross morphology (*e.g.* body plan and organ systems in animals) are reproducible across a wide variety of environments and genetic backgrounds. Other traits are less canalized. In *C. elegans*, for example, genetic and environmental perturbation readily gives rise to differences in gender

distribution, fecundity, and fat storage, but has less impact on cell number and lineage or movement and development of the pharynx, vulva, and other organs[1]. In contrast to animals, plant body plans and morphologies are far more responsive to environmental change due to continuous development; nevertheless, organ identity is largely preserved even in the face of severe stress[2].

As outlined in several previous reviews, the remarkable phenotypic robustness of wild-type organisms is commonly attributed to features of the underlying genetic networks, such as genetic redundancy, network connectivity, feedback loops, modularity, and the presence of microRNAs[1,3-27]. In model organisms, perturbation of any of these mechanisms or environmental change can decrease phenotypic robustness and reveal cryptic genetic variation[3,9-11,19,28-33].

Canalization can be advantageous in constant environments, or even in the presence of modest fluctuations, maintaining a mean distribution of phenotypes that hews closely to what has been adaptive to an ancestral population[34]. Yet extreme canalization can create a phenotypic 'lock-in' that could be disadvantageous if the environment shifts such that the prior distribution of phenotypes is maladaptive[35]. In this chapter, I focus on the stress-regulated molecular chaperone HSP90 as a mechanism for canalization that offers some resolutions to this paradox, linking the degree of trait canalization to the severity of environmental change.

1.1.2 HSP90 provides a molecular mechanism for de-canalization mediated by stress

Seminal studies investigating the concept of canalization were carried out more than half a century ago by the 'father of epigenetics,' Conrad Hal Waddington. While conducting heat shock experiments with *Drosophila* pupae, Waddington noted that a small fraction of the resulting adult flies developed crossveinless wings[36]. Selection enriched this phenotype to near fixation in the population, suggesting a stable epigenetic or genetic basis. Remarkably, after a

few generations of selection, the crossveinless phenotype was evident even in the absence of stress[36] (**Figure 1.1B**); that is, this once rare and environmentally contingent phenotype was readily assimilated into the population as a stable trait. This observation laid the groundwork for many future studies of canalization (and de-canalization) and its possible contribution to evolutionary change. In the intervening decades, these concepts have been applied to many other systems, ranging from assimilation of tadpole body size mediated by dietary changes[37] to caterpillar body color driven by temperature shifts[38].

Working half a century after Waddington, Rutherford and Lindquist observed a strikingly similar set of phenomena linked to the activity of the molecular chaperone HSP90. Investigating *D. melanogaster* harboring heterozygous mutants of the *HSP83* gene, which encodes HSP90, they noticed that rare individuals developed crossveinless wings, among other morphological abnormalities[32]. The specific kind of HSP90-dependent phenotype observed strongly depended on the genetic background examined, consistent with an underlying genetic basis. Thermal stress produced the same phenotypes in the same backgrounds. Just as in Waddington's studies, selection over several generations enriched these phenotypes in the population, consistent with a stable epigenetic or genetic basis. Selection on an eye and a wing trait also rendered these phenotypes independent of perturbation by either direct interference with HSP90 function or environmental stress. These observations implicated HSP90 as a possible molecular mechanism contributing to Waddington's seminal observations.

Subsequent studies, highlighted in later sections, have extended the hypothesis that HSP90 broadly influences the phenotypic manifestation of genetic diversity beyond *D. melanogaster*[16,17,39]. HSP90 influences the phenotypic outcomes of diverse genetic variants in plants (*A. thaliana*)[40], zebrafish[33], fungi[29,41], worms[42], Mexican cavefish[43], and even humans[44-46]

(**Figure 1.2A-D**). The broad conservation of HSP90's role in shaping phenotype highlights the importance of canalization in understanding the trajectory from genotype to phenotype, in particular with regard to understanding complex human diseases.

1.1.3 HSP90: A special chaperone

HSP90 is one of the most abundant proteins in eukaryotes[47]. It is normally expressed at high levels – beyond what is required for growth in organisms where it has been tested[48] – and it is induced by myriad environmental stresses. In some instances, however, even this increased expression of HSP90 cannot contend with the increasing number of unfolded proteins under stress, resulting in a reduction of net chaperone activity[41,49] It has been hypothesized that the basal reservoir of HSP90 activity in unstressed conditions allows cells to rapidly respond to modest levels of environmental fluctuations.

Over one thousand proteins have been identified in physical interaction screens using HSP90 as bait[50]; however, HSP90 clients are not a random sampling of all proteins, but a select cohort enriched in kinases and transcription factors[51] that are known to be conformationally dynamic. These clients reside in nearly every developmental and signaling pathway in eukaryotes[52-55], providing a plausible explanation for HSP90's broad influence on the relationship between genotype and phenotype.

HSP90's N-terminus contains a conserved ATPase domain that powers conformational dynamics linked to client folding[56], and its C-terminus is critical for dimerization (**Figure 1.3A**). The basis of client recognition is far more complex. Structural studies with a range of client proteins suggest that interactions with the middle region are important[57-59], but the interfaces identified also include some portions of the N- and C-termini[60-62]. Combinatorial recognition with co-chaperones also plays an important role in this process (see below). Subdomain-FRET-

analyses and crystal structures have illuminated the dynamic cycles that fuel the 'molecular clamp' mechanism of HSP90 binding and release driven by ATP hydrolysis (**Figure 1.3B**)[63,64]. **Figure 1.3B** illustrates the chaperone cycle that has been well defined for the progesterone receptor, a model client of HSP90[65]. However, our mechanistic knowledge is incomplete; *e.g.* researchers are unable to predict whether a particular protein is an HSP90 client or whether a mutation will confer or revoke client status. Clients are often directed to HSP90 via other (co)chaperones, dozens of which are known. For instance, HSP90's capacity to catalyze the folding of many of its kinase client proteins is dependent on the Cdc37 co-chaperone[61,66-71]. Like other HSP90 clients, these kinases are thought to be initially metastable, but they are stabilized through interaction with HSP90 and become functional. Other client proteins rely on other co-chaperones such as SQUINT in *A. thaliana*[72]. I point the reader to recent reviews detailing the extended family of HSP90 proteins, diverse co-chaperones, post-translational control, and mechanisms of action of all chaperone proteins[52,66,71,73-82]. Our knowledge of the multitude of HSP90 client proteins continues to expand with the utilization of new techniques[51]. Collectively, these studies demonstrate that HSP90 is a hub-of-hubs, linked to nearly every process within the cell (**Figure 1.3C**).

1.1.4 Missing heritability, canalization, and the evolving genotype-to-phenotype

Decoding how genetic variation gives rise to phenotypic diversity is the central challenge of genetics and genomics. Modern genomic technologies have enabled unprecedented strides toward cataloging genetic variation across many individuals and mapping functional genomic regions; nevertheless, the complexity of most biological traits, including many diseases, poses enormous challenges for predicting phenotype from sequence. For example, genome wide association studies have been employed in large cohorts of individuals to identify genetic

variants that contribute to complex human diseases. These studies have successfully associated thousands of genetic variants with various quantitative phenotypes. However, most of these variants contribute little to disease risk and explain only a small proportion of the observed heritability in families. This "missing heritability" has been attributed to several factors including unidentified sequence variation (*e.g.* copy number variation in repetitive DNA, large genomic rearrangements)[83], rare alleles of large effect[84,85], inflated heritability values in families[84], the failure to account for epistasis (*i.e.* genetic interactions)[84,85], epigenetic variation[84,85], variable levels of robustness[86,87], and cryptic genetic variants. HSP90 and molecular hubs like HSP90[30,86] are likely to play a major role in shaping complex traits through their role as strong genetic modifiers.

1.2 Principles and theories

1.2.1 Epistasis with an environmental contingency

Traditionally, epistasis refers to a non-reciprocal interaction between two alleles in which the phenotypic effect of one allele is dependent upon the presence of the other. The extent of epistasis in genetic networks is vast. For example, systematic studies in yeast have tested all pairs of viable gene deletion alleles, and identified genetic interactions between them[88]. Even in the compact yeast genome and examining only a single growth condition, these >23 million double mutants revealed nearly one million instances of epistasis. Notably, systematic studies like this one reveal that not all genes exhibit the same degree of epistasis, allowing us to understand and build genetic networks[89]. Genes at the hub of such networks – HSP90 key among them – show epistatic interactions with a large number of other genes[51]. For example, studies of ~65,000 pairs of genes in *C. elegans* identified 350 genetic interactions; over a quarter of these

involved six hub genes, all encoding chromatin regulators[30]. In other words, network hubs like HSP90 and chromatin regulators represent a special case of epistasis in which one gene interacts epistatically with many others.

The direct link between HSP90 activity and environmental conditions make this relationship even more remarkable, and important for linking phenotypic diversification to environmental change. Indeed, because HSP90 activity itself serves as a 'stress sensor', this system ensures that phenotypic diversity, the substrate for selection, can increase in the face of environmental change across entire populations in contrast to mutations that affect only a few individuals. Although other hubs have been shown to act as strong genetic modifiers[30], there is less evidence that their phenotypic robustness (or 'buffering') function is environmentally responsive. Without plausible paths for individuals becoming less phenotypically robust across many in a population, genetic variation will remain cryptic and will remain unable to contribute to phenotype. Nevertheless, one can imagine mutations that disrupt such hub genes in certain individuals, a scenario that has been invoked as contributing to complex human diseases[30,86]. With regard to HSP90, common environmental stresses and changes in cell physiology during malignant transformation can modulate its activity and hence its interactions with many other genes. The classic example of HSP90's effect on malignant transformation is the well-studied interaction between HSP90 and v-Src kinase, without which the kinase is not functional (**Figure 1.4A-C**)[90,91]. Thus, changes in the intra-and extracellular environment can readily lead to the release (and masking) of genetic variation, higher variation of phenotypes, and ultimately the assimilation of such traits via selection.

Although environmental stress provides a common trigger for changes in HSP90 activity, genetic and even epigenetic mechanisms may also affect its function. HSP90 and associated co-

chaperones are highly conserved in eukarya, but variation has been observed in some organisms. For example, some *Drosophila* populations harbor *HSP83* variants that can affect phenotypic robustness[92,93]. In *C. elegans,* the penetrance of several mutant alleles in developmental pathways can be predicted by endogenous HSP90 levels in juvenile animals[42]. HSP90 polymorphisms are also surprisingly common in humans, an exciting topic for future study.

1.2.2 Genetic assimilation of environmentally responsive traits

One of the most striking – and thus far least experimentally dissected – aspects of HSP90-dependent capacitance is the genetic assimilation of previously environmentally and HSP90-dependent traits. Empirically, such genetic assimilation has been observed in the laboratory. In Waddington's original experiments, assimilation of the crossveinless wing trait in *D. melanogaster* was rapid. After several generations of selective breeding the trait was fixed[36] (**Figure 1.1B**). Likewise, Rutherford and Lindquist observed rapid assimilation of analogous, HSP90-dependent traits in *D. melanogaster*[32] (**Figure 1.2A**). Laboratory studies with different organisms and employing other environmental triggers have come to conceptually similar conclusions. For example, heritable variation was observed in tadpole body size, developmental stage, and gut length after shifting to a rich shrimp diet[37].

Although HSP90 activity can be affected by all environmental stimuli that compromise protein folding, it has long been debated whether HSP90-dependent variation and its release upon stress can contribute to evolutionary trajectories in nature. Rohner et al. investigated this question in the context of the Mexican cavefish *A. mexicanus*[43]. Recent geological events have repeatedly isolated sub-populations of this river fish in different cave environments. These isolated populations have experienced a series of highly reproducible changes, specifically loss of pigmentation and eyes. Multiple lines of evidence suggest that these phenotypes are adaptive

in the cave environment[43]. Rohner et al. exposed developing river fish with normal eyes to low concentrations of HSP90 inhibitor, noticing significant variation (de-canalization) of orbit size. Selective breeding of fish with small orbit size led to rapid assimilation of the trait. That is, progeny from such crosses showed small orbits even without any HSP90 inhibition (**Figure 1.2B**). Most remarkably, exposure to cave water conditions, an ecologically relevant stress, also de-canalized orbit size in river fish, analogous to the treatment with the HSP90 inhibitor. Although determining whether HSP90-dependent de-canalization has contributed to the cave-specific phenotypes in nature stands as a goalpost for future work, this study establishes the expression of HSP90-dependent, formerly cryptic variation as a plausible explanation for this rapid and recurring adaptation.

1.3 Evidence for the evolutionary importance of HSP90-dependent variation

Although it is challenging to devise experiments to conclusively prove that HSP90-dependent variation contributed to eye loss or other traits, the existence and relative importance of HSP90-dependent evolution can be detected in genomes, in particular by comparing the evolutionary rates of client and non-client proteins. The capacitor hypothesis posits that clients should be allowed to acquire more and potentially more harmful mutations than non-clients. Evolutionary rate is influenced by many factors, including protein stability, protein interactions, and gene expression. These factors will confound any effect that interaction with HSP90 may have, making it imperative to conduct analyses of evolutionary rate among genes encoding comparable client and non-client proteins. One solution has been to compare pairs of recent gene duplicates that differ little in sequence and expression. In *A. thaliana*, the HSP90-client *BES1,* a transcription factor in the brassinosteroid pathway, shows relaxed selection compared to its

closest paralog the non-client *BZR1*[94]. *BES1* bears hallmarks of neo- and sub-functionalization, and shows dynamic HSP90 client status across independent evolutionary paths. In yeast, HSP90 clients also evolve faster than their non-client paralogs[94]. The authors concluded that HSP90 may facilitate the divergence of gene duplicates, but noted the scarcity of suitable pairs of gene duplicates.

The availability of large-scale data on HSP90 clients, in particular on human kinases[51], has finally enabled the systematic exploration of HSP90's role in protein evolution across the mammalian lineage. Kinases are monophyletic, akin to the prior studies of gene duplicates. Kinases identified as clients in humans show significantly higher evolutionary rates than non-client kinases across the mammalian lineage; this effect is independent of gene expression and protein interaction, the two major factors influencing evolutionary rate, and comparable in effect size[95]. Across several thousand sequenced humans, genes encoding client kinases showed greater nucleotide diversity than those encoding non-clients. Moreover, the genetic variants in client kinases were predicted to be more damaging to protein function than those in non-clients, consistent with HSP90's hypothesized capacitance function. If so, one would predict that once a kinase acquires HSP90 client status, it would be unlikely to lose it again. Indeed, this outcome is often the case. Kinases are of outsized importance in shaping development, physiology, and evolutionary trajectories; they also play a major role in many human diseases, including various cancers. In this context, HSP90's role in promoting their divergence and in maintaining their function in the face of accumulating genetic variation is particularly noteworthy.

In contrast to Eukarya, HSP90 is not essential in bacteria, and a broad characterization of its molecular function and possible role in capacitance is lacking in this domain of life. A recent study used genome-scale phylogenetic analysis to identify genes that co-evolve with bacterial

HSP90[96]. Genes whose gains and losses are coordinated with HSP90 throughout bacterial evolution tended to function in large protein complexes associated with motility and secretion, suggesting that HSP90 may aid the assembly of protein complexes. Indeed, experimental validation identified HSP90 clients such as the flagellar protein FliN and the chemotaxis kinase CheA; *E. coli hsp90* mutants showed impaired motility and chemotaxis. The presence of bacterial HSP90 across all sequenced species is associated with a preference for multiple habitats. Taken together, bacterial HSP90 appears to aid the assembly of membrane protein complexes and facilitates adaptation to novel environments, both functions that seem to preface its much larger and essential role in protein folding and evolution in Eukarya.

To summarize, these studies confirm one of the two predictions of the capacitor hypothesis: genetic variation indeed accumulates in genes encoding client proteins. The other prediction of the capacitor hypothesis posits that intermittent stress leads to expression of this accumulated variation followed by selection. This prediction has also been addressed in recent studies, as I will discuss in more detail below (**see Chapter 1.5.3**).

1.4 Protein folding as a general mechanism

1.4.1 Open questions

Studies from yeast to human have established HSP90's conserved capacity to buffer genetic variation. Although several HSP90-dependent loci have been mapped in natural populations[97-99] it has largely remained unresolved how precisely HSP90 perturbation enables cryptic genetic variation to contribute to phenotype. Does this variation occur in client proteins, or can it occur in non-clients, or even regulatory regions? Could any variant in a client protein be

HSP90-responsive? In short, what variation can the chaperone buffer? Below I synthesize results from experiments seeking to answer these questions.

1.4.2 HSP90 reveals cryptic genetic variants responsible for many traits

Our understanding of how the HSP90 affects cryptic genetic variation is driven by a series of genetic studies across model organisms. In flies, plants, yeast, fish, and other model systems, HSP90 perturbation generates background-specific traits[43,44,100,101] (**Figure 1.2**), allowing HSP90-dependent loci to be mapped in some systems[97-99]. Thus far, however, few HSP90-dependent variants have been identified at the gene level[97,102]. As a result, our mechanistic understanding of HSP90-mediated capacitance is thus limited, while biochemical studies of HSP90 function have flourished[55]. In the absence of systematic studies of HSP90-dependent variation in a wide array of client and non-client proteins, it has been impossible to rigorously determine features that render a given variant HSP90-responsive. The handful of known examples suggests that HSP90-dependent variants can occur in clients, non-clients that interact with client proteins, and even in regulatory regions that are bound by clients. I discuss specific examples in section 4. Recent studies suggest that disease-associated variants in various proteins often show HSP90-dependence[44]; early work found this to be true for mutations in oncogenic proteins[91,103].

1.5 Specific examples across Eukarya

1.5.1 Alleles that are buffered

A capacitor stores electrical energy for later rapid release. HSP90 has been proposed to function analogously for genetic variants, allowing them to accumulate (or be 'stored') as phenotypically silent mutations, only to be expressed after a shift in environment. That is,

ensuing reduction of HSP90 function may unmask the phenotypic consequences of genetic variants that were previously cryptic. As discussed above our understanding of specific variants that are influenced by this mechanism is incomplete, although there is convincing evidence that they are common in natural populations[29,98,99].

Greater detail on buffered variants is emerging from saturating mutagenesis studies of individual genes. For example, "deep mutational scanning" has identified HSP90-buffered variants of the Ste12 transcription factor in *S. cerevisiae*[102] (**Figure 1.4D**). The wild-type Ste12 protein is not a client of HSP90. At standard growth conditions, the HSP90-dependent Ste12 variants were competent for both mating and invasion. Ste12 drives the expression program for both traits, which are mutually exclusive, yet share many signaling components, including Ste12. Upon HSP90 inhibition or thermal stress, cells harboring the HSP90-dependent variants lose the capacity to mate, but become dominantly hyperinvasive even in the absence of the known invasion cofactor. The ability to engage in invasive growth is a property strongly associated with pathogenesis[104-107]. Indeed, temperature-regulated invasiveness is a common phenotype of fungal pathogens. The Ste12 example is so striking because loss of HSP90 does not simply lead to degradation of the respective protein and loss of function; rather, loss of HSP90 shifts the trait preference of Ste12 towards invasion by altering its binding to DNA. Although HSP90-dependent Ste12 variants are rare, they are accessible through a single amino acid change, suggesting that the chaperone could facilitate a mutational path toward a pathogenic fungal lifestyle by minimizing mating costs at normal temperature and enhancing invasion at the higher host temperature.

In yeast, fine mapping studies have identified several natural genetic variants that are affected by chaperone activity[97]. Two arise in HSP90 clients: Mec1, the sentinel DNA damage

kinase, and Nfs1, an essential sulfur donor in FeS cluster biogenesis and tRNA thiolation. Under normal growth conditions, natural genetic variation in these genes is phenotypically silent. But upon pharmacological or environmental inhibition of HSP90 activity, vineyard (RM) alleles of these genes give rise to new phenotypes. The vineyard allele of Mec1 produces resistance to DNA damage induced by UV-irradiation (**Figure 1.4E**), and the vineyard allele of Nfs1 produces resistance to rapamycin. Each of these phenotypes is explained by the known function of the polymorphic genes and their well-characterized interaction with the chaperone. HSP90 also buffers resistance to the oxidative stressor 1-chloro-2,4-nitrobenzene derived from vineyard alleles of the Ndi1 gene. Remarkably, this trait arises from mutations in the 3'-untranslated sequence of the gene. Upon HSP90 inhibition, levels of *NDI1* mRNA increase by nearly 100-fold in strains harboring the vineyard allele. Forced overexpression of Ndi1 also produces CDNB resistance. Several HSP90 clients are known to bind to the 3'-UTR of this mRNA, providing a plausable rationale for this HSP90-responsive phenotype.

Genotypes and phenotypes have been measured extensively across many dozens of yeast isolates from diverse ecological niches. This approach has made it feasible to assess the global relationship among HSP90, genotype and phenotype in this organism. Across >100 growth conditions and without HSP90 perturbation, the correlation between genotype and phenotype is statistically significant, but surprisingly weak. This correlation increases considerably in response to HSP90 inhibition, suggesting that a considerable fraction of the 'silent' genetic variation in this organism has phenotypic consequences in the presence of HSP90 inhibition[97].

Another striking example comes from mice, where HSP90 buffers the regulatory influence of certain endogenous retroviruses on neighboring developmental genes[108]. This effect on *cis*-regulatory variation arises because HSP90 chaperone activity is required for

TRIM28/KAP1-mediated epigenetic silencing of endogenous retroviral elements. This example provides yet another mechanism by which HSP90 can buffer natural genetic variation, and raises the question of whether the capacitor function of HSP90 may have facilitated exaptation of endogenous retroviruses as modifiers of gene expression.

As discussed earlier, as the number of sequenced human genomes expands, so does our ability to detect the broad effects of HSP90 and protein folding in general on human phenotypes. Across >1,500 disease alleles, a recent study found that their relative association with HSP90 was highly predictive of disease severity, especially when compared to association with HSP70, another chaperone (**Figure 1.2D**)[44]. This finding, which is remarkable given the diversity of genetic causes of disease, illustrates how even specific aspects of chaperone function are fundamentally integrated into the trajectory between genotype and phenotype. A more detailed examination of mutations associated with the cancer-prone syndrome Fanconi Anemia (FA) revealed that HSP90 perturbation amplified FA-related sensitivities to chemotherapeutics. Although an integrated understanding of how chaperone activity influences specific disease alleles will require many more both detailed and systematic studies, it is clear that these effects are likely highly significant and widespread.

1.5.2 Alleles that are potentiated

HSP90 can also potentiate some mutations; that is, when HSP90 activity is reduced, the capacity of these variants to produce new traits is eliminated. Like buffering, potentiation is linked to the activity of the chaperone and reflects its wide-spread epistasis with genes residing in nearly all pathways. The first oncogene discovered, v-Src, provides a particularly striking example (**Figure 1.4A-C**). v-Src arose from mutations in the c-Src progenitor kinase that lead to its constitutive activation. However, these same mutations render v-Src thermodynamically

unstable, making its folding and function dependent on HSP90[91,109] (**Figure 1.4C**). Many other oncogenes have since been shown to require HSP90 for function[103].

Another fascinating example is the BCR-ABL gene fusion that encodes a constitutively active tyrosine kinase. The BCR-ABL inhibitor Imatinib, known commercially as Gleevec, was one of the earliest and most successful targeted therapies for chronic myelogenous leukemia. However, emergence of resistance has been a common failure mode of this and most other oncogene-directed therapies. A majority of patients treated with Imatinib at an advanced stage will relapse due to a point mutation in BCR-ABL that renders its inhibition ineffective[110]. However, treatment with an HSP90 inhibitor leads to degradation of the HSP90-client BCR-ABL and loss of Imatinib resistance (**Figure 1.4F**)[45,111], highlighting the need to understand the role of HSP90 and other buffering factors in enabling the accumulation of mutations favorable to cancer cells.

Like buffering, potentiation can also occur indirectly. A striking example is resistance to fluconazole, a main line antifungal drug, in the fungal pathogen *Candida albicans.* Mutations in *ERG3* enable resistance to fluconazole[112], but also result in the production of a toxic sterol. Such variants persist in the population because HSP90 mediates the function of its client Calcineurin and other proteins integral to stress response circuitry. Mutations in several other genes also potentiated fluconazole resistance dependent on Hsp90 including *erg6Δ*, *osh1Δ*, *scs2Δ*, and *cka2Δ* (**Figure 1.4G**). Genetic assimilation of initially HSP90-dependent antifungal drug resistance has been observed in multiple clinical isolates evolving in human hosts, suggesting that this process may have a strong influence on human health. Remarkably, dependence on HSP90 was abrogated by high temperatures, pointing to a potential clinical benefit of fever.

1.5.3 Buffering and potentiation arise naturally from HSP90's chaperone function

Although HSP90's relationship with phenotype is remarkable, it is decidedly not magic. HSP90 does not have the capacity to buffer or potentiate every mutation in every gene; rather, its effects on phenotype are a consequence of its biochemical function. HSP90's client proteins – largely kinases and transcription factors – occupy key nodes in signaling cascades that govern a multitude of cellular and developmental pathways[51,52]. Relative to other chaperones, HSP90 catalyzes folding steps that occur late in the maturation of its client proteins[52]. A case in point is the family of steroid hormone receptors, a class of closely related transcription factors that were among the earliest HSP90 clients identified and studied. These proteins bind to HSP90 in an immature but mostly folded state[113]. In the presence of hormone, the protein acquires a fully folded and functional conformation, leading to concomitant release from the chaperone. Other clients have different trajectories; they require phosphorylation or other modifications to reach their stable state or reach their final cellular destination. Loss of HSP90 activity severely disrupts client protein function, often through degradation or failure to signal or productively interact in protein complexes[17].

As discussed, HSP90's biochemical activity and regulation is tightly coupled to fluctuations in the environment. Together with HSP70, HSP90 interacts and suppresses Hsf1, the major regulator of the conserved heat shock response that ensues upon proteotoxic stress. It has been appreciated for decades that, upon stress, Hsf1 trimerizes and releases HSP90 and HSP70 to act on unfolding proteins; as soon as protein folding has recovered, HSP90 and HSP70 are once more available to suppress Hsf1[114,115]. Active, trimeric Hsf1 activates expression of many chaperones, including HSP90. There are also many post-transcriptional and post-translational mechanisms that regulate HSP90 activity – and these are also linked to environmental inputs –

including phosphorylation, acetylation, and nitrosylation[52,116]. HSP90 also changes its interaction with co-chaperones in different environments, lineages, and disease states that affects its substrate specificity. Together, these regulatory inputs generally up- or down-regulate HSP90 activity, or direct its activity toward particular cohorts of clients.

As a result of its complex regulation, HSP90's epistatic relationship with genetic variants is not static, but highly dependent on specific environmental circumstances, developmental stages, and even diurnal cycles (**Figure 1.5**). Thus, organisms have likely experienced environmentally-driven changes in these epistatic relationships during their evolutionary histories. This predictability of HSP90 activity changes may expose HSP90-dependent genetic variation to significant selection, purging deleterious alleles. Indeed, the distribution of fitness effects revealed upon HSP90 inhibition in wild isolates of *S. cerevisiae* is heavily skewed toward adaptive phenotypes (~50%) relative to the distribution of fitness effects that would be expected for spontaneous mutations (where adaptive effects are rare)[117,118], arguing for intermittent release of and selection on HSP90-dependent variation. In *A. thaliana* plants, deep mutagenesis revealed significantly greater penetrance of EMS mutations upon HSP90 inhibition; however, many of the HSP90-dependent phenotypes (but not all) are also observed in wildtype plants treated with HSP90 inhibitors (**see Chapter 2**). These observations in yeast and plants are consistent with two key points I wish to make: first, not all loci are HSP90-responsive, and second, HSP90-dependent variants in these loci in natural populations likely experience intermittent release and selection, purging those that are deleterious[119]. Deeper investigation of these observations stands as a goalpost for future studies.

1.6 Links between HSP90 and *de novo* variation

1.6.1 HSP90 impacts genome instability

Genome instability encompasses an increased genome-wide frequency of point mutations, insertions/deletions, microsatellite slippage events, somatic homologous recombination, and transposon activity. In human cells, HSP90 perturbation increases mutation rates of microsatellites[120], and decreases resistance to ionizing radiation[121]. In yeast, HSP90 reduction can increase rates of aneuploidy[122] and overexpression of HSP90 results in reduced efficiency of DNA repair[123]. In metazoans, HSP90 inhibition increases transposon transcription and mobility through the disruption of PIWI-protein function (*D. melanogaster*, *C. elegans*, mice, and human cells)[82,124-130]. In the plant *A. thaliana*, perturbation of HSP90 increases somatic homologous recombination[86] and susceptibility to ionizing radiation[131]. HSP90 perturbation is therefore correlated with, and in some instances causative of, genome instability in eukaryotes (**Figure 1.5**). HSP90's wide-reaching effects on genome stability is readily explained by its role in chaperoning many proteins functioning in the various DNA maintenance and repair pathways. In addition to the above mentioned PIWI-proteins, these include the above mentioned Mec1 in yeast, telomerase, FANCA in the Fanconi anemia pathway[44], DNA Polymerase subunits, BRCA proteins, and Rad proteins to name a few examples (See reference [132] for database of HSP90 interactors).

However, given the breadth of standing genetic variation that is responsive to HSP90 perturbation[29,41,43,44,100,101,108], mutations that newly arise in response to HSP90 inhibition likely play only a minor role in most HSP90-dependent phenotypes. Most previous studies validate their genotype-specific HSP90-dependent phenotypes through treatment of embryos with highly specific HSP90 inhibitors and moderate temperature stress. Drug and temperature treatment

produce the same genotype-specific phenotypes, which is inconsistent with major contributions of *de novo* mutations. *De novo* mutations due to these treatments would be somatic mutations, and these most certainly occur at an increased rate in response to HSP90 inhibition as I and others have shown[86]. However, somatic mutations occurring in individual embryos are extremely unlikely to affect many embryos of the same genotype in the same way; they are also extremely unlikely to be transmitted to the next generation. As the issue of HSP90-dependent *de novo* mutations has caused some controversy in the past, I would like to state clearly that although HSP90 perturbation increases genome instability, the majority of HSP90-dependent phenotypes described to date are highly unlikely a consequence of *de novo* mutations, in particular if these phenotypes have been validated through drug or environmental treatments of embryos.

The observation that perturbation of a hub like HSP90 is associated with genomic instability may have broader implications. Increased genome instability via HSP90 or via perturbation of other hubs may be a general hallmark for loss of robustness, which in turn may affect penetrance of genetic variation. In support of this hypothesis, yeast studies identified hub genes in which deletion decreased phenotypic robustness; one-fourth of ~300 identified hubs were genes with critical roles in genome stability[9]. Similarly, environmental stress is known to decrease phenotypic robustness; in many cases, it is also associated with increased genome instability[133,134]. As genome instability and robustness levels appear to be associated, it has been previously proposed that levels of genome instability could be used as a marker for robustness levels in humans and non-model organisms (and hence as markers for penetrance levels of genetic variation)[86].

1.7 Conclusions and Future Directions

It has been nearly two decades since Rutherford and Lindquist proposed that HSP90 might impact the relationship between genotype and phenotype, and suggested that this might provide a link between environmental change and evolutionary processes[32]. Their work attracted a great deal of interest; yet, it was also highly controversial. And, it must be said, for good reasons. As exciting as the initial findings in *D. melanogaster* were, the adaptive value of the traits exposed upon HSP90 inhibition, and the nature of their underlying genetics, was unclear.

Since then, many studies have moved the capacitance model from a compelling hypothesis to a plausible mechanism that has contributed to the evolution of genomes. Work in plants, fungi, and human cancers have identified many genetic variants and loci that are affected by HSP90 activity. Indeed, the pervasive influence of HSP90 on mutations linked to cancer has sparked great interest in the therapeutic value of chaperone inhibitors[103,135-137]. In a wide variety of fungal pathogens, HSP90 fuels the rapid acquisition of mutations that confer resistance to environmental stressors, including antifungal drugs[138-142], contributing to the interest in HSP90 as a therapeutic target.

Perhaps the strongest evidence for HSP90's influence on evolution comes from systematic studies of genotype-to-phenotype relationships. In *Saccharomyces cerevisiae* strains from diverse ecotypes, inhibiting HSP90 leads to a far more adaptive distribution of fitness effects than would be expected from random mutations, suggesting that selection has previously acted on the genetic variation responsible for these traits. Modest reduction in HSP90 function (elicited either pharmacologically or by a moderate environmental stress) improved the correlation between genotype and phenotype across more than 100,000 polymorphisms in sequenced yeast strains. Even more compelling evidence has come with systematic annotation of

human kinase clients of HSP90 function. A key tenet of the original capacitor hypothesis is that HSP90 client proteins should be able to accumulate mutations at a higher rate than non-clients. Indeed, across the human protein kinase superfamily – and mammals more generally – HSP90 client status promotes increased evolutionary rate. Collectively, these studies provide strong evidence that HSP90 has played an important role in shaping the evolution of current genomes.

Although HSP90 exerts a large influence on the phenotypic manifestation of genetic and epigenetic variation, it is not magic and clearly does not universally act on any type of variation. In fact, the most universal mechanism for buffering the effects of genetic variation is being diploid, which prevents most mutations from having a phenotypic impact (because they are recessive). Yet even being diploid fails at buffering dominant mutations, which are estimated to constitute *ca.* 10-20% of variants from studies in *Drosophila* and *S. cerevisiae*[143,144]. Likewise, several human diseases arise from haploinsufficiency[145]. Experiments in plants and yeast suggest that HSP90 activity can influence many natural genetic variants[29,31], and the polymorphisms that have been fine-mapped to date are plausibly linked to HSP90 chaperone function[29]. These observations are a natural consequence of HSP90's interaction with large swaths of cellular circuitry integral to growth and development. Theory holds that in any sexually reproducing organism the costs of maintaining a system for increasing variation will eventually be separated from beneficial variants via meiotic recombination[146]. Yet because HSP90's chaperone activity is required for nearly all aspects of eukaryotic biology; such separation is likely impossible. Furthermore, the large number of HSP90 clients and their distribution throughout the genome makes it likely that combinatorial gain (and loss) of chaperone-dependent variants can occur at each generation.

HSP90's influence on evolutionary processes is now indisputable – scientists can detect the chaperone's impact in genomes. Yet a better understanding of the genotype-to-phenotype map across multiple environments will improve our understanding of how this chaperone alters adaptive landscapes (**Figure 1.7**). Fortunately, researchers have new tools in hand to achieve this goal. Using deep mutational scanning, it is now possible to systemically interrogate how HSP90 affects variants at *every* position within a protein. Likewise, new crossing strategies in model organisms and advances in human functional genomics will enable identification of HSP90-dependent genetic variants at single nucleotide resolution and on an unprecedented scale. These powerful new approaches promise to transform our mechanistic understanding of how the HSP90 chaperone acts as a global regulator of the evolving genotype-to-phenotype map.

1.8 Focus of the dissertation

How do organisms, particularly sessile plants, remain robust to environmental and genetic perturbations? Furthermore, to what degree to do phenotypic buffering mechanisms overlap? Clearly, HSP90 does a great in deal in buffering both environmental and genetic disturbances. For studies reviewed in **Chapter 1**, mostly pre-existing genetic variation is well-characterized for its interactions with HSP90. While these data are invaluable, they do not tell us what proportion of new genetic variation HSP90 can interact with. Data from cancer research and a few model organism examples imply that HSP90 does interact with *de novo* genetic variation, albeit rarely. Although invaluable, previous studies have not assayed the phenotypic consequences of decreased buffering capacity when large-scale perturbations to the genome are introduced. These ideas will be addressed in **Chapter 2**.

HSP90 lends phenotypic capacitance to pre-existing, often hidden, genetic variation within populations. Is such a phenomenon unique to HSP90 or are there other robustness master regulators that maintain constant phenotype in the face of genetic and environmental changes? Do the genetic targets of HSP90 and these novel buffering factors overlap? These questions will be addressed in **Chapters 3 and 4**, where I characterize a key player in microRNA-mediated gene regulation, ARGONAUTE 1, and its roles in buffering cryptic genetic variation and integration of environmental signals.

Highly connected genetic hubs, like HSP90, provide robustness to complex phenotypes from developmental noise. Is the robustness provided by these hubs emergent from networks or can it be explained by a particular genetic interactor? Do non-hub genes buffer developmental variation across genetically identical siblings? These questions will be addressed in **Chapters 5**. In total, these studies help define more of the rules about HSP90's and ARGONAUTE 1's roles in buffering *de novo* genetic variation, pre-existing genetic variation, developmental noise, and environmental stimuli.

1.9 Main figures

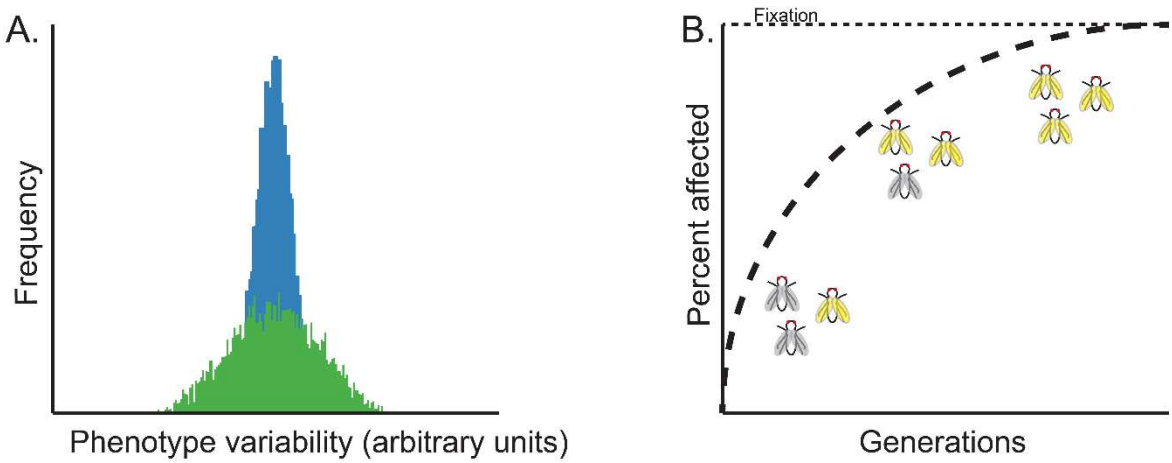

Figure 1.1: Canalization minimizes phenotypic variation. (A) Quantitative traits exhibit some degree of variation, represented here by a distribution. A canalized, phenotypically robust trait shows tight distributions (blue) regardless of genetic or environmental perturbation. Some traits can be de-canalized by environmental or genetic perturbations which increases the degree of phenotypic variation (green). **(B)** A possible mechanism of assimilation of a new phenotype occurs via de-canalization. Over several generations of selection for a crossveinless wing phenotype in *Drosophila*, the rare phenotype was assimilated to a large fraction of the population.

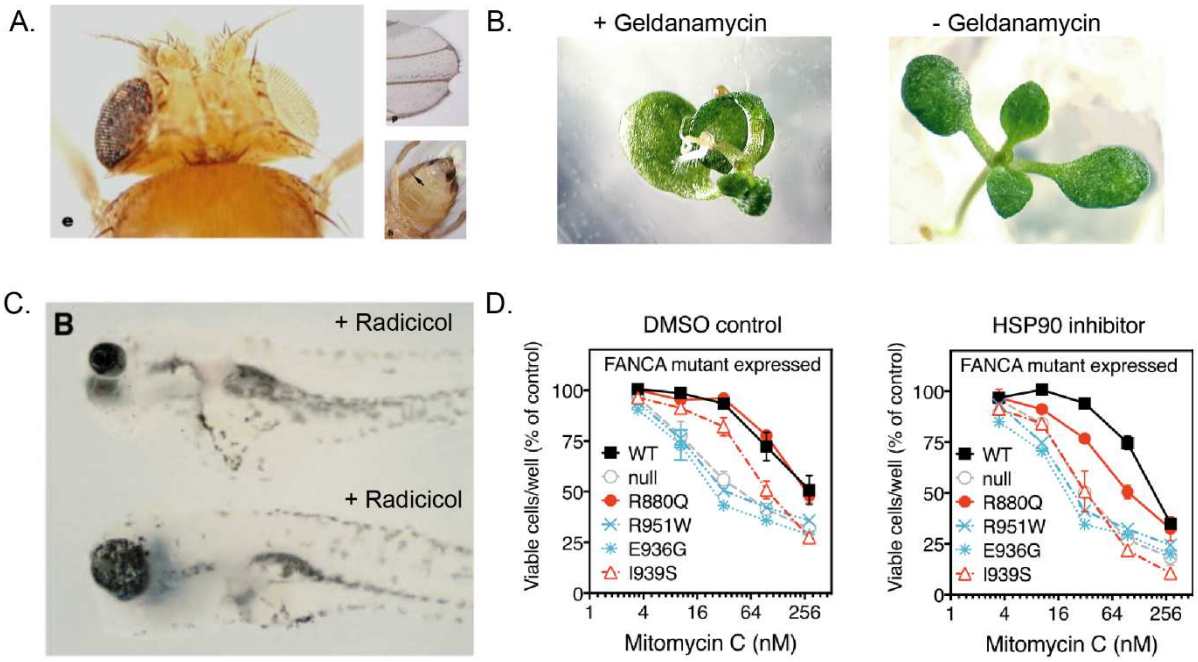

Figure 1.2: Phenotypic variability revealed by inhibition of HSP90. (A) Inhibition of HSP90 in *Drosophila* reveals phenotypes including black facets in one eye, notched wings, and extraneous tissue. **(B)** Inhibition of HSP90 by Geldanamycin in *A. thaliana* reveals phenotypes including disruption of typical symmetry and oval shaped, flat leaves. **(C)** Inhibition of HSP90 in Mexican cavefish, *A. mexicanus*, results in variable eye size of larval fish. **(D)** Human cells expressing the FANCA mutant allele R880Q exhibit increased sensitivity to HSP90 inhibitor Mitomycin C but a wild type allele or non-buffered alleles do not. In this case the detrimental growth phenotype revealed upon HSP90 inhibition is only observed in a specific FANCA mutant background.

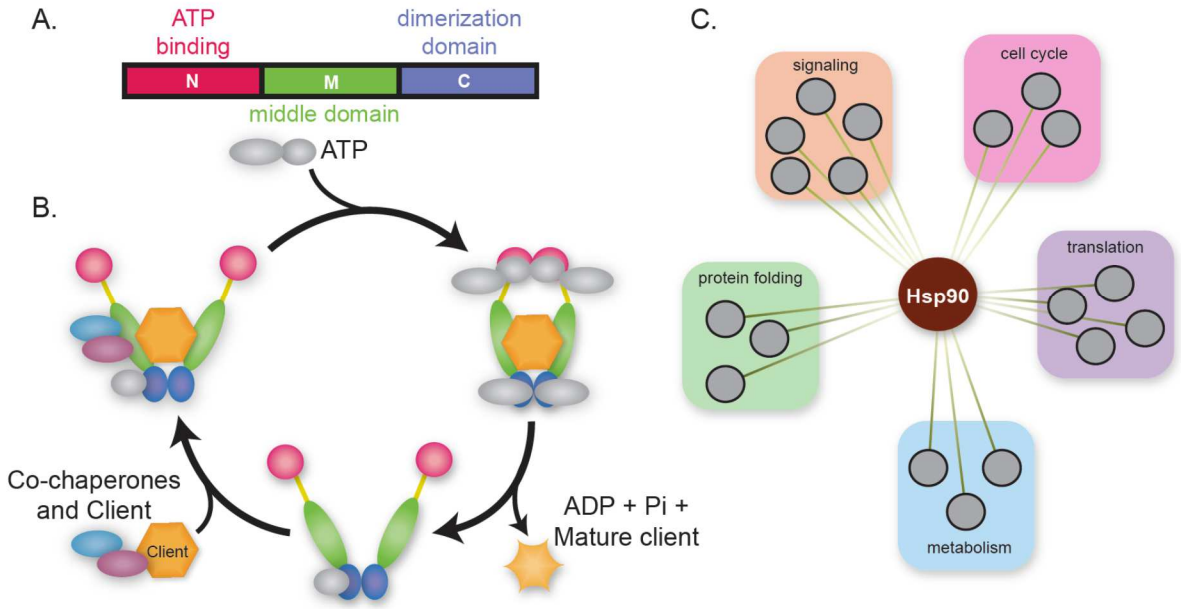

Figure 1.3: HSP90 structure and function. (A) The N-terminus of HSP90 contains a conserved ATP binding domain, the middle domain may bind client proteins and co-chaperones, and the C-terminal domain is responsible for dimerization. **(B)** The HSP90 chaperone cycle begins with the binding of co-chaperones and clients. Here all co-chaperones, and ATP, are drawn in gray. The progesterone receptor is one of the best understood clients. It binds HSP40, then recruits HSP70. Then HSP90-HOP binds HSP70, resulting in the delivery of the progesterone receptor client. After ATP binding, the dimer clamps together. This final hydrolysis step includes binding of p23 (Sba1 in yeast) as well as ATP, which leads to the dissociation of HOP and HSP70. Upon ATP hydrolysis, the clamp opens, releasing a mature client protein. **(C)** Protein interaction studies have defined the vast interaction network of HSP90 interactors. HSP90 interacts with hundreds of proteins of diverse functions including protein folding, signaling, cell cycle, translation and metabolism.

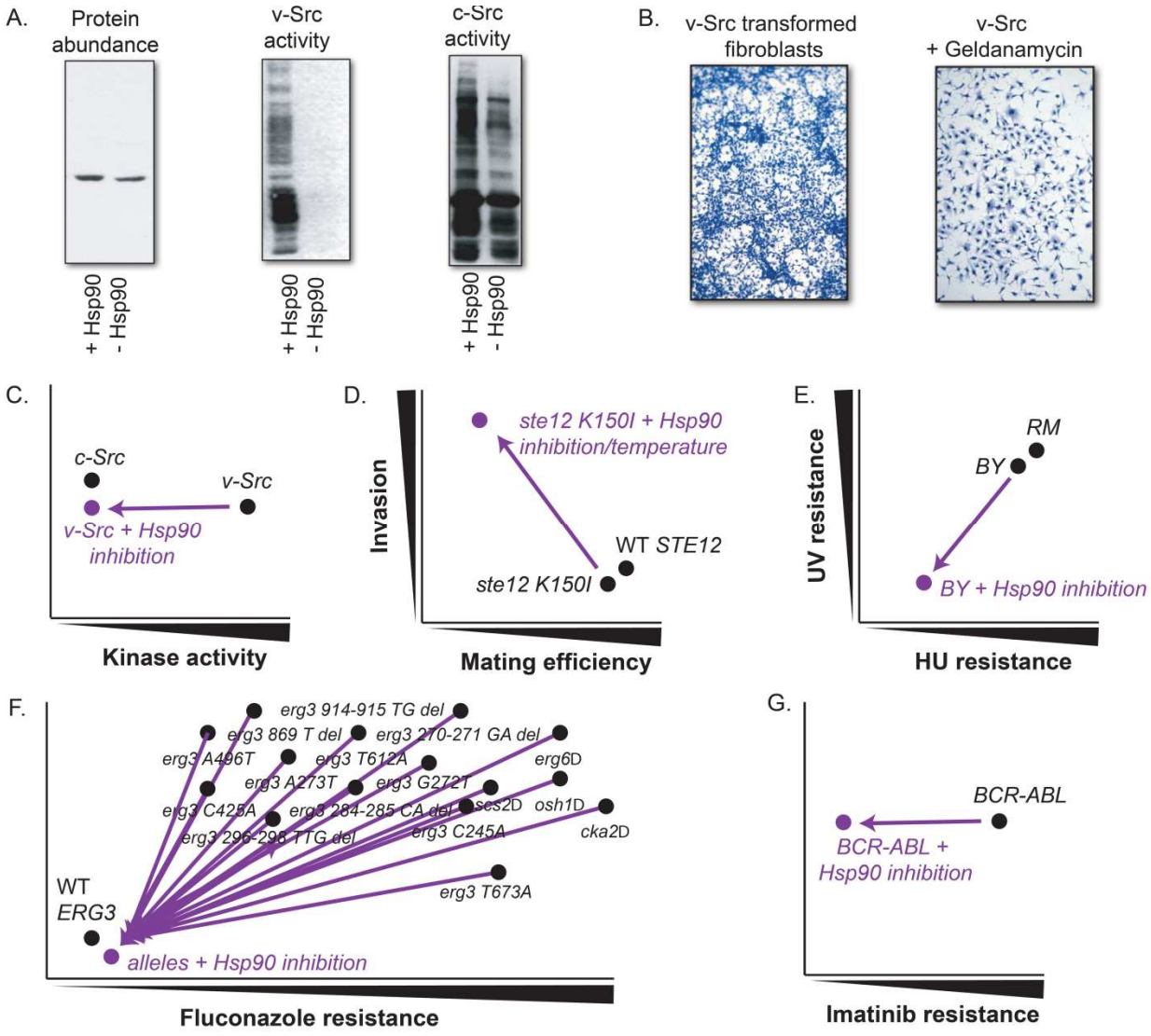
A.
Protein abundance
v-Src activity
c-Src activity
+ Hsp90
- Hsp90
B.
v-Src transformed fibroblasts
v-Src + Geldanamycin
C.
c-Src
v-Src
v-Src + Hsp90 inhibition
Kinase activity
D.
ste12 K150I + Hsp90 inhibition/temperature
WT STE12
ste12 K150I
Invasion
Mating efficiency
E.
RM
BY
BY + Hsp90 inhibition
UV resistance
HU resistance
F.
erg3 914-915 TG del
erg3 869 T del
erg3 270-271 GA del
erg3 A496T
erg3 T612A
erg6D
erg3 A273T
erg3 G272T
erg3 C425A
erg3 284-285 CA del
ses2D
osh1D
erg3 296-298 TTG del
erg3 C245A
cka2D
erg3 T673A
WT ERG3
alleles + Hsp90 inhibition
Fluconazole resistance
G.
BCR-ABL
BCR-ABL + Hsp90 inhibition
Imatinib resistance

Figure 1.4: Mechanistic examples of buffering and potentiating. (A) Activity of v-Src but not -Src is dependent on Hsp90 (reprint from Xu and Lindquist, 1993). **(B)** Likewise, malignant transformation with v-Src is also dependent on HSP90. Upon treatment with the HSP90 inhibitor Geldanamycin, normal contact inhibition of growth is restored (reprint from Whitesell *et al*., 1994). **(C)** Graphic illustration of HSP90 potentiating oncogenic v-Src constitutively active kinase activity. The original observed phenotype is graphed on a phenotypic scale in black. The phenotype dependent on HSP90 is graphed in purple with a vector designating the phenotypic difference of buffered alleles[90,109]. **(D)** Ste12 contributes to both mating and invasion. A WT *STE12* allele results in normal mating efficiency and invasion. *ste12 K150I* allele results in decreased mating efficiency only at high temperature or upon inhibition of Hsp90. The same allele results in increased invasion only at high temperature[102]. **(E)** In the RM background, the *MEC1* allele is not dependent on HSP90. In the BY background, the *MEC1* allele is dependent on HSP90; HU-resistance and UV-resistance decreases when Hsp90 is inhibited[147]. **(F)** HSP90 potentiates fluconazole resistance in several *erg3* alleles and other gene deletions[112]. **(G)** Hsp90 potentiates BCR-ABL imatinib resistance[45,111].

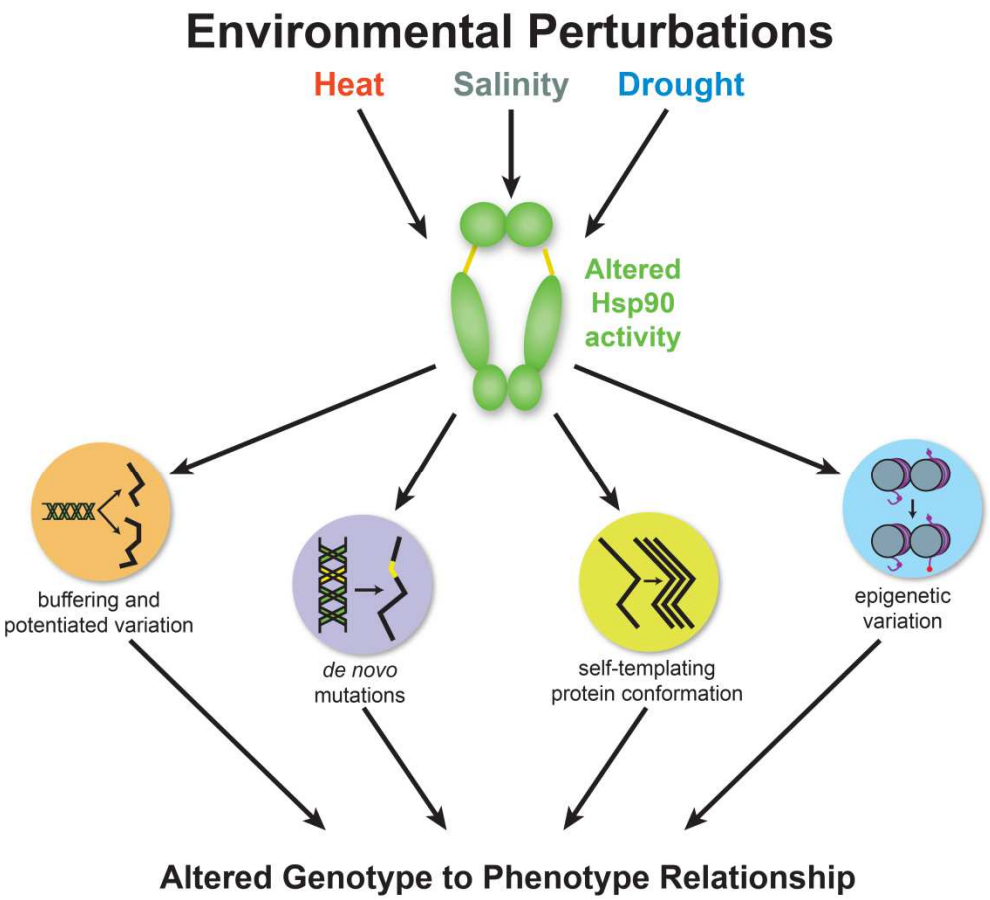

Figure 1.5: Environmental perturbations regulate HSP90, a central node that integrates stress sensing with the manifestation and generation of de novo variants. Many environmental perturbations including heat, salinity, and drought have the potential to alter HSP90 activity. This altered activity affects cryptic genetic variation, buffered and potentiated variants, *de novo* mutations, self-templating protein conformations, and epigenetic variation. All of these will in turn alter the relationship between genotype and phenotype.

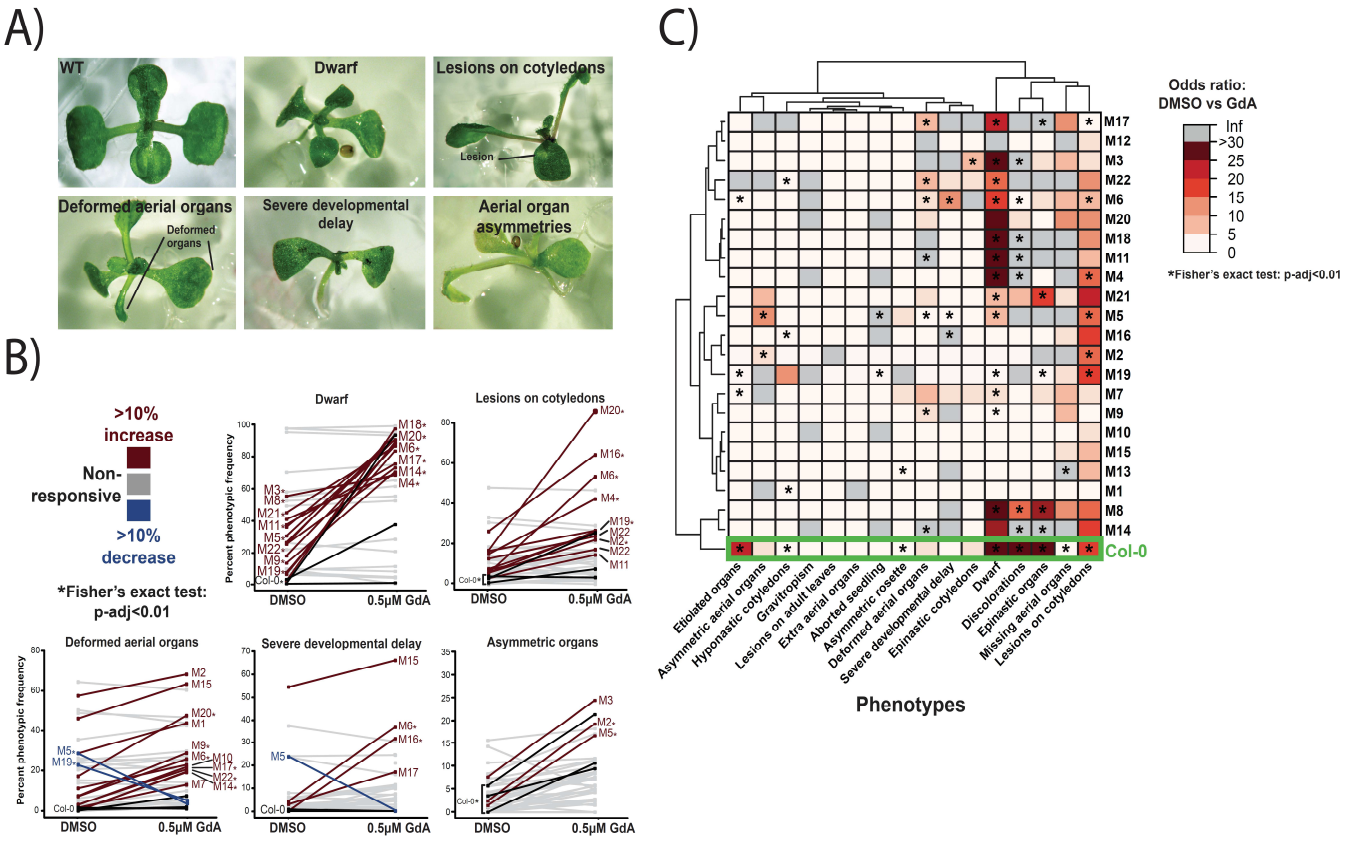

Figure 6: HSP90-responsive phenotypes in deeply mutagenized Col-0 seedlings often resemble those commonly arising in the wild-type Col-0 background but their frequency the population and severity is significantly increased. This observation is consistent with mutations affecting genes encoding clients that are already susceptible to Hsp90 perturbation in the wild-type through standing variation. Novel Hsp90-dependent phenotypes are also observed; genetic variation in the genes underlying these phenotypes has likely been purged in the wild-type Col-0 population. A) Phenotype examples of EMS mutagenized seedlings in the Col-0 background. B) Response to Hsp90 perturbation (Geldanamycin: GdA) in Col-0 and mutagenized lines (M_3 generation). Dark red color denotes 10% increase in frequency of phenotypes under Hsp90-reduced conditions. Dark blue color denotes 10% decrease in frequency of phenotypes under Hsp90-reduced conditions. Black lines represent frequency phenotypic frequency in the Col-0 background. An asterisk (*) denotes a significant p-value for Fisher's Exact test (p-adj<0.05). C) Odds ratios of seedling phenotypes in M_3 lines derived from EMS mutagenized Col-0. Seedlings were assayed for 16 early-seedling phenotypes under Geldanamycin (GdA) and mock (DMSO) treatment. Increasing red intensity reflects higher Odds Ratios, with grey color reflecting an infinite Odds Ratio for that comparison. An asterisk (*) denotes a significant p-value for Fisher's Exact test (p-adj<0.05).

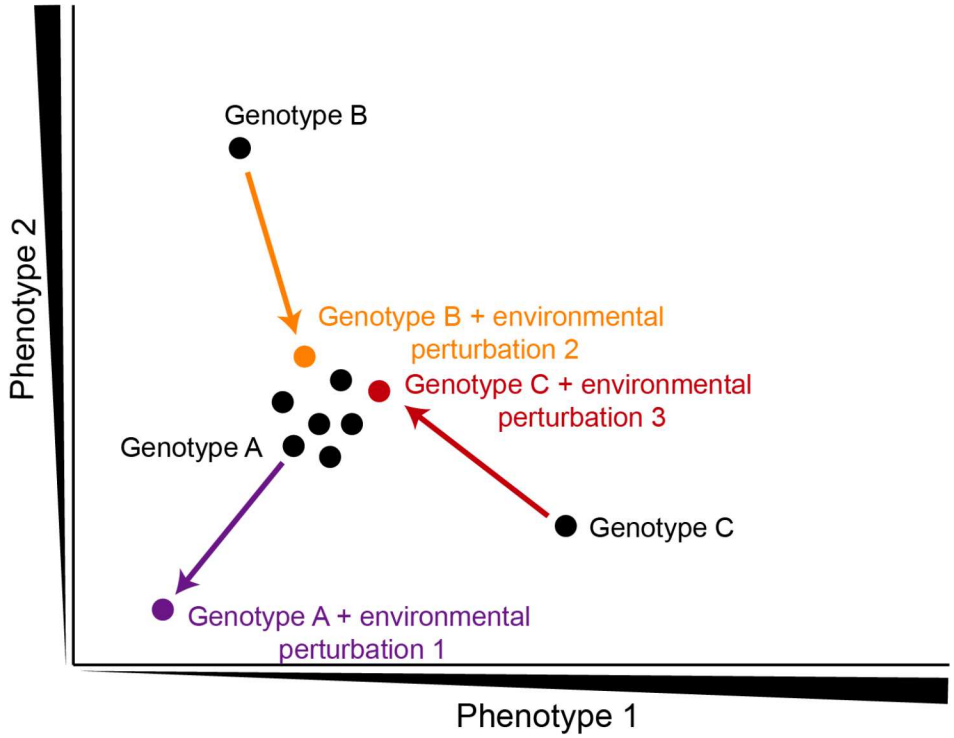

Figure 1.7: Phenotypic neighborhoods are rewired by changes in environment. In this cartoon example, two phenotypes are plotted in two-dimensional space (*x* and *y* axes). Each point represents a different genotype. The genotype is graphed twice when it presents a different phenotype in a different environmental condition (colored points). Phenotypes dependent on the three different environmental perturbations are graphed (purple, orange, and red) at the end of vectors representing the difference due to buffering or potentiation. Research illuminating examples such as these will greatly advance our understanding of how HSP90 and environmental perturbations alter phenotypic landscapes.

Chapter 2: HSP90 interacts with new genetic variation[2,3]

Abstract

Phenotypic robustness is the measure of an organism's ability to lessen the impact of adverse effects, caused by aberrant genetic and environmental factors, on an organism's appearance and function. Loss of robustness has been shown to increase the severity of certain mutations in model organisms. The best characterized regulator of robustness is the protein chaperone HSP90, which aids in proper protein folding and allows accumulation of phenotypically silent genetic variation in its select group of client proteins. In *Arabidopsis thaliana*, my lab has previously shown that by inhibiting HSP90, the penetrance (*i.e.* frequency of a mutant phenotype) and heritability of natural genetic variation increases. I therefore hypothesized that *A. thaliana* seedlings with low-levels of HSP90 would show a higher frequency of aberrant phenotypes after introduction of new mutations via chemical mutagenesis. By analyzing 16 distinct early seedling phenotypes, I observed that HSP90-reduced seedlings show a higher frequency of detrimental phenotypes after mutagenesis compared to controls. Additionally, I have screened our mutagenized populations and demonstrate that some these mutant phenotypes are heritable and HSP90-dependent. To my knowledge, this work is the first time the effects of HSP90 buffering have been measured on thousands of *de novo* mutations.

[2] This chapter will be published as a manuscript in the near future as "Massively mutated plant lines provide evidence that HSP90 buffers penetrance of newly induced mutations," *G.A. Mason, K. Bubb, K.D. Carlson, M.O. Press. and **C. Queitsch. *First author, **corresponding author.

[3] G.A.M., K.D.C., and C.Q. conceived the project. G.A.M. and K.D.C. executed early mutagenesis experiments. G.A.M. performed all phenotypic screening and validation. G.A.M. and K.B. performed data analysis and created figures.

2.1 Introduction

The protein chaperone HSP90 stabilizes, or buffers, organismal phenotypes in the face of genetic and environmental variation (**see Chapter 1**). HSP90 is essential in multicellular organisms, highly connected in genetic networks, and plays a crucial role in integrating environmental signals[50,51,86,148-154]. These phenomena are an outcome of HSP90's essential role in protein folding[54,155]. Interaction with HSP90 allows its protein substrates (*i.e.* clients) to accumulate mutations that would otherwise impact function and phenotype[94,95]. For example, human kinases that are strong HSP90 interactors[149] also tend to be under relaxed selection rather than weak- or non-interactors, implying HSP90's role in buffering new genetic variation[95].

Loss of HSP90 increases the severity of a few mutations and many natural variants in model organisms and humans[28,44,86,147,156-158](**see Chapter 3**). In worms, naturally varying HSP90 levels predict the expressivity of a transcription factor mutation[157]. In yeast, loss of HSP90 in certain deep mutational scanning mutants results in decreased mating behavior but increased invasiveness[159]. In humans, HSP90 buffers the effects of mutations in a Fanconi anemia-associated protein[160], resulting in reduced disease impact under normal conditions[44]. In plants, HSP90 perturbation increases the frequency of lesion affected individuals in an already sensitized background (**see Chapter 3**). These data imply that HSP90's buffering capacity has obvious relevance for both new disease-causing mutations in humans, such as cancer, and non-model organism studies on evolution and adaptation (**see Chapter 1**). However, the spectrum of genetic variation that is buffered by HSP90 remains largely unknown.

Despite HSP90's evident importance for protein stability and phenotypic buffering, I contend that while HSP90-dependent traits are common[147,156], HSP90-dependent genetic variants are likely rare in the context of the genome – for example, only 7% of 850 tested human

transcription factors and 61% of 314 kinases are HSP90 interactors[149]. Furthermore, not every mutation affecting a client protein will alter its HSP90 dependence (**see Chapter 1.6.1**); a random mutation within a genome is also unlikely to render a previously non-client protein as an HSP90 client[159].

To determine the frequency of new HSP90-buffered genetic variation, I introduced thousands of random mutations into Col-0, the *Arabidopsis thaliana* reference wild-type, and RNAi lines with reduced HSP90 levels[152] (**Figure 2.1A**). After mutagenesis, I scored plant phenotypes in the M_1 generation (somatic, heterozygous mutations), and self-fertilized adult M_1 plants to score phenotypes in the resulting M_2 generation (both heterozygous and homozygous mutations) (**Figure 2.1A**). If HSP90 has the capacity to buffer at least some induced mutations, I should observe greater severity and/or frequency of mutant phenotypes in HSP90-reduced plants.

In my analysis of ~16 distinct early seedling phenotypes (**Figure 2.1B**), I demonstrate that HSP90-reduced seedlings show a significant increase in the frequency of affected seedlings and the severity of mutant phenotypes in the M_1 and M_2 generations. I show in the M_2 generation that HSP90-RNAi seeds have a higher penetrance of embryonic lethality compared to controls. In the M_3 generation, I observed that HSP90-responsive phenotypes in mutagenized seedlings often resemble those commonly arising in the wild-type Col-0 background; however, their frequency in the population was significantly increased. I also detected novel HSP90-dependent phenotypes in the M_3 generation (*i.e.* rare in Col-0); genetic variation in the genes underlying these phenotypes has likely been purged in the wild-type Col-0 population. Broadly, my results support the idea that HSP90 can interact with new genetic variation.

2.2 Results

2.2.1 HSP90-perturbation *increases penetrance of embryonic lethal mutations*

To introduce many new single nucleotide mutations into the *A. thaliana* genome, I performed chemical mutagenesis on wild-type (Col-0) and two HSP90-RNAi lines with the chemical mutagen ethyl methanesulfonate (EMS) (Detlef Weigel, personal communication). In my pilot experiment I used two concentrations of EMS on Col-0 seeds, 0.2% (v/v) and 0.4% (v/v). After I applied EMS, I transferred seeds (M_1 generation) to soil and allowed them to grow into adults. One silique was collected from 50 individuals within a genotype and treatment. I then counted the number of live and dead seeds for each silique to estimate mutagenesis efficiency.

In my pilot experiment, I found that the number of live seeds per silique greatly decreased in EMS treated groups, with 0.4% EMS treatment resulting in the largest decrease in live seeds (Student's unpaired t-test: $p<0.05$) (**Figure 2.2B**). A similar susceptibility to EMS was detected when I performed mutagenesis on HSP90-RNAi lines and a second wild-type control (Student's unpaired t-test: $p<0.05$) (**Figure 2.2B**).

To estimate mutagenesis efficiency, I calculated the average number of embryonic lethal mutations per diploid genome for each mutagenized genotype and, in the case of Col-0, each concentration of EMS. Dead seeds are representative of individuals with lethal mutations and can therefore be reliably used to estimate mutation burden after mutagenesis[161].

For a Poisson value of 0, let X equal the number of siliques without dead seeds, let Y equal the total number siliques observed, and let μ equal the average number of embryonic lethal mutations per diploid genome. To calculate μ, I used the following equation:

$$\mu = \ln Y - \ln X$$

If μ is greater than one, or <36% of observed siliques do not have dead seeds, mutagenesis is successfully saturated[161].

I observed in the pilot experiment that EMS increases μ in a dose dependent manner (Generalized linear model, family=Poisson: p<1.0E-06) (**Figure 2.2C**). In my second mutagenesis experiment, I saw that EMS-treated HSP90 RNAi-C1, but not EMS-treated HSP90 RNAi-A1, appeared to have nearly twice the amount of embryonic lethal mutations as compared to EMS-treated Col-0 (Generalized linear model, family=Poisson: p<1.0E-06) (**Figure 2.2C**). One explanation for this result is that HSP90 RNAi-C1 plants could have been more susceptible to EMS and thereby carried more mutations than EMS-treated wild-type. It is well established that reduced HSP90 levels in a variety of model organisms can increase frequency of genome instability events (**see Chapter 1.6.1**). Furthermore, HSP90-reduced seeds that are exposed to ionizing radiation tend to have a high frequency of abnormal defects[131]. To exclude this possibility, I performed whole-genome sequencing of six M_2 HSP90 RNAi-C1 and six M_2 Col-0 plants to estimate mutation frequencies in each background.

After whole genome sequencing and private SNV calling, I observed that both backgrounds had highly similar counts of unique mutations within each individual (**Figures 2.2D and 2.2E**) (**see Supplemental figure 1 for analysis pipeline**). M_2 individuals had on average ~1000 new, high confidence mutations; my estimated mutation frequencies are also in concordance with similar studies[162] (**Supplemental table 2.1**). I therefore concluded that the more frequent and severe embryonic lethal phenotypes observed in the mutagenized HSP90 RNAi-C1 background are due to the increased effect of induced mutations.

2.2.2 HSP90 perturbation increases penetrance of mutant-like phenotypes in the M_1 and M_2 generations

Having established that newly introduced mutations are more likely to cause lethality in HSP90-reduced plants than in controls, I next examined the effects of HSP90 reduction on the frequency of aberrant morphological phenotypes. As such plant phenotypes are qualitative in nature, I used a mutant scoring index to estimate the frequency of 16 complex early seedling traits, categorized by severity (**Figure 2.1B and C**).

I first examined the frequency of these aberrant phenotypes in the M_1 plants, in which the EMS-induced mutations are heterozygous and can occur only somatically, generating chimeras (as opposed to be present in cells throughout a plant). It has been previously observed that heterozygous mutations can show increased penetrance and cause dominant mutant phenotypes when HSP90 is inhibited [163]. Indeed, M_1 HSP90 RNAi-C1 seedlings, but not M_1 HSP90 RNAi-A1 seedlings, displayed a modest yet significant increase in the frequency of individuals with mutant index scores ≥ 2 (Fisher's exact test: p-value<0.05, OR=1.5) (**Supplemental figure 2.2B**).

Next, I used the highly specific HSP90 inhibitor geldanamycin (GdA) to examine whether I would observe a similar trend in the EMS-mutagenized Col-0 M_1 plants when HSP90 was inhibited pharmaceutically (as opposed to genetically in the RNAi lines). Indeed, GdA treatment significantly increased phenotype frequency and severity in this population (**Supplemental Figure 2.2C**). I conclude that HSP90 perturbation appears to increase expressivity of heterozygous or even somatic mutations with regard to seedling morphology phenotypes.

Second, I tested the response to HSP90 perturbation, both pharmaceutically and genetically, in the M_2 generation using the same mutant phenotype index. In the M_2 generation, the newly introduced mutations are segregating, some will be homozygous and others heterozygous. HSP90 perturbation should increase the expressivity and penetrance of these mutations and thereby cause a higher frequency of severely aberrant morphological phenotypes. Consistent with this expectation, I observed significantly greater frequency of severe phenotypes among the EMS-mutagenized seedlings grown with different concentrations of the HSP90 inhibitor as compared to un-mutagenized seedlings and seedlings grown with the inhibitor's solvent DMSO (**Figure 2.3B**).The most significant effect on phenotype frequency was observed at an intermediate GdA dose (Fisher's exact test: p-adj<1.0E-15, OR=4.6). Most likely, the lower GdA dose inhibited HSP90 less strongly while the higher, more toxic GdA dose somewhat diminished differences between mutagenized and un-mutagenized populations. Genetic HSP90 perturbation yielded similar results: the M_2 HSP90 RNAi-C1 seedlings produced significantly more aberrant phenotypes than comparable M_2 Col-0 seedlings (Fisher's exact test: p-adj<1.0E-07, OR=2.2) (**Figure 2.3C**). I conclude that HSP90 perturbation increase the frequency and severity of aberrant phenotypes after mutagenesis.

2.2.3 Tracking heritability of new HSP90-responsive phenotypes

The assays in the M_2 generation reveal that HSP90 reduction does affect the penetrance of *de novo* mutations, but had certain limitations. Specifically, I could not (1) directly compare phenotypic outcomes for plants with identical *de novo* mutations grown in GdA or mock conditions, or (2) test heritability of the HSP90-responsive phenotype, thus testing for the presence of a genetic mutation.

Because it is impossible to test a single plant in two different growth conditions, I generated multiple M_3 lines from M_2 parents that displayed aberrant phenotypes under HSP90-inhibited or control conditions (**see Materials and methods**). This protocol allowed me to test groups of plants with similar mutations (siblings) under both control and test conditions. I generated the M_3-lines specifically using M_2s with the deformed aerial organs phenotype, because these were easy to identify and some forms of them are known to be HSP90-responsive[164]. When examining M_3 seedlings, however, I looked for 16 different phenotypes (like dwarfism, *etc.*). I distinguish between M_3-lines grown from M_2 parents with aberrant phenotypes that were present on either the mock treatment or GdA treatment as DM and GM, respectively (**see Supplemental table 2.3 for summary of M_2-parent phenotypes**).

There are several possible scenarios for HSP90's putative interactions with new genetic loci in the DM and GM lines. I considered a trait to be penetrant if it occurs at greater than 15% frequency in either or both HSP90-reduced and mock treatments. For a given seedling trait in an M_3-line, genetic variation (either *de novo* or pre-existing) is responsive to HSP90 perturbation if one of the following scenarios is met.

Let X= (%) Phenotypic Frequency Affected Seedlings:

1) If $X_{\mathrm{GdA,\ M3}} - X_{\mathrm{DMSO,\ M3}} \geq 10\%$, the trait is positively responsive to HSP90 perturbation.

2) If $X_{\mathrm{DMSO,\ M3}} - X_{\mathrm{GdA,\ M3}} \leq 10\%$, the trait is negatively responsive to HSP90 perturbation.

Genetic variation is un-responsive to HSP90 perturbation if the following scenario is met:

3) If $X_{\mathrm{GdA,\ M3}} - X_{\mathrm{DMSO,\ M3}} \approx 0$, the trait is un-responsive to HSP90 perturbation.

If I observe response to HSP90 inhibition in an M_3-line, it may be due to variation in the Col-0 background responding to HSP90 perturbation. Therefore:

4) If $X_{GdA,\ M3} - X_{DMSO,\ M3} \approx X_{GdA,\ Col\text{-}0} - X_{DMSO,\ Col\text{-}0}$, Col-0 genetic variation is epistatic to *de novo* variation.

The two major findings were as follows. First, as expected, M_3-lines had higher rates of aberrant phenotypes in both HSP90-reduced and mock conditions, most likely because a higher fraction of variants are homozygous. Second, while most of the M_3-line phenotypes were not responsive to HSP90 inhibition, of the ones that were responsive, they were much more likely to result in increased penetrance after HSP90 perturbation. I show in **Figure 2.4B** five representative early seedling traits: dwarf, severe developmental delay, deformed aerial organs, lesions on cotyledons, and aborted seedlings (**see Supplemental figures 2.3 and 2.4 for data summaries and additional phenotypic frequencies**).

Dwarf and severe developmental delay phenotypes are complex and known to be HSP90 responsive in a background dependent manner[165]. For the trait of dwarfed seedlings, I observed that Col-0 is highly responsive to GdA treatment. This result is not surprising because HSP90 chaperones several growth-related proteins, such as genes in the auxin and brassinosteroid signaling pathways[77,94,166-168] (**see Chapter 5**). For many of the M_3 lines, I observed that they are also highly responsive to HSP90 reduction, implying that variants within the Col-0 background are epistatic to EMS-generated variants (**Figure 2.4B**). I observed for the dwarf phenotype one significant instance of negative interaction with HSP90 (Fisher's exact test: p-adj<0.01, OR=0.3). For severe developmental delay, I observed that while this trait was somewhat frequent among the M_3-lines, few were significantly responsive to HSP90-inhibition. Specifically, I observed two GM lines and one DM line that possessed a significant positive interaction with HSP90; I saw no significant negative interactions for this trait (Fisher's exact test: p-adj<1.0E-03, OR>13.07) (**Figure 2.4B**).

Like the previously described size-related traits, deformed aerial organ traits are HSP90-responsive in a background-dependent fashion[152,165]. Furthermore, many of our M_3-lines had parents that were selected for deformed aerial organ phenotypes, and as expected, many of these selected traits were heritable (21/32 lines). I detected in our data six GM lines and one DM line with a significant and positive interaction to HSP90 perturbation (Fisher's exact test: p-adj<0.05, OR>4.3). Five out of seven of these significantly responsive lines possessed low penetrance of deformed organs in DMSO conditions; such a phenomenon supports previous observations that HSP90-dependent phenotypes exist at low frequencies in un-perturbed conditions[157,158,169]. Adhering to the predicted scenarios, I also detected two GM lines with significant negative responses to HSP90 perturbation (Fisher's exact test: p-adj<0.05, OR<0.03).

The trait of lesions on cotyledons is responsive to HSP90 perturbation in the Col-0 background[152] (**see Chapter 3**). Lesions are often representative of the hypersensitive response, a plant defense strategy to ward off pathogen attack through localized cell death[170]. Several immune-related signaling receptors and R-proteins are HSP90 clients, making a plausible mechanistic link between HSP90-inhibition and aberrant plant immune responses[77,153,171-173]. Like frequency of dwarfed seedlings, I saw in Col-0 and many M_3-lines that frequency of this trait significantly increases when HSP90 function is reduced (**Figure 2.4B**). Five GM lines and one DM line were significantly responsive to HSP90 perturbation in the positive direction (Fisher's exact test: p-adj<0.05, OR>5.0). No negative interactions were observed. One explanation for these data is that lesion-associated variants in the Col-0 background are epistatic to EMS-derived variants. However, I do observe for five M_3 lines that the lesion phenotype is significantly more penetrant than in Col-0, suggesting that genes contributing to this this trait are

frequent and possibly sensitized to perturbation from new mutations, even more so if HSP90 cannot buffer them (Fisher's exact test: p-adj<0.05, OR>2.0) (**Figure 2.4B**).

I predicted that genes associated with seedling lethality, like embryonic lethality, may be sensitized to HSP90 perturbation. Indeed, I detected a modest increase in frequency of this phenotype under low HSP90 conditions for some M_3-lines. Specifically, I observed one GM line with a significant positive interaction and one DM line with a significant negative interaction with HSP90 perturbation (Fisher's exact test: p-adj<0.05, OR>2.0) (**Figure 2.4B**). In contrast to our initial prediction, I did not observe widespread increased penetrance of this phenotype, suggesting that already by the M_3 generation lethal genetic variants have been mostly selected against.

To detect larger patterns in the M_3 data, I clustered the ORs of Col-0 and each tested M_3 line for DMSO *vs*. GdA comparisons (**Figure 2.4C**). I found substantial and significant increase in the incidence of at least one aberrant phenotype in almost every M_3-line tested (**Figure 2.4C**). Furthermore, I detected one distinct cluster in our data reflecting ~½ of the M_3-lines that behave similarly to Col-0 when HSP90 is perturbed (**Figure 2.4C**). The traits of discolorations and epinastic organs also cluster closely together and maybe reflective of a general response to HSP90 inhibition or the growth conditions required for GdA experiments. I also observed that deformed aerial organ, epinastic cotyledon, and severe developmental delay traits cluster closely together, suggesting that these phenotypes are highly correlated in our data. When looking at clustered ORs calculated from comparing GdA-treated Col-0 to each GdA-treated M_3 line, I observed evidence of increased effect size for deformed organ phenotypes in over ½ of M_3 lines, thus adding support that selected phenotypes were heritable (**Supplemental figure 2.5**).

To further confirm the genetic nature of some of these HSP90-responsive traits, I selected three lines that displayed increased penetrance of deformed organ phenotypes under HSP90-reduced conditions (OR>4.5) and backcrossed them to Col-0 to further characterize their inheritance patterns in the F_2 generation. I chose lines GM6, GM9, and GM17 for further analysis because they possessed significantly high ORs compared to GdA-treated Col-0 and their DMSO-treated M_3 counterparts (Fisher's exact test: p-adj<0.05, OR>4.5). I observed for all three F_2 populations that selected deformed organ phenotypes were partially penetrant in mock conditions and significantly increased in penetrance under HSP90-reduced conditions (Fisher's exact test: p-adj<0.05, OR>2.0) (**Supplemental figure 2.6**).

2.3 Discussion

I present data supporting that HSP90 interacts with new genetic variation. In the M_1 and M_2 generations, I observed that HSP90 perturbation by either genetic or pharmacological insult significantly increases the penetrance of EMS-generated mutations. In the M_2 generation, I also found that populations enriched for deleterious variants had more aberrant phenotypes regardless of HSP90 status. In the M_3 generation, I tracked heritability of putative HSP90-dependent phenotypes and observed that 13/32 M_3-lines possessed heritable phenotypes that were HSP90-responsive. I validated our results in the M_3 generation by backcrossing selected individuals to wild-type and assaying inheritance patterns in F_2 populations. In the F_2 generation, I saw that HSP90-responsive phenotypes were heritable, and some were at least partially penetrant under mock conditions. Just as with pre-existing genetic variation[32,147,156,174,175], HSP90 appears to play a role in buffering phenotype against some *de novo* genetic variation.

Currently, I am performing mapping-by-sequencing for the generated F_2 populations to further validate our findings. For these experiments, recombinant F_2 seedlings with abnormal phenotypes are pooled and deeply sequenced. Specifically, I will sequence two pools of mutants: 100 DMSO-grown affected F_2s and 100 GdA-grown affected F_2s. After sequencing, I should observe a strong association between certain EMS-induced mutations and their presence in the mutant-phenotype pools. Once identified, I will validate these variants with standard genetic analyses.

One limitation of our studies is that almost all the phenotypes I assayed, with exceptions of lesion and lethality traits, are not only partially penetrant, they are continuous traits that were reduced to binary categories. My approach was amenable to quickly phenotyping many individuals. However, I may have reduced our discovery power and only been able to detect only variants with high expressivity. To address this limitation, future work could focus on examining M_2 and M_3 populations for complex quantitative phenotypes, such flowering traits, dark-grown embryonic stem length (**see Figure 6.1**), response to pathogens, response to heat stress, *etc*[152,156,176-178]. Future experiments may also benefit from automated phenotyping methods that take advantage of image analysis software[179]. Such proposed experiments will be discussed in **Chapter 6.2**.

I set out gain a better understanding of how rare or common *de novo* HSP90-responsive genetic variation is. While it is still hard to predict what portion of the genome is responsive to HSP90-perturbation on the single variant level, I do provide some evidence that while HSP90-responsive loci may be common, *de novo* HSP90-sensitized loci within the *A. thaliana* genome are likely rare. Specifically, I can use the data to provide rough estimates of how likely a random mutation would interact with HSP90. In this calculation, I will use data estimates from our

private SNV calling and the deformed organ phenotype analyses. Because deformed organ traits were uncommon in the wild-type background, they are likely caused by EMS-variants.

Let us assume that each of the 32 examined M_3-lines had 500 – 2,000 unique SNVs, creating a pool of 16,000 – 64,000 *de novo* SNVs. In the data, I detected nine M_3-lines that were significantly responsive to HSP90 perturbation for deformed organ phenotypes. Assuming a false discovery rate of 5%, at least one line was mis-phenotyped, thus giving me eight responsive lines. Let us assume the simplest scenario that in each responsive line, a single SNV is the causative allele, numbering a total of eight SNVs. If I divide the number of causative alleles by the pool of EMS-variants, there is a 5.0E-04 – 1.24E-04 probability that a single variant will be HSP90-responsive for severely deformed aerial organ traits. These numbers become smaller when taking in to account the starting pool of EMS-mutants that our lines were selected from (~800 individuals), or when considering a rarer trait such as defective gravitropism. Based on this estimate, *de novo* HSP90-responsive variants are not common.

Previous studies from yeast mutation accumulation (MA) lines have implicated that *de novo* HSP90-responsive variation is common and that HSP90 can only potentiate new genetic variation[180]. It is worth noting that the examained 94 MA lines on average each accumulated ~4 single-nucleotide mutations per haploid genome, equaling ~380 new SNVs[181]. Experimentally, the results supporting these conclusions were reported as high variance across MA lines for a given trait in mock conditions, and modestly decreased variance of that trait under HSP90-reduced conditions[180].

In my data, I did not observe widespread potentiation as described by Geiler-Samerotte *et al.* Instead I found that while *de novo* HSP90-responsive variants can be found, they are not common. I also detected many instances of genetic variation in the Col-0 background behaving

epistatically to new genetic variation. It is therefore likely that because Geiler-Samerotte *et al.* started with a small pool of variants they did not observe widespread interactions with HSP90, but rather background-specific epistasis for response to HSP90 inhibition.

It should of course be stated that my estimates are just merely estimates. For instance, these calculations do not consider the percentage of the genome that is functional and would be sensitized to *de novo* genetic variation. I also do not know the number of *A. thaliana* genes that are HSP90 clients or are regulated by HSP90 clients; I therefore cannot include these parameters in my calculations. Additionally, as discussed early, the assays are designed to be able to detect the most severe phenotypes, and I therefore may have missed HSP90-responsive variants with low expressivity. Nevertheless, the scarcity of these variants is in line with other observations.

In yeast, for example, deep mutational scanning experiments of the non-client protein Ste12 has provided some clues as to how likely a change to a non-client would result in HSP90 dependence. Dorrity *et al.* detected only two (out of ~20,000) highly sequence specific amino acid substitutions that displayed a significant HSP90-dependence for mating behavior (see **Chapter 1.5.1** for more details)[169]. Studies from cancer also posit that *de novo* HSP90-dependent variants in oncogenes are highly sequence specific and rare[44,91,109]. Given the breadth of standing genetic variation that is responsive to HSP90 perturbation[29,41,43,44,100,101,108], mutations that newly arise likely play only a minor role in most HSP90-dependent phenotypes.

2.4 Main figures

(A)

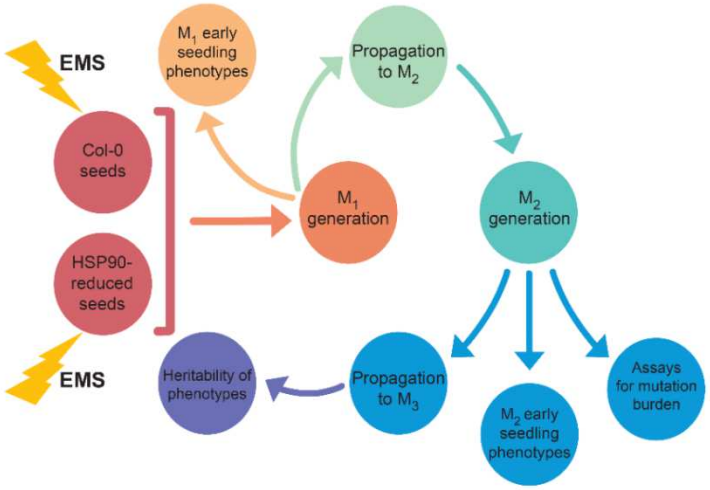

(B)

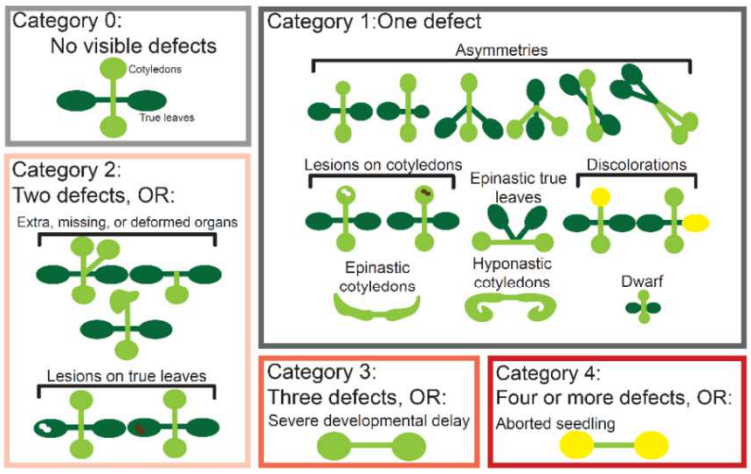

(C)

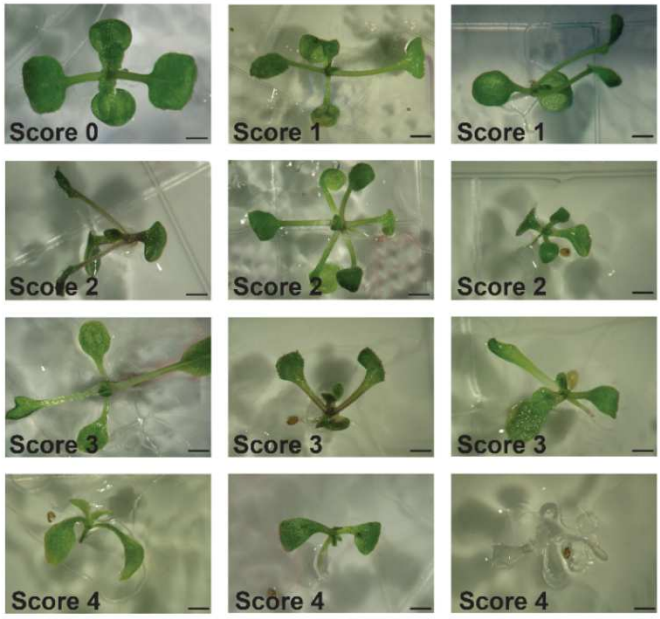

Figure 2.1: Experimental set-up of mutagenesis experiments. (A) Experimental guide for analyzing phenotypes in the M_1, M_2, and M_3 generations. **(B)** Mutant phenotype index for 10-day-old seedling traits going from wild-type-like (0) to very mutant-like (4). **(C)** Example seedlings from the M_2 generation that show a variety of mutant phenotypic scores and severity of phenotypes. Scale bars equal 1 mm.

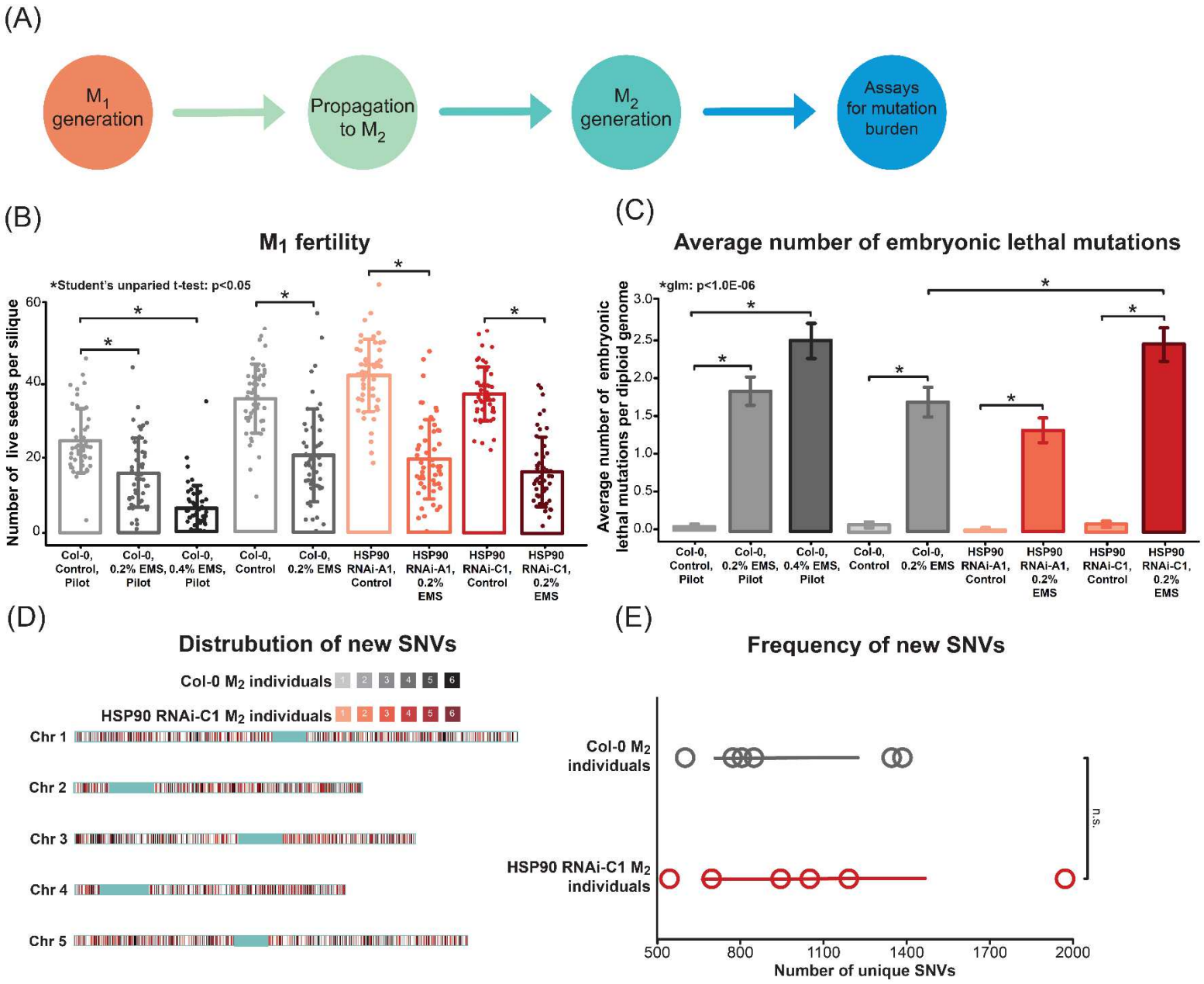
(A)
M1 generation
Propagation to M2
M2 generation
Assays for mutation burden
(B)
M1 fertility
*Student's unparied t-test: p<0.05
Number of live seeds per silique
Col-0, Control, Pilot
Col-0, 0.2% EMS, Pilot
Col-0, 0.4% EMS, Pilot
Col-0, Control
Col-0, 0.2% EMS
HSP90 RNAi-A1, Control
HSP90 RNAi-A1, 0.2% EMS
HSP90 RNAi-C1, Control
HSP90 RNAi-C1, 0.2% EMS
(C)
Average number of embryonic lethal mutations
*glm: p<1.0E-06
Average number of embryonic lethal mutations per diploid genome
(D)
Distrubution of new SNVs
Col-0 M2 individuals
HSP90 RNAi-C1 M2 individuals
Chr 1
Chr 2
Chr 3
Chr 4
Chr 5
(E)
Frequency of new SNVs
Col-0 M2 individuals
HSP90 RNAi-C1 M2 individuals
n.s.
Number of unique SNVs

Figure 2.2: HSP90-reduced seeds show a higher penetrance of embryonic lethal mutations. (A) Schematic showing experimental guide for Figure 2.2. **(B)** Live seeds per silique after EMS treatment. EMS-treated seeds were placed on soil and grown into self-fertilizing adults. One silique was collected from 50 individuals for each genotype/treatment and number of live and dead seeds per silique were counted. *p<0.05, Student's unpaired t-test. Error bars represent standard deviation. **(C)** Estimated number of embryonic lethal mutations per diploid genome after EMS mutagenesis. μ (average number of embryonic lethal mutations per diploid genome) was calculated by using the following the equation: $\mu=ln(Y)-ln(X)$, where Y equals the number of siliques collected from M_1's within a genotype/treatment and X equals the number of those siliques without dead seeds. *p<1.0E-06, Poisson regression. Error bars represent standard error as calculated from the Poisson distribution. **(D)** Distribution of detected unique SNVs after whole genome sequencing of six Col-0 M_2 and six HSP90 RNAi-C1 M_2 individuals. Read color denotes SNVs detected in HSP90 RNAi-C1 M_2 plants, and gray color denotes SNVs in Col-0 M_2 plants. **(E)** Frequency of new SNVs in Col-0 M_2 and HSP90-RNAi M_2 individuals. Error bars represent 95% confidence intervals. p=0.4979, Student's unpaired t-test.

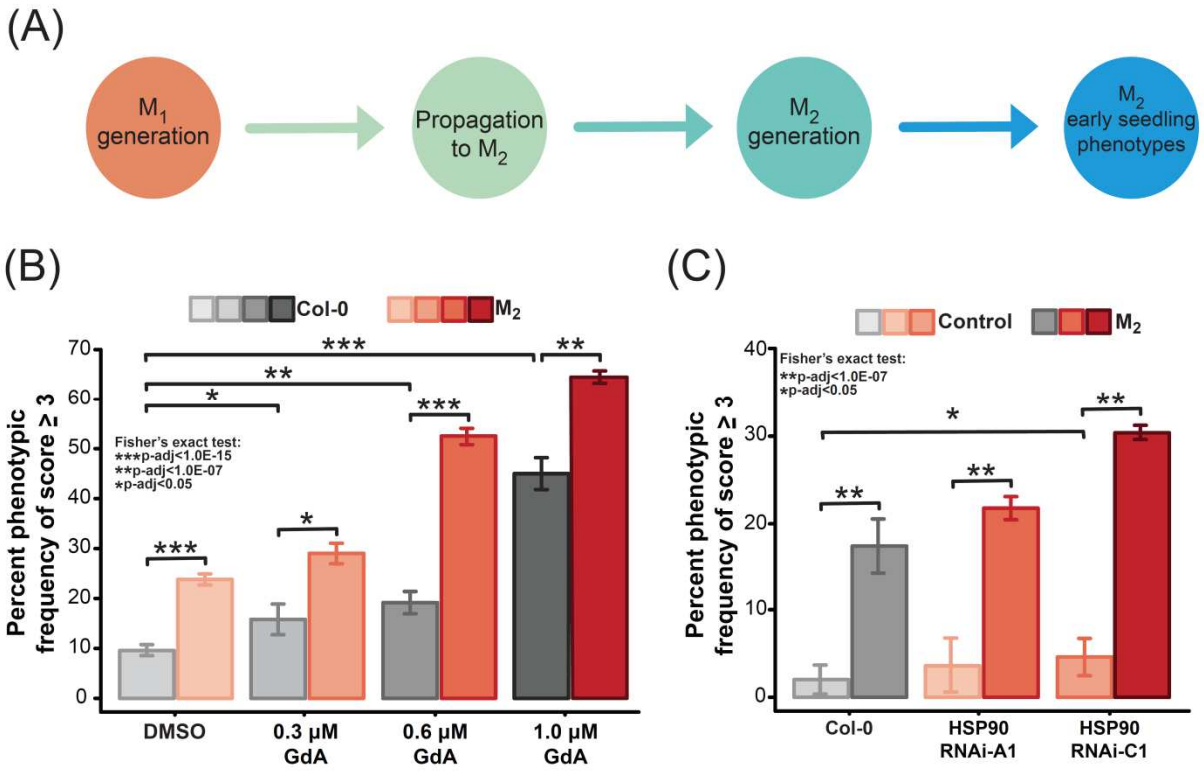

Figure 2.3: HSP90 perturbation increased penetrance of new mutations in the M_2 generation. (A) Schematic showing experimental guide for Figure 2.3. **(B)** Dose response to the HSP90 inhibitor to Geldanamycin (GdA) in Col-0 and M_2 seedlings. Y-axis measures percent phenotypic frequency of seedlings with phenotypic scores $\geq$ 3 (highly mutant-like individuals) (See **Figure 2.1** for mutant phenotype index). Col-0 groups: DMSO, n=731; 0.3 µM GdA, n=143; 0.6 µM GdA, n=319; 1.0 µM GdA, n=243. M_2 groups: DMSO, n=1394; 0.3 µM GdA, n=492; 0.6 µM GdA, n=933; 1.0 µM GdA, n=1488. *p-adj<0.05, **p-adj<1.0E-07, ***p-adj<1.0E-15, Fisher's exact test. See **Supplemental table 2.2** for all Odds Ratios and p-values. **(C)** Genetic perturbation of *HSP90* results in increased penetrance of new mutations in M_2 seedlings. Col-0 groups: control, n=347; M_2, n=817. HSP90 RNAi-A1 groups: control, n=314; M_2, n=688. HSP90 RNAi-C1 groups: control, n=362; M_2, n=632. *p-adj<0.05, **p-adj<1.0E-07, Fisher's exact test. Error bars represent standard error as calculated by: SE = sqrt(p(100-p)/n), where p equals the percentage of affected seedlings and n equals the number of observations.

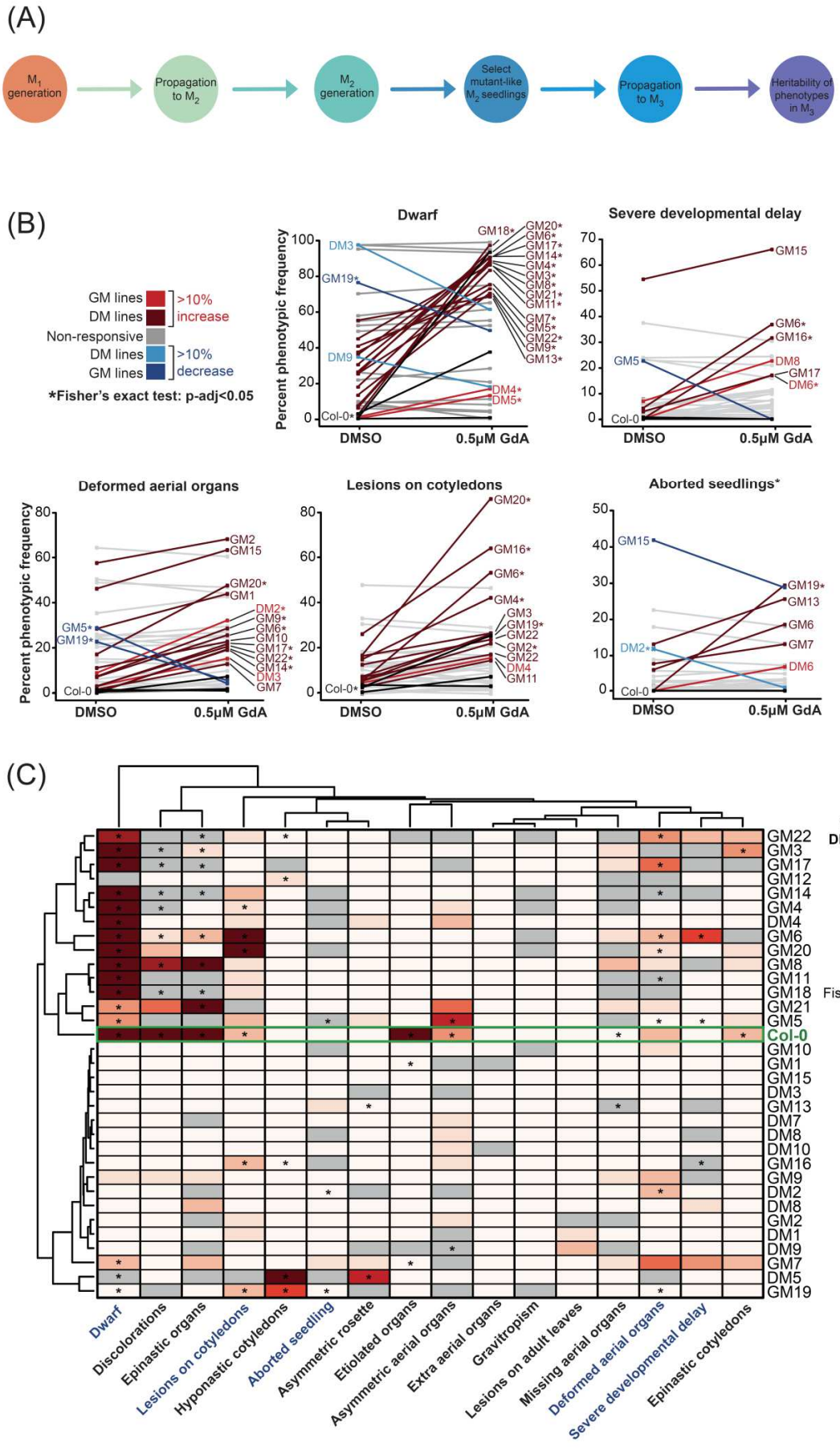
(A)
M1 generation
Propagation to M2
M2 generation
Select mutant-like M2 seedlings
Propagation to M3
Heritability of phenotypes in M3
(B)
GM lines
DM lines
>10% increase
Non-responsive
DM lines
GM lines
>10% decrease
*Fisher's exact test: p-adj<0.05
Dwarf
Severe developmental delay
Deformed aerial organs
Lesions on cotyledons
Aborted seedlings*
Percent phenotypic frequency
DMSO
0.5µM GdA
Col-0
(C)
Odds ratio: DMSO vs. GdA
Inf
>20
15
10
5
0
Fisher's exact test:
*p-adj<0.05
Col-0
Dwarf
Discolorations
Epinastic organs
Lesions on cotyledons
Hyponastic cotyledons
Aborted seedling
Asymmetric rosette
Etiolated organs
Asymmetric aerial organs
Extra aerial organs
Gravitropism
Lesions on adult leaves
Missing aerial organs
Deformed aerial organs
Severe developmental delay
Epinastic cotyledons

Figure 2.4: Assays for heritability of HSP90-responsive phenotypes. (A) Schematic showing experimental guide for Figure 2.4. **(B)** Frequencies of selected phenotypes in Col-0 and M_3-lines in response to HSP90-reduced (0.5 μM GdA) or mock conditions (DMSO). Black lines represent Col-0 response to HSP90-perturbation across three biological replicates. Red colors denote 10% (5% for frequency of aborted seedlings) increase in phenotypic frequency under HSP90-reduced conditions and blue colors denote 10% decrease in phenotypic frequency under HSP90-reduced conditions (5% for frequency of aborted seedlings). Gray color denotes non-responsive lines. Per treatment: n~144 for Col-0 groups and n~72 for M_3 groups. *p-adj<0.05, Fisher's exact test. *p-adj<0.05, Fisher's exact test. **(C)** Heatmap of clustered odds ratios for GdA *vs*. DMSO comparisons as calculated for Col-0 (green box) and the M_3-lines across 16 early seedling phenotypes. Blue labeled phenotypes correspond to phenotypes shown in Figure 4.4B. *p-adj<0.05, Fisher's exact test.

2.5 Materials and Methods

Plant Growth Conditions: Columbia-0 (Col-0) was used as wild-type reference. HSP90 RNAi-A1 and HSP90 RNAi-C1 were in the Col-0 background[152]. For experiments, seeds were sterilized with ethanol and plated onto 1× Murashige and Skoog (MS) basal salt medium supplemented with 1× MS vitamins, 1% (wt/vol) sucrose, 0.05% MES (wt/vol), and 0.24% (wt/vol) Phytagel. After stratification in the dark at 4 °C for 5 days, plates were transferred to an incubator (Conviron) that was set to long day (LD) (16L:8D at 22 °C:20 °C), with light supplied at 100 µmol·m−2·s−1 by cool-white fluorescent bulbs; for Geldanamycin experiments, plates were placed under a long-pass yellow filter that blocks 454 nm light[182]. Seedlings were then scored for mutant phenotypes at day 10. Geldanamycin was purchased from Sigma Aldrich (G3381), diluted in DMSO, and used for M_1 and M_2 experiments. Geldanamycin was purchased from LC Laboratories (G-4500), diluted in DMSO, and used in the M_3 heritability experiments.

M_3 heritability experiments: I selected 44 M_2 individuals with aberrant phenotypes, grown on either 0.5 µM GdA or DMSO (**Supplemental table 2.3 for parental phenotypes of surviving parents**). For the selected seedlings, ~50% survived the transfer and produced progeny (**Supplemental Figure 2.4A**). The resulting M_3 progeny, called either DM (DMSO-grown, M_2-parent) or GM (GdA-grown, M_2-parent) lines were then assayed for 16 early seedling phenotypes with 0.5 µM GdA and DMSO. For phenotyping of M_3-lines, each line was assigned a non-matching number and was plated and scored blindly. Seedlings were photographed with a Canon Power Shot S5 IS camera and were edited using Adobe Photoshop CC 2017.

EMS Mutagenesis: For each genotype and treatment, 50 mg of seeds were weighed out (~2500 seeds). Seeds were sterilized by a 10-minute wash in 70% ethanol (v/v) with 0.1% Triton-X (v/v), followed by a five-minute wash with 95% ethanol (v/v) and one wash with sterile water. Seeds were then transferred to a tube containing 12 ml of 0.0005% Tween (v/v). EMS (ethyl methanesulfonate, Sigma-Aldrich, M0880) was added to a final concentration of either 0.2% (v/v) or 0.4% (v/v) in each experimental tube. Control samples received only Tween treatment but no EMS. Samples were then rotated at room temperature for 15 hours. Samples were washed eight times for 10 minutes in sterile water and then plated on plant media.

Whole genome sequencing: *A. thaliana* genomic DNA was extracted from one adult leaf per individual using the CTAB method[161]. Total DNA was then quantified using the Qubit HS dsDNA assays according to the manufacturer's instructions. Sequencing libraries were generated using the Nextera (Illumina) sample kit according to the manufacturer's instruction. Libraries were then quality checked on the Agilent 2100 bioanalyzer using a DNA high-sensitivity chip (Agilent). The samples were sequenced by Genewiz on an Illumina Hi-seq in a 100-bp paired-end run to an average depth of 12x-coverage.

Data analysis for whole genome sequencing: WGS reads were aligned to the TAIR10 release genome (http://www.arabidopsis.org/) using the default parameters of BWA[183]. Aligned reads with MapQ scores less than 35 were discarded. A VCF file was then generated using SAMtools (http://samtools.sourceforge.net). Variants were further filtered for the following criteria: minimum coverage = 6, minimum base quality = 25, minor allele frequency = 0.3. I filtered each VCF file for unique mutations (*i.e.* unshared with any other sample within either Col-0 or HSP90

RNAi-C1) as these were likely caused by EMS mutagenesis. After identifying unique and private SNVs, I counted the number of total non-reference transitions and transversions for each individual. See **Supplemental Table 1** for information about variants called.

Statistical analysis: All statistical analyses were performed in R Version 3.2.5. Comparisons of seedling mutant frequencies were performed with Fisher's exact test. Embryonic lethality comparisons were modeled with Poisson regression using a general linear model. Student's t-tests performed for live seed data and mutation frequency data. When appropriate, p-values were adjusted using the R package "p.adjust," with method= "fdr."

2.6 Supplemental materials

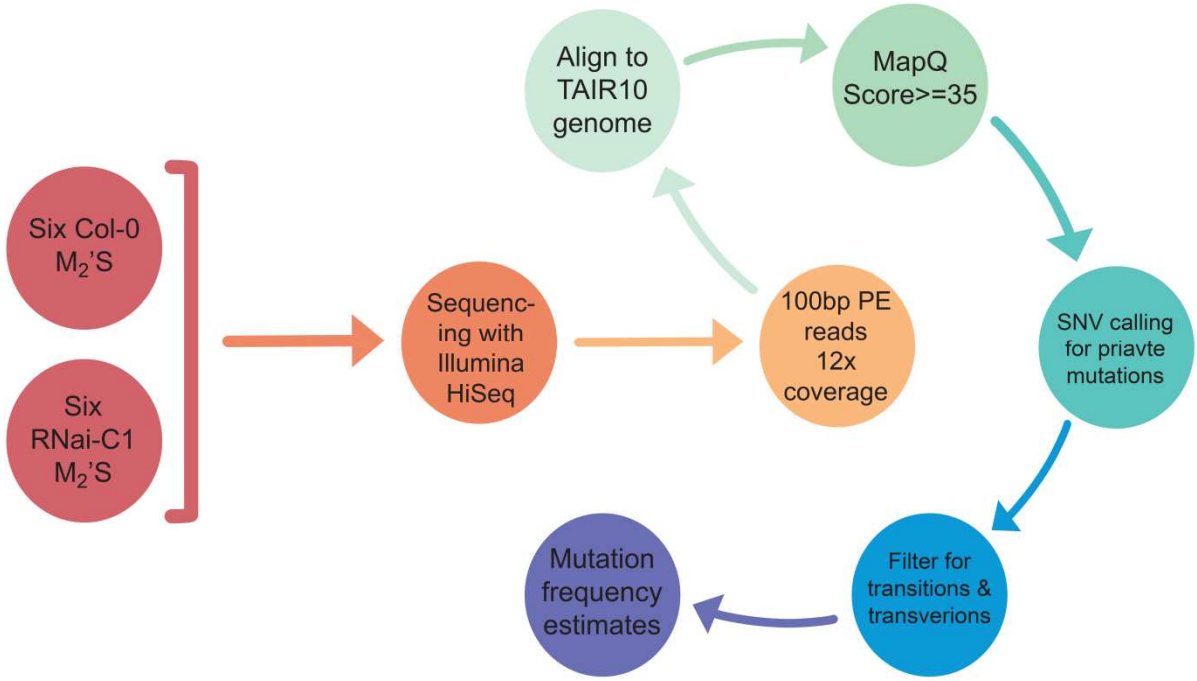

Supplemental Figure 2.1: Analysis pipeline for SNV calling in M_2 plants. One leaf was collected from six wild-type-like Col-0 M_2 and six wild type-like HSP90 RNAi-C1 M_2 adult plants. DNA was then extracted using the CTAB method[161]. DNA was quantified using the Agilent Bioanalyzer DNA 1000 chip to determine fragment sizes and concentration of DNA. Only samples with high molecular weight DNA were used (fragments $\geq$ 10 kb). To generate sequencing libraries, the Nextera (Illumina) library preparation kit was used according to the manufacturer's instructions. Libraries were then sent out for sequencing with Genewiz. Sequencing was performed with an Illumina HiSeq in a paired-end, 100 bp run. Samples were sequenced to an average depth of ~12x-coverage. Sequencing reads were aligned to the TAIR10 genome with BWA[183] and reads with MapQ scores < 35 were discarded. SNV calling was performed using SAMtools version 1.2 and BCFtools version 1.3.1. The following command was used: samtools mpileup -Ou -f TAIR10_chr_all.fas in.bam | bcftools call -Ov -mv > out.vcf. Variants were further filtered for base quality of 25, 0.3 minor allele frequency, and at least six reads of coverage. Filtered variants were then compared to each individual within a genotype to identify unique, un-shared SNVs for each individual. SNVs were then classified as either transitions or transversions.

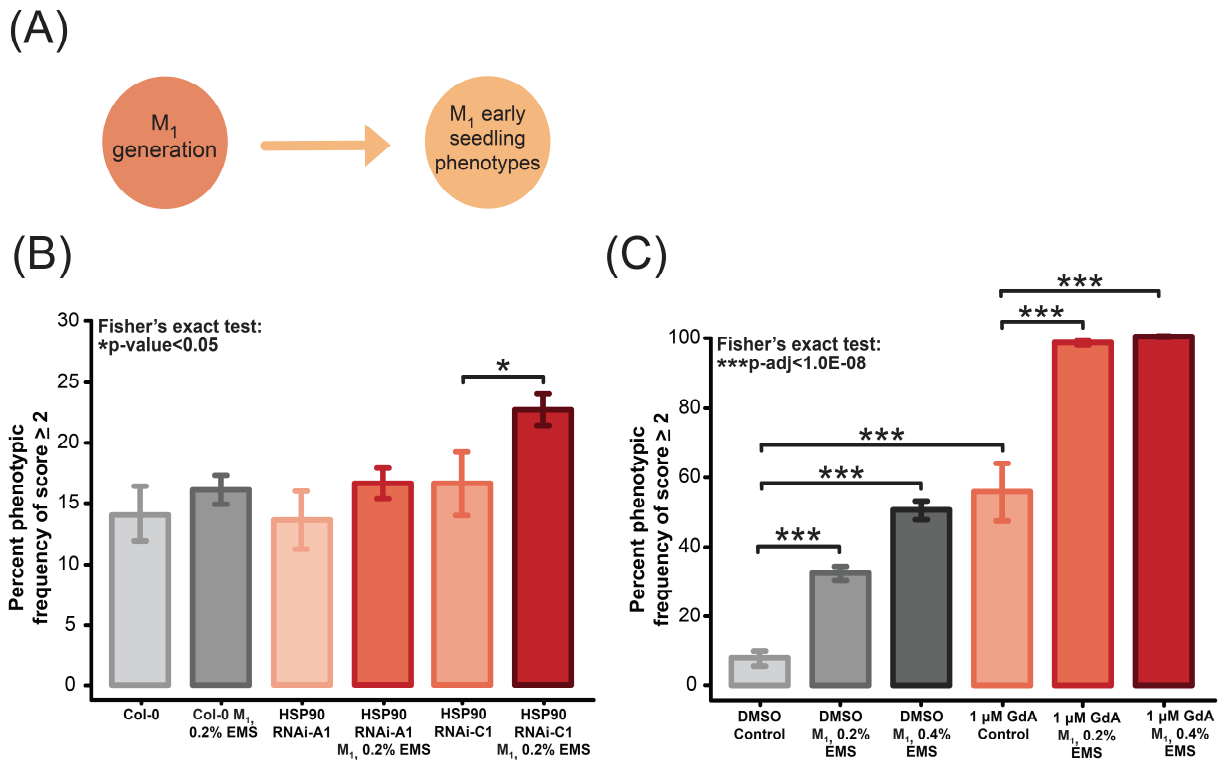

Supplemental Figure 2.2: HSP90 perturbation increases penetrance of new mutations in the M_1 generation. (A) Schematic showing experimental guide for Supplemental figure 2. **(B)** Genetic perturbation of *HSP90* results modestly increased penetrance of new mutations in M_1 seedlings. Seeds were treated with 0.2% EMS and scored for abnormal phenotypes at day 10. Col-0 groups: control, n=213; M_2, n=948. HSP90 RNAi-A1 groups: control, n=206; M_1, n=1009. HSP90 RNAi-C1 groups: control, n=206; M_1, n=961. *p-adj<0.056, Fisher's exact test. Error bars represent standard error as calculated by: SE = sqrt(p(100-p)/n), where p equals the percentage of affected seedlings and n equals the number of observations. Please see **Supplemental Table 2** for all Odds Ratios and p-values. **(C)** Pharmacological inhibition of HSP90 results in increased frequency of abnormal M_1 seedlings. Seeds were treated with two doses of EMS and plated on media containing either DMSO or 1.0 µM GdA and scored for abnormal phenotypes at day 10 (See **Figure 2** for mutant phenotype index). DMSO groups: control, n=144; 0.2% EMS, n=530; 0.4% EMS, n=355. 1.0 uM GdA groups: control, n=36; 0.2% EMS, n=540; 0.4% EMS, n=329. ***p-adj<1.0E-08, Fisher's exact test.

(A)

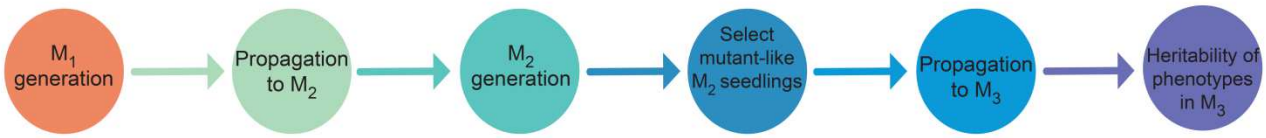

(B)

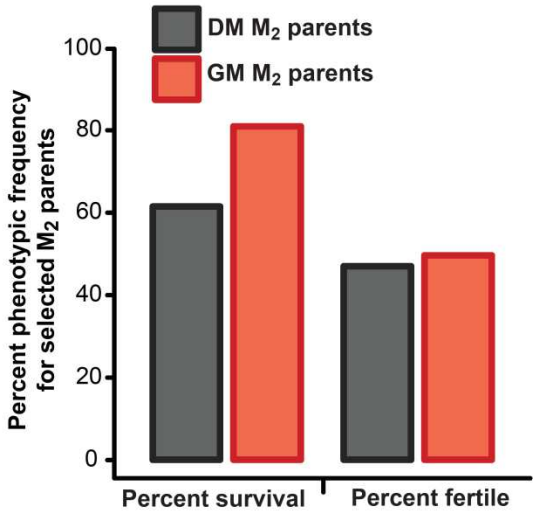

(C)

	DM lines	GM lines
Number of lines	10	22
Number of with at least one heritable phenotype	8	21
Number of lines with at least one HSP90-responsive and heritable phenotype	2	17
Number of lines with at least one significant, HSP90-responsive, and heritable phenotype	1	12
Number of parental phenotypes	13	48
Number of heritable phenotypes	9	36
Number of HSP90-responsive and heritable phenotypes	2	21
Number of significant, HSP90-responsive, and heritable phenotypes	1	15

Supplemental Figure 2.3: Summary M_3-line data. (A) Schematic showing experimental guide for Supplemental figure 2.3. **(B)** 21 DMSO-grown and 44 Geldanamycin (GdA)-grown M_2 seedlings were selected for deformed aerial organ traits. Of those selected lines, ~50% survived transfer and were fertile. **(C)** Summary of heritability of phenotypes in the 32 M_3-lines.

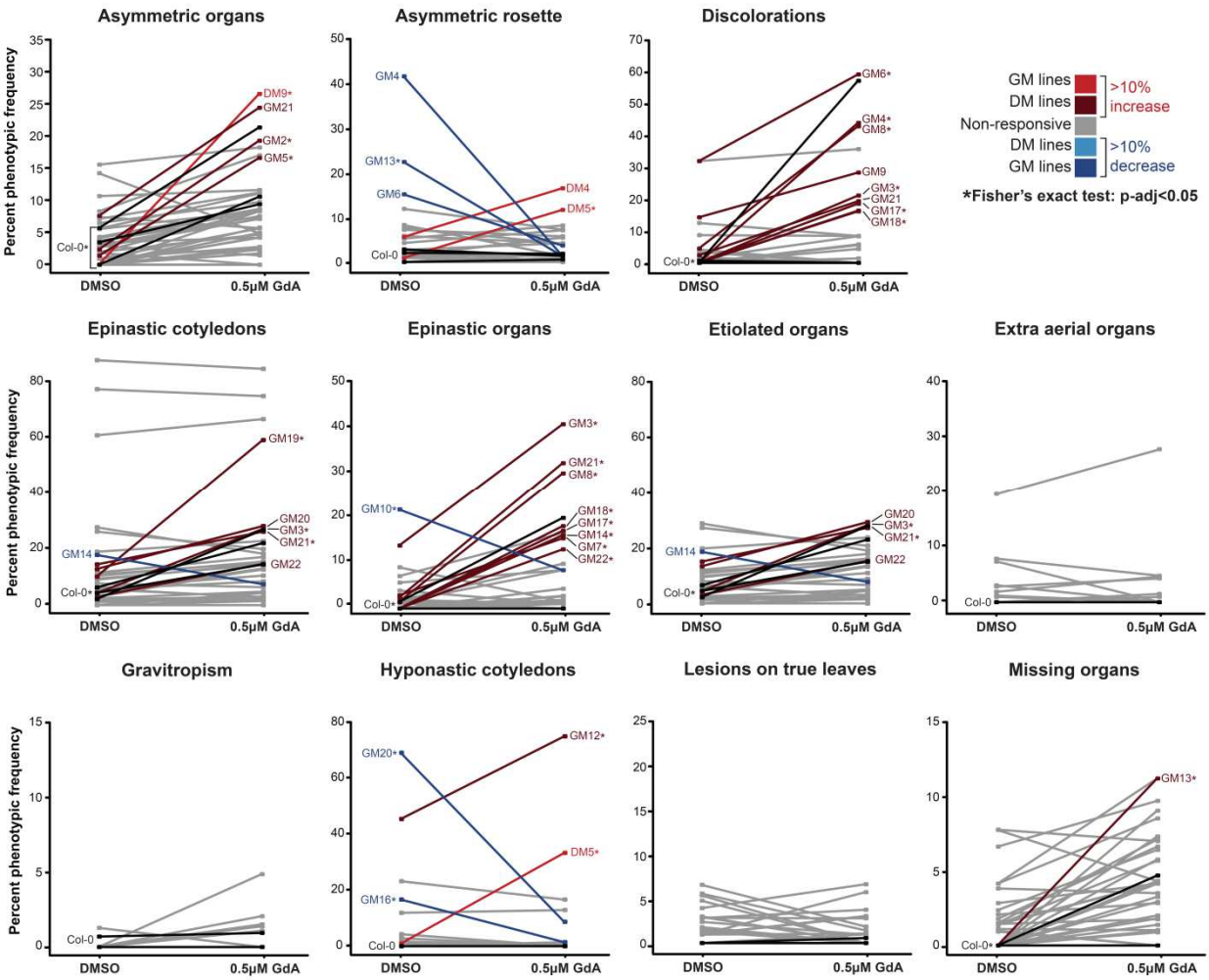

Supplemental Figure 2.4: Assays for heritability of HSP90-responsive phenotypes not shown in Figure 2.4. Frequencies of selected phenotypes in Col-0 and M_3-lines in response to HSP90-perturbation (0.5 uM GdA) or mock conditions (DMSO). Black lines represent Col-0 response to HSP90-perturbation. Red color denotes 10% increase in phenotypic frequency under HSP90-reduced conditions and blue color denotes 10% decrease in phenotypic frequency under HSP90-reduced conditions. Gray color denotes non-responsive lines. Per treatment: n~144 for Col-0 groups and n~72 for M_3 groups. *p-adj<0.05, Fisher's exact test.

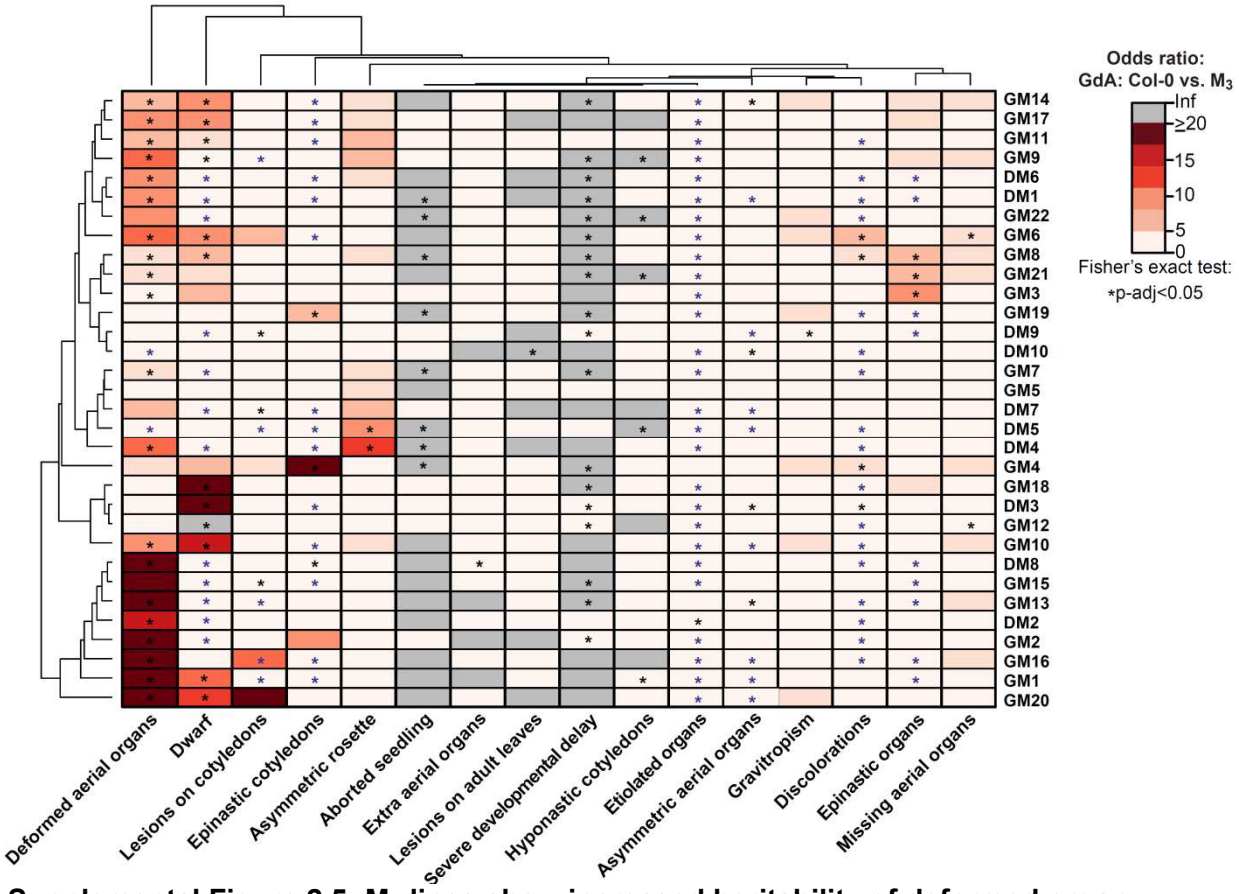

Supplemental Figure 2.5: M_3-lines show increased heritability of deformed organ phenotypes. Heatmap of clustered odds ratios for 0.5 µM GdA-treated Col-0 vs. 0.5 µM GdA-treated M_3-lines comparisons as calculated across 16 early seedling phenotypes. Black asterisk (*), p-adj<0.05, Fisher's exact test, significance towards the M_3-line. Blue asterisk (*), p-adj<0.05, Fisher's exact test, significance towards Col-0.

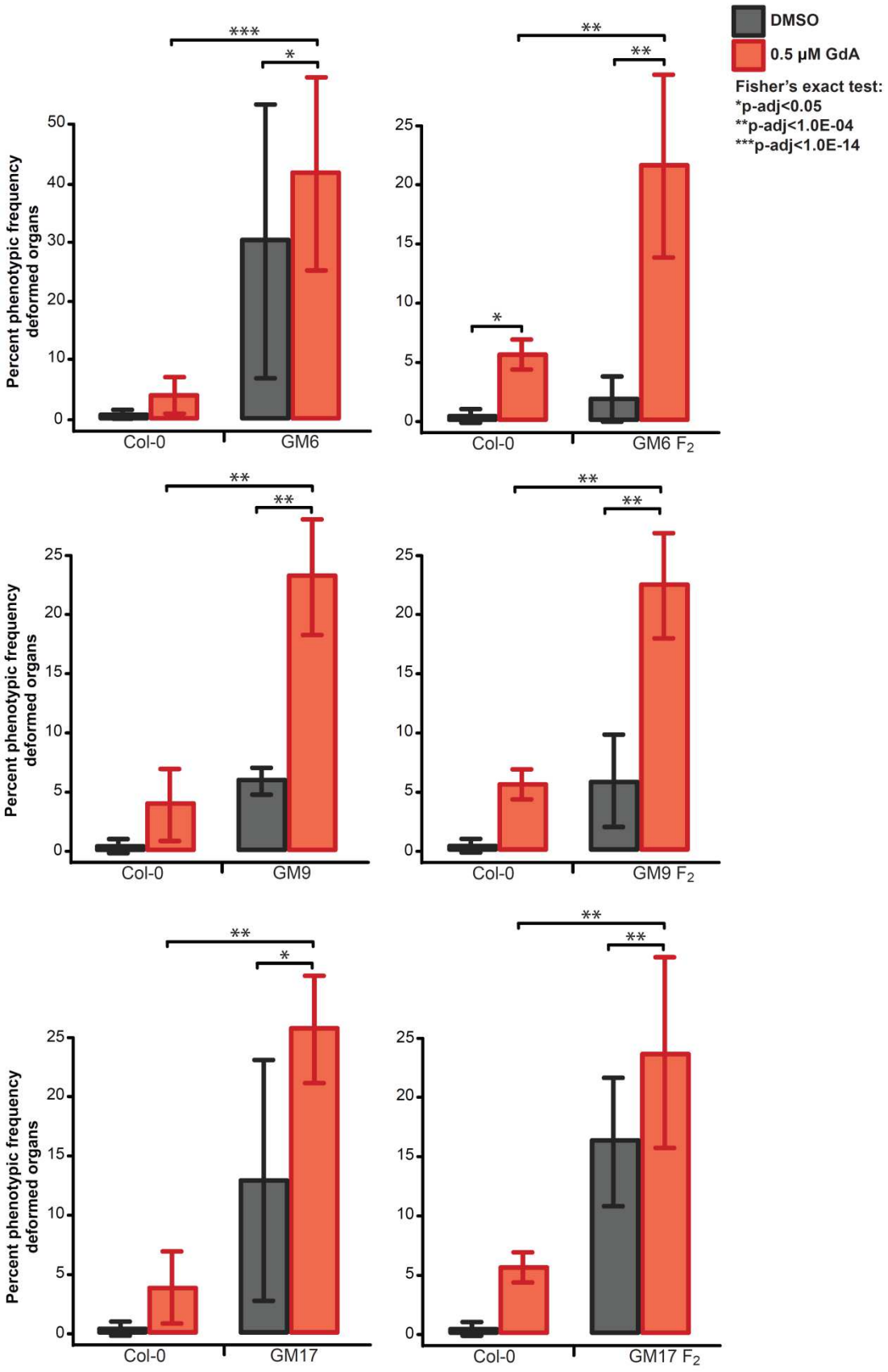
DMSO
0.5 µM GdA
Fisher's exact test:
*p-adj<0.05
**p-adj<1.0E-04
***p-adj<1.0E-14
Percent phenotypic frequency deformed organs
Col-0
GM6
GM6 F2
GM9
GM9 F2
GM17
GM17 F2

Supplemental Figure 2.6: Selected HSP90-responsive phenotypes are heritable. Three M_3-lines that showed evidence of deformed organ phenotypes that are HSP90-repsonsive were selected to be backcrossed to Col-0. The resulting F_2 populations show increased penetrance of deformed organs traits when HSP90 is inhibited. Left column: selected M_3-lines and response to 0.5 μM GdA treatment. Right column: M_3-line F_2 populations and response to 0.5 μM GdA treatment. Errors bars represent standard error of the mean across two biological replicates. *p-adj<0.05, **p-adj<1.0E-04, ***p-adj<1.0E-14, Fisher's exact test.

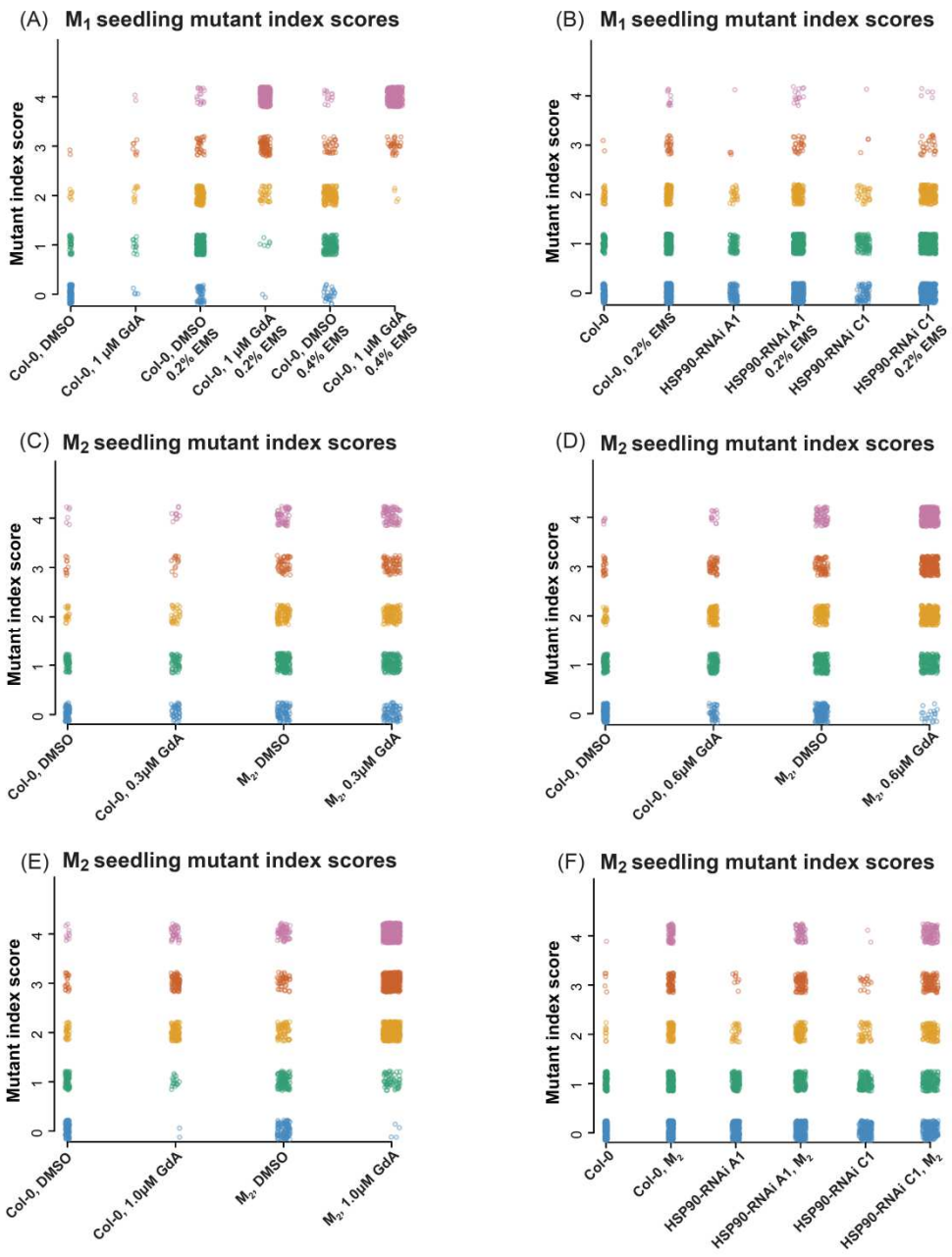

Supplemental Figure 2.7: Scatter plots of M_1 and M_2 scores shown in Figure 2.3 and Supplemental figure 2.2. Scores from each genotype and treatment are displayed. For the M_1 generation, a phenotypic cutoff was placed at seedlings with mutant index scores $\geq$ 2. For M_2 experiments, a phenotypic cutoff was placed seedlings with mutant index scores $\geq$ 3.

Genotype	Individual	X-coverage	Transitions (Ti)	Transversions (Tv)	Ti/Tv	SNVs/kb
Col-0 M_2	1	10.06	687	119	5.77	1.29E-08
Col-0 M_2	2	15.00	812	535	1.51	1.4E-08
Col-0 M_2	3	12.03	437	162	2.70	7.77E-08
Col-0 M_2	4	12.34	664	144	4.61	1.05E-08
Col-0 M_2	5	11.68	698	152	4.59	1.04E-08
Col-0 M_2	6	13.14	941	445	2.11	1.61E-08
HSP90-RNAi C1 M_2	1	7.41	621	73	8.51	1.41E-08
HSP90-RNAi C1 M_2	2	10.67	934	114	8.19	1.54E-08
HSP90-RNAi C1 M_2	3	14.32	768	173	4.44	1.20E-08
HSP90-RNAi C1 M_2	4	14.67	1292	477	3.13	1.87E-08
HSP90-RNAi C1 M_2	5	13.86	754	432	1.75	1.20E-08
HSP90-RNAi C1 M_2	6	9.77	447	93	4.81	8.35E-08
Average	**--**	**12.08**	**754.58**	**243.25**	**4.34**	**2.48E-08**

Supplemental table 2.1: Summary of whole genome sequencing and private SNV calling for selected M_2 individuals.

Comparison	Figure	Test	p-value	adjusted p-value	Note
Col-0 vs. Col-0 0.2% EMS, number of live seeds, pilot	Figure 2.2B	Student's unpaired t-test	<1.0E-04	N/A	
Col-0 vs. Col-0 0.4% EMS, number of live seeds, pilot	Figure 2.2B	Student's unpaired t-test	<1.0E-04	N/A	
Col-0 vs. Col-0 0.2% EMS, number of live seeds	Figure 2.2B	Student's unpaired t-test	<1.0E-04	N/A	
HSP90 RNAi-A1 vs. HSP90 RNAi-A1 0.2% EMS, number of live seeds	Figure 2.2B	Student's unpaired t-test	<1.0E-04	N/A	
HSP90 RNAi-C1 vs. HSP90 RNAi-C1 0.2% EMS, number of live seeds	Figure 2.2B	Student's unpaired t-test	<1.0E-04	N/A	
Col-0 0.2% EMS vs. HSP90 RNAi-A1 0.2% EMS, number of live seeds	Figure 2.2B	Student's unpaired t-test	0.62	N/A	
Col-0 0.2% EMS vs. HSP90 RNAi-C1 0.2% EMS, number of live seeds	Figure 2.2B	Student's unpaired t-test	0.06	N/A	
Col-0 control pilot vs. Col-0 control, number of live seeds	Figure 2.2B	Student's unpaired t-test	<1.0E-04	N/A	
Col-0 0.2% EMS pilot vs. Col-0 0.2% EMS, number of live seeds	Figure 2.2B	Student's unpaired t-test	0.03	N/A	
Col-0 0.2% EMS vs. HSP90 RNAi-C1 0.2%, number of dead seeds	Figure 2.2C	GLM, dead.seeds ~ (Genotype), poisson	3.70E-08	N/A	
Col-0 0.2% EMS vs. HSP90 RNAi-C1 0.2% EMS, number of dead seeds	Figure 2.2C	GLM, dead.seeds ~ (Genotype), poisson	1.22E-07	N/A	
Col-0 0.2% EMS vs. HSP90 RNAi-A1 0.2% EMS, number of dead seeds	Figure 2.2C	GLM, dead.seeds ~ (Genotype), poisson	0.13	N/A	
Col-0 0.2% EMS vs. Col-0, number of dead seeds, pilot	Figure 2.2C	GLM, dead.seeds ~ (Genotype), poisson	<2.0E-16	N/A	
Col-0 0.4% EMS vs. Col-0, number of dead seeds, pilot	Figure 2.2C	GLM, dead.seeds ~ (Genotype), poisson	1.08E-11	N/A	
Col-0 M_2 SNVs vs. C1 M_2, number of SNVs	Figure 2.2E	Student's unpaired t-test	0.5	N/A	
M_1 DMSO vs. M_1 1 µM GdA, 0.2% EMS, score $\geq$ 2	Supplemental figure 2.2C	Fisher's exact test	2.20E-16	3.85E-16	OR: 138.87
Col-0 1 µM GdA vs. M_1 1 µM GdA, 0.2% EMS, score $\geq$ 2	Supplemental figure 2.2C	Fisher's exact test	7.18E-16	1.01E-15	OR: 51.85
Col-0 DMSO vs. M_1 DMSO, 0.2% EMS, score $\geq$ 2	Supplemental figure 2.2C	Fisher's exact test	1.83E-10	2.13E-10	OR: 5.75
Col-0 DMSO vs. M_1 DMSO, 0.4% EMS, score $\geq$ 2	Supplemental figure 2.2C	Fisher's exact test	2.20E-16	3.85E-16	OR: Inf
M_1 DMSO vs. M_1 1 µM GdA, 0.4% EMS, score $\geq$ 2	Supplemental figure 2.2C	Fisher's exact test	2.20E-16	3.85E-16	OR: Inf
Col-0 1 µM GdA vs. M_1 1 µM GdA, 0.4% EMS, score $\geq$ 2	Supplemental figure 2.2C	Fisher's exact test	2.20E-16	3.85E-16	OR: 12.17
Col-0 1 µM GdA vs. Col-0 DMSO, score $\geq$ 2	Supplemental figure 2.2C	Fisher's exact test	1.14E-09	1.14E-09	OR: 14.34
Col-0 M_1 vs. HSP90 RNAi-C1 M_1, score $\geq$ 2	Supplemental figure 2.2B	Fisher's exact test	7.28E-03	1.70E-02	OR: 1.731
Col-0 M_1 vs. HSP90 RNAi-A1 M_1, score $\geq$ 2	Supplemental figure 2.2B	Fisher's exact test	5.40E-01	6.86E-01	OR: 1.171
HSP90 RNAi-C1 vs. HSP90 RNAi-C1 M_1, score $\geq$ 2	Supplemental figure 2.2B	Fisher's exact test	3.21E-02	5.61E-02	OR: 1.55
HSP90 RNAi-A1 vs. HSP90 RNAi-A1 M_1, score $\geq$ 2	Supplemental figure 2.2B	Fisher's exact test	6.76E-09	4.732E-08	OR: 8.82
Col-0 vs. Col-0 M_1, score $\geq$ 2	Supplemental figure 2.2B	Fisher's exact test	0.60	0.69	OR: 1.14
Col-0 vs. HSP90 RNAi-C1, score $\geq$ 2	Supplemental figure 2.2B	Fisher's exact test	0.69	0.69	OR: 1.12
Col-0 vs. HSP90 RNAi-A1, score $\geq$ 2	Supplemental figure 2.2B	Fisher's exact test	9.56E-06	1.59E-05	OR: 0.13
M_2 DMSO vs. M_2 0.6 µM GdA, score $\geq$ 3	Figure 2.3B	Fisher's exact test	2.2E-16	5.50E-16	OR: 3.52
M_2 DMSO vs. M_2 1 µM GdA, score $\geq$ 3	Figure 2.3B	Fisher's exact test	2.2E-16	5.50E-16	OR: 5.79
Col-0 DMSO vs. Col-0 1 µM GdA, score $\geq$ 3	Figure 2.3B	Fisher's exact test	2.2E-16	5.50E-16	OR: 7.55
Col-0 0.6 µM GdA vs. M_2 0.6 µM GdA, score $\geq$ 3	Figure 2.3B	Fisher's exact test	2.2E-16	5.50E-16	OR: 4.62
Col-0 1 µM GdA vs. M_2 1 µM GdA, score $\geq$ 3	Figure 2.3B	Fisher's exact test	1.37E-08	2.74E-08	OR: 2.22
Col-0 DMSO vs. Col-0 0.6 µM GdA, score $\geq$ 3	Figure 2.3B	Fisher's exact test	3.34E-05	4.77E-05	OR: 2.21
Col-0 0.3 µM GdA vs. M_2 0.3 µM GdA, score $\geq$ 3	Figure 2.3B	Fisher's exact test	1.66E-03	2.10E-03	OR: 2.16
M_2 DMSO vs. M_2 0.3 µM GdA, score $\geq$ 3	Figure 2.3B	Fisher's exact test	0.026	0.03	OR: 1.31
Col-0 DMSO vs. Col-0 0.3 µM GdA, score $\geq$ 3	Figure 2.3B	Fisher's exact test	0.04	0.04	OR: 1.75
Col-0 DMSO vs. M_2 DMSO, score $\geq$ 3	Figure 2.3B	Fisher's exact test	2.25E-16	2.25E-16	OR: 2.90
HSP90 RNAi-C1 vs. HSP90 RNAi-C1 M_2, score $\geq$ 3	Figure 2.3C	Fisher's exact test	2.2E-16	3.67E-16	OR: 8.84
Col-0 vs. Col-0 M_2, score $\geq$ 3	Figure 2.3C	Fisher's exact test	2.2E-16	3.67E-16	OR: 12.25
HSP90 RNAi-A1 vs. HSP90 RNAi-A1 M_2, score $\geq$ 3	Figure 2.3C	Fisher's exact test	2.2E-16	3.67E-16	OR: 10.69
Col-0 vs. HSP90 RNAi-C1, score $\geq$ 3	Figure 2.3C	Fisher's exact test	0.03	0.04	OR: 2.80
Col-0 vs. HSP90 RNAi-A1, score $\geq$ 3	Figure 2.3C	Fisher's exact test	0.59	0.59	OR: 1.48
GM6 DMSO vs. GM6 0.5 µM GdA, 2 replicates, frequency of deformed organs	Figure 2.3C	Fisher's exact test	0.01	0.02	OR: 4.68
Col-0 0.5 µM GdA, vs. GM6 0.5 µM GdA, 2 replicates, frequency of deformed organs	Figure 2.3C	Fisher's exact test	2.20E-16	3.96E-15	OR: 55.71
GM6 F_2 DMSO vs. GM6 F_2 0.5 µM GdA, 2 replicates, frequency of deformed organs	Supplemental figure 2.6	Fisher's exact test	2E-08	1.20E-07	OR: 18.00
Col-0 0.5 µM GdA, vs. GM6 F_2 0.5 µM GdA, 2 replicates, frequency of deformed organs	Supplemental figure 2.6	Fisher's exact test	3.76E-03	6.77E-03	OR: 3.23
GM9 DMSO vs. GM9 0.5 µM GdA, 2 replicates, frequency of deformed organs	Supplemental figure 2.6	Fisher's exact test	1.28E-04	2.56E-04	OR: 4.76
Col-0 0.5 µM GdA, vs. GM9 0.5 µM GdA, 2 replicates, frequency of deformed organs	Supplemental figure 2.6	Fisher's exact test	2.35E-07	1.06E-06	OR: 8.25
GM6, GM9, GM17 control: Col-0 DMSO vs. Col-0 0.5 µM GdA, 2 replicates, frequency of deformed organs	Supplemental figure 2.6	Fisher's exact test	0.05	0.054	OR: 7.64
GM9 F_2 DMSO vs. GM9 F_2 0.5 µM GdA, 2 replicates, frequency of deformed organs	Supplemental figure 2.6	Fisher's exact test	9.81E-05	2.21E-04	OR: 4.59
Col-0 0.5 µM GdA, vs. GM9 F_2 0.5 µM GdA, 2 replicates, frequency of deformed organs	Supplemental figure 2.6	Fisher's exact test	2.2E-05	5.66E-05	OR: 5.12
GM6, GM9, GM17 F_2 control: Col-0 DMSO vs. Col-0 0.5 µM GdA, 2 replicates, frequency of deformed org	Supplemental figure 2.6	Fisher's exact test	0.05	0.05	OR: 6.64
GM17 DMSO vs. GM17 0.5 µM GdA, 2 replicates, frequency of deformed organs	Supplemental figure 2.6	Fisher's exact test	4.80E-04	7.86E-03	OR: 2.34
Col-0 0.5 µM GdA, vs. GM17 0.5 µM GdA, 2 replicates, frequency of deformed organs	Supplemental figure 2.6	Fisher's exact test	1.33E-09	1.197E-08	OR: 10.28
GM17 F_2 DMSO vs. GM17 F_2 0.5 µM GdA, 2 replicates, frequency of deformed organs	Supplemental figure 2.6	Fisher's exact test	9.02E-07	3.25E-06	OR: 8.10
Col-0 0.5 µM GdA, vs. GM17 F_2 0.5 µM GdA, 2 replicates, frequency of deformed organs	Supplemental figure 2.6	Fisher's exact test	1.62E-05	4.86E-05	OR: 5.15
GM6, GM9, GM17 control: Col-0 DMSO vs. Col-0 0.5 µM GdA, 2 replicates, frequency of deformed organs	Supplemental figure 2.6	Fisher's exact test	0.048	0.05	OR: 7.64
GM6, GM9, GM17 F_2 control: Col-0 DMSO vs. Col-0 0.5 µM GdA, 2 replicates, frequency of deformed org	Supplemental figure 2.6	Fisher's exact test	0.05	1	OR: 6.659

Supplemental table 2.2: Summary of p-values used Figure 2.2, Figure 2.3, Supplemental Figure 2.2, and Supplemental Figure 2.6.

Line number	Parental phenotypes: heritability	Parental phenotypes responsive (+/-) *p-adj<0.05
DM1	Deformed aerial organs: yes	Deformed aerial organs: no
DM2	Dwarf: yes Epinastic cotyledons: yes Deformed aerial organs: yes	Dwarf: no Epinastic cotyledons: no Deformed aerial organs: yes (+)*
DM3	Deformed aerial organs: yes	Deformed aerial organs: yes (+)
DM4	Deformed aerial organs: yes	Deformed aerial organs: no
DM5	Deformed aerial organs: no	
DM6	Deformed aerial organs: yes	Deformed aerial organs: no
DM7	Deformed aerial organs: yes	Deformed aerial organs: no
DM8	Epinastic true leaves: yes Deformed aerial organs: yes	Epinastic true leaves: no Deformed aerial organs: no
DM9	Deformed aerial organs: no	Deformed aerial organs: no
DM10	Deformed aerial organs: no	Deformed aerial organs: no
GM1	Epinastic cotyledons: yes Deformed aerial organs: yes Discolorations: no	Epinastic cotyledons: no Deformed aerial organs: yes (+)
GM2	Dwarf: yes Deformed aerial organs: yes	Deformed aerial organs: yes (+)
GM3	Dwarf: yes Asymmetric rosette: no Deformed aerial organs: no	Dwarf: yes (+)*
GM4	Epinastic cotyledons: yes Deformed aerial organs: yes	Epinastic cotyledons: no Deformed aerial organs: no
GM5	Dwarf: yes Epinastic cotyledons: yes	Dwarf: yes (+)* Epinastic cotyledons: no
GM6	Deformed aerial organs: yes Asymmetric aerial organs: no	Deformed aerial organs: yes (+)*
GM7	Deformed aerial organs: yes	Deformed aerial organs: yes (+)
GM8	Epinastic cotyledons: yes Deformed aerial organs: yes	Epinastic cotyledons: no Deformed aerial organs: no
GM9	Extra aerial organs: no	
GM10	Dwarf: yes Epinastic cotyledons: yes Deformed aerial organs: yes	Dwarf: no Epinastic cotyledons: no Deformed aerial organs: yes (+)
GM11	Dwarf: yes Extra aerial organs: no Deformed aerial organs: yes	Dwarf: yes (+)* Deformed aerial organs: yes (+)*
GM12	Dwarf: yes	Dwarf: no
GM13	Epinastic true leaves: no Deformed aerial organs: yes	Deformed aerial organs: no
GM14	Deformed aerial organs: yes	Deformed aerial organs: yes (+)*
GM15	Severe developmental delay: yes Dwarf: yes Deformed aerial organs: yes	Severe developmental delay: yes (+) Dwarf: no Deformed aerial organs: yes (+)
GM16	Dwarf: yes Lesions on cotyledons: yes Deformed aerial organs: yes	Dwarf: no Lesions on cotyledons: yes (+)* Deformed aerial organs: no
GM17	Severe developmental delay: no Dwarf: yes Missing aerial organs: no	Dwarf: yes (+)*
GM18	Dwarf: yes Lesions on cotyledons: yes Deformed aerial organs: no	Dwarf: yes (+)* Lesions on cotyledons: no
GM19	Dwarf: yes Deformed aerial organs: yes	Dwarf: yes (-)* Deformed aerial organs: yes (-)*
GM20	Dwarf: yes Deformed aerial organs: yes	Dwarf: yes (+)* Deformed aerial organs: yes (+)*
GM21	Dwarf: yes Deformed aerial organs: no	Dwarf: yes (+)*
GM22	Missing aerial organs: no Deformed aerial organs: yes	Deformed aerial organs: yes (+)*

Supplemental table 2.3: Summary M_3-line parental phenotypes and heritability of traits.

Chapter 3: ARGONUATE 1 is a source of environmental robustness[4,5]

Abstract

The crucial role of miRNAs in plant development is exceedingly well supported; their importance in environmental robustness is studied in less detail. Here, we describe a novel, environmentally-dependent phenotype in hypomorphic *ago1* mutants and uncover its mechanistic underpinnings. AGO1 is a key player in miRNA-mediated gene regulation. We observed transparent lesions on embryonic leaves of *ago1*-mutant seedlings. These lesions increased in frequency in full spectrum light. Notably, the lesion phenotype was most environmentally responsive in *ago1-27* mutants. This allele is thought to primarily affect translational repression, which has been linked with response to environmental perturbation. Using several lines of evidence, we found that these lesions represent dead and dying tissues due to an aberrant hypersensitive response. Although all three canonical defense hormone pathways - salicylic acid, jasmonate, and jasmonate/ethylene pathways - were upregulated in *ago1* mutants, we demonstrate that jasmonate perception drives the lesion phenotype. Double mutants of *ago1* and *coi1*, the jasmonate receptor, showed greatly decreased frequency of affected seedlings. The chaperone HSP90, which maintains phenotypic robustness in the face of environmental perturbations, is known to facilitate AGO1 function. HSP90 perturbation has been previously shown to upregulate jasmonate signaling and to increase plant resistance to herbivory. Although single HSP90 mutants showed subtly elevated levels of lesions, double mutant analysis disagreed

[4] This chapter is published as "The mechanistic underpinnings of an *ago1*-mediated, environmentally-dependent, and stochastic phenotype," Plant Physiology: 170(4), 2016, pp. 15.01928, by *G.A. Mason, T. Lemus, and **C. Queitsch. *First author, **Corresponding author.

[5] T.L. noted *ago1*-dependent lesions. G.A.M., T.L., and C.Q. conceived experiments. G.A.M. and T.L. performed experiments. G.A.M. performed data analysis. G.A.M. and C.Q. wrote the article. All authors read, commented on, and improved the article.

with a simple epistatic model for *HSP90* and *AGO1* interaction; rather, both appeared to act non-additively in producing lesions. In summary, our study identifies AGO1 as a major, largely HSP90-independent, factor in providing environmental robustness to plants.

3.1 Introduction

ARGONAUTE 1 (AGO1) is an ancient, highly conserved essential protein. One of 10 functionally distinct AGO proteins in the plant *Arabidopsis thaliana*, AGO1 uses microRNAs (miRNAs) to decrease the expression of target genes. AGO1 and the miRNA pathway are crucial for many regulatory processes throughout development and in response to environmental stimuli. As frequent components of feed forward loops, miRNAs also play important roles in controlling gene expression noise and maintaining phenotypic robustness of specific traits in several organisms, including plants[184].

AGO1 and miRNAs are also critical for proper plant responses to abiotic stress. Expression levels of miRNAs respond to heat shock, cold, drought, oxidative stress, ultra-violet light exposure, and hypoxia[185]. For example, in response to drought, the expression of miR169 decreases and expression of its target gene, encoding the transcription factor NFYA5, increases in *A. thaliana*[186]. Increased expression of NFYA5 supports plant survival in drought conditions. Transgenic plants overexpressing NYFA5 have drought-tolerant phenotypes; in contrast, plants overexpressing miR169 are drought-sensitive[186].

In addition to orchestrating proper responses to abiotic stress, miRNAs are also implicated in response to biotic factors such as defense against pathogens and herbivores[187-190]. There is abundant evidence from expression studies[187,188,191] that links miRNA expression to disease resistance pathways. For example, *MIR393* is upregulated in response to bacterial flg22,

a potent trigger of innate immunity in plants[192]. miR393 represses expression of auxin receptor genes, which are involved in plant growth and development[191]

A highly effective plant defense mechanism is the hypersensitive response (HR), which restricts the growth of some pathogens through 'programmed' cell death[170]. Pathogen perception triggers complex multi-faceted responses, including altered ion fluxes, the initiation of MAPK signaling cascades, the accumulation of reactive oxygen species (ROS), the induction of downstream defense genes, and callose deposition at the cell wall, all of which are thought to contain pathogen growth[193-196]. The phytohormones salicylic acid, jasmonate, and ethylene are of particular importance in HR and are critical for defense against pathogens and/or herbivores[177,197]. The jasmonate and ethylene pathways contain several, well-characterized miRNA targets[198,199]. All three hormone pathways interact in a complex manner to coordinate plant defenses in the face of constantly changing environmental challenges in nature[177].

Salicylic acid (SA) plays a central role in resistance against biotrophic pathogens, such as *Pseudomonas syringae* and turnip crinkle virus[200]. SA and ROS can act synergistically to lead to HR-mediated localized cell death[201,202]. Jasmonate (JA) regulates many processes ranging from plant development (*e.g.* fertility) to defense against herbivores[203-208]. JA modulates ROS production, specifically the production of hydrogen peroxide[209]. JA and SA are often thought to act antagonistically; however, the crosstalk between these two hormones is complex[177].

Ethylene (ET) is a positive regulator of ripening and senescence[210]. In plant defense, ET potentiates some branches of SA-responsive gene expression[211], but globally represses SA-responsive genes[212]. ET and JA synergistically promote defense against necrotrophic fungal pathogens through ethylene responsive transcription factors (ERFs)[213]. However, ET represses JA-dependent herbivory responses[214] antagonizing the transcription factor MYC2[213,215,216].

Here, we provide evidence that AGO1 maintains phenotypic robustness in the face of an environmental challenge and integrates environmental signals through these canonical defense pathways. We show that *ago1* mutant plants develop lesions on embryonic leaves (cotyledons) when grown under full spectrum light conditions. We demonstrate that these lesions represent localized cell death and originate due to stochastically occurring, aberrant HR. We show that SA, JA, and JA/ET signaling pathways are all significantly upregulated in full spectrum light-grown *ago1* cotyledons, and use genetic analysis to demonstrate that lesions arise primarily due to the JA-dependent pathway.

We also test the interaction of AGO1 with the molecular chaperone HSP90, which is known to provide robustness to environmental perturbations in plants. HSP90 plays crucial roles in response to abiotic and biotic factors such as herbivores and pathogens[152,171,172]. Moreover, HSP90 facilitates AGO1 folding and function in a wide range of organisms, including plants[217-219]. Consistent with HSP90's well-established role in altering penetrance of genetic variation[156,158,220,221], we find that decreased HSP90 levels increase the penetrance of *ago1* mutations. Our results indicate that AGO1 and HSP90 act together in maintaining plant robustness and buffering development from environmental perturbations.

3.2 Results

3.2.1 argonaute 1 *mutant seedlings develop lesions in full spectrum light conditions*

In addition to previously characterized *ago1* phenotypes[222-224], such as hyponastic cotyledons and developmental delay (**Figure 3.1C and D**), we observed that *ago1* mutant seedlings frequently produced white, often raised, lesions, which resided primarily on cotyledons (**Figure 3.1**). Wild type seedlings (Col-0) showed these lesions at low frequency in both filtered

light (yellow long-pass filters, blocking <454 nm[182] and full spectrum light) (**Figure 3.1A and 3.1B**). We grew an allelic series of *ago1* mutations in both light conditions and scored the frequency of affected seedlings (**Figure 3.1B**). We scored affected seedlings rather than frequency of lesions because lesions often fused with each other, confounding frequency measures. For the *ago1*-25, *ago1-27*, and *ago1-46* mutant seedlings[223,225], the frequency of affected seedlings increased significantly in full spectrum light compared to wild-type (**Figure 3.1B**). We selected the *ago1-27* mutant for subsequent investigation of the molecular underpinnings of the lesion phenotype for two reasons. First, we were intrigued by the strong dependency of its lesion phenotype on growth conditions (General linear mixed model, family=binomial [GLMM]: p< 1.0E-04). Second, *ago1-27* mutants, albeit carrying a stronger allele than *ago1-46* mutants, show fewer and less severe unrelated developmental abnormalities than *ago1-25* mutant seedlings[223].

The raised, transparent morphology of the *ago1*-dependent lesions superficially resembled undifferentiated tissue, *i.e.* ectopic callus tissue[226]. Notably, previous studies described callus-like tissue on cotyledons of hypomorphic *serrate* mutant plants without experimental follow-up[227]. The zinc-finger protein SERRATE is involved in primary miRNA biogenesis; *serrate* mutants show pleiotropic phenotypes due to perturbed meristem function and leaf axial patterning[227].

We tested the callus hypothesis by analyzing expression of genes implicated in callus formation[228] and by testing the propensity of lesions to facilitate callus formation[161]. However, genes implicated in callus formation and shoot apical meristem identity showed wild-type expression levels in *ago1-27* cotyledons (**Supplemental figure 3.1**). To test callus formation, we dissected lesions from both *ago1-27* and wild-type and tested callus formation on hormone-

containing media. At low hormone dose, *ago1-27* lesion tissue performed worse than wild-type or *ago1-27* unaffected tissue; at high hormone dose, no difference was observed (Supplemental Figure 2). We conclude that the observed lesions do not represent undifferentiated, callus-like tissue.

To explore the origin and identity of the lesion tissue, we employed scanning electron microscopy (SEM) (**Figure 3.1F-H**). SEM revealed that both wild-type and *ago1-27* lesions 'erupt' from beneath the epidermis, suggesting that mesophyll cells are primarily affected (**Figure 3.1F-H**). Cells within lesions appeared to be ruptured, suggesting that at least some lesions represented dead or dying tissue[229].

To exclude the possibility that ruptured cells were an artifact of SEM sample preparation, we used vital dye staining to validate our findings. Localized cell death is induced in plants as part of the hypersensitive response (HR) upon pathogen attacks. We hypothesized that the *ago1* lesions were a result of stochastically occurring, aberrant HR that was enhanced in *ago1* seedlings by exposure to full spectrum light. Localized cell death is examined by staining with vital dyes such as Trypan blue, which stains dead and dying tissue dark blue[161]. We performed Trypan blue staining of unaffected and affected cotyledon tissue (**Figure 3.2**). Cotyledons exhibiting lesions retained the dye, with lesions exhibiting dark blue staining indicative of ruptured cell walls (**Figure 3.2**). In fact, even unaffected *ago1-27* cotyledons showed deeper staining than wild-type cotyledons, suggesting increased susceptibility to cell wall rupture. To confirm these results, we performed 3,3'-diaminobenzidine (DAB) staining (**Figure 3.2**). DAB staining indicates the presence of reactive oxygen species, specifically hydrogen peroxide, which is a reliable marker of HR-mediated localized cell death[161]. Indeed, we observed DAB staining

coinciding with lesions (**Figure 3.2**). Based on both Trypan blue and DAB stainings, we concluded that *ago1-27* cotyledons show lesions that resemble HR-mediated localized cell death.

3.2.2 ago1-27 *cotyledons overexpress canonical SA, JA, and JA/ET signaling markers in full spectrum light*

Phytohormones mediate all major aspects of a plant's response to environmental perturbations, including defense against biotic stresses. The three phytohormones salicylic acid (SA), ethylene (ET), and jasmonate (JA) are the canonical defense hormones. As previous results link light conditions (UV-B) with defense hormone response[230,231], we set out to examine whether the SA, JA, or JA/ET pathways were responsible for the lesions on *ago1* cotyledons. We measured expression of marker genes for SA, JA, or JA/ET signaling in 10-day-old cotyledons of wild-type, *ago1-46*, *ago1-27,* and *ago1-25* mutant seedlings grown in the lesion-inducing, full spectrum light condition. Specifically, we assessed expression of *PATHOGENESIS-RELATED GENE 1(PR1)*, *VEGETATIVE STORAGE PROTEIN 1(VSP1)*, and *PLANT DEFENSIN 1.2 (PDF1.2)*, which are upregulated in defense-triggered SA, JA, and JA/ET-signaling, respectively[206,213,232-235]. All three marker genes were significantly upregulated in *ago1* cotyledons compared to wild-type (**Figure 3.3**); hence, more detailed analysis was required to identify the involved pathway(s).

ago1 plants are susceptible to virus infection, implying a direct link between SA-mediated defense and AGO1 activity[223,236,237]. As the SA marker gene *PR1* was most strongly upregulated in *ago1* cotyledons, we first examined the expression of additional genes in SA signaling. Although there are no known miRNA targets in the SA signaling pathway, altered light conditions change the expression of many miRNAs[238]. Based on previous studies, we selected three SA-signaling genes. The first*, NONEXPRESSOR OF PR GENES 1 (NPR1),* was

selected because it contributes to activation of *PR*-genes after SA perception[239]. *NPR1* is also a key modulator in SA-JA crosstalk[214]. The second, *SUPPRESSOR OF NPR1-1* (*SNC1),* was previously reported to be upregulated in *ago1-36* mutants[240]. The third, *ENHANCED DISEASE SUSCEPTIBILITY 1* (*EDS1*), is a component of R gene-mediated disease resistance in *Arabidopsis thaliana*[241]*;* EDS1 is also required for production of SA in some conditions involving pathogen challenge[242]. All three genes were significantly upregulated in *ago1-27* cotyledons (**Figure 3.4A**).

We next investigated additional marker genes in JA signaling. In *A. thaliana,* miR319a represses specific members of the *TEOSINTE BRANCHED/CYCLOIDEA/PCF (TCP)* family of transcription factors, which positively regulate JA biosynthesis[243]. TCP4 promotes JA biosynthesis by activating the expression of *LIPOXYGENASE2* (*LOX2*)[199,243]. JASMONATE INSENSITIVE 1 (JIN1/MYC2), a master regulator of the response to herbivores, also activates expression of *LOX* genes[213,233]. TCP4-regulated LOX2 catalyzes an early step of jasmonate biosynthesis[204]. Lastly, *JASMONATE RESISTANT 1* (*JAR1)* functions in the synthesis of biologically active jasmonate-isoleucine[244]. All four tested genes – *TCP4, LOX2, MYC2,* and *JAR1* – were significantly upregulated in *ago1-27* cotyledons (**Figure 3.4B**).

Lastly, we examined additional genes known to function in JA/ET signaling. We selected *ETHLYLENE INSENSITIVE 2 (EIN2)* because it is the key integrator of JA/ET stress responses[245] and is required for *PDF1.2* expression[245]. We also examined the transcription factor *ORESARA 1*(*ORE1),* which is a direct target of miR164ab and which together with *EIN2* regulates ethylene signaling via a trifurcate feed-forward loop[198]. JA and ET also activate expression of *AP2*/*ERF*-domain transcription factors[246] such as *OCTADECANOID-RESPONSIVE ARBIDOPSIS AP2/ERF* 59 (*ORA59*) and *ETHYLENE RESPONSE FACTOR 1*

(*ERF1*)[211,247]. Overexpression of *ERF1*[248] or *ORA59*[211] enhances resistance against fungal pathogens. Overexpression of *ORA59* also suppresses *MYC*-dependent signaling in defense against herbivores, making plants more susceptible to herbivores[249].

All but one gene were significantly upregulated in *ago1-27* cotyledons (**Figure 3.4C**). The outlier, *EIN2,* was significantly downregulated at about half of wild-type levels. Given the strong upregulation of *PDF1.2*, this specific result is likely a consequence of extensive feedback relationships. In summary, all three stress response pathways were upregulated, suggesting that *ago1* mutants no longer interpret environmental signals correctly and may be overly sensitive to the subtle stress of full spectrum light[182].

3.2.3 Exogenous JA and ET treatments, but not SA treatment, suffice to induce lesions in wild type

The consistent upregulation of all three candidate pathways necessitated a different approach to identify the molecular origin(s) of the lesions in *ago1* cotyledons. We applied all three phytohormones separately and in combination and assayed the frequency of affected *ago1-27* and wild-type seedlings. Specifically, we sprayed five-day-old seedlings grown in full spectrum light with increasing concentrations of phytohormones[152,161,250] and scored affected seedlings at day 10. As SA signaling marker genes were upregulated, we predicted that exogenous SA treatment would increase the number of affected individuals in both *ago1-27* and wild-type. However, the frequency of affected *ago1-27* seedlings decreased; there was no significant response in wild-type (**Figure 3.5A**). This result excludes SA as the cause of the observed lesions.

We next tested whether application of methyl jasmonate (MeJA) would increase the frequency of affected seedlings and whether we could detect differences in the response of *ago1-*

27 and wild-type. In wild-type, the frequency of affected individuals increased dramatically at 50 μM MeJA. Thus, JA treatment suffices to cause lesions (**Figure 3.5B**). In *ago1-27* seedlings, the number of affected individuals increased significantly at low MeJA dosage (10 μM) but did not further increase at high MeJA dosage (50 μM). This result suggests that *ago1-27* is hypersensitive to JA at low concentrations but its response plateaus at higher concentrations (**Figure 3.5B**). We compared the responses of wild-type and *ago1-27* to MeJA using a generalized linear model with genotype and treatment as fixed effects and replicate as a random effect. Indeed, *ago1-27* mutants were significantly more responsive to MeJA at 10 μM conditions (GLMM: $p<1.0E-04$), whereas at 50 μM wild-type was more responsive (GLMM: $p<1.0E-04$), indicating that *ago1-27* mutants have a lower threshold for JA perception and saturation.

Lastly, we tested whether ethylene treatment could increase the number of affected seedlings using the ethylene precursor 1-aminocyclopropane-1-carboxylic acid (ACC) (**Figure 3.5C**). At the lowest dose of ACC (1 μM), the frequency of affected *ago1-27* seedlings increased sharply. Comparing *ago1-27* and wild-type response to ACC, we found that *ago1-27* mutants were significantly more responsive at 1 μM conditions (GLMM: $p<1.0E-04$). However, with increasing ACC doses, the frequency of affected seedlings decreased subtly but significantly in *ago1-27* and remained unchanged in wild-type (GLMM: $p<1.0E-04$). Thus, ET treatment does increase the number of affected *ago1-27* individuals at low doses and decreases the frequency of affected *ago1-27* seedlings at high doses, but it fails to fully mimic the mutant phenotype in wild-type.

As both JA and ET treatment produced an increase in affected seedlings, we wanted to test the effect of both hormones in combination. We performed these experiments with 10 μM

MeJA, the highly responsive dose for *ago1-27* mutant seedlings, and at various concentrations of ACC. The presence of ACC did not significantly change the frequency of affected *ago1-27* and wild-type individuals observed at 10 μM MeJA (**Figure 3.5D**). Thus, we conclude that JA, but not ET or SA, is likely the main driver of the environmentally-sensitive lesion phenotype in *ago1-27*.

3.2.4 Disruption of JA perception dramatically reduces lesions in ago1-27 *mutant seedlings*

Thus far, our expression results and exogenous hormone treatments point to JA as the key hormone underlying the lesion phenotype in *ago1-27* mutant seedlings. To test whether JA causes the lesion phenotype, we created a double mutant of *ago1*-27 and *coi1-1* to block JA perception. *CORONATINE INSENSITIVE 1* (*COI1*) encodes the main receptor of biologically active JA; the well-characterized *coi1-1* mutant carries an amino acid substitution in the F-box motif of COI1[232,251]. The *coi1-1* homozygous seedlings showed significantly fewer individuals with lesions than wild-type (**Figure 3.6**). The frequency of affected seedlings in the *ago1-27; coi1-1* double mutants was dramatically reduced compared to *ago1-27* single mutants, albeit higher than in wild-type (**Figure 3.6**). Disruption of JA perception and signaling appears to strongly suppress the environmentally-sensitive lesions in both *ago1-27* and wild-type.

To explore the possible interplay of JA and ET perception and signaling genetically, we created triple mutants of *ago1-27* with *coi1-1* and *ein2-1*. EIN2 is a membrane bound transport protein; *ein2-1* mutants carry an early stop mutation resulting in a truncated protein[245]. Consistent with our expression data for *EIN2* in *ago1-27* mutant seedlings, the *ein2-1* homozygous seedlings produced significantly more lesions than wild-type and were statistically similar to *ago1-27* mutant seedlings (**Supplemental figure 3.3**). Thus, loss of ET perception increases rather than decreases the lesion phenotype. Double mutants of *ago1-27* and *ein2-1*

resembled *ago1-27* single mutants (**Supplemental figure 3.3**), suggesting that lesions in both mutant genotypes arise through the same pathway. The *coi1-1* mutation was epistatic in both the double mutant with *ein2-1* and the triple mutant *ago1-27;coi1-1;ein2-1* (**Supplemental figure 3**), identifying JA perception as causal for lesions in single *ago1-27* and *ein2* mutants. We conclude that the observed environmentally-sensitive, *ago1-27*-dependent lesions are primarily driven by JA and that the effects of exogenous ET are likely due to the known cross-regulation of both pathways.

3.2.5 ARGONAUTE1 *and* HSP90 *interact genetically in producing the lesion phenotype*

Recent studies in both animals[218,219] and plants[217] demonstrate that the molecular chaperone HSP90 is required for different aspects of AGO function. HSP90-reduced plants show overexpression of genes involved in JA biosynthesis and are more resistant to herbivores than wild-type[152]. Therefore, we wanted to explore if the observed environmentally-and JA-dependent lesion phenotype was affected by perturbing HSP90. To do so, we created a double mutant of *ago1-27* with a previously published RNAi line, RNAi-A1[152]. This line primarily affects levels of the environmentally-responsive, heat-inducible HSP90.1 paralog, which could be plausibly involved in the environmentally-dependent lesion phenotype. We refrained from using highly specific inhibitors of the chaperone, as these compounds are highly sensitive to full spectrum light[182]. Indeed, we observed a subtle but significant increase in affected seedlings in single HSP90-mutants (HSP90 RNAi-A1) compared to wild-type seedlings (**Figure 3.7**). This result is consistent with the previously described role of HSP90 in JA signaling[152]. However, HSP90 perturbation produced far fewer affected seedlings than AGO1 perturbation, inconsistent with simple epistasis of both genes. Assuming that the HSP90 RNAi-A1 lesion phenotype arises as the result of an AGO1-HSP90 interaction, there should be no further increase in the frequency of

affected seedlings in the double mutant. If, however, HSP90 and AGO1 act independently, we should observe additive effects. These simple assumptions are complicated by the fact that both *ago1-27* and HSP90 RNAi-A1 are weak, partial loss-of-function mutants. Our result deviated subtly but significantly from additive expectations (GLMM: p<1.0E-04) **(Figure 3.7**), suggesting a non-additive relationship between the chaperone and AGO1 in this phenotype. Non-additivity is supported by our expression analysis of HSP90 across all three mutant backgrounds (**Supplemental figure 3.4**). In full-spectrum light conditions, HSP90 RNAi-A1 mutants showed strong downregulation of the chaperone and significantly more seedlings with lesions than wild-type; the *ago1-27* mutants showed significant upregulation of HSP90 compared to wild-type, consistent with experiencing stress, and many more affected seedlings than both wild-type and single HSP90 mutants; finally, the double mutant showed reduced HSP90 levels compared to wild-type, albeit to a lesser extent than in the single HSP90 RNAi-A1, and the highest frequency of seedlings with lesions. The non-additive higher incidence of affected seedlings in this double mutant is consistent with previous observations that HSP90 perturbation increases the penetrance of genetic variants[220,252]. In summary, our results indicate that although AGO1 and HSP90 appear to be inter-dependent with regard to responding properly to environmental perturbations, neither contribution is fully explained by the other. Furthermore, AGO1 appears to be the principal integrator of environmental signaling for proper repression of lesion formation, with a much reduced role for the environmentally-responsive HSP90.1 paralog.

3.3 Discussion

Here, we present a previously undescribed phenotype in *ago1* mutant plants – apparently stochastic lesions in cotyledons – and uncover its molecular underpinnings. Our initial

observation and subsequent investigation of the lesion phenotype identifies AGO1 as a key integrator of environmental signals and hormone signaling, thereby providing robustness to micro-environmental challenges as was previously observed for the molecular chaperone HSP90. The spontaneous lesions that we observed in *ago1* seedlings, especially in response to full spectrum light, appear to be dead and dying tissue bearing the hallmarks of HR due to upregulated JA/ET signaling. In wild-type, functional AGO1 appears to play a key role in properly deploying HR only upon pathogen attack.

Previous studies have implicated AGO1 in different plant defense pathways through gene expression[253,254] and genetic studies[240]. It is tempting to speculate that the observed lesions in *ago1* mutants involve mis-regulation of R-genes[240], although empirical evidence is lacking thus far. In contrast, the role of AGO1 in defense against viruses is exceedingly well studied; viruses employ several strategies to counteract AGO1 upon infection, including translational repression and protein degradation[255-260].

Notably, *ago1-27* mutants were far more responsive to full spectrum light than other *ago1* mutants, presumably due to the functional differences between mutant alleles. AGO1-dependent regulation of gene activity occurs through two principal mechanisms, mRNA cleavage[237] and translational repression[261]. In plants, AGO1 was previously thought to function primarily through RNA cleavage because of the near perfect base pairing of plant miRNAs with their target sequences[262]. More recently, however, several studies have provided evidence for translational repression[263-265], in particular with regard to the heat stress-induced downregulation of SPL transcription factors[266,267]. Translational repression, which is reversible, has been proposed as a mechanism for facilitating recovery after environmental stress[268,269]. In fact, the environmentally-responsive *ago1-27* allele[223] is thought to affect primarily translational

repression[237,265]. Our *ago1-27* results are consistent with a recent report demonstrating that *ago1-27* seedlings are more responsive to heat stress compared to *ago1-25* seedlings[266]. Similarly, as we show, translational repression appears to be relevant for the response to the subtle stress of full spectrum light.

Our study also links light conditions to JA signaling, which is supported by several previous studies. Specifically, solar UV-B radiation renders plants more resistant to herbivory, primarily due to upregulation of the JA pathway[231,270,271]. Consistent with these prior findings, the *ago1*-dependent lesions were much less frequent in filtered light conditions which exclude UV-B radiation[182].

Similarly, HSP90 perturbation is known to increase JA signaling and it yields greater resistance to herbivores[152]. As expected, mutants with reduced HSP90 levels show subtly but significantly greater frequency of affected seedlings. HSP90 plays important roles in plant defense, especially in defense against microbial pathogens[53,77,153,272]. HSP90 is also implicated in chaperoning AGO1[217]. Our double mutant and expression analyses, however, suggest a synergistic, rather than a simple epistatic or additive relationship. *ago1-27* single mutants show many more affected seedlings than HSP90 RNAi-A1 seedlings. Although HSP90 expression levels in the double mutant are considerably higher than in the single HSP90 mutant, the number of affected seedlings increases further in double mutants beyond additive expectations. Note that the interpretation of this double mutant result is complicated by the fact that both mutants represent weak partial mutants of essential genes. The increased penetrance of the *ago1-27* mutation upon HSP90 perturbation is consistent with the notion that HSP90 is critical for buffering deleterious mutations[86]. Our results further suggest that fluctuations in environmental conditions are buffered by both AGO1 and HSP90.

In our gene expression studies, we observed that SA marker genes, just like JA and ET marker, were also highly upregulated. We conclude that *ago1* plants generally upregulate these hormone pathways, presumably in part due to complex cross-regulation. However, as our exogenous hormone treatments and genetic analyses demonstrate, JA is the main driver of the lesion phenotype. In summary, AGO1 and the miRNA pathway appear to minimize variation in phenotype among isogenic seedlings and suppress aberrant mis-regulation of plant defense pathways similar to previous observations for the phenotypic capacitor HSP90.

3.4 Main figures

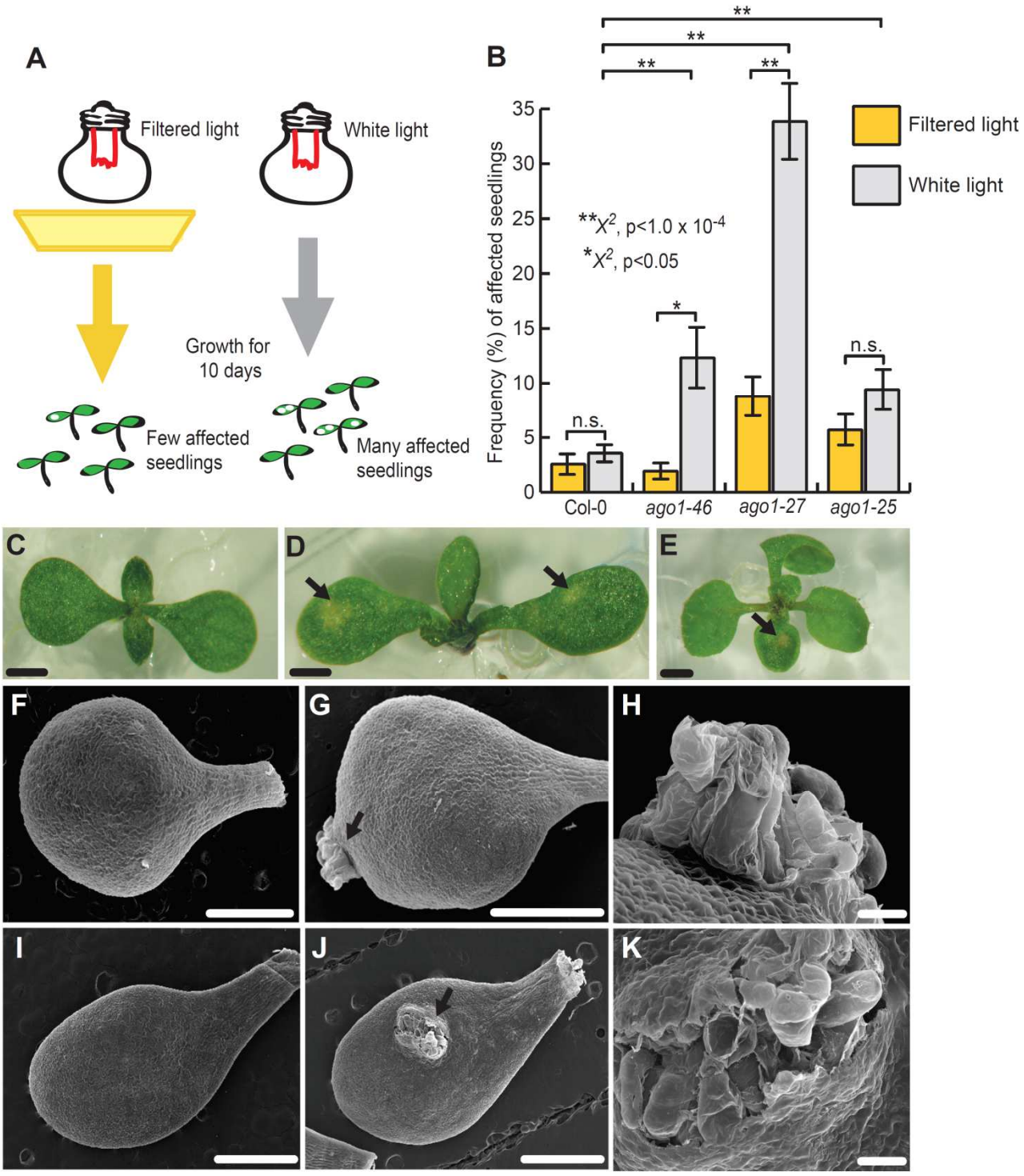

Figure 3.1: Hypomorphic *argonaute 1* mutants showed increased frequency of seemingly stochastic lesions. (A) Experimental set-up: when grown in yellow, filtered light conditions for 10 days, few *ago1* seedlings showed lesions on cotyledons. When grown in full spectrum light, many more *ago1* seedlings developed lesions. **(B)** In full spectrum light, *ago1-46, ago1-27,* and *ago1-25* mutants showed significantly increased frequency of affected seedlings compared to wild-type. *ago1-27* and *ago1-46* mutants showed significantly more affected individuals in unfiltered versus filtered light conditions; a similar, albeit non-significant tendency was observed for seedlings carrying the *ago1-25* allele. Error bars are standard error of mean across at least three replicates with n = 25-72 seedlings per replicate. Statistical significance was calculated using χ^2-test of significance (**p<1.0E-04, *p<0.05, for all possible p-values, refer to Supplemental Table 4). **(C-D)** Lesions in wild-type and *ago1-27* mutant seedlings show distinct morphology. **(C)** Full spectrum light-grown, 10 day-old, unaffected *ago1-27* seedling. **(D)** Full spectrum light-grown, 10 day-old, affected *ago1-27* seedling with lesions denoted by arrows. **(E)** Full spectrum light-grown, 10 day-old, affected wild-type seedling with lesion denoted by arrow. **(C-E)** Scale bar: 1 mm. **(F-K)** Scanning electron micrographs of 10 day-old cotyledons grown in full spectrum light. **(F)** Unaffected wild-type cotyledon. **(G)** Wild-type cotyledon with lesion denoted by arrow. **(H)** Magnified view of lesion from **(G)**. (I) Unaffected *ago1-27* cotyledon. **(J)** *ago1-27* cotyledon with lesion denoted by arrow. **(K)** Magnified view of lesion from **(I)**. **(F, G, I, and J)** Scale bar: 1 mm. **(H, K)** Scale bar: 500 microns.

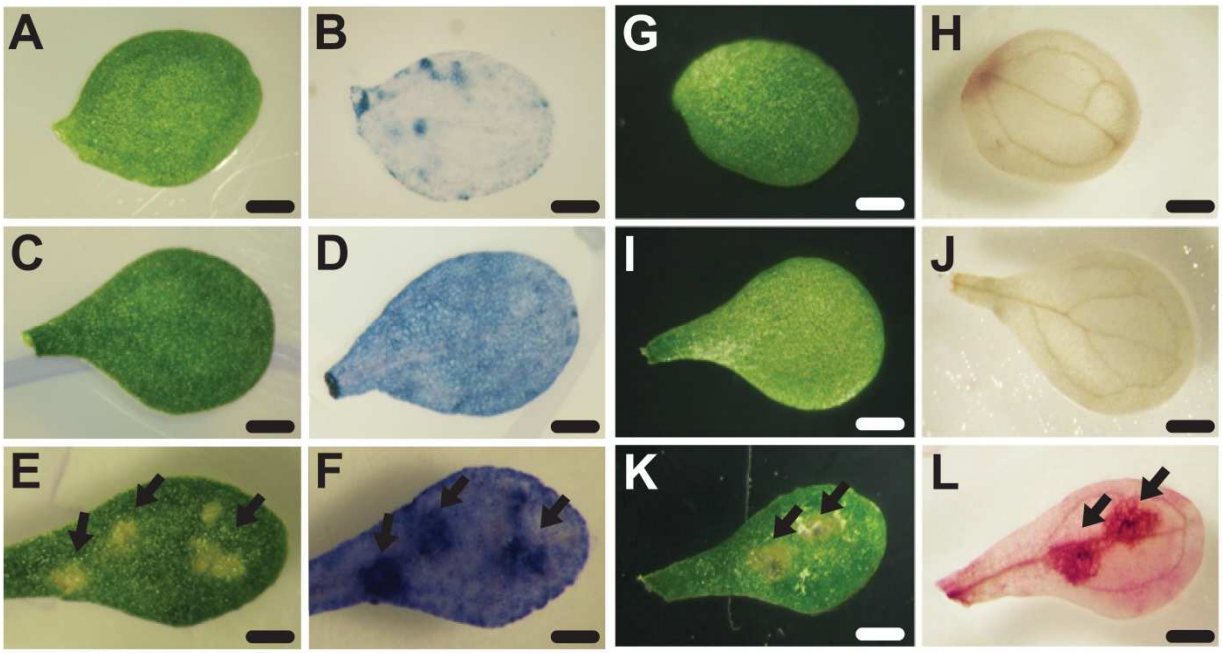

Figure 3.2: Vital staining of unaffected and affected tissue from wild-type and *ago1-27* cotyledons. (A, G) Unaffected wild-type cotyledons prior to staining. **(B)** Unaffected wild-type cotyledon after Trypan blue staining showed little dye accumulation. **(G)** Unaffected wild-type cotyledon after DAB staining showed little dye polymerization. **(C, I)** Unaffected *ago1-27* cotyledons prior to staining. **(D)** Unaffected *ago1-27*cotyledon after Trypan blue staining showed some dye accumulation. **(L)** Unaffected *ago1-27* cotyledon after DAB staining showed no dye polymerization. **(E,K)** Affected *ago1-27* cotyledons prior to staining. **(F)** Affected *ago1-27*cotyledon after Trypan blue staining showed strong accumulation of dye in lesions (arrows). **(L)** Affected *ago1-27* cotyledon after DAB staining showed strong dye polymerization in lesions (arrows). Scale bar: 1 mm.

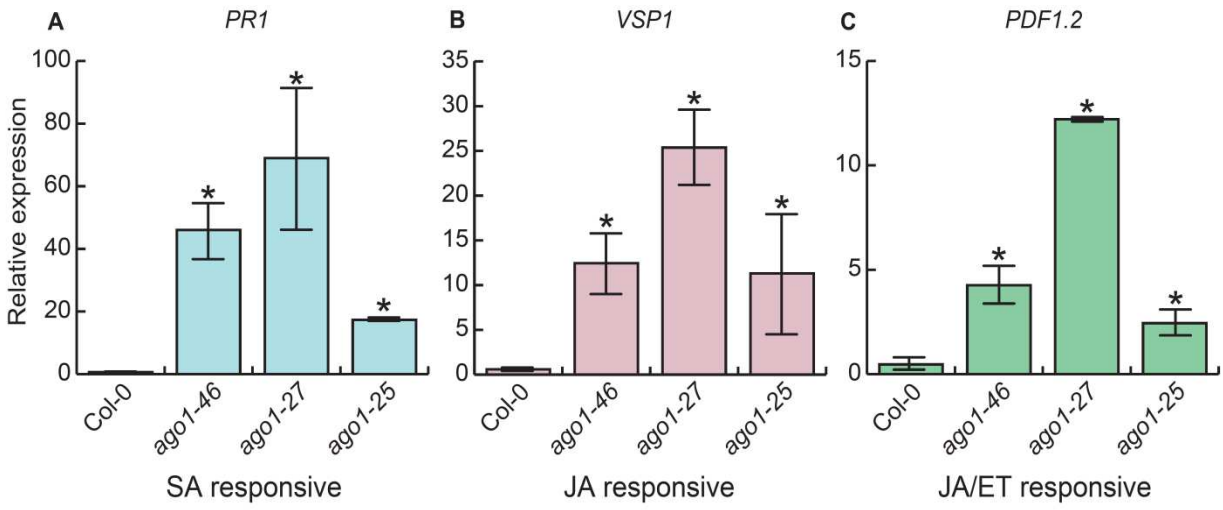

Figure 3.3: Marker genes of all three canonical defense hormone pathways were upregulated in *ago1* cotyledons. (A) *PR1* (salicylic acid [SA] responsive); **(B)** *VSP1* (jasmonate [JA] responsive); **(C)** *PDF1.2* (jasmonate/ethylene [JA/ET] responsive) expression were dramatically upregulated in 10 day-old *ago1-46*, *ago1-27,* and *ago1-25* cotyledons in full spectrum light. Expression was measured by qRT-PCR; all assayed genes were normalized to *UBC* expression. Error bars indicate standard error of the mean across at least two replicates of cotyledons harvested from 18 pooled seedlings.

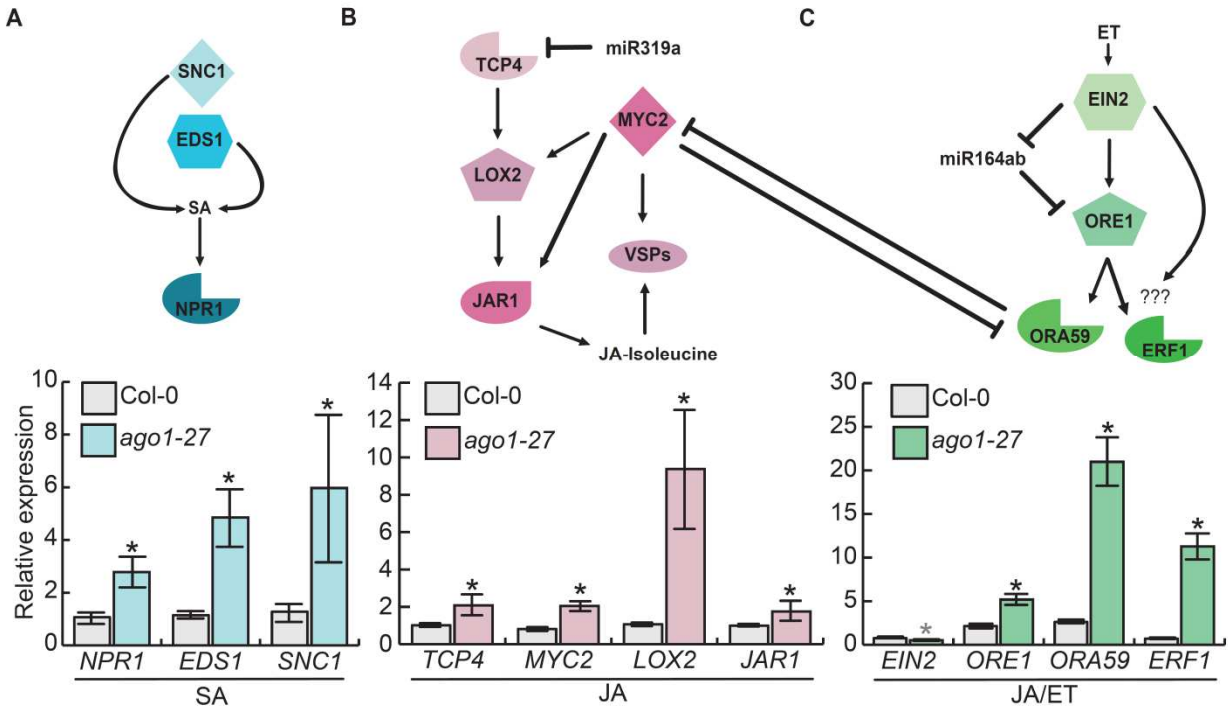

Figure 3.4: Genes in all three defense hormone pathways, including miRNA target genes, were upregulated in *ago1-27* cotyledons. (A) Top, pathway diagram indicates pathway connection of three tested SA genes, none of which are miRNA targets. Bottom, *NPR1, EDS1,* and *SNC1* were upregulated in *ago1-27* seedlings relative to wild-type. **(B)** Top, pathway diagram indicates pathway connection of four tested JA genes, the most upstream of which, TCP4, is a miRNA target gene. Bottom, the canonical jasmonate signaling and biosynthesis genes *TCP4, LOX2, MYC2, VSP2* and *JAR1* were strongly upregulated. **(C)** Top, pathway diagram indicates pathway connection of four tested JA/ET genes. The most upstream gene, *EIN2*, acts in an incoherent feed-forward loop with mir164ab and its target gene *ORE1*. ET and JA pathways show cross-regulation via *ORA59* and *MYC2.* Bottom, (JA/ET) markers *ORE1, ORA59,* and *ERF1* were significantly upregulated in *ago1-27* cotyledons relative to wild-type; in contrast, *EIN2* was significantly downregulated in *ago1-27* cotyledons. All assayed genes are normalized to *UBC* expression. Error bars indicate standard error of the mean across three to four replicates of cotyledons harvested from 18 pooled seedlings. Black stars represent significant upregulation in *ago1-27* cotyledons; grey star (*EIN2*) represents significant downregulation in *ago1-27* cotyledons.

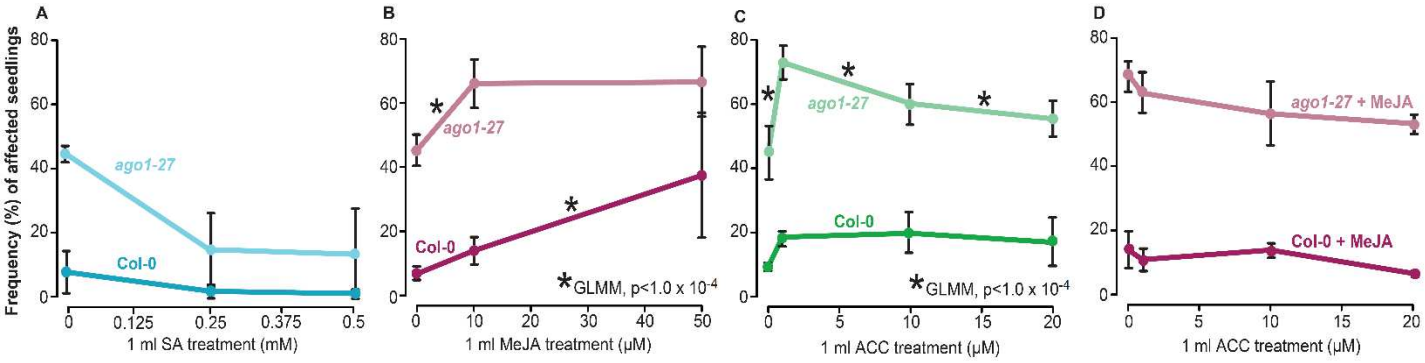

Figure 3.5: Methyl jasmonate (MeJA) treatment was sufficient to induce lesions. (A) Under high salicylic acid conditions, fewer seedlings were affected for both wild-type and *ago1-27* in full spectrum light. **(B)** At 10 µM MeJA, *ago1-27* was significantly more responsive compared to wild-type (GLMM, testing for interaction between genotype and treatment: p< 1.0E-04) whereas at the 50 µM MeJA treatment, wild-type was more responsive (GLMM: p<1.0E-04). **(C)** At 1 µM ACC (ethylene pre-cursor molecule), *ago1-27* was more responsive than wild-type, (GLMM: p<1.0E-04), reaching a frequency of affected seedlings similar to *ago1-27* seedlings at 10 µM MeJA. At higher doses, ACC repressed the lesion phenotype in *ago1-27* (GLMM, p< $1x10^{-4}$) and had no further effect on wild-type. **(D)** Combining10 µM MeJA with varying ACC concentrations yielded no significant change, albeit frequencies of affected seedlings declined. n = 72-144 individuals per replicate, two to five replicates. The difference in responsiveness between genotypes was modeled using GLMM, testing for interaction between genotype and treatment with replicate and number of seedlings set as random variables (p<1.0E-04, for all possible p-values, refer to **Supplemental table 3.4**).

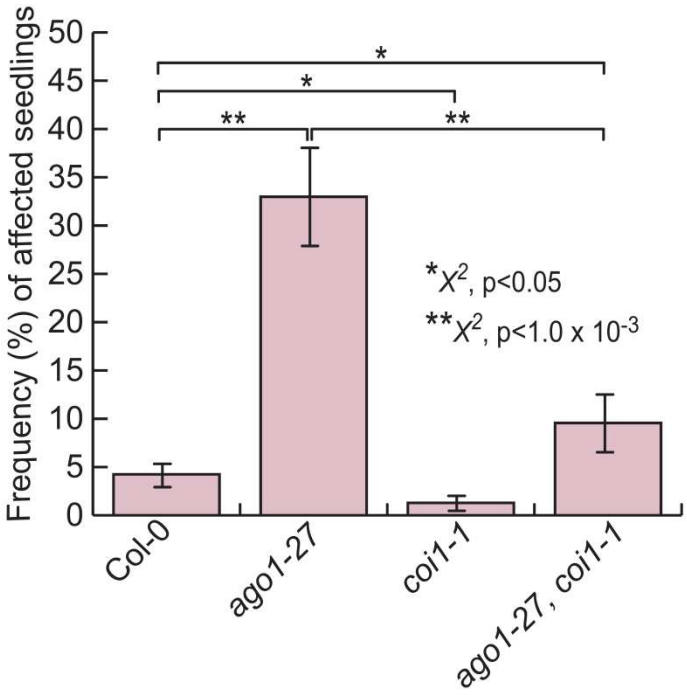

Figure 3.6: Disruption of JA perception suppresses lesion phenotype. *coi1-1* mutant seedlings showed significantly fewer affected seedlings than wild-type ($p<0.05$). *ago1-27; coi1-1* double mutant seedlings showed dramatically fewer affected seedlings than *ago1-27* single mutant seedlings ($p<1.0E-03$); however, frequency of affected seedlings was significantly higher than in wild-type ($p<0.05$). Statistical significance was calculated using χ^2-test of significance (**$p<1.0E-03$, *$p<0.05$, for all reported p-values, refer to **Supplemental table 3.4**). n = 72-144 individuals per replicate, four replicates; error bars represent standard error of the mean across biological replicates.

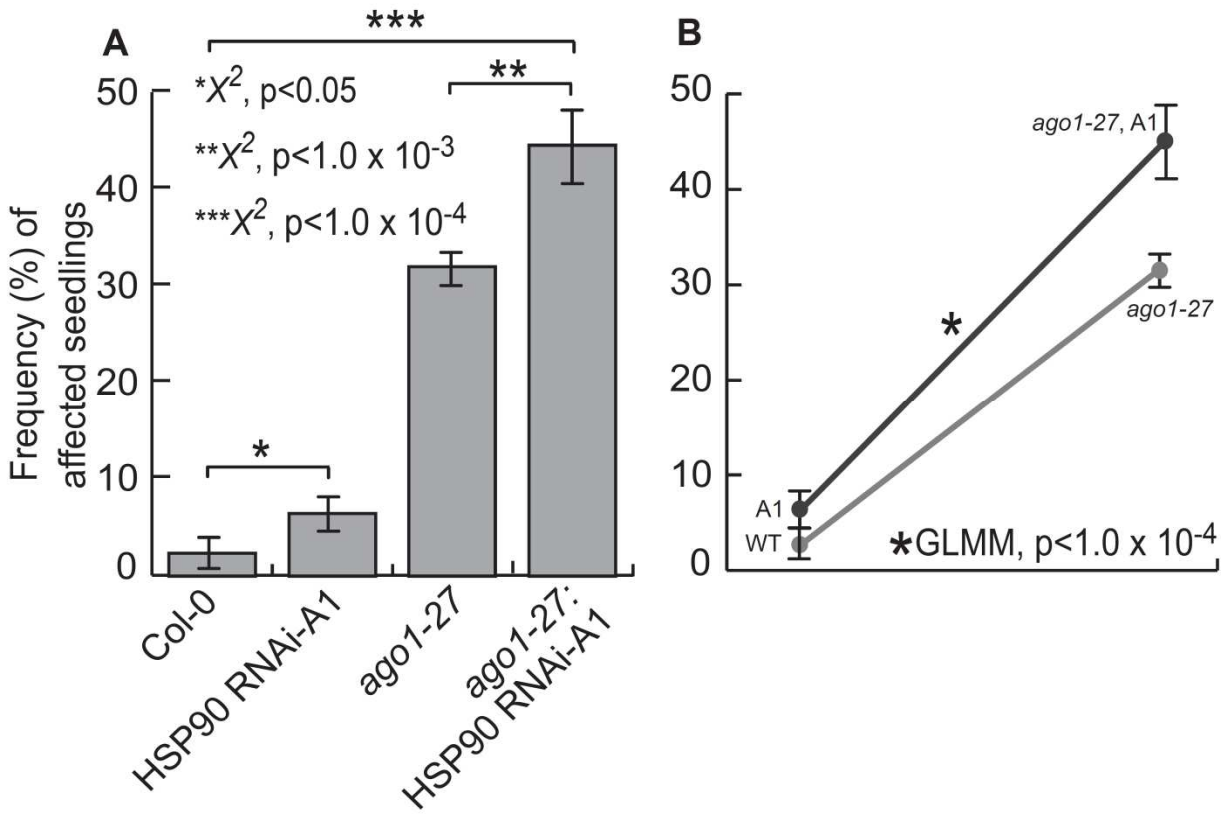

Figure 3.7: *AGO1* and *HSP90* genetically interact. (A) HSP90 RNAi-A1 seedlings showed significantly more affected seedlings than wild-type ($p<0.05$). *ago1-27;* HSP90 RNAi-A1 double mutant seedlings showed significantly more affected seedlings than *ago1-27* single mutant seedlings ($p<1.0E-03$). Error bars represent standard error of the mean across two replicates of n = 108 seedlings. (B) The *ago1-27* mutation showed higher penetrance in the presence of HSP90 RNAi-A1 (*ago1-27*, A1) in full spectrum light (GLMM, $p<1.0E-04$). Statistical significance was calculated using χ^2-test of significance (***$p<1.0E-04$, ** 1.0E-03, *$p<0.05$, for all possible p-values, refer to **Supplemental table 3.4**). n = 72-144 individuals per replicate, two replicates. Error bars represent standard error of the mean across biological replicates.

3.5 Materials and Methods

Plant Growth Conditions: Columbia-0 (Col-0) was used as wild-type reference. *ago1-46*, *ago1-27*, and *ago1-25*, HSP90 RNAi-A1, *coi1-1* and *ein2-1* were in the Col-0 background (**Supplemental table 3.2**). For experiments, seeds were sterilized with ethanol and plated onto 1× Murashige and Skoog (MS) basal salt medium supplemented with 1× MS vitamins, 1% (wt/vol) sucrose, 0.05% MES (wt/vol), and 0.24% (wt/vol) phytagel. After stratification in the dark at 4 °C for 5 days, plates were transferred to an incubator (Conviron) that was set to long day (LD) (16L:8D at 22 °C:20 °C), with light supplied at 100 μmol·m−2·s−1 by cool-white fluorescent bulbs; for control plates (filtered light), a long-pass yellow filter that blocks 454 nm light was placed in front of the bulbs. Seedlings were then scored for lesions at day 10. The accession numbers for genes analyzed in this research are listed in **Supplemental table 3.2.**

Genotyping and gene expression analyses:

RNA Extractions and Quantitative Real-Time PCR: Total RNA was extracted from 30 mg frozen tissue using the SV Total RNA Isolation System (Promega). Subsequently, 2 μg of RNA were subjected to DNase treatment using Ambion Turbo DNA-free Kit (Applied Biosystems). RNA integrity and purity were checked with an Agilent Bioanalyzer using the RNA 6000 Nano Kit (Agilent Technologies). For cDNA synthesis, 200 ng of DNase-treated RNA was reverse-transcribed using the Transcriptor First Strand cDNA Synthesis Kit (Roche) and oligo dT primers. Transcript abundance was determined by real-time quantitative PCR using the LightCycler 480 system (Roche), with LightCycler 480 SYBR Green I Master (Roche) and the following PCR conditions: 5 min at 95 °C, followed by 35 cycles of 15 s at 95 °C, 20 s at 55 °C, and 20s at 72 °C. To ensure that PCR products were unique, a melting curve analysis was

performed after the amplification. *UBC* expression (AT5G25760) was used as a reference. All quantitative RT-PCR primers were designed with Primer3Plus software (http://www.primer3plus.com/). Sequences for real-time PCR primers are shown in **Supplemental table 3.1**. The accession numbers for genes analyzed in this research are listed in **Supplemental table 3.2**. Relative quantification was determined with the ΔΔCT Method (Fryer et al., 2011). Error was calculated using standard error of the mean across at least three biological replicates.

DNA Extractions and genotyping: Arabidopsis genomic DNA was extracted for genotyping analysis by PCR using the CTAB method (Weigel and Glazebrook, 2002). The RNAi-A1, ago1-27, coi1-1, and *ein2-1* alleles were genotyped by using the primers in **Supplemental table 3.3**. PCR conditions for *ago1-27* genotyping is as follows: 5 min at 94 °C, followed by 35 cycles at 30 s at 94 °C, 30 s at 55 °C, 1 min at 72 °C. PCR product was then digested with Bsp1286I at 37 °C, which cuts wild type sequence. PCR conditions for *coi1-1* genotyping is as follows: 5 min at 94 °C, followed by 35 cycles at 30 s at 94 °C, 30 s at 55.7 °C, 1 min at 72 °C. PCR product was then digested with XcmI, which cuts the wild type sequence. PCR conditions for *ein2-1* genotyping is as follows: 5 min at 94 °C, followed by 35 cycles at 30 s at 94 °C, 30 s at 63.2 °C, 2 min at 72 °C. PCR product was then digested with BsrBI, which cuts the wild type sequence. HSP90 RNAi-A1 plants were genotyped using two PCR assays. For RNAi construct identification, the Lm1 and Rc3 primers (**Supplemental table 3.3**) were used with following parameters: 3 min at 95 °C, followed by 30 cycles of: 30 s at 95 °C, 30 s at 55 °C, and 1 min 15 s at 72 °C. For wild type sequence identification, the Lw1 and Rc3 primers (**Supplemental table 3.3**) were used with the previously described PCR conditions.

Hormone response assays:

Methyl Jasmonate: Seedlings were grown as previously described in **Plant Growth Conditions** under full spectrum light conditions. Five days post germination seedlings in groups of 36 were sprayed with 1 ml of water, 1 ml of 10 μM methyl jasmonate solution (Sigma Aldrich), or 1 ml of 50 μM methyl jasmonate solution and returned to incubator. Seedlings were then scored for lesions at day 10.

Salicylic acid: Seedlings were grown as previously described in **Plant Growth Conditions** under full spectrum light conditions. Five days post germination seedlings in groups of 36 were sprayed with 1 ml of 1xPBTx, 1ml of 10 μM salicylic acid in 1xPBTx, or 1 ml of 100 μM salicylic acid in 1xPBTx and returned to incubator. Seedlings were then scored for lesions at day 10.

ACC (ethylene precursor): Seedlings were grown as previously described in **Plant Growth Conditions** under full spectrum light conditions. Five days post germination seedlings in groups of 36 were sprayed with 1 ml of water, 1 ml of 1 μM ACC, 1 ml of 10 μM ACC or 1 ml of 20 μM ACC in water and returned to incubator. Seedlings were then scored for lesions at day 10.

Callus induction: To test for callus-hormone responsivity, plants were grown for 10 days under full spectrum light conditions. Affected and unaffected tissue was then excised using a Pasteur pipette tip and plated on media with varying levels of callus inducing hormones. Media with the low concentration of callus-inducing hormones: 250 μl of 2000x 2,4-D (final concentration 0.25 mg/liter), 250 μl 2000x kinetin (final concentration 0.025mg/liter), 1x Gamborg's B5 salts, 20g glucose, 0.5g MES, pH 5.7. Media with high concentration of callus-inducing hormones: 500 μl of 2000x 2,4-D (final concentration 0.5 mg/liter), 500 μl 2000x kinetin (final concentration 0.05mg/liter), 1x Gamborg's B5 salts, 20g glucose, 0.5g MES, pH 5.7. Plates were then placed

under yellow filter light conditions (to maintain quality of hormones) and were then scored at 10 days post callus induction using scoring index described in **Supplemental Figure3. 2**.

Hypersensitive response assays:

Trypan Blue staining: Fresh affected and unaffected cotyledons were collected and then treated with Trypan blue staining solution. Trypan blue staining solution was prepared as follows: add Trypan blue (Sigma Aldrich) to lactophenol (10 ml lactic acid, 10 ml glycerol, 10 ml phenol, 10 ml water) to a concentration of 2.5 mg/ml. Two volumes ethanol were then added to Trypan blue/lactophenol solution. Staining solution was added to fresh tissue and boiled for 1 min (100 oC). Tissue was then allowed to incubate in staining solution for 5-10 minutes at room temperature while rotating. Stain solution was removed by washing with lactophenol/ethanol solution. Samples were then mounted on glass slides with glycerol (70% w/v) and photographed with a Canon Power Shot S5 IS camera. Images were edited using Adobe photoshop CS3.

DAB: Fresh affected and unaffected cotyledons were collected and then treated with 3,3'-diaminobenzidine (DAB, Sigma Aldrich) (1mg/ml, pH 3.8) staining solution for 8 hours. Tissue was then de-stained with 100% ethanol. Samples were then mounted on glass slides with glycerol (70% w/v) and photographed with a Canon Power Shot S5 IS camera. Images were edited using Adobe photoshop CS3.

Phenotyping assays: Methyl jasmonate screening: 10 day old seedlings were sprayed with 50-100 uM methyl jasmonate (Sigma Aldrich) solution in water. Seedlings were incubated for an additional three days and were then screened for response to jasmonate (i.e. anthocyanin accumulation)

ACC screening: For experiments, seeds were sterilized with ethanol and plated onto 1× Murashige and Skoog (MS) basal salt medium supplemented with 1× MS vitamins, 1% (wt/vol) sucrose, 0.05% MES (wt/vol), and 0.24% (wt/vol) phytagel. Experimental plates were made to 10 μM ACC. After stratification in the dark at 4 °C for 5 d, plates were transferred to an incubator (Conviron) that was set to long day (LD) (16L:8D at 22 °C:20 °C), with light supplied at 100 μmol·m−2·s−1 by cool-white fluorescent bulbs; for control plates (filtered light) for three hours and then wrapped in aluminum foil. Plates were incubated for seven days and then scored for triple response.

Statistical analysis: All statistical analyses were performed in R Version i386 3.1.2. Comparisons of seedling lesion frequencies were performed with the $\chi 2$-test. Seedling lesion frequency was modeled with binomial regression using a mixed model from the MASS package's glmmPQL function (Ripley et al., 2015). Replicate and individual within a replicate were designated as random effects, whereas genotype and treatment were designated as fixed effects.

3.6 Supplemental materials

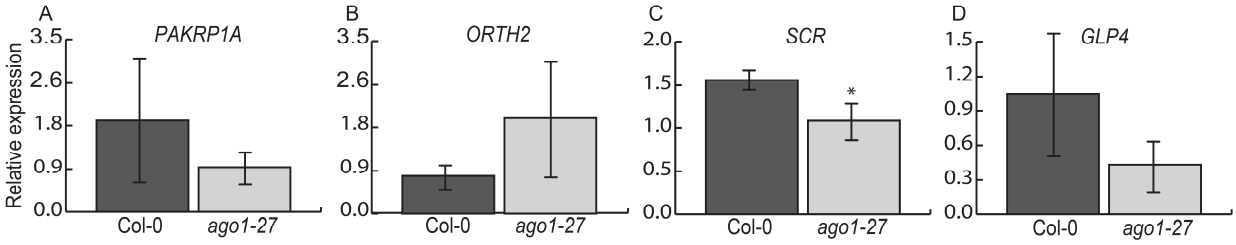

Supplemental figure 3.1: Plant stem cell marker genes are not upregulated in full spectrum light-grown *ago1-27* seedlings. (A-D) *ago1-27* cotyledons did not show significantly higher expression of the stem cell marker genes *PAKRP1A* (shoot apical meristem marker), *ORTH2* (shoot apical meristem marker), *SCR* (root apical meristem marker), and *GLP4* (root apical meristem marker). Expression of all assayed genes was normalized to *UBC21* expression. Error bars indicate standard error of the mean across three to four replicates of cotyledons harvested from 18 pooled seedlings. Black star represents significant downregulation in *ago1-27* cotyledons.

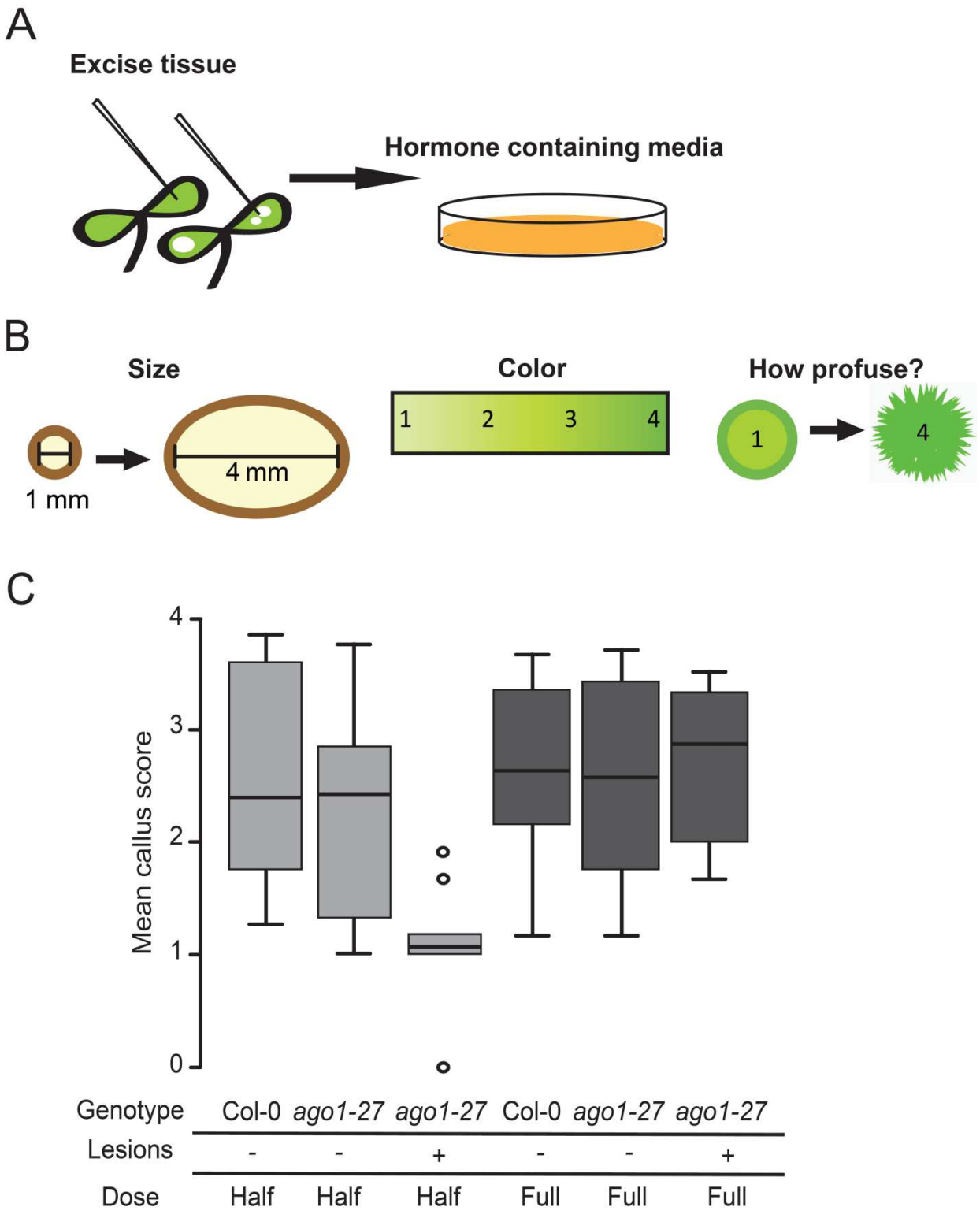
A
Excise tissue
Hormone containing media
B
Size
1 mm
4 mm
Color
1
2
3
4
How profuse?
1
4
C
Mean callus score
0
1
2
3
4
Genotype
Col-0
ago1-27
ago1-27
Col-0
ago1-27
ago1-27
Lesions
-
-
+
-
-
+
Dose
Half
Half
Half
Full
Full
Full

Supplemental figure 3.2: *ago1-27* lesion tissue did not show enhanced callus formation. **(A)** Schematic representation of experimental procedure. Affected and unaffected tissue was excised from 10 day-old *ago1-27* cotyledons and 10 day-old unaffected tissue was excised from wild-type cotyledons. Tissue was placed on callus-inducing media at the recommended hormone doses and half the recommended doses as described previously (Weigel and Glazebrook, 2002). Plates were scored five days later for callus induction. **(B)** Callus scoring index. Callus formation was scored based on three criteria: length at longest axis, color, and profuseness. These separate criteria were given a score of 1-4, with a score of 4 being the most callus-like of criteria. Scores were averaged to compute callus scores. **(C)** Mean callus score of tested genotypes and treatments. At the lower hormone dose, *ago1-27* lesion tissue does not form callus tissue at all.

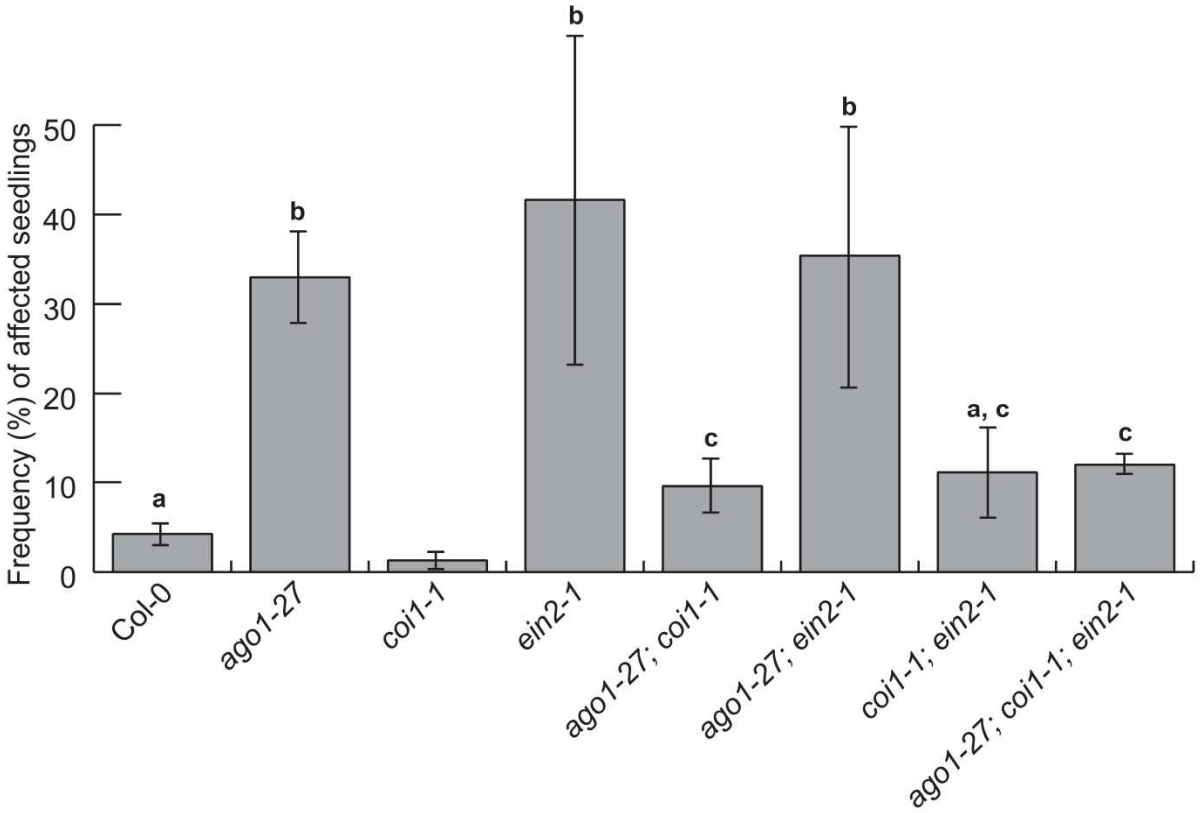

Supplemental figure 3.3: The disruption of JA perception in *coi1-1* is epistatic to both *ago1-27*- and *ein2-1*-dependent lesion phenotypes. *ago1-27* and *ein2-1* single mutant seedlings showed similar frequencies of affected individuals as *ago1-27*; *ein2-1* double mutant seedlings. *coi1-1* suppressed the lesion phenotype in all three combinations: *coi1-1*; *ein2-1*, *ago1-27*; *coi1-1*, and *ago1-27*; *coi1-1*; *ein2-1*. Statistical significance was calculated using the χ2-test of significance. Shared letters (a, b, c) denote statistically similar genotypes. Data for Col-0, *ago1-27*, *coi1-1*, and *ago1-27*; *coi1-1* also appears in Figure 6. For all reported p-values, refer to Supplemental Table 4. n =72-144 individuals per replicate, two-four replicates; error bars represent standard error of the mean across biological replicates.

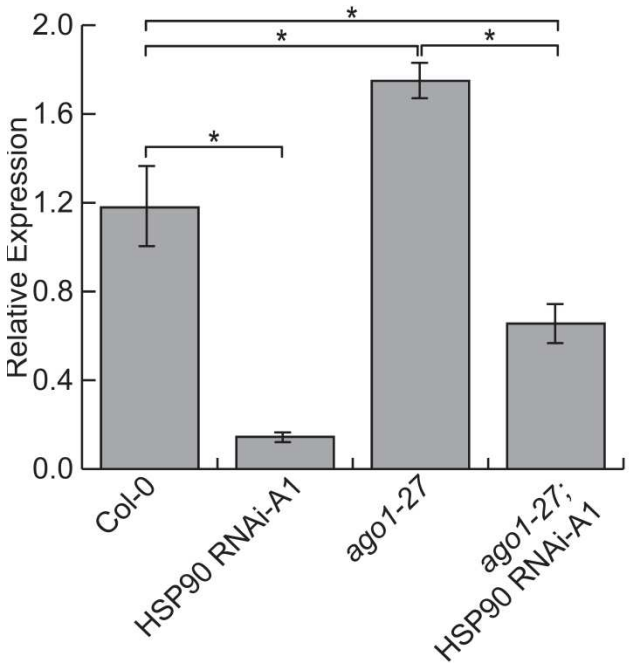

Supplemental figure 3.4: HSP90 expression under white light conditions is reduced by RNAi. qRT-PCR shows that *HSP90* expression is significantly reduced in both the single HSP90 RNAi-A1 mutant and the double mutant *ago1-27*; HSP90 RNAi-A1. Error bars indicate values for standard error of the mean across three biological replicates. *HSP90* expression was normalized to the housekeeping gene *UBC21*.

Supplemental Table 1: qRT-PCR primers

Gene	Accession number	Primer	Primer sequence
GLP4	AT1G18970	GLP4 F 1	ATGGCTTTCCATGCAAATCA
		GLP4 R 1	TCGAGATTCCTAAAGTGTTTAGACC
SCR	AT3G54220	SCR F 1	CTCAAACTTTCGAACCTCTCTATC
		SCR R 1	GGGAACAGTGGCCGTCA
ORTH2	AT1G57820	ORTH2 F 1	GTCTCACAAGGAGAAGCG
		ORTH2 R 1	GGCTCATTGTCACATCTAACGAA
PAKRP1A	AT4G14150	PAKRP1A F 1	GGATGTGTCATCATGCCC
		PAKRP1A R 1	TATTTCTAATCGTAGGAGAGACGC
PDF1.2	AT5G44420	PDF1.2 F 1	ATGGCTAAGTTTGCTTCCA
		PDF1.2 R 1	TTAACATGGGACGTAACAGATAC
PR1	AT2G14610	PR1 F 1	TCTTCCCTCGAAAGCTCAAG
		PR1 R 1	AAGGCCCACCAGAGTGTATG
VSP1	AT5G24780	VS1 F 1	ACCTCTTGGAACTCGGGATT
		VSP1 R 1	ACCACTTGCGTCAACTTCG
EDS1	AT3G48090	EDS1 F 1	TCTGTGGAAATGGCTGTGAG
		EDS1 R 1	CCAAAGGAGCTCCAAATGTC
NPR1	AT1G64280	NPR1 F 1	AGGCACTTGACTCGGATGAT
		NPR1 R 1	CCTCGGATTCCTATGGTTGA
SNC1	AT4G16890	SNC1 F 1	GCCGGATATGATCTTCGGAA
		SNC1 R 1	CGGCAAGCTCTTCAATCATGG
TCP4	AT3G15030	TCP4 F 1	CAACATCACCACCACACCTC
		TCP4 R 1	ACAGAAACCCTCCTCCGTTT
LOX2	AT3G45140	LOX2 F 1	TGAGGACTCATGCCTGTACG
		LOX2 R 1	ATTCCACCTCCGTTGACAAG
JAR1	AT2G46370	JAR1 F 1	TACGCGGGTGATCTACCTCT
		JAR1 R 1	AACCAACCGGTTTCTCCTCT
MYC2	AT1G32640	MYC2 F 2	GTGACGGATACGGAATGGTT
		MYC2 R 2	ATGCATCCCAAACACTCCTC
EIN2	AT5G03280	EIN2 F 1	AAAACCGGCTAAAGGCAAAT
		EIN2 R 1	TCAAAACCGAAGCCAAATTC
ORE1	AT5G39610	ORE1 F 1	CTGCTACTGCCATTGGTGAA
		ORE1 R 1	TCCAATAACCGGCTTCTGTC
ERF1	AT3G23240	ERF1 F 1	GATGGTTGTTCTCCGGTTGT
		ERF1 R 1	CCCAAAAGCTCCTCAAGGTA
ORA59	AT1G06160	ORA59 F 1	GGCTCTCGCTTATGATCAGG
		ORA59 R 1	GGACGGTTTCTCATGGAGTG
UBC	AT1G04810	UBC F 1	GACCAAGATATTCCATCCTA
		UBC R 1	GTTAAGAGGACTGTCCG
HSP90	AT5G52640	HSP90 F 1	GGTTCTGAAAACTTCTAATATGTCG
		HSP90 R 1	TGACACAAACCCAACCCTAGA

Supplemental Table 2: Accession numbers of genes analyzed

Gene	Accession number
AGO1	AT1G48410
COI1	AT2G39940
EIN2	AT5G03280
GLP4	AT1G18970
SCR	AT3G54220
ORTH2	AT1G57820
PAKRP1A	AT4G14150
PDF1.2	AT5G44420
PR1	AT2G14610
VSP1	AT5G24780
EDS1	AT3G48090
NPR1	AT1G64280
SNC1	AT4G16890
TCP4	AT3G15030
LOX2	AT3G45140
JAR1	AT2G46370
MYC2	AT1G32640
EIN2	AT5G03280
ORE1	AT5G39610
ERF1	AT3G23240
ORA59	AT1G06160
HSP90.1	AT5G52640
UBC	AT1G04810

Supplemental Table 3: Genotyping primers

Gene	Accession number	Primer	Primer sequence	Restriction enzyme/allele cut
AGO1	AT1G48410	F	ACCACGTTCTTTGGGATGAG	Bsp1286I/wild-type
		R	TCTACCCATTCCACCTC	
COI1	AT2G39940	F	GGGGAGATAAGGGATATGAATGC	Xcm1/wild-type
		R	TTGTGGAAACCCCAAAACTC	
EIN2	AT5G03280	F	CGCCATCTTTGTTTCAACAATCAGATCC	BsrB1/wild-type
		R	CCAGAGGAAAGAGAGTTGGATGTAAAGTACTCTACCGCT	
HSP90-RNAi A1	AT5G52640	Lw1	GATGCGGGATATGGCTGGACT	Produces 1194 bp band with Rc3 primer for wild-type
		Lm1	CGGCAGTTCATCAGGGCTAA	Produces 850 bp band with Rc3 primer for mutant
		Rc3	TATCACCTCGTTAGGGGCCA	

Supplemental Table 4: Reported p-values

Figure	Comparison	Test	P-value
1	Col-0 Yellow vs. Col-0 White	Chi-square	0.89
1	Col-0 Yellow vs. *ago1-27* Yellow	Chi-square	0.77
1	Col-0 Yellow vs. *ago1-46* Yellow	Chi-square	0.26
1	Col-0 White vs. *ago1-27* White	Chi-square	4.00E-21
1	Col-0 White vs. *ago1-46* White	Chi-square	8.00E-04
1	*ago1-27* Yellow vs. *ago1-27* White	Chi-square	9.00E-26
1	*ago1-46* Yellow vs. *ago1-46* White	Chi-square	5.00E-04
1	*ago1-25* White vs. Col-0 White	Chi-square	1.00E-05
1	*ago1-25* Yellow vs. *ago1-25* White	Chi-square	0.95
1	*ago1-25* Yellow vs. Col-0 Yellow	Chi-square	1.00E-06
1	*ago1-27* White vs. *ago1-25* White	Chi-square	2.00E-09
1	*ago1-27* vs. *ago1-25*	GLMM	< 1.00E-04 (towards *ago1-27*)
5	Col-0 vs. *ago1-27*, 0 and 10 µM MeJA	GLMM	< 1.00E-04 (towards *ago1-27*)
5	Col-0 vs. *ago1-27*, 0 and 50 µM MeJA	GLMM	< 1.00E-04 (towards Col-0)
5	Col-0 vs. *ago1-27*, 10 and 50 µM MeJA	GLMM	< 1.00E-04 (towards Col-0)
5	Col-0 vs. *ago1-27*, all MeJA treatments	GLMM	< 1.00E-04 (towards Col-0)
5	Col-0 vs. *ago1-27*, 0 and 250 µM SA	GLMM	0.71
5	Col-0 vs. *ago1-27*, 0 and 500 µM SA	GLMM	0.86
5	Col-0 vs. *ago1-27*, 250 and 500 µM SA	GLMM	0.51
5	Col-0 vs. *ago1-27*, all SA treatments	GLMM	0.91
5	Col-0 vs. *ago1-27*, 0 and 1 µM ACC	GLMM	< 1.00E-04 (towards *ago1-27*)
5	Col-0 vs. *ago1-27*, 0 and 10 µM ACC	GLMM	0.35
5	Col-0 vs. *ago1-27*, 0 and 20 µM ACC	GLMM	< 1.00E-04 (towards *ago1-27*)
5	Col-0 vs. *ago1-27*, 1 and 10 µM ACC	GLMM	< 1.00E-04 (towards *ago1-27*)
5	Col-0 vs. *ago1-27*, 1 and 20 µM ACC	GLMM	< 1.00E-04 (towards *ago1-27*)
5	Col-0 vs. *ago1-27*, 10 and 20 µM ACC	GLMM	0.07
5	Col-0 vs. *ago1-27*, all ACC treatments	GLMM	0.09
5	Col-0 vs. *ago1-27*, 0 and 1 µM ACC, 10 µM MeJA	GLMM	0.22
5	Col-0 vs. *ago1-27*, 0 and 10 µM ACC, 10 µM MeJA	GLMM	0.15
5	Col-0 vs. *ago1-27*, 0 and 20 µM ACC, 10 µM MeJA	GLMM	0.38
5	Col-0 vs. *ago1-27*, 1 and 10 µM ACC, 10 µM MeJA	GLMM	0.21
5	Col-0 vs. *ago1-27*, 1 and 20 µM ACC, 10 µM MeJA	GLMM	0.88
5	Col-0 vs. *ago1-27*, 10 and 20 µM ACC, 10 µM MeJA	GLMM	0.20
5	Col-0 vs. *ago1-27*, all ACC treatments, 10 µM MeJA	GLMM	0.07
6	Col-0 vs. *ago1-27*	Chi-square	1.15E-55
6	Col-0 vs. *ago1-27; coi1-1*	Chi-square	3.60E-03
6	Col-0 vs. *coi1-1*	Chi-square	0.02
6	ago1-27 vs. *ago1-27; coi1-1*	Chi-square	2.69E-15
6	ago1-27 vs. *ago1-27; ein2-1*	Chi-square	0.35
Supp. 4	Col-0 vs. *ago1-27; coi1-1; ein2-1*	Chi-square	1.8E-03
Supp. 4	Col-0 vs. *coi1-1; ein2-1*	Chi-square	0.76
Supp. 4	Col-0 vs. *ein2-1*	Chi-square	1.30E-27
Supp. 4	ago1-27 vs. *ago1-27; coi1-1; ein2-1*	Chi-square	1.76E-07
Supp. 4	ago1-27 vs. *coi1-1; ein2-1*	Chi-square	3.86E-21
Supp. 4	ago1-27 vs. *ein2-1*	Chi-square	0.31
7	Col-0 vs. HSP90 RNAi-A1	Chi-square	0.40
7	Col-0 vs. *ago1-27*	Chi-square	4.67E-09
7	Col-0 vs. *ago1-27*; HSP90 RNAi-A1	Chi-square	3.98E-25
7	*ago1-27* vs. *ago1-27*; HSP90 RNAi-A1	Chi-square	7.6E-03
7	*ago1-27* White vs. *ago1-27;* HSP90 RNAi-A1	GLMM	< 1.00E-04 (towards *ago1-27;* RNAi-A1)

Chapter 4: ARGONAUTE 1 buffers standing genetic variation[6,7]

Abstract

Phenotypic robustness, a fundamental property of biological systems, is the measure of an organism's ability to withstand genetic and environmental perturbations. Robustness is thought to arise from features of genetic networks, such as connectivity, redundancy, and feedback. Targeted perturbation of these features can lead to expression of previously hidden genetic variation often with significant effects on phenotype. We used STAIRS (STepped Aligned Inbred Recombinant Strains) made between Landsberg *erecta* and Col-0 backgrounds, and crossed them with an *argonaute 1* (*ago1*) mutation (Col-0 background). If *AGO1* could confer genetic robustness, we would observe several genomic loci revealing genetic variation for correlated phenotypes, examples of which are days to flowering and leaf number at flowering time. Using these tools, we found a background-specific locus on chromosome 5 that decouples days to flowering and leaf number at flowering time. To further identify causative variants in this region, we performed bulk segregant analysis for individuals that had six or fewer leaves at flowering. We identified the Landsberg *erecta hua2-5* (*enhancer of ag-4 2*) allele as causative of the phenotypic uncoupling. Based on these data, we predict that HUA2 and AGO1-miRNAs have overlapping regulation of flowering-related phenotypes.

[6] Portions of this chapter are adapted from "Loss of *ARGONAUTE1* and *HUA2* uncouple flowering time traits in *Arabidopsis thaliana,*" Manuscript in preparation, by T. Lemus*, G. A. Mason*, J. Cuperus**, and C. Queitsch. Co-first authors*. Corresponding author**.

[7] T.L. and C.Q. conceived the project. T.L. and G.A.M executed early seedling phenotyping experiments. T.L. performed STAIRS crosses and analyses. T.L. and G.A.M. performed data analysis and created figures. T.L., G.A.M., and J.C. performed mapping by sequencing. G.A.M. and J.C. performed validation experiments.

4.1 Introduction

Genetic networks are robust to environmental and genetic perturbations. This robustness ensures that developmental and physiological processes remain stable to produce stereotyped traits[273-275]. Network disruptions are thought to decrease robustness and produce increased phenotypic variation on the scale of single to many phenotypes[9,276-278].

One source of developmental and environmental robustness include post-transcriptional regulation by small RNAs. Small RNAs regulate the expression of target genes in a sequence-specific manner by either degrading their mRNA[279,280] or inhibiting their translation[281]. Small RNAs are loaded into one of the ARGONAUTE (AGO) effector proteins to form the RNA-induced silencing complex (RISC)[237]. In plants, most endogenous post-transcriptional gene regulation is mediated by AGO1 loaded with microRNAs[279,280]. Some microRNAs (miRNAs) are known to act as robustness regulators by buffering stochastic[282], environmental[10] and genetic variation[283].

Several studies in various organisms suggest that AGO proteins are chaperoned by HSP90. HSP90 physically interacts with AGO proteins in yeast[284], flies[126,285,286], humans[287], *Tetrahymena*[288], and tobacco cell extracts[218,289]. Because of miRNAs' role in buffering environmental and genetic perturbations and AGO1's HSP90-client status, we set out to investigate the extent to which AGO1 perturbation (1) affects phenotypic variation in isogenic *A. thaliana* seedlings, (2) releases genetic variation in divergent backgrounds, and (3) whether AGO1-dependent loci overlap with HSP90-dependent loci.

We found that AGO1 perturbation alone sufficed to significantly increase phenotypic variation in several early seedling traits. Next, we set out to test whether AGO1 perturbation releases cryptic genetic variation. To do so, we crossed the hypomorphic *ago1-27* mutant with

Col-0 lines with single chromosome substitutions from the divergent *A. thaliana* strain, Landsberg *erecta* (L*er)* (STAIRS, STepped Aligned Inbred Recombinant Strains)[290]. We then measured five well-studied quantitative traits and found instances of AGO1-dependent buffered variation. Specifically, we observed that *ago1-27* combined with the presence of L*er* DNA on the top of chromosome 5 uncoupled flowering time from rosette leaf number, two highly correlated traits that are used interchangeably to assess the onset of flowering[291,292]. We go on to demonstrate that the AGO1-dependent polymorphism resides in *ENHANCER OF AG-4 protein 2* (*HUA2*), a known regulator of flowering time[176,293]. Finally, we show that days to flowering and number of leaves at flowering time are uncoupled in presence of both *HUA2* and *AGO1* malfunction in the Col-0 background.

4.2 Results

4.2.1 ago1 *mutant plants show increased phenotypic variation*

We examined several morphological and quantitative phenotypes of hypomorphic *ago1-46* and *ago1-27* mutants. We observed that 10-day old *ago1-46* and *ago1-27* seedlings showed increased phenotypic variation in morphological features such as lesions in cotyledons, rosette symmetry, and organ defects compared to wild-type (Col-0) seedlings (Student's unpaired t-test: $p<0.05$) (**Figure 4.1A**). The more severe *ago1-27* mutant also showed subtly higher numbers of abnormal phenotypes compared to the less severe *ago1-46* mutant (**Figure 4.1A)**.

We next examined hypocotyl length in dark grown seedlings, a readily assayed quantitative trait that is known to show increased variance in response to HSP90 perturbation[294]. Like earlier results with HSP90[152], we found that dark-grown *ago1-27* seedlings showed a lower mean (Wilcoxon test: $p<1.0E-15$) and significantly greater variance of hypocotyl length than

Col-0 (Levene's test: p<1.0E-03) (**Figure 4.1B**). We therefore concluded that fully functional AGO1 maintains phenotypic robustness and buffers developmental noise among isogenic seedlings for both early morphological and quantitative traits, as was observed for HSP90[152,274,294].

4.2.2 AGO1 *perturbation reveals and conceals* genetic *variation*

HSP90 buffers both developmental noise and genetic variation[274,294]. Therefore, we next tested if *AGO1* perturbation could reveal genetic variation and whether AGO1-dependent loci overlap with known HSP90-dependent loci. We crossed the *ago1-27* mutant (Col-0 background) to four STepped Aligned Inbred Recombinant Strains (STAIRS)[290]. STAIRS are Col-0 lines with partial chromosome substitutions from the divergent *A. thaliana* strain Landsberg *erecta* (L*er*) and exist for chromosomes 1, 3 and 5. Since *AGO1* is located on chromosome 1, we excluded the respective STAIRS from our analyses. The resulting progeny from the *ago1-27* x STAIRS crosses should contain recently acquired genotypic differences that have not had time to evolve new network regulations to compensate for them, and therefore depend on capacitors like HSP90 to attain robust phenotypes.

We measured dark-grown hypocotyl length, seedling root length, rosette diameter at flowering, rosette leaf number at flowering, and days to flowering time for each *ago1-27* x STAIRS F_2 population. These phenotypes were selected because they are well-studied, readily measurable, and show evidence of HSP90 buffered variation in previous studies[295], enabling the planned comparisons of HSP90-dependent and putative AGO1-dependent variation.

AGO1 reveals genetic variation affecting a quantitative trait *X* if one of the following scenarios is met: (1) wild-type plants of Col-0 and L*er* backgrounds have similar distributions of a trait, but the distribution of that trait in Col-0 *ago1-27* and L*er ago1-27* plants differ

significantly, or (2) wild-type Col-0 and L*er* plants differ significantly in their distribution of a trait, yet Col-0 *ago1-27* and L*er ago1-27* plants show a significantly different relationship than observed for wild-type comparison.

Fundamentally, we assume that *AGO1* perturbation may alter the contributions of underlying genetic variation to a given quantitative trait. Therefore, revealing variation (*i.e.* increasing the contribution of a particular locus to a quantitative trait with a certain overall genetic contribution) should also be as common as concealing other variation (*i.e.* decreasing the contribution of other loci). Indeed, this phenomenon has been previously observed for HSP90 perturbation across many traits in *A. thaliana* Col-0-L*er* recombinant inbred lines[295]. We may also observe that the L*er* introgression acts epistatically and suppresses phenotypic differences between wild-type and *ago1-27*.

As predicted, we observe all three scenarios of epistasis (**Figure 4.1C**; **see Supplemental figure 4.1A for more details**). Despite the mounting evidence that HSP90 facilitates some aspects of AGO function in many organisms, including plants, we did not observe an overlap of HSP90 and AGO1-dependent loci[295] (**Supplemental figure 4.1A**). Although our findings could indicate that AGO1 and HSP90 simply buffer different variants, this interpretation is compromised by the fact that both previous work on HSP90[295] and our analyses used partial mutants. Hence, our results may be the consequence of differential sensitivity such that identified HSP90-dependent loci are those most strongly and directly affected by HSP90 perturbation. We may therefore be unable to detect those loci that are indirectly affected because perturbation of the chaperone decreases AGO1 function.

4.2.3 ago1 *uncouples closely related flowering time traits in a background-specific manner*

One example of AGO1-dependent genetic variation particularly captured our attention. When *AGO1* is perturbed, the closely linked flowering time traits of rosette leaf number and days to flowering become uncoupled. The close link between these traits makes intuitive sense, as the resources for flower and seed development are generated in rosette leaves. In *A. thaliana*, days to flowering and rosette leaf number are so closely linked that they are often used interchangeably to measure the onset of flowering[291,292]. There are only a few reported cases in which such uncoupling has been observed, involving certain early flowering mutants[296] and in response to a particular environmental perturbation[297]; the mechanistic underpinnings of these findings remain unknown. With these data in mind, we decided to characterize this example of AGO1-dependent variation.

This uncoupling in flowering traits arises when *ago1-27* reveals genetic variation localized on L*er* chromosome 5 with the coordinates 1 – 9,479,000 bp (STAIRS0942, hereafter referred to as L*er*) (**Figure 4.2**). Rosette leaf number differed significantly between Col-0 wild-type and L*er* wild-type, which is consistent with the known disruption of the flowering repressor *FLC* in the L*er* background[298-301] (Wilcoxon test: p<1.0E-11). Rosette leaf number also differed significantly between Col-0 *ago1-27* and L*er ago1-27* (Wilcoxon test: p<1.0E-11). While L*er ago1-27* showed a decrease in rosette leaf number with respect to wild-type L*er*, Col-0 *ago1-27* showed an increase in rosette leaf number with respect to Col-0 wild-type (**Figure 4.2A**). In contrast, using the measure of days to flowering, L*er* wild-type and L*er ago1-27* were indistinguishable (Wilcoxon test: p=0.4714) (**Figure 4.2B**). Thus, *AGO1* perturbation significantly affected leaf number in a background-specific manner, uncoupling these two closely correlated traits.

4.2.4 FLC *as an epistatic factor contributing to rosette leaf number.*

A major player in flowering time phenotypes is *FLOWERING LOCUS C* (*FLC*), which prevents flowering by suppressing the expression of the flowering activator *FT*[302]. *FLC* expression is repressed when plants are exposed to cold temperatures for a long period of time (*i.e.* vernalization or winter period)[302]. Many natural strains that do not require vernalization to flower carry null *FLC* mutations, as is the case in the parental L*er* ecotype used to create the STAIRS[290].

To determine the extent to which *FLC* contributes to the observed phenotypic differences, we repressed expression of *FLC* by vernalization[302]. We vernalized the Col-0 wild-type, L*er* wild-type, Col-0 *ago1-27,* and L*er ago1-27* plants and measured rosette leaf number and days to flowering as before (**Supplemental figure 4.2**). If differences in *FLC* expression were fully responsible for the reduced Ler *ago1-27* rosette leaf number, vernalized L*er ago1-27* and Col-0 *ago1-27* plants should show similar numbers of rosette leaves. Although vernalization treatment subtly increased L*er ago1-27* rosette leaves, L*er ago1-27* plants still had significantly fewer leaves than Col-0 *ago1-27* (Wilcoxon test: $p<1.0E-11$) (**Supplemental figure 4.2A**). This result indicates that *FLC* contributes to the reduced L*er ago1-27* rosette leaf number, but does not fully account for the observed phenotype.

4.2.5 Identifying the genetic variants that uncouple rosette leaf number from days to flowering

To identify the polymorphism(s) underlying the AGO1-dependent uncoupling of rosette leaf number and days to flowering, we performed bulk segregant analysis and focused on genes with known functions in regulating flowering time[300,301,303] and are polymorphic between Col-0 and L*er*[304] (**Figure 4.3C**).

We performed bulk segregant analysis following a flowering time experiment using four genotypes: Col-0, L*er*, Col-0 *ago1-27*, and L*er ago1-27* F_2s. We selected ~100 *ago1-27* L*er* F_2 plants that possessed six or fewer leaves at flowering time (**Figure 4.3A and 4.3B**). After extraction, DNA samples were pooled and sequenced to a depth of 51x-coverage. Parental samples were collected in parallel and sequenced to a depth ~20x-coverage. We then performed mapping by sequencing using the SHOREmap method for outcrossed segregating populations[305].

We used SHOREmap to visualize the allele frequency estimations at the *Ler* specific loci. Selection for the upper arm of chromosome 5 became apparent through an allele frequency distortion in the region. The loss of function L*er*-specific allele of *hua2-5* (*ENHANCER OF AG-4 2*) appeared as the strongest candidate for causing the uncoupling of flowering time and rosette leaf number. We proceeded to PCR genotype the plants analyzed in the mapping experiment at the *HUA2* region and found that 47 of 48 plants were homozygous for the L*er hua2-5* allele (**Figure 4.3D**).

4.2.6 HUA2 malfunction uncouples flowering time and leaf number in the ago1 *background*

Single *hua* mutants are early flowering and have reduced levels of *FLC* mRNA[293]. In Col-0, HUA2 is required for expression of floral repressors and enhances function of the transcription factor AGAMOUS (AG)[293,306]. Furthermore, HUA2 is highly connected in genetic networks based on a large-scale phenotypic screen between L*er* and Cvi[176]. The L*er* parent used to generate the STAIRS carries a nucleotide substitution described as the *hua2-5* allele[293], which was confirmed by sequencing the *HUA2* gene in our parental STAIRS line. By contrast, the Col-0 background carries a functional *HUA2* allele.

To confirm whether *HUA2* disruption uncouples flowering time from rosette leaf in the *ago1-27* background, we performed double mutant analysis between the two genes. *hua2-4*

mutants showed significantly reduced time to flowering and leaf number compared to Col-0 (Wilcoxon test: p<1.0E-08) (**Figure 4.4A and 4.4B**). Compared to Col-0, *ago1-27* mutants displayed significantly delayed flowering time but no significant change in rosette leaf number (Wilcoxon test: p<1.0E-11) (**Figure 4.4A and 4.4B**). As we previously found for the STAIRS cross, *ago1-27; hua2-4* mutants had fewer than six leaves at flowering (Wilcoxon test: p<1.0E-11) (**Figure 4.4A**). With exception of a late few outliers, we observed that most homozygous *ago1-27*; *hua2-4* mutants flowered at ~24 days (Wilcoxon test: p<1.0E-03) (**Figure 4.4A and 4.4B)**. We also found that many *ago1-27* plants heterozygous for *hua2-4* also flower with six or fewer leaves, thus providing evidence of haploinsufficiency (**Figure 4.4C**).

4.3 Discussion

We provide evidence that genetic perturbation of *AGO1* amplifies developmental noise and thereby increases phenotypic variation in isogenic seedlings similar to previous studies examining HSP90 perturbation[152,274,294]. Prompted by this finding, we investigated whether partial loss of function *ago1* would affect the contribution of genetic variation to complex developmental traits, such as flowering and hypocotyl elongation in the dark. Previous studies found that HSP90 buffers flowering-related traits and hypocotyl elongation in Col-L*er* RILs; other studies showed that AGO1 requires HSP90 for some aspects of its function[218,289]. Therefore, we expected that AGO1-responsive loci would largely overlap those that are responsive to HSP90.

We observed that *AGO1* perturbation readily revealed (or concealed) genetic variants; *AGO1*-buffered loci were common and affected several quantitative traits. However, in contrast to our expectation, there was no overlap among *AGO1*-dependent and *HSP90*-dependent loci.

This finding is consistent with the existence of largely independent, or at least insulated, mechanisms of phenotypic robustness, even though there is evidence for functional relationships between HSP90 and AGO1 in plants[218,289]. The tested mutants for *HSP90* and *AGO1* were hypomorphs (null mutants are lethal)[152,223,295]. As such, our finding may indicate different thresholds for either HSP90 or AGO1 perturbation for a given trait or variant rather than indicating true independence of both buffering mechanisms. The apparent redundancy of molecular robustness mechanisms is no surprise given the evolutionary need to maintain phenotype; however, thus far their interplay has received little attention. Nevertheless, the observed differences in buffered loci would still be evolutionarily relevant because environmental stresses affecting either HSP90 or AGO1 function will produce partially inhibited proteins rather than complete loss of function.

Phenotypic capacitators, such as HSP90, have been proposed to allow genetic variants to accumulate as phenotypically silent mutations in their genetic targets. These silent variants are only expressed after a shift in environment that perturbs the capacitator's buffering function (*e.g.* exposure to moderate heat stress) (**see Chapter 1**). Although genetic hubs other than HSP90 have been shown to act as strong genetic modifiers that buffer phenotypes[30], there is less evidence that their buffering function is environmentally responsive. Like HSP90, AGO1 and AGO1-related miRNAs appear to be important for response to environmental stress[185,307] and buffering of micro-environmental fluctuations[308](**see Chapter 3**). AGO1's function is also environmentally contingent due to its direct interaction with HSP90 as well as several plant pathogens directly targeting AGO1 or its translation[255-260]. These observations provide a hypothetical mechanism for intermittent release of AGO1-dependent cryptic genetic variation outside of the lab.

To understand the underlying genetics of *AGO1*-buffered variation, we studied the surprising uncoupling of two flowering time traits – final leaf number and days to flowering – which depended on AGO1 perturbation in the L*er* background, and discover an example of dramatic pathway rewiring. We show that in the L*er* background, *AGO1* plays a crucial role in maintaining the important correlation between final rosette leaf number and days-to flowering traits, which assures that a plant has enough resources for setting seeds. Contrary to this expectation, in the Col-0 background, vernalization (which suppresses *FLC* expression) disrupts the leaf number-days to flowering correlation. The L*er* background used for creating the STAIRS contains null alleles of both *FLC* and *HUA2*[290,309,310]. Together, these mutations ensure tight coupling of the leaf number and days-to-flowering traits. This L*er*-specific coupling is perturbed when *AGO1* function is disrupted, thereby revealing its existence. This ecotype-specific pathway wiring illustrates the necessity to explore pathways beyond commonly used laboratory strains, in particular when working with inbreeding species that can readily fix mutations. It also illustrates the enormous flexibility in pathway wiring to yield a certain trait – here coupling of resources (leaves) to seed setting (flowering time) – when selection is strong enough.

Although we identify a significant genetic interaction between *HUA2, FLC,* and *AGO1*, the exact mechanistic underpinning that connects these genes remains unclear. HUA2 is predicted to have transcription factor activity that enhances the floral morphology gene AGAMOUS[306]. Phenotypically, single *hua2* mutants are early flowering and have reduced levels of *FLC* mRNA[293]. There is evidence that mutant alleles of the miRNA processing gene *HEN1*[311] are sensitized in a *hua1; hua2* background with regards to flower morphology [312], consistent with *HUA2* being involved in gene regulation through the miRNA pathway. *HUA2* has also been

suggested as a candidate gene for a quantitative trait locus that buffers thousands of molecular and hundreds of organismal phenotypes, including flowering related traits[176,310].

Previous studies have reported that specific miRNAs buffer noise in the pathways which they target to maintain robust phenotypes[282,283,313-315]. The frequency of observed revealed and concealed genetic variation on L*er* chromosomes 3 and 5 suggests that *AGO1*-dependent genetic variation is rather common in *A. thaliana*. We assume many more AGO1-dependent loci exist across *A. thaliana* ecotypes and that these may represent miRNA genes or their targets, many of which are known to harbor functionally relevant natural variation[316,317]. A logical next step for future work is to use bulk segregant analysis to identify other buffered genetic variants in our STAIRS crosses.

Regardless of the precise mechanistic reasons for the largely missing overlap between AGO1 and HSP90 buffered loci, our findings are relevant for understanding the rules of phenotypic buffering. In our data, HSP90 and AGO1 do maintain robustness in some of the same traits, though it is appear to be through buffering of non-overlapping genetic variants. This redundancy may maintain phenotypic robustness in the face of environmental perturbations that are specific to AGO1 or HSP90, thus ensuring that traits remain robust to a variety of environments and different genetic variants.

4.4 Main figures

A)

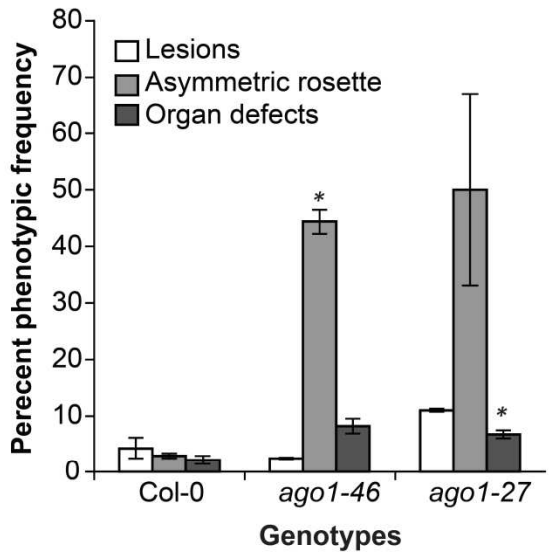

B)

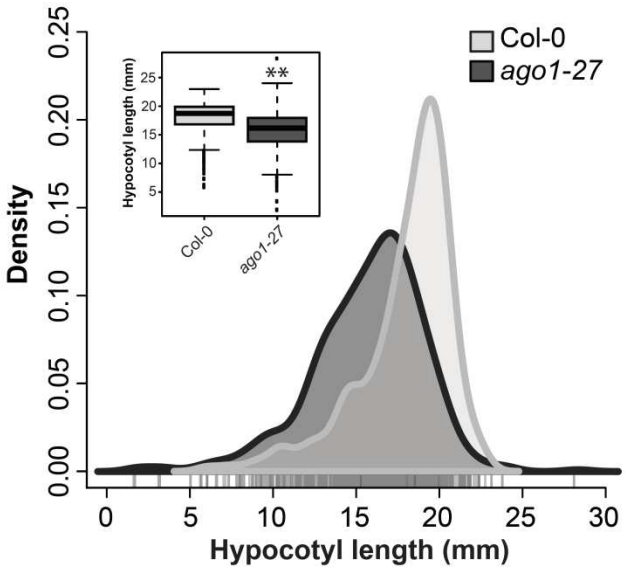

C)

Trait	*Ler* on Chr 3 1 - 9,742,000	*Ler* on Chr 3 18,230,000 - 23,459,830	*Ler* on Chr 5 1 - 9,479,000	*Ler* on Chr 5 9,479,000 - 26,975,502
Rosette leaf number	epistatic	--	reveals	conceals
Days to flowering	conceals	epistatic	epistatic	--
Rosette diameter	reveals	conceals	--	--
Hypocotyl length	--	--	--	--
Root length	reveals	--	--	--

Figure 4.1: *ago1* plants show more variation in qualitative and quantitative traits.
(A) Early morphology trait measures for wild-type (WT), *ago1-46*, and *ago1-27* seedlings. Ten-day old seedlings were scored for three different morphological traits. The data represent two biological replicates (two replicates, n = 144 for *ago1* mutants, and n = 216 for Col-0, *p<0.05, t-test). **(B)** Hypocotyl length for 7-day old, dark-grown seedlings. The variance for Col-0 and *ago1-27* distributions is different (Levene's test, p<1.0E-03; n = 475 for *ago1-27*, n = 486 for WT). **Inset:** boxplots of hypocotyl length distribution. Y-axis represents hypocotyl length (mm), **p<1.0E-15, Mann-Whitney Wilcoxon test. **(C)** Table for results of for *ago1-27* x STAIRS crosses. Across the five quantitative traits measured, we observe instances of *AGO1* perturbation revealing and concealing phenotypes as well as examples where L*er* loci are epistatic Col-0 and *ago1-27*. For p-values of comparisons, please **Supplemental figure 4.1**.

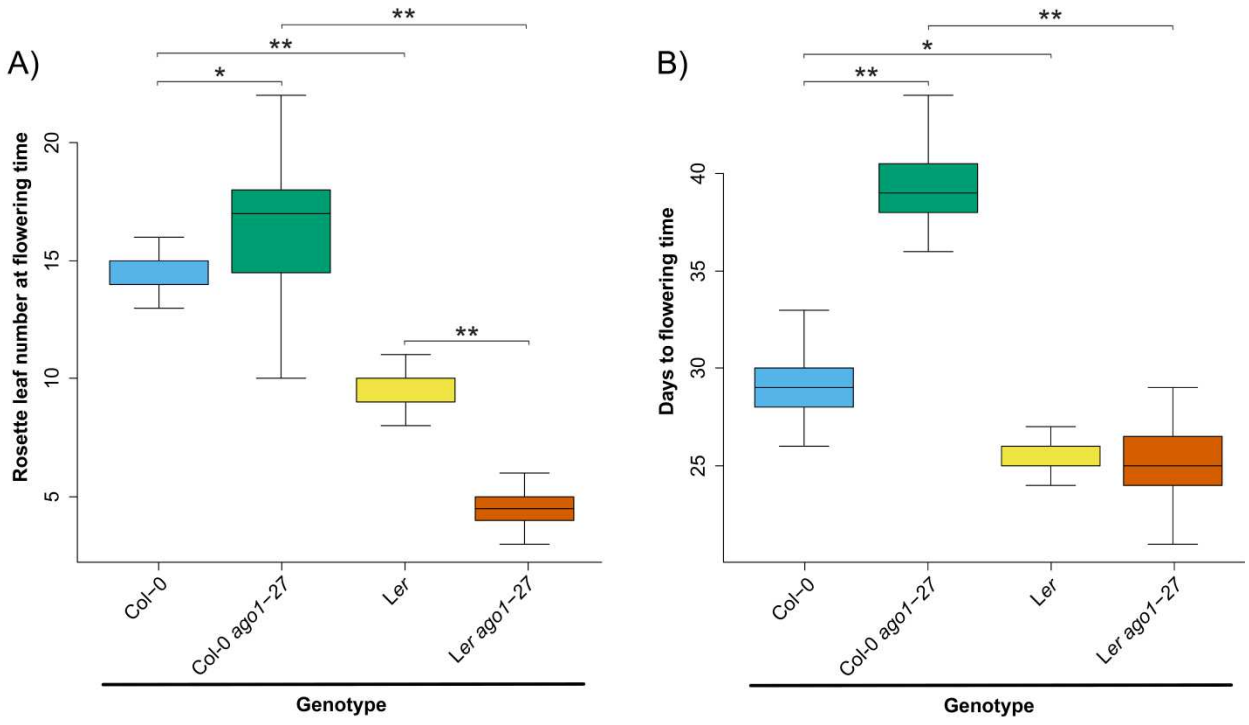

Figure 4.2: AGO1 perturbation uncouples flowering time from rosette leaf number. Plants for Col-0, L*er* (STAIRS0942), Col-0 *ago1-27* and L*er* (STAIRS0942) *ago1-27* were grown on soil in LD at 23˚C, n = 30-36. **(A)** Rosette leaf number was measured at time of flowering. We observed that *AGO1* perturbation reveals this phenotype in the L*er* background. **(B)** Days to flowering was measured when floral bolts reached 1cm in height. For this phenotype, we found that the L*er* introgression was epistatic to *ago1-27*. *p<0.0001, **p < 1.0E-11, Mann-Whitney Wilcoxon test.

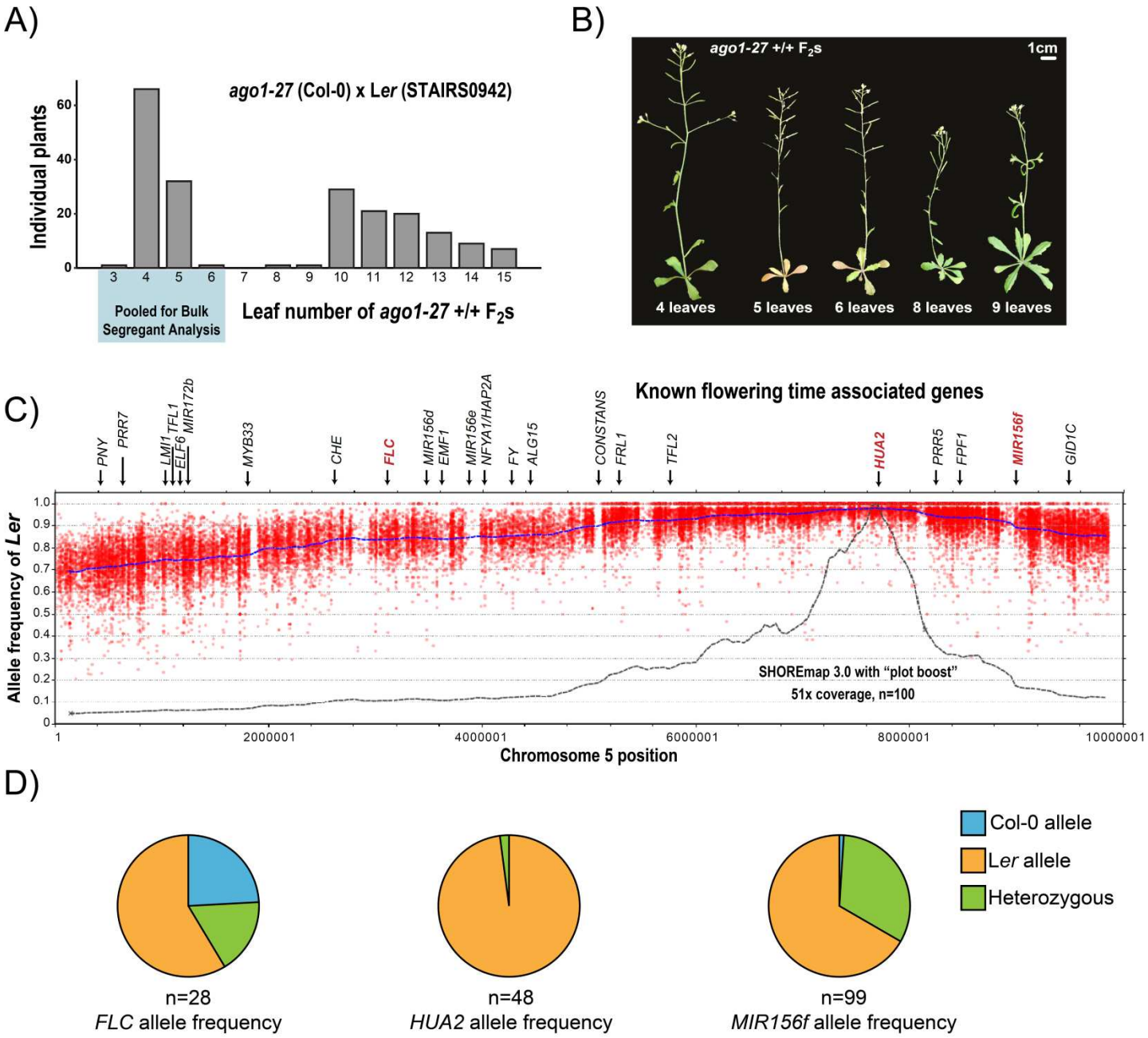
A)
ago1-27 (Col-0) x Ler (STAIRS0942)
Individual plants
Pooled for Bulk Segregant Analysis
Leaf number of ago1-27 +/+ F2s
B)
ago1-27 +/+ F2s
1cm
4 leaves
5 leaves
6 leaves
8 leaves
9 leaves
C)
Known flowering time associated genes
PNY
PRR7
LMI1
TFL1
ELF6
MIR172b
MYB33
CHE
FLC
MIR156d
EMF1
MIR156e
NFYA1/HAP2A
FY
ALG15
CONSTANS
FRL1
TFL2
HUA2
PRR5
FPF1
MIR156f
GID1C
Allele frequency of Ler
SHOREmap 3.0 with "plot boost"
51x coverage, n=100
Chromosome 5 position
D)
Col-0 allele
Ler allele
Heterozygous
n=28
FLC allele frequency
n=48
HUA2 allele frequency
n=99
MIR156f allele frequency

Figure 4.3: Bulk segregant analysis of *ago1-27* x STAIRS0942 cross identifies HUA2 polymorphisms as candidate loci for un-coupling of flowering related traits. **(A)** F_2 plants from *ago1-27* x L*er* (STAIRS0942) cross were grown in LD at 23˚C and genotyped for the *ago1-27* allele. For F_2 plants that were *ago1-27* (+/+), we observed a distribution of rosette leaf number at flowering time. For bulk segregant analysis, we selected *ago1-27* (+/+) that flowered with six or fewer leaves (n=100). **(B)** Representative F_2 *ago1-27* (+/+) plants with nine or fewer leaves at flowering. Scale bar = 1cm. **(C)** Bulk segregant analysis[318] of *ago1-27* x L*er* (STAIRS0942) cross for ago1-27 (+/+) plants with six or fewer leaves. Red dots represent allelic frequencies of L*er* loci on chromosome 5 (bp, x-axis). Allele frequencies (y axis) were estimated as the fraction of reads supporting the L*er* allele divided by the number reads mapping to that loci. Dashed blue line represents sliding window based allele frequencies at estimated by SHOREmap[318]. Dashed black line represents window-based plot boost as estimated by SHOREmap. The L*er hua2-5* allele was found to be a candidate locus as local allele frequencies appeared higher as compared with other regions on chromosome 5. **(D)** F_2 *ago1-27* (+/+) plants with nine or fewer leaves at flowering were PCR genotyped for alleles at *FLC*, *HUA2*, and *MIR156f* loci after our bulk segregant analysis. This results further support *HUA2* as the candidate buffered locus.

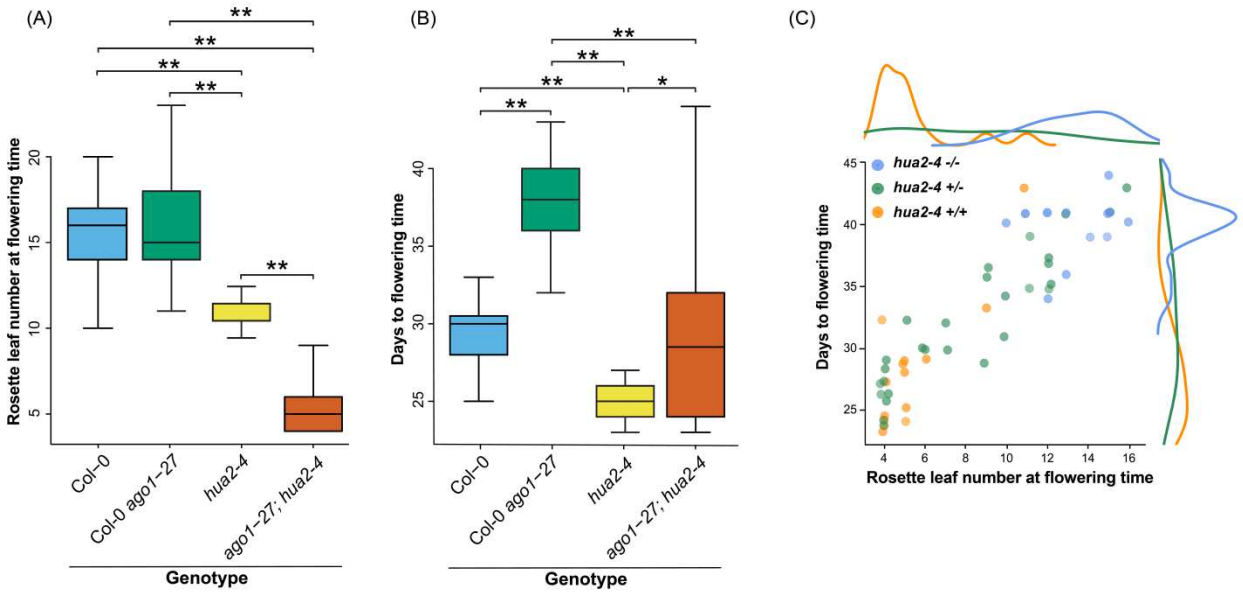

Figure 4.4: *ago1-27; hua2-4* mutants decouple flowering time from leaf number. Plants for Col-0, *ago1-27* and *ago1-27* x *hua2-4* F_2s were grown on soil in LD at 23˚C. n=30-36 for parental genotypes and Col-0, and n=72 for *ago1-27*; *hua2-4* F_2s. **(A)** Rosette leaf number was measured at flowering time. As was observed for the initial STAIRS0942 (L*er*) cross, we also observed that *ago1-27*; *hua2-4* plants flower with few leaves. **(B)** Days to flowering was measured when floral bolts reached 1cm in height. Like our previous results, we saw that *hua2-4* is epistatic to *ago1-27*. *p<1.0E-05, **p<1.0E-08, Mann-Whitney Wilcoxon test.
(C) Scatter plot of flowering related traits in *ago1-27* (+/+) F_2 population that is segregating for *hua2-4*.

4.5 Materials and Methods

Plant Materials and Growth Conditions: The following parental lines were used: Col-0, *ago1-27* in the Col-0 background [319], and STAIRS N9448, N9456, N9472, N9501[290]. *ago1-27* plants were crossed into the STAIR lines and F_2's that had the wild-type and *ago1-27* allele in both Col-0 and the STAIRS backgrounds were isolated. Selected F_2's and their progeny were used to perform the described experiments. For the hypocotyl and root length assays, the plants were grown on MS media containing 0.0005% MES hydrate, 0.004% vitamin solution, 3% Phytagel, and 1% sucrose.

Genotyping of F_2 plants: PCR was used to genotype the F_2s from each STAIRS – *ago1-27* cross. PCR conditions for *ago1-27* genotyping is as follows: 5' at 94 °C, followed by 35 cycles at 30 s at 94 °C, 30 s at 55 °C, 1 min at 72 °C. PCR product was then digested at 37°C with Bsp1286I, which cuts wild-type sequence. To genotype for the STAIRS portion of each cross, please **Supplemental Table 1** for primers. The *hua2-4* and *hua2-5* alleles were genotyped using the primers in **Supplemental Table 1.**

Hypocotyl and root length assays: Seeds from different genotypes were laid on agar plates in a random, 10-seeds per plate arrangement. The plates were stacked in racks, wrapped in foil, and transferred to 4˚C for five days. Then they were unwrapped, and exposed to light for two hours. After that, the plates were wrapped in foil again, to prevent further light exposure and were transferred to a 23˚C tissue culture incubator for seven days. The plants were grown vertically. After that, the plates were taken out, and photographed. The photographs were used to measure the seedlings' hypocotyls and roots using the ImageJ software (http://rsbweb.nih.gov/ij/).

Early morphology traits analysis: Seeds from the different genotypes were plated on agar (36 seeds/per plate). For experiments, seeds were sterilized with ethanol and plated onto 1x Murashige and Skoog (MS) basal salt medium supplemented with 1x MS vitamins, 1% (w/w) Suc, 0.05% (w/w) MES, and 3% (w/w) phytagel. After stratification in the dark at 4°C for 5 d, plates were transferred to an incubator (Conviron) that was set to long days (16 h of light/8 h of dark at 22°C/20°C), with light supplied at 100 mmol m22 s21 by cool-white fluorescent bulbs and a long-pass yellow filter that blocks 454-nm light was placed in front of the bulbs. Seedlings were then scored for phenotypes at day 10.

Flowering time experiments: Seeds from different genotypes were embedded in 1mL of 0.1% agar, and then stratified for 5 days at 4˚C. Then, they were sowed on soil in 36-pot trays. Flowering time was measured by scoring both the number of rosette leaves and days to flowering. The traits were recorded when the primary inflorescence of the plant had reached a height of 1cm. Flowering time experiments were performed in long days (LD, 16 hours of light, 8 hours of dark), at 23˚C. **Rosette diameter measurements:** The diameter of the rosette was measured on the day that the primary inflorescence of the plant reached a height of 1cm.

Library preparation and sequencing: Approximately 400 L*er ago1* F_2 plants were sown, and leaf samples of equal size were collected from 100 plants scored as flowering with few leaves. Additionally, individuals were genotyped to be sure they had the correct L*er* chromosome fragments (See Supplemental Table 1 for genotyping primers). In parallel, leaf samples were collected from Col-0 - *ago1-27* and L*er*-Col-0. DNA was extracted using CTAB extraction[161] and quantified using the Qubit HS dsDNA assays. Samples were then pooled and libraries were

generated using the Nextera sample kit according to the manufacturer's instruction (Illumina). Libraries were then quality checked on the Agilent 2100 bioanalyzer using DNA high-sensitivity chip (Agilent). The samples were sequenced on an Illumina Nextseq in a 75-bp paired end run.

Bulk segregant analysis: We applied BWA[183] to independently align the read sets to the Col-0 reference. Using the function SHORE import, raw reads were trimmed or discarded based on quality values with a cutoff Phred score of +38. After correcting the paired-end alignments with an expected insert size of 300-bp, we applied SHORE consensus to identify variations between the mutants and reference. SHOREmap[318,320] was then used to calculate allele frequency estimates were calculated as the ratio of the reads of mutant alleles divided by all reads at a particular locus. Sequence changes in the region that featured evidence for selection were annotated for their effect on gene identity using the TAIR10 gene annotation.

4.5 Supplemental materials

A)

P -values for Wilcoxon tests

STAIRS 9448	Chr3: 18,230,000 - 23,459,830					
Phenotype	Wt comparison Col-0 vs Ler	*ago1-27* comparison Col-0 vs *Ler*	Col-0 comparison Wt vs *ago1-27*	Ler comparison Wt vs *ago1-27*	Interaction	Overlap with HSP90-loci for the selected trait?
Hypocoyl length	*1.74E-02*	*1.06E-04*	1.34E-01	*1.02E-08*	*2.36E-02*	No
Root length	*1.67E-10*	1.05E-01	*4.66E-13*	*1.55E-06*	*2.07E-06*	No
Days to flowering	***9.67E-03***	8.63E-01	***5.19E-13***	***3.66E-12***	1.15E-01	No
Rosette leaf number	*1.10E-02*	*1.93E-02*	1.83E-01	*1.76E-06*	*5.62E-04*	No
Rosette diameter	***4.06E-02***	3.56E-01	***3.84E-02***	3.68E-01	***2.90E-02***	No

STAIRS 9459	Chr3: 1 - 9,742,000					
Phenotype	Wt comparison Col-0 vs Ler	*ago1-27* comparison Col-0 vs *Ler*	Col-0 comparison Wt vs *ago1-27*	Ler comparison Wt vs *ago1-27*	Interaction	Overlap with HSP90-loci for the selected trait?
Hypocoyl length	*4.40E-14*	*2.09E-04*	*8.90E-07*	*2.35E-05*	7.91E-01	No
Root length	3.06E-01	***5.95E-02***	***< 2.2e-16***	***3.71E-11***	***1.90E-02***	No
Days to flowering	***1.03E-11***	3.45E-01	***2.34E-12***	6.14E-01	***1.73E-02***	No
Rosette leaf number	***7.55E-11***	5.09E-01	2.71E-01	***6.74E-04***	***1.48E-03***	No
Rosette diameter	4.10E-01	***7.12E-03***	***2.85E-09***	***2.33E-03***	***3.96E-02***	No

STAIRS 9472	Chr5: 1 - 9,479,000					
Phenotype	Wt comparison Col-0 vs Ler	*ago1-27* comparison Col-0 vs *Ler*	Col-0 comparison Wt vs *ago1-27*	Ler comparison Wt vs *ago1-27*	Interaction	Overlap with HSP90-loci for the selected trait?
Hypocoyl length	*5.65E-02*	*3.89E-02*	*3.29E-12*	*3.35E-10*	*4.73E-03*	No
Root length	*2.41E-08*	*1.42E-02*	*< 2.2E-16*	*3.19E-08*	*9.54E-03*	No
Days to flowering	***5.36E-11***	***4.66E-12***	5.51E-12	4.71E-01	***< 2.2 E -16***	No
Rosette leaf number	***2.60E-12***	***3.45E-12***	***1.02E-04***	***2.33E-12***	***< 2.2E-16***	No
Rosette diameter	*< 2.2E-16*	*< 2.2E-16*	*1.10E-10*	< 2.2E-16	*8.53E-04*	No

STAIRS 9501	Chr5: 9,479,000 - 26,975,502					
Phenotype	Wt comparison Col-0 vs Ler	*ago1-27* comparison Col-0 vs *Ler*	Col-0 comparison Wt vs *ago1-27*	Ler comparison Wt vs *ago1-27*	Interaction	Overlap with HSP90-loci for the selected trait?
Hypocoyl length	***4.50E-07***	3.96E-01	6.37E-01	***6.66E-05***	7.07E-02	Yes
Root length	*2.36E-04*	*3.40E-05*	*1.33E-07*	*1.46E-05*	5.58E-01	Yes
Days to flowering	*1.86E-04*	3.84E-01	*6.10E-12*	*4.06E-13*	1.49E-01	No
Rosette leaf number	***1.28E-03***	***1.08E-02***	***4.55E-04***	1.51E-01	***7.50E-05***	No
Rosette diameter	*3.82E-03*	3.22E-01	*4.48E-16*	*8.94E-12*	1.94E-01	No

B) *ago1-27* reveals on Chr3

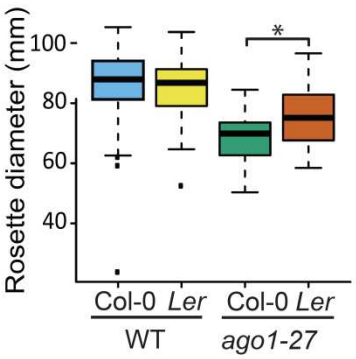

C) *ago1-27* conceals on Chr3

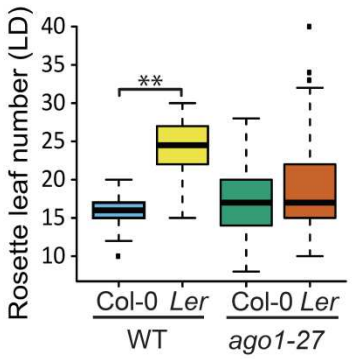

D) *Ler* Chr3 is epistatic to *ago1-27*

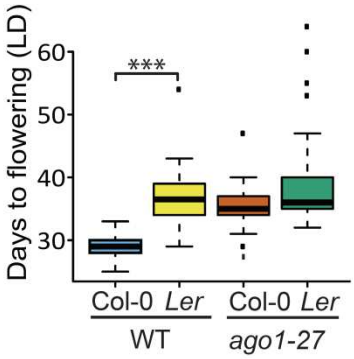

Supplemental figure 4.1: *AGO1* perturbation reveals and conceals genetic variation. **(A)** p-values for the comparisons per line per phenotype measured. Mann-Whitney Wilcoxon tests were used to test significance. The column "interaction" contains the p-value of the ANOVA interaction term genetic-background*mutant status. Red marks instances in which *ago1* reveals genetic variation; blue, when *ago1* conceals genetic variation; and green, cases in which the L*er* introgression was epistatic to *ago1*. For the "HSP90 overlap" column, we searched if the portions of L*er* chromosomes that harbor AGO1-dependent loci overlapped with published HSP90 –dependent loci that affect the same measured traits. All the experiments were done in Long day (LD) (16h light / 8h dark) at 23˚C. **(B)** *ago1* reveals genetic variation for rosette diameter. **(C)** *ago1* conceals genetic variation for rosette leaf number. **(D)** The L*er* introgression is epistatic to *ago1* mutation. Asterisks represent significant p-values. * = p<0.005, ** = p< 1.0E-10, *** = p<1.0E-11, Mann-Whitney Wilcoxon test.

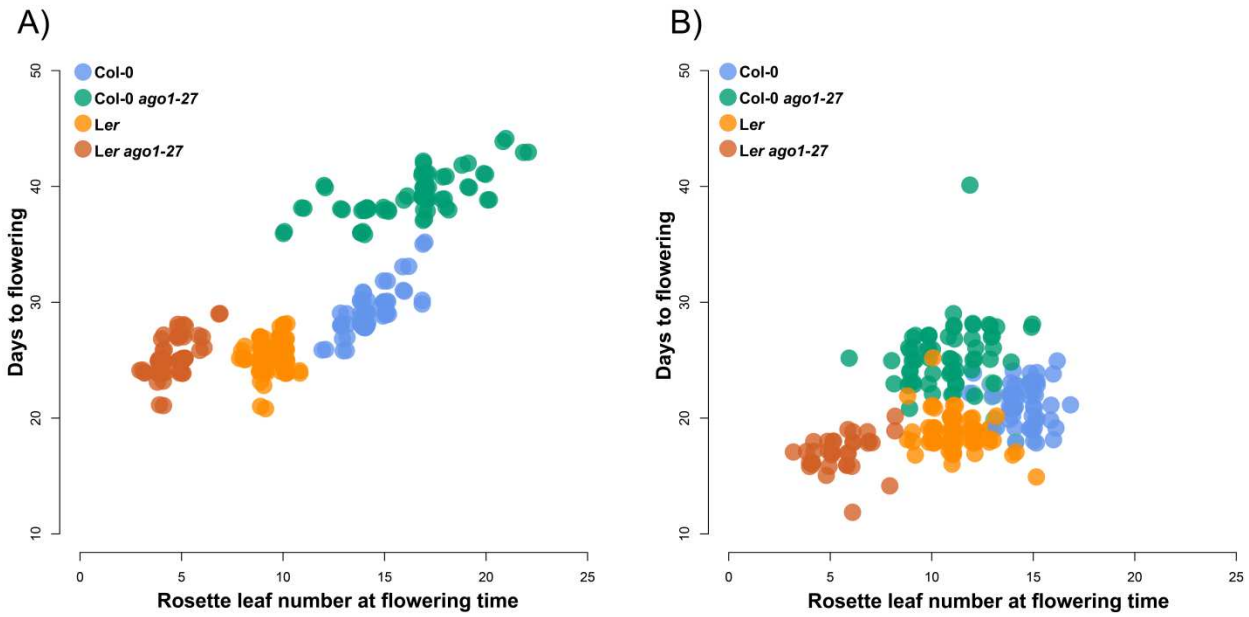

Supplemental figure 4.2: Effect of *FLC* in the decoupling of days to flowering and rosette leaf number. Vernalization treatment partially rescues the decoupling phenotype. **(A)** Plants were grown in LD at 23˚C. Data is also shown in **Figure 4.2**. **(B)** Plants were grown for 5 days under long-day conditions at 23˚C, and then vernalized for 40 days at 4˚C. Here, days to flowering are the days after vernalization treatment was stopped.

Supplemental Table 1: Genotyping Primers

Gene	Accession number	Primer	Primer sequence	Notes
AGO1	AT1G48410	F	ACCACGTTCTTTGGGATGAG	Bsp1286I cuts the wild-type allele
		R	TCTACCCATTCCACCTC	
hua2-4	AT5G23150	LP	TCTATCAGAGCCACCTGCTTC	Used for SALK genotyping with LbB1 primer
		RP	TTACTCGGTCAGATTCCATGG	
hua2-5	AT5G23150	F	CTTCACAATCATTAACAACTCAG	110 bp for Ler allele
		R	TGCTGCATAGATCCTGGGTA	
Ler 1,738,567		F	GCGATGAAGGCAGCTATTGT	Col-0 amplicon: 616 bp *Ler* amplicon: 486 bp
		R	TTCACGAACATTACGCCATT	
Ler 2,680,451		F	TTGTGGAAACTGGAAACAGC	Col-0 amplicon: 514 bp *Ler* amplicon: 470 bp
		R	AAGCTAGGCTGGTGGAGACA	
Ler 3,184,117		F	TGTTCTCTCTGCCTCTTCTGC	Col-0 amplicon: 526 bp *Ler* amplicon: 495 bp
		R	CCATATTTAGGCAAACGAAACA	
Ler 5,383,687		F	CCTTTGAAAAACCGCCATTA	Col-0 amplicon: 1658 bp *Ler* amplicon: 523 bp
		R	AGATCTCATACCGCCGGAGT	
Ler 5,938,745		F	ATGCTTACTGGTCCCGTCAC	Col-0 amplicon: 662 bp *Ler* amplicon: 564 bp
		R	GTTGACCCTGTCTGCGATTT	
Ler 6,248,348		F	GTCGTTTCATCGACACTTGC	Col-0 amplicon: 474 bp *Ler* amplicon: 434 bp
		R	TCTGGCCAGTTTGAAAGACC	
Ler 7,825,812		F	CGCGATGTAATCGGTCTTTT	Col-0 amplicon: 807 bp *Ler* amplicon: 575 bp
		R	CGCGATGTAATCGGTCTTTT	
Ler 8,803,872		F	TCATTGATTTCCCTCGATCA	Col-0 amplicon: 659 bp *Ler* amplicon: 555 bp
		R	TCTTGAAATGTGTAATTTCGGTGT	
Ler 9,478,916		F	TGTGGCACAGGGTTTGTAAG	Col-0 amplicon: 538 bp *Ler* amplicon: 490 bp
		R	AAAGCCAGCCAATGTTTCAC	

Chapter 5: Redundancy, feedback, and robustness in the *Arabidopsis thaliana BZR/BEH* gene family[8,9]

Abstract

Organismal development is remarkably robust, tolerating stochastic errors to produce consistent, so-called canalized adult phenotypes. The mechanistic underpinnings of developmental robustness are poorly understood, but recent studies implicate certain features of genetic networks such as functional redundancy, connectivity, and feedback. Here, we examine the *BRZ*/*BEH* gene family, whose function is crucial for embryonic stem development in the plant *Arabidopsis thaliana*, to test current assumptions on functional redundancy and trait robustness. Our analyses of *BRZ*/*BEH* gene mutants and mutant combinations revealed that functional redundancy among gene family members does not contribute to trait robustness. Connectivity is another commonly cited determinant of robustness; however, we found no correlation between connectivity among gene family members or their connectivity with other transcription factors and effects on robustness. Instead, we found that only *BEH4*, the most ancient family member, modulated developmental robustness. We present evidence that regulatory cross-talk among gene family members is integrated by *BEH4* and promotes wild-type levels of developmental robustness. Further, the chaperone HSP90, a known determinant of developmental robustness, appears to act via BEH4 in maintaining robustness of embryonic stem length. In summary, we demonstrate that even among closely related transcription factors, trait robustness can arise

[8] This chapter adapted from "Redundancy, feedback, and robustness in the *Arabidopsis thaliana BZR/BEH* gene family," BioRXiv: doi: https://doi.org/10.1101/053447, by *J. Lachowiec, G. A. Mason, K. Schultz, **C. Queitsch. *First author, **Corresponding author.

[9] J.L. and C.Q. conceived the project. G.A.M. performed expression assays. J.L. and K.S. executed hypocotyl assays. J.L. and G.A.M. performed data analysis.

through the activity of a single gene family member, challenging common assumptions about the molecular underpinnings of robustness.

5.1 Introduction

Development relies on the coordinated action of low concentrations of regulatory factors diffusing within and between cells, which inevitably results in random developmental errors. Typically, organisms tolerate developmental errors, resulting in canalized, wild-type-like individuals[252,277,278,321,322]. Robustness to developmental errors is an intrinsic property of all organisms and is genetically controlled[221,323-328]. However, the molecular mechanisms that regulate developmental robustness are poorly understood, which is largely due to the technical obstacles of studying this phenomenon in complex, multicellular organisms.

A feature of genetic networks commonly associated with developmental robustness is functional redundancy among genes[276]. Functional redundancy will compensate for stochastic losses of function in specific gene family members or paralogs[329,330]. Gene duplication is one obvious source of network redundancy, and thereby developmental robustness. In *Arabidopsis thaliana*, one-third of genes belong to multi-member gene families[331], which have arisen through three well-supported whole genome duplications[332,333], in addition to segmental and tandem duplication events[334]. Duplication of transcription factor genes provides a plausible but potentially complex form of robustness regulation. Transcription factor family members recognize highly similar DNA motifs[335] and often regulate one another[336], showing functional redundancy as well as feedback regulation[337-339]. At the same time, transcription factors are particularly vulnerable nodes for developmental robustness due to their often low cellular concentrations and positions as both master regulators[340] and endpoints of signaling cascades[341].

It is unclear how these different features of transcription factors and their gene families converge to regulate developmental robustness.

The *BES1/BZR1 HOMOLOG* (*BEH)* transcription factors belong to a small gene family exclusive to plants. With only six members[342], this family is tractable for studying the role of redundancy, connectivity, and feedback on developmental robustness. The well-studied founding members of the *BEH* family, *BRI1-EMS-SUPRESSOR1* (*BES1*) and *BRASSINAZOLE-RESISTANT1* (*BZR1*) result from the most recent whole genome duplication in the *A. thaliana* lineage and are highly similar in sequence[343]. They are thought to be the primary transcription factors in brassinosteroid signaling; studies of phenotypic effects are largely restricted to dominant mutants[342,344,345]. Brassinosteroid signaling regulates a large number of physiological processes in plants, ranging from seed maturation to senescence[346]. Brassinosteroids are recognized by the membrane-associated receptor BRI1 that then represses the activity of the GSK3 kinase BIN2. In the absence of brassinosteroids, BIN2 phosphorylates and inhibits BES1 and BZR1[344]. In this phosphorylated state, BES1 and BZR1 are prohibited from entering the nucleus[347]. In the presence of brassinosteroids, BES1 and BZR1 are dephosphorylated[348] and localize to the nucleus, where they activate and repress different sets of targets genes[349-352]. BES1 and BZR1 are known to interact with several other proteins to regulate transcription. For example, BES1 dimerizes with BIM family proteins[349] to increase DNA binding affinity *in vitro*, interacts with its target gene MYBL2[353], and works with ISW1[354], ELF6, and REF6[355] to alter chromatin accessibility. Some studies have revealed differences in BES1 and BZR1 protein interactions. For example, BES1, but not BZR1, interacts with the known robustness regulator HSP90[94,356].

In contrast, the other family members *BEH1-4* are little studied, largely due to the lack of well-characterized loss-of function or dominant mutants. As BES1 and BZR1, BEH1, BEH2, BEH3, and BEH4 are thought to act as transcription factors[342,350]. Moreover, BEH1, BEH2, BEH3, and BEH4 are phosphorylated in a manner similar to BES1 and BZR1[349], and yeast two-hybrid analyses show that BEH2, in addition to BES1 and BZR1, interacts with a GSK3 kinase[357]. In sum, previous studies support that BEH1, BEH2, BEH3, and BEH4 act redundantly with the well-studied transcription factors BES1 and BZR1[353,358].

Previously, we systematically examined the entire *BEH* family for effects on developmental robustness through the lens of redundancy[359]. Contrary to commonly held assumptions about the importance of redundancy and connectivity in robustness, we observed that robustness in hypocotyl growth arises largely due to the function of a single gene, *BEH4,* which appears to maintain proper cross-talk among *BEH* family members.

Here, we characterize expression feedback and cross-regulation amongst members of the *BEH* family in both light and dark conditions. We found that two genes, *BEH3* and *BEH4*, are the most highly connected genes in the network. We then go on to take advantage of genome-wide chromatin accessibility data to gain a better understanding of the *BEH* family-mediated regulatory network underlying dark-grown seedling development; we did not observe that any one family was enriched for BEH-family binding motifs that could explain phenotypic differences amongst the mutants. Finally, we trace HSP90's role in maintaining robustness of hypocotyl length to the function of *BEH4*, thereby elucidating how this well-known regulator of global developmental robustness specifically affects this trait.

5.2 Results

5.2.1 Expression feedback among members of the BEH *family in the light and dark*

We wanted to further explore the putative functional integration among *BEH* family members that may underlie *BEH4*-dependent developmental robustness. Specifically, we hypothesized that *BEH4* acts as hub gene among *BEH* family members. Highly connected hub genes such as the well-characterized HSP90 are thought to affect robustness through their interaction with many other loci; hub perturbation results in large-scale phenotypic effects and loss of robustness[176,252,339,360]. BES1 and BZR1 ChIP results[351,352] suggest that all other *BEH* family members are potential transcriptional targets of BES1 and BZR1 (**Supplemental table 5.1**), consistent with direct or indirect regulation among family members. Further, expression of *BEH2* is up-regulated in RNAi lines in which *BES1* is targeted[361], and *BZR1* expression is reduced in *bes1-1* mutants[362]. To test our hypothesis that BEH4 is the most highly connected gene in this gene family, we determined the relative expression of each *BEH* family member in each single *lof* mutant background. If mean gene expression was altered more than 2-fold in a given mutant background, we assumed a direct or indirect genetic interaction between the assayed and the mutated gene. Disproving our hypothesis, we found that *BEH3* was the most highly connected gene among the *BEH* family, not *BEH4* (**Figure 5.1**). Seven connections among *BEH3* and other family members were counted, with *BEH3* directly or indirectly regulating three family members and *BEH3* expression affected in four mutants. Two of these interactions were reciprocal, in which *BEH3* and *BEH4* regulate each other, as well as *BEH3* and *BES1*. Similar to *BEH3*, *BEH4* directly or indirectly affected gene expression of three family members, but only two mutants influenced *BEH4* expression. Notably, the *lof beh3-1* mutant showed no decrease in developmental robustness; hence, connectivity, another frequently cited

cause of developmental robustness[339,360], is apparently not majorly involved in robustness of hypocotyl growth. This interpretation does not consider possible interactions at the protein level through heterodimers among family members or connections of *BEH4* with genes outside its gene family.

Although connectivity was not associated with phenotypic effects, gene duplicate age appeared to be associated with the number of connections among family members. *BES1* and *BZR1* are the most recently duplicated members of the family, followed by *BEH1* and *BEH2*, with *BEH3* and *BEH4* being the most ancestral[343]. With three connections, BZR1 and *BES1* were the least connected genes; *BEH1* and *BEH2* each showed four direct or indirect regulatory connections. These results are consistent with closely related transcription factors gaining regulatory complexity over time as paralogs are added.

To further explore the regulatory network underlying hypocotyl elongation in the dark, we analyzed recent DNaseI-seq data of dark grown seedlings[338]. We and others have suggested that robustness regulators may be characterized by numerous regulatory inputs and few outputs, an architecture well suited to buffer noise[30,325,360,363]. Therefore, we identified and counted transcription factor (TF) binding motifs in the accessible chromatin marking the putative promoters of all *BEH* gene family members (**Supplemental table 5.2**). The promoter-proximal accessible chromatin of *BEH4* and *BEH3* each contained 25 TF binding motifs; 26 TF motifs were found for *BEH2* and 35 for *BZR1*. In contrast, no TF motifs were detected for *BEH1,* and only six TF motifs were found for *BES1*. We conclude that at least for the BEH gene family the number of regulatory inputs (measured as number of promoter TF binding sites) is not associated with the severity of phenotypic effects on developmental robustness or trait mean. We were unable to assess regulatory outputs because the binding motifs of individual *BEH* family

members are unknown. *BES1* and *BZR1* both recognize the BRZ motif, which resided in accessible, promoter-proximal chromatin of 230 genes. Although *BEH4* most strongly affects phenotype among the BEH family members, neither connectivity nor regulatory architecture is consistent with the hypothesized role of BEH4 as a hub gene.

5.2.2 HSP90 likely maintains developmental robustness of dark-grown hypocotyls via BEH4

HSP90 function is crucial for developmental robustness of dark-grown hypocotyls and other traits[152,156,221,364]. As HSP90 chaperones the *BEH* family member BES1[94,356], we hypothesized that the dominant role of *BEH4* in developmental robustness may involve HSP90. To test this hypothesis, we assessed the genetic interaction of HSP90 and *BEH4*, using the potent and highly specific inhibitor Geldanamycin (GdA) to reduce HSP90 function. As previously observed, HSP90 inhibition in wild-type seedlings decreased robustness (**Figure 5.2A**). HSP90 inhibition in *bes1-2* mutant seedlings also decreased robustness, closely resembling the phenotypic effect observed in wild-type (**Figure 5.2A**). In stark contrast, *beh4-1* exhibited no change in developmental robustness upon HSP90 inhibition (Levene's test: $p=0.296$). In fact, *BEH4* appeared to be epistatic to HSP90 in mediating developmental robustness of dark-grown hypocotyls, suggesting that HSP90 acts via BEH4 in this pathway.

The most obvious mechanism by which HSP90 would act via BEH4 to mediate developmental robustness is by chaperoning BEH4. The BEH family member BES1, but not BZR1, is an HSP90 client[94,356]. Due to the high similarity among BEH family members, it is certainly likely that others are also HSP90 substrates, as client status is often shared among family members[149,365]. HSP90 inhibition typically compromises the function of its clients due to mis-folding and degradation[148]. The observed epistasis of BEH4 with HSP90 in developmental

robustness (lack of response in *beh4-1* upon HSP90 inhibition) is consistent with the hypothesis that BEH4 is an HSP90 client.

To further test this hypothesis, we analyzed trait means of all single mutants of the *BEH* family members with and without HSP90 inhibition. As expected from our previous studies[94], the *lof* mutant of the HSP90 client BES1, *bes1-2*, was significantly less sensitive than wild-type to HSP90 inhibition (LMM: $p<0.05$) (**Figure 5.2B**). Moreover, both *beh3-1*, and *beh4-1* were significantly less affected than wild type (LMM: $p = 0.01$, $p<1.0E-04$, respectively) (**Figure 5.2B**). In contrast, BRZ1, which is not chaperoned by HSP90[94,356], BEH1 and BEH2 behave like wild-type. These results are consistent with our hypothesis that BEH4, and possibly BEH3, are HSP90 clients.

5.3 Discussion

Developmental robustness is thought to emerge from the topology of gene networks, including the activity of redundant genes, gene connectivity, and regulatory architecture[339]. Here, we trace robustness of the model trait hypocotyl length to a specific member of the *BEH* gene family, *BEH4*. Contrary to our expectations, *BEH4*'s role in developmental robustness of dark-grown hypocotyls does not appear to arise through functional redundancy with closely related family members. Loss of another family member did not further decrease developmental robustness; rather, we observed partial rescue. *BEH4,* the ancestral member of the *BEH* family, also showed the largest effect on the trait mean phenotype. Our observations challenge a prior theory that additional connections (here paralogs), added later, may stabilize traits[366]. Instead, at least for this particular trait and gene family, the ancestral gene remained the largest player for both trait mean and variance (developmental robustness). Previous studies frequently found that

loci that affect trait robustness also affect trait mean[221,323,326,367]. This frequently observed overlap makes intuitive sense: a gene that significantly affects trait mean when disrupted will perturb the underlying stabilizing genetic network and may so decrease trait robustness[322]. As stabilizing selection on genetic variants that affect both mean and variance will be far stronger than selection on variants that affect only trait variance, genes such as *BEH4* will play critical roles in maintaining phenotypic robustness.

Gene network hubs are thought to be crucial for developmental robustness, presumably due to their high number of connections with other loci. This assumption is certainly supported by several prior studies in plants, yeast and worms[29,30,152,325,360]. At the small scale of the *BEH* gene family this assumption did not hold true. We did, however, observe that the older gene duplicates, *BEH3* and *BEH4*, tended to engage in more regulatory connections than other family members, consistent with previous studies finding that number of protein interactions correlates with gene age[368-370]. However, *beh3-1* did not exhibit altered developmental robustness, indicating that connectivity alone does not suffice to explain effects on developmental robustness.

One may argue that our experiments did not thoroughly test *BEH4* as a hub, as we primarily restricted our analysis to the *BEH* family. The known genetic network underlying hypocotyl dark growth is certainly complex[371], and thus far *BEH4*'s role within this network has been unknown. Our analysis of DNaseI-seq data for dark-grown seedlings revealed the putative number of TFs regulating different *BEH* family members (**Supplemental table 5.1**). The number of potential regulatory inputs for individual family members did not correlate with the severity of the phenotypic effects in their mutants; several family members showed equal or more inputs that *BEH4*.

Our data best support the alternative hypothesis that *BEH4*'s role in developmental robustness arises through the topology of its connections with other family members. For example, feedback loops are known to promote robustness[339,372-374]. We found that *BEH4* positively regulates *BEH3* and *BEH1*, which in turn, both negatively regulate *BEH4*. Hence, loss of robustness in *beh4* mutants likely arises through the loss of finely tuned regulation among family members. This hypothesis is supported by our observation that in the *bes1-2*; *beh4-1* double mutant developmental robustness is partially rescued, possibly because the fine-tuned balance among family members is partially restored in the double mutant.

The BEH family member BES1 is known to be a client of the developmental robustness regulator HSP90[94,356]. HSP90 presumably governs developmental robustness by chaperoning its client proteins, which function in diverse developmental pathways[148]. HSP90 inhibition leads to destabilization and loss of function for its many clients[149,375]. Notably, loss of BES1 function did not affect robustness, indicating that HSP90 does not regulate robustness through its client BES1. Instead, we observed that HSP90-dependent robustness of hypocotyl growth is likely due to *BEH4* function—unlike wild type, the *beh4-1* mutant showed no response to HSP90 inhibition with regard to developmental robustness. Together, this result and the significantly diminished mean response of *beh4-1* mutant to HSP90 suggest that BEH4 is also an HSP90 client. In sum, we propose that HSP90 regulates developmental robustness of dark-grown hypocotyls through the activity of BEH4, which is central for fine-tuned cross-regulation among all *BEH* family members.

5.4 Main figures

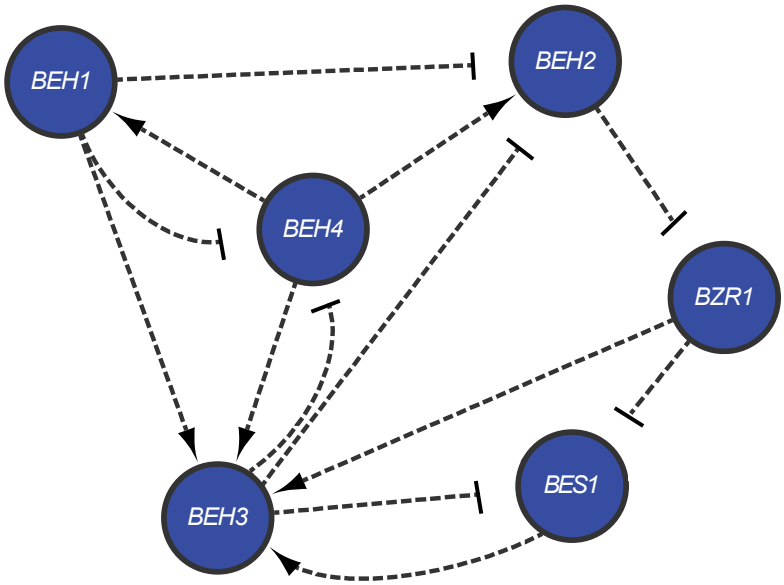

Figure 5.1: *BEH* family members engage in extensive regulatory cross-talk. Direct or indirect regulatory relationships among *BEH* family members were determined using qPCR. A regulatory relationship was called for a gene if a greater than a 2-fold expression difference between wild-type and mutant backgrounds was measured. Both positive and negative regulatory relationships are indicated.

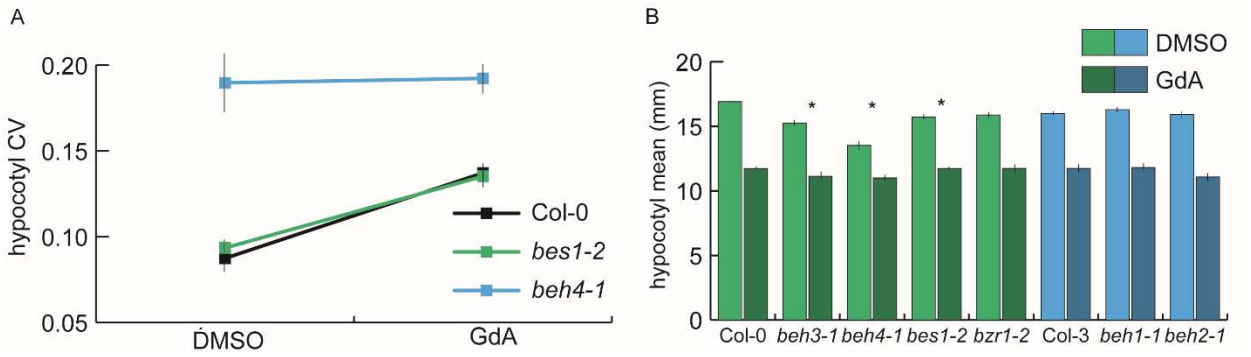

Figure 5.2: Robustness provided by HSP90 likely arises from the chaperone's interaction with BEH4. A) Seedlings were grown with or without HSP90, and hypocotyl length was measured in three replicate experiments. CV was calculated for each replicate (n~210) and the standard errors of the mean for n = 3 are shown. BES1 is a known HSP90 client in this gene family. **B)** Hypocotyl length mean data for the same conditions are shown. One representative replicate experiment with standard error of the mean for n > 20 is shown. *Significant differences in mean trait response to HSP90 inhibition are shown ($p < 0.03$, linear mixed model with genotype, treatment, and interaction effects as fixed effects and replicate as a random effect).

5.5 Materials and Methods

Plant materials and growth conditions: *bes1-2* (Lachowiec *et al.* 2013), *bzr1-2* (GABI_857E04), *beh3-1* (SALK_017577), and *beh4-1* (SAIL_750_F08) are in the Col-0 background. *beh1-1* (SAIL_40_D04) and *beh2-1* (SAIL_76_B06) are in the Col-3 background. Using qPCR (see below), we confirmed that none of the mutants produced full-length transcripts; most produced no transcript at all. For hypocotyl length assays, seeds were sterilized for 10 minutes in 70% ethanol, 0.01% Triton X-100, followed by 5 minutes of 95% ethanol. After sterilization, seeds were suspended in 0.1% agarose and spotted on plates containing 0.5x Murashige Minimal Organics Medium and 0.8% bactoagar. Seeds on plates were then stratified in the dark at 4°C for 3 days and then transferred to an incubator cycling between 22° for 16 hours and 20° for 8 hours to imitate long days. Plate position was changed every 24 h to minimize position effect for light grown seedlings. Racks of plates containing dark-grown seedlings were wrapped in foil. For HSP90-inhibitor assays, 1μM geldanamycin (Sigma) was suspended in the medium. Equivalent amounts of the solvent DMSO were used for control treatment.

Phenotyping: For estimates of hypocotyl CV, three replicates of $n > 50$ were measured. Assays of mean hypocotyl length were completed in triplicate with $n > 15$. Photos were taken of each plate, and individual hypocotyls were manually measured using NIH ImageJ1.46r.

qPCR: Three biological replicates of sixty pooled 5-day dark grown seedlings were harvested. Tissue was frozen in liquid nitrogen and ground by hand with a pestle. RNA was extracted using the SV Total RNA Isolation kit (Promega). To remove contaminating DNA, a second DNase

treatment was completed according to the Turbo DNase protocol (Ambion). Poly-A tail cDNA was produced using LightCycler kit with oligo-dT primers (Life Technologies). qPCR primers are listed in Table S3. In both the *bzr1-2* and *beh2-1* mutants these qPCR primers amplified products. The absence of the full-length transcripts was confirmed using primers that target the full-length transcript.

5.6 Supplemental Materials

Gene	Target of BES1[1]	Target of BZR1[2]
At1g19350 BES1	X	X
At1g75080 BZR1		X
At3g50750 BEH1	X	X
At4g36780 BEH2	X	X
At4g18890 BEH3		X
At1g78700 BEH4	X	

Supplemental table 5.1: Co-regulation of family members and response to brassinosteroids. [1]Yu et al 2011, [2]Sun et al 2010. Targets of BES1 were determined with ChIP-chip using an anti-BES1 antibody on material collected from *bes1-D* 14d seedlings on plates or the BZR1 ChIP-chip (Yu *et al.* 2011). Targets of BZR1 were determined using ChIP-chip using an anti-GFP antibody on rosette tissue of transgenic BZR1-GFP fusion plants.

Supplemental table 5.2: Putative transcription factors regulating members of the *BEH* family.

transcription factor	putative target gene
ABF1	BEH2
ABF3	BEH2
ABI5	BEH2
AGL9_SEP3	BEH2
AMS	BEH2
AT1G01260	BEH2
AT4G17950	BEH2
AT4G29000	BEH2
ATAREB1	BEH2
AtbZIP63	BEH2
bHLH34	BEH2
BIM2	BEH2
bZIP68	BEH2
BZR1	BEH2
BZR1	BEH2
GBF1	BEH2
GBF2	BEH2
GBF3	BEH2
HY5	BEH2
ILR3	BEH2
MYC3	BEH2
MYC4	BEH2
PIL5	BEH2
POC1	BEH2
SOL1	BEH2
SPT	BEH2
ZCW32	BEH2
ANL2	BEH3
APRR2	BEH3
ARR1	BEH3
ARR10	BEH3
ARR14	BEH3
ARR2	BEH3
ASIL1	BEH3
AT3G53600	BEH3
AT5G05090	BEH3
AtPHR1	BEH3
bZIP68	BEH3

CCA1	BEH3
GATA1	BEH3
GATA26	BEH3
GATA27	BEH3
GATA3	BEH3
GATA4	BEH3
GBF1	BEH3
GBF2	BEH3
GBF3	BEH3
HY5	BEH3
MYB77	BEH3
PDF2	BEH3
PHL1	BEH3
WRKY40	BEH3
AGL9_SEP3	BEH4
AT1G01260	BEH4
AT2G18300	BEH4
AT5G48560	BEH4
ATHB16	BEH4
ATHB6	BEH4
BEE2	BEH4
bHLH34	BEH4
BIM1	BEH4
BIM2	BEH4
BIM3	BEH4
bZIP68	BEH4
GBF2	BEH4
GBF3	BEH4
ILR3	BEH4
MYC3	BEH4
MYC4	BEH4
PIL5	BEH4
POC1	BEH4
RD22BP1	BEH4
SPT	BEH4
TCP2	BEH4
TCP20	BEH4
UNE10	BEH4
ZCW32	BEH4
anac025	BES1
AT3G53600	BES1
AT5G51910	BES1
NAC083	BES1

TCP20	BES1
TEM2	BES1
ABI5	BZR1
AT1G01260	BZR1
AT1G64620	BZR1
AT3G53600	BZR1
AT5G51910	BZR1
AtbZIP63	BZR1
ATHB16	BZR1
ATWOX13	BZR1
AZF1	BZR1
bHLH34	BZR1
BIM2	BZR1
bZIP68	BZR1
CCA1	BZR1
CDF2	BZR1
cdf3	BZR1
DOF5.6	BZR1
GATA26	BZR1
GATA27	BZR1
GBF1	BZR1
GBF2	BZR1
GBF3	BZR1
HAT3	BZR1
HB-1	BZR1
HY5	BZR1
ILR3	BZR1
INO	BZR1
MYC3	BZR1
MYC4	BZR1
PIL5	BZR1
POC1	BZR1
SPT	BZR1
STZ	BZR1
TCP20	BZR1
YAB5	BZR1
ZCW32	BZR1

TF-binding motifs located within DNaseI-seq peaks

Supplemental table 5.3: Primers used for qPCR of *BEH* family members.

Target gene	Oligo
BEH1 F	TTTGTCTTGAAGCTGGTTGGATCG
BEH1 R	TTCTGTTGGTCGAGAACCCTTTC
BEH2 F	TATCCAACAGTGCGCCTGTGAC
BEH2 R	AGTTTCCGCTTCGAACCACGAG
BEH3 F	TGCAATGAAGCTGGTTGGACTG
BEH3 R	TCCATTGGTTTGCATCCCTTGC
BEH4 F	GCACTCTGTAACGAAGCTG
BEH4 R	TGGCTGATAGGAAGAGCA
BES1 F	GGCTGGTTTAACTCAAATCAACGG
BES1 R	TCCGTCAGACGTCATCTTCTTCG
BZR1 F	TTGTGTTGAAGCTGGTTGGGTTG
BZR1 R	GTAAAGGCTTGCATCCCTTGCG

Chapter 6: Discussion and future directions

6.1 Introduction

I set out to understand more of the mechanisms that make organisms, particularly plants, robust to mutagenic and environmental disturbances. I focused on the best characterized regulator of robustness, HSP90, to answer my questions about new genetic perturbations. Using standard genetic analyses, I demonstrated that less robust backgrounds are more susceptible to aberrant phenotypes after mutagenesis. To answer my questions about overlap in targets between robustness master regulators, I characterized AGO1's putative phenotypic and environmental buffering functions. Through rigorous experimentation, I found that AGO1's phenotypic and environmental buffering capabilities appear to be mostly independent of HSP90, despite reports that some aspects of AGO1's functions are HSP90-dependent. Finally, I conducted experiments to better understand how redundancy in gene families buffers developmental phenotypes. I found that robustness for a single trait was ensured by the activities of a single, highly connected family member. By pursuing these topics, I have furthered what we know about the mechanistic details that govern phenotypic buffering and integration of environmental stimuli. In this chapter, I share my final thoughts on these projects, discuss outstanding questions, and propose future experiments to address them.

6.2 Additional methods to detect *de novo* HSP90-responsive phenotypes

In Chapter 2, one of my goals was to gain a better understanding of how rare or common HSP90-responsive *de novo* genetic variation is. After mutagenesis, I observed that mutant-like phenotypes were somewhat common; when HSP90 levels were reduced in mutagenized backgrounds, the frequency of aberrant phenotypes significantly increased. The data I generated

indicate that HSP90 can significantly interact with some, but certainly not all, *de novo* genetic variation. When I followed phenotypes across generations, I observed that the most common type of HSP90-interaction for *de novo* variation is no interaction with HSP90. I also observed that when HSP90 was reduced, decreased penetrance of phenotypes was rarer than increased penetrance, but this may reflect experimental limitations. Finally, while my results support HSP90's role in buffering genetic variation, it does not inform us if other phenotypic buffering agents would also have these properties for *de novo* variation.

It remains to be discovered if disruption of other robustness master regulators could sensitize organisms to many new mutations. Good candidates for such experiments would be AGO1 and genes involved in chromatin stability that also buffer phenotype[30,360]. In the case of AGO1 malfunction, one may predict that miRNAs and miRNA-targets are particularly susceptible to perturbation from *de novo* genetic variation. If these experiments were to be conducted, I would strongly advise to use some level of automation for assaying phenotypes.

6.2.1 Future directions

As I discussed in **Chapter 2.3**, I reduced complex phenotypes that are likely continuous to categorical binary states. Reducing these complex traits may have biased my discovery power to only identify phenotypes with high expressivity. For example, dwarf-related phenotypes are certainly continuous and were particularly problematic to categorize consistently between experiments unless only the most extreme cases were counted.

To address this issue, I propose examining M_2 (possibly M_3) populations for complex quantitative phenotypes where a metric can be used to assign a measurement with some accuracy. Examples of these phenotypes are: embryonic stem (hypocotyl) length, flowering traits, response to pathogens, response to heat stress, *etc*. In doing so, I could still measure

penetrance of mutant phenotypes, but I could also assign expressivity of aberrant phenotypes to individuals.

Take dark-grown hypocotyl length for example. Hypocotyl length is known to be regulated by several HSP90 clients[77,94,166-168] and therefore makes an excellent complex trait to study whether HSP90-reduced backgrounds are sensitized to *de novo* variation. For instance, I may observe that HSP90-reduced M_2 seedlings are more likely to produce short hypocotyls compared to wild-type. Indeed, M_2 seedlings were significantly responsive to modest HSP90 perturbation while wild-type was unchanged between conditions (Linear regression: $p=0.539$, $p<1.0E-08$, respectively) (**Figure 6.1**). This observation is consistent with mutations affecting genes encoding HSP90 clients that are already susceptible to HSP90 perturbation due to pre-existing variation in the wild-type. Based on this result, I propose large scale phenotyping of other quantitative traits in the M_2 generation.

High-throughput phenotyping, or 'phenomics,' has recently made leaps and strides in the plant community with the goal of being applied to selective crop breeding. The Danforth center in St. Louis, MO has such a platform optimized for *A. thaliana* time-course studies of many adult life-history traits across hundreds of individuals[179]. On this platform, plants are randomized in location and several cameras capture images daily to measure phenotypes. These phenotypes include: flowering-related traits, growth-rate estimates, size phenotypes, photosynthetic rates, photo-pigment abundances, and some leaf-morphology traits. As a pilot experiment, I would send the genotypes of Col-0 (wild-type) and modestly affected HSP90 RNAi-C1 to the Danforth center and measure life-history traits on their platform. I would compare these assayed data to previous experiments performed for HSP90 RNAi-C1[152,156]. I should observe high correlation between newly generated data and previous studies for similar traits. If I observe promising

differences in some traits between Col-0 and HSP90 RNAi-C1, I would then request phenotyping of 1,000 M_2 plants for both genotypes. Based on my assays in the M_2 and M_3 generations, I have some predictions for what I may observe regarding size- and stress-related phenotypes.

Based on the lesion data, M_2 HSP90 RNAi-C1 plants may show higher penetrance and expressivity of stress-related phenotypes, such as increased anthocyanin pigmentation and necrotic lesions. Loss of apical dominance and growth-related phenotypes are also more abundant in HSP90 RNAi-C1 plants. Therefore, these traits may behave similarly to the hypocotyl experiment I performed, where M_2 plants that are HSP90-reduced display more extreme defects. Many of these life-history traits are highly correlated; as such, I may observe increased incidence of certain redundant phenotypes becoming uncoupled in HSP90-reduced M_2 individuals, similar to what I observed in Chapter 4.

6.3 Blue light as candidate driver of *ago1*-lesions

In Chapter 3, I presented experiments dissecting a mutant phenotype in *ago1* plants – apparently stochastic lesions on cotyledons – and traced the molecular underpinnings to an aberrant defense response. Like previous studies involving miRNAs[10,185,199,269,307,376,377], AGO1 behaves as a key integrator of environmental signals and phytohormone signaling, thereby providing robustness to micro-environmental challenges as was previously observed for HSP90[31,148,221]. In the wild-type background, functional AGO1 appears to play a key role in properly deploying immune responses to pathogen attack.

My data also links light conditions to herbivory-related jasmonate (JA) signaling, which is supported by several previous studies. Specifically, solar UV-B radiation renders plants more

resistant to herbivory, primarily due to upregulation of the JA pathway[214,231,271]. Consistent with these prior findings, the *ago1*-dependent lesions were much less frequent in filtered light conditions which exclude UV-B radiation[182]. Also excluded in the filtered light conditions was blue light, a possible regulator of reactive oxygen species (ROS) production in roots[378].

6.3.1 Future directions

After my work came out, a paper from the del Pozo lab was published describing how exposure to only blue light results in negative phototropism, where roots grow away from light sources[378]. This makes intuitive sense because roots need to grow away from the direction of light and into soil to properly orient plants. In this paper, the authors demonstrate that exposure to blue light induces production of flavanol, a ROS scavenger, to stimulate growth away from blue light sources. The authors go on to speculate that ROS may serve as the chemical messenger for production of flavanols. ROS production has also been linked to normal root gravitropic responses[379]. These findings have led me to predict that the conditions where I grew my *ago1* seedlings (clear media and full spectrum light) may have led production to production of ROS in roots, which could have sensitized the plants to produce lesions.

Previously, I detected that *ago1* mutants had large amounts of ROS in their cotyledons (**Figure 3.2**). Furthermore, excluding short wavelengths of light, such as blue light, rescued the lesion phenotype in *ago1* (**Figure 3.1B**). Although this did not make it into the final publication, I found that for *ago1* seedlings grown on opaque plant media, which moderately blocked light from roots, the lesion phenotype was completely rescued (**Figure 6.2A**). Furthermore, I never observed lesions on soil-grown *ago1* seedlings. Based on the existing literature, it may be possible that full-spectrum light exposed *ago1* roots produce ROS, just like wild-type, but rather

than only inducing negative phototropic responses, they instead misinterpret the ROS as a signal of defense.

To test this prediction, I would take advantage of D-Root, a seedling culturing system that can block light from roots, leaving only aerial tissue exposed to light sources of choice. Without too much elaboration, this system consists of a black methacrylate box in which a square Petri plate tightly fits[380] (**Figure 6.2B**).

For my experiments, I would grow wild-type and *ago1* seedlings in the D-Root apparatus and expose their roots to darkness, yellow light, full-spectrum light, and blue light. I expect dark- and yellow light-exposed *ago1* plants to have no lesions on cotyledons. In contrast, the full-spectrum and blue light exposed roots should result in many lesion-affected *ago1* seedlings (**Figure 6.2C**). If I observed only partial-induction of the lesion phenotype in blue light-exposed *ago1*, I would argue that light perception in aerial tissue also contributes to aberrant JA response. Alternatively, I could repeat my full-spectrum light treatments on *ago1* crossed into blue light photo receptor mutants. In this context, I predict that loss of perception of blue light would rescue the lesion phenotype.

It is also possible that the *ago1* plants are sensitized to herbivory-related JA signaling, regardless of what tissue perceives light. I say this because I have anecdotal evidence of *ago1* soil-grown adults being highly resistant to a recent Arabidopsis pest infestation in the lab; the *ago1* plants were largely ignored by the invaders.

6.4 Flowering-related miRNAs as a putative buffer of null *HUA2* alleles

In Chapter 4, I report data supporting the hypothesis that AGO1 is a robustness master regulator, independent of HSP90. We demonstrated that *AGO1* perturbation reveals and

conceals genetic variants; these loci appear to be common and affect several quantitative traits. We went on to characterize one specific case of *AGO1* perturbation that resulted in the uncoupling of flowering time traits and identified that *AGO1* malfunction reveals a *HUA2*-dependent polymorphism in the *Landsberg erecta* (*Ler*) background. *HUA2* is predicted to have transcription factor activity that activates expression of flowering suppressors, such as *FLC*[293].

Despite the significant genetic interaction between *HUA2* and *AGO1*, the exact mechanistic link between these genes remains unclear. Previous studies have linked the *hua1;hua2* background to sensitizing plants to mutations in miRNA processing gene *HEN1*[311,312]. *HUA2* has also been identified as a candidate gene responsible for buffering thousands of molecular and hundreds of organismal phenotypes, including flowering related traits[176]. We therefore predict that *AGO1* buffers *lof* alleles in *HUA2* through the miRNA pathway.

6.4.1 Future directions

We propose that regulation of flowering is buffered through the miRNA pathway when *lof hua2* is present. An excellent candidate miRNA that provides this buffering is a principal regulator of the flowering-related aging: miR156[381-383]. Mir156 represses flowering by suppressing expression of several *SQUAMOSA PROMOTER BINDING LIKE* (*SPL*) transcription factors, which in turn upregulate the expression of the floral activators *FUL*, *AP1* and *LFY* [384]. The *SPL*-gene family is comprised of 15 genes, of which 11 are targeted by miR156[381].

To determine if there was mis-regulation of *SPL*-miR156 targets in our *ago1-27* x L*er* (STAIRS0942) cross, we measured expression of 10 miR156-*SPL* target genes (**Figure 6.3**). We observed that five *SPL* genes displayed increased expression in L*er ago1-27* relative to Col-0

ago1-27 (**Figure 6.3**). Based on these data, we predict that miR156-*SPL* targets, and perhaps other flowering-related miRNA-targets, are mis-regulated in the presence of *hua2* and *ago1*.

To confirm our predictions, we will perform RNA-seq on 14 day-old plants of the following genotypes: Col-0, L*er* (STAIR0942), Col-0 *ago1-27*, L*er ago1-27, hua2-4,* and *ago1-27; hua2-4*. Similar to the *SPL* qPCR data, genotypes without fully functional *AGO1* may have up-regulation of flowering-related miRNA targets. For genotypes where both *HUA2* and *AGO1* function is disrupted, we predict to see global dis-regulation of flowering-related miRNA targets. If we observe these trends, we will have provided data supporting that the miRNA pathway buffers *hua2 lof* alleles to maintain robust flowering phenotypes. If we detect strong candidate miRNA-targets that are dysregulated, we will validate our findings in the *hua2* background with *lof* and *gof* miRNA-candidate mutants. Null miRNA mutants should display similar finale rosette leaf number and days to flowering uncoupling in the *hua2* background. It is harder to predict phenotypes of overexpression mutants; however, in this case of the *hua2* background, miRNA overexpression may result in extreme late-flowering phenotypes with a high number of rosette leaves.

6.5 Robust response to environmental stress may be reliant on gene redundancy

HSP90's buffering of genetic variation and developmental noise is thought to arise from its high connectivity within genetic networks. In Chapter 4, we tested if other putative, highly connected hubs within a genetic network also possess this characteristic. In our studies, we observed that a single gene, the brassinosteroid-signaling transcription factor *BEH4*, was a strong regulator of developmental stability for hypocotyl length.

Current predictions posit that when HSP90'S function is reduced, the activity of many other genes regulating the trait of interest have altered functionality and result in increased variance for a developmental trait[363]. Our experiments on the *BEH* family do not support this prediction. For the variance in hypocotyl length, robustness due to HSP90 appears to be provided through its interaction with one other gene, *BEH4*, not many. Based on phenotypic similarities between *bes1-2* (an HSP90 client) and *beh4-1*, we speculate that BEH4 is a likely HSP90 client. It should of course be clearly stated that response to HSP90 perturbation alone cannot designate a protein as a client[148]; it can however be suggestive of further studies.

Despite these data, we still do not know the mechanistic reason why the *BZR/BEH* family has six members with putatively redundant functions for transcriptional regulation. One explanation may be that proper response to environmental stimuli is highly reliant on gene redundancy, rather than developmental stability of a single complex trait.

6.5.1 Future directions

The transcription factors BZR1 and BES1 have well-characterized functions in regulating response to drought[385,386]. In the lab, droughts conditions can be mimicked through application of the phytohormone abscisic acid (ABA). When ABA is applied, plants will induce expression of transcription factors, such as *ABI3* and *ABI5,* to activate expression of drought-responsive genes while suppressing genes associated with growth[387,388]. Generally, ABA and brassinosteroid signaling are mutually antagonistic[39]. For instance, when ABA is not present, BES1 and BZR1 suppress expression of *ABI3* and *ABI5* to promote growth, respectively[385,386,389]. Phenotypically, the dominant *gof* mutants *bzr1-D* and *bes1-D* were reported as un-responsive to ABA treatment[385,386], while the *lof* mutant $bes1^{KO}$ was observed to be modestly hypersensitive[385].

It remains unknown if the other *BEH* family members also significantly contribute to mediating the trade-off between growth and response to ABA treatment.

I propose testing the *beh* mutants used in Chapter 5 for response to ABA treatment. As a preliminary experiment, I would test wild-type and single *beh* mutants for root growth in response to increasing doses of ABA[161,385]. If the *beh* mutants behave like *lof bes1*, we may observe slightly shorter roots compared to wild-type after ABA treatment. If gene redundancy plays an important role in response to ABA, single mutants should behave similarly to wild-type, while double and triple mutants are highly responsive. If we observe only the largest effects of ABA treatment in one of the single mutants, it is likely that gene redundancy within the *BEH* family does ensure proper response to drought.

Similar to our previous assays, I would also measure expression of all *BEH* family members in all of our mutants under normal and ABA-treated conditions. Here, I predict that there is network 're-wiring' of the *BEH* family in response to ABA-treatment. Under normal conditions, we may observe network connections similar to our previous results amongst the family members. ABA-treatment, on the other hand, may result in *BZR1* and/or *BES1* behaving as network hubs to possibly repress the other family members. It is also possible that we observe no particular connection changes in response to ABA-treatment, with *BEH3* and *BEH4* still acting as network hubs. While it is hard to predict specific phenotypic results, these experiments would still provide invaluable data for understanding the advantages of having gene duplicates and whether that ensures proper response to environmental stress.

6.6 Parting thoughts

I came to graduate school with a deep interest and love of watching organisms grow and develop. I was particularly attracted to plants because of their phenotypically plastic development. I came to appreciate (and was sometimes frustrated by!) just how plastic that growth and development was regarding environmental changes. I came to the Queitsch lab because I recognized the value in understanding the mechanistic details of genetic epistasis. My studies on robustness and large-scale epistasis have taught me to always consider the genetic background of whatever genetic data I am considering. As I saw many times in my studies, a change to just a single locus can have vast, sometimes unexpected, effects on phenotype. My studies on integration of environmental signals have prepared me to tackle the next phase of my training: a post-doctoral position studying the relationship between development and defense in wild and cultivated tomato.

6.7 Main figures

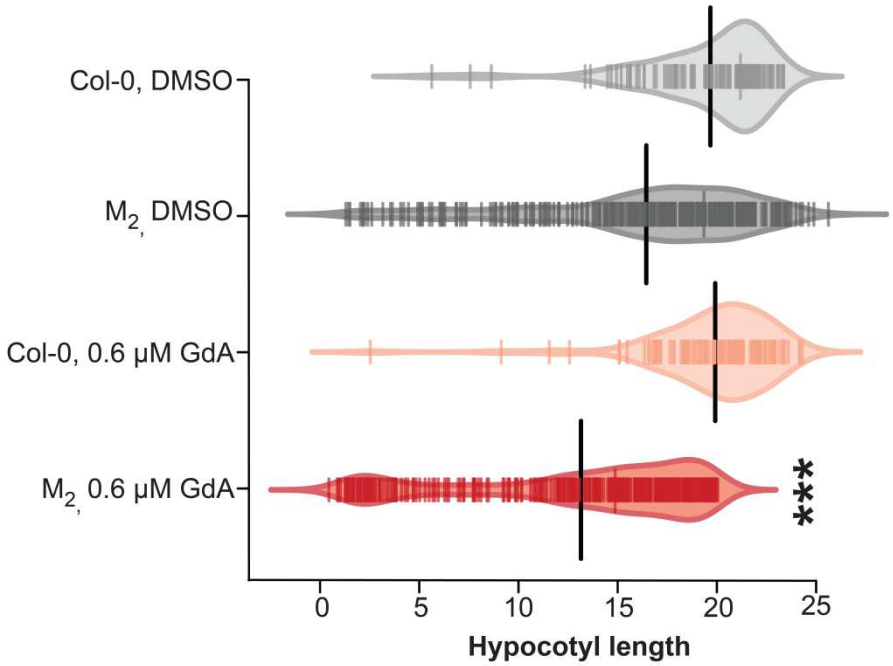

Figure 6.1: M_2 seedlings are highly responsive to HSP90 perturbation. Seedlings were treated with 0.6 µM Geldanamycin (GdA) or DMSO (mock) and measured for embryonic stem (hypocotyl) length after 7 days of growth in the dark. M_2 hypocotyls are highly responsive to modest amounts HSP90 perturbation, while Col-0 (wild-type) is not. Black lines represent mean hypocotyl length. ***p=1.77E-09, linear regression, testing for interaction between genotype and treatment. Col-0 groups: DMSO, n=113; GdA, n=106. M_2 groups: DMSO, n=405; GdA=413.

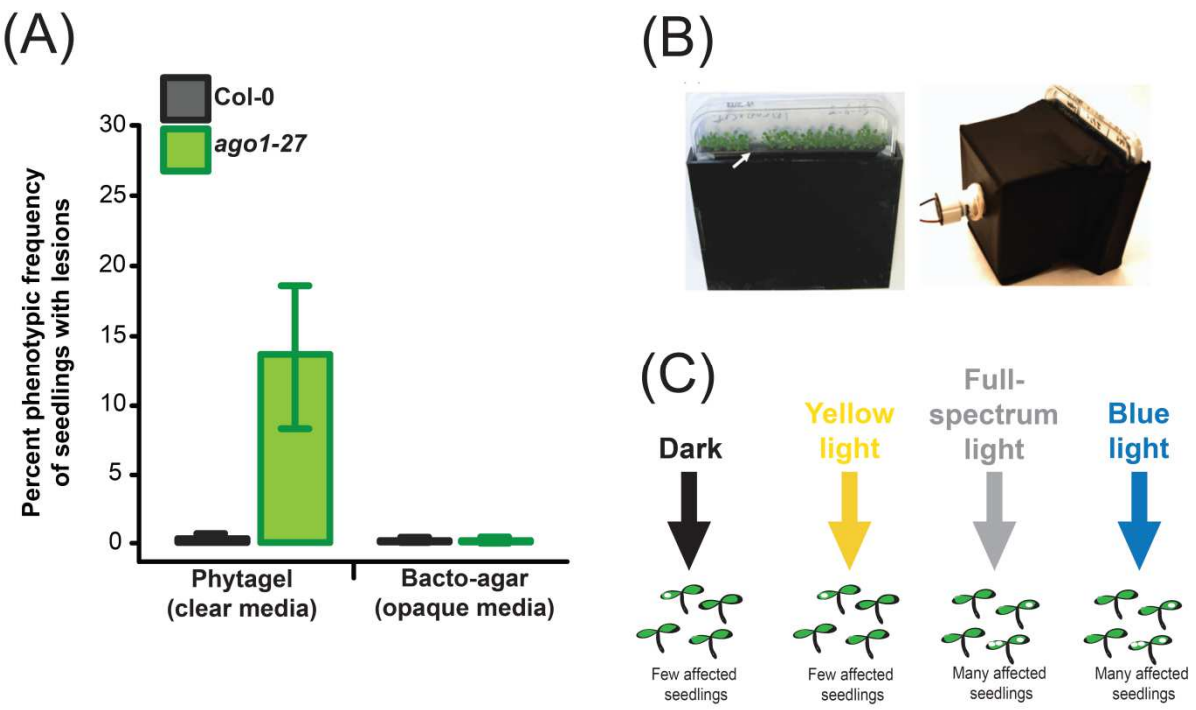

Figure 6.2: Proposed experiments for testing if blue light on roots induces lesions on *ago1* seedlings. (A) *ago1-27* seedlings produce few lesions affected individuals when grown on opaque media that partially blocks light from roots. Error bars represent standard error of the mean across three replicates of ~18 seedlings. **(B)** D-Root experimental set-up using black methacrylate to block light from roots, not aerial tissue. Adapted from Silva-Navas *et al.,* 2015. **(C)** Experimental expectations of **(B)**. Full-spectrum and blue light exposure should result in many lesion-affected *ago1* seedlings, while yellow light and darkness rescues the lesion phenotype.

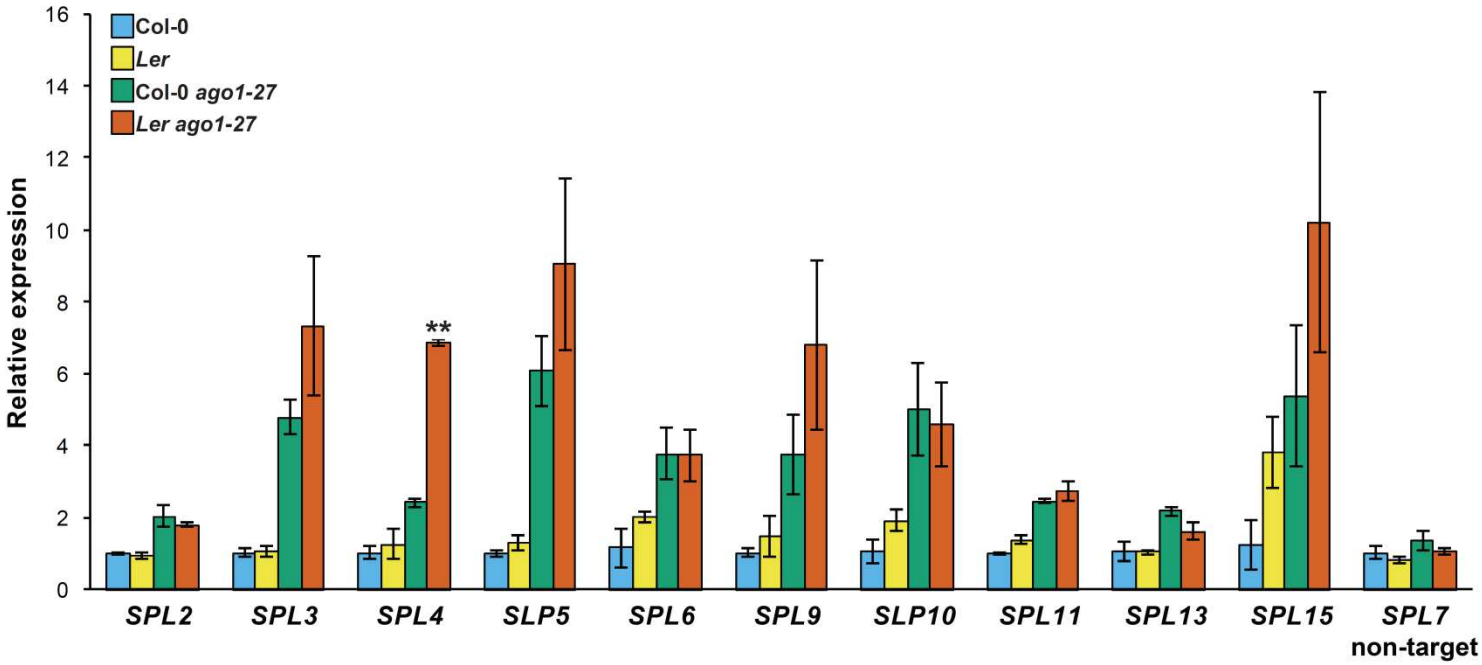

Figure 3: Assessing the effect of miR156 in the decoupling of days to flowering and rosette leaf number. *SPL3, SPL5, SPL9*, and *SPL15* are upregulated in L*er ago1*-27 compared Col-0 *ago1-27. SPL7* is not a miR156 target, and its expression was measured as a control. 14-day old plant tissue was collected at ZT16. Gene expression was normalized to the housekeeping gene *UBC21*. Mean expression data represent two biological replicates, each with three technical replicates. **p<0.005, Student's unpaired t-test.

Appendix A: Evidence that long-term memory of acquired thermotolerance requires H2A.Z in *Arabidopsis thaliana*[10]

Abstract

Like many other organisms, the flowering plant *Arabidopsis thaliana* possesses protective, stress-inducible mechanisms to increase its survivability when exposed to extreme environmental changes, such as heat stress (HS). Exposure to an extreme, noxious HS is lethal for *A. thaliana*. However, survivability can be increased if plants are first exposed to a mild HS prior to the severe, lethal HS. This phenomenon, known as acquired thermotolerance, is well understood at the level of protein stability but not at the level of transcriptional memory. We hypothesize that the *A. thaliana* genome undergoes changes in chromatin in response to HS to allow for the rapid re-induction of HS genes. In addition, changes in chromatin accessibility in response to HS may make available regulatory elements that enhance the activity of genes necessary for acquiring thermotolerance. To test these hypotheses, ATAC-seq, H2A.Z-ChIP-seq, and RNA-seq will be performed on wild-type and after they are exposed to different temperature conditions. To identify loci important for transcriptional memory, these experiments were also performed in an H2A.Z deposition mutant, *arp6-1*. H2A.Z is a histone variant of H2A that has been implicated in the HS response and is thought to play a role in transcriptional memory by marking genes for rapid re-induction. This 'marking' is dependent on histone deposition through the SWR1 complex. Since *arp6-1* loses both acquired and basal thermotolerance before Col-0, studying *arp6-1* will help identify loci essential for retaining the memory of previous heat stresses.

[10] This chapter contains data will be used for a future publication. Co-authors include: Cristina Alexandre, Kerry Bubb, Ken Jean-Baptiste, amongst others. This appendix is to serve as guide for others in the lab who follow-up on these experiments.

A.1 Main figures

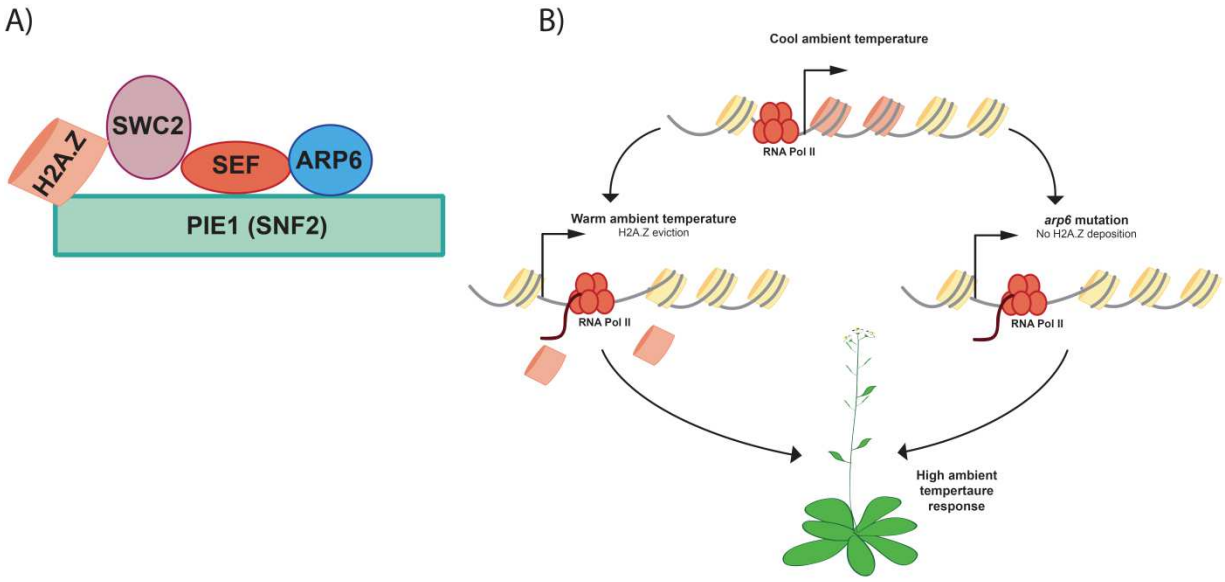

Figure A.1: H2A.Z deposition is associated with promoters and gene bodies of environmentally responsive genes. (A) Schematic representation of known interactions between subunits of the putative *A. thaliana* SWR1 complex that inserts H2A.Z containing nucleosomes into chromatin. Mutants from genes in this pathway display global depletion of H2A.Z in chromatin[390-395]. Adapted from March-Diaz and Reyes, 2009. **(B)** H2A.Z-containing nucleosomes can modulate transcription in a temperature-dependent manner. At cool ambient temperatures, H2A.Z is incorporated into transcription start sites and gene bodies of temperature-responsive genes. When plants are warmed, H2A.Z containing nucleosomes are evicted and transcription is up-regulated[391]. There is some evidence that H2A.Z levels in heat-specific genes increases after long-term exposure to heat stress[396]. *arp6* mutants have globally depleted levels of H2A.Z and therefore phenotypically behave as if they have been exposed to high ambient temperatures. It remains unknown if H2A.Z plays a role in long-term memory of acquired thermotolerance in plants. Adapted from Kumar and Wigge, 2010.

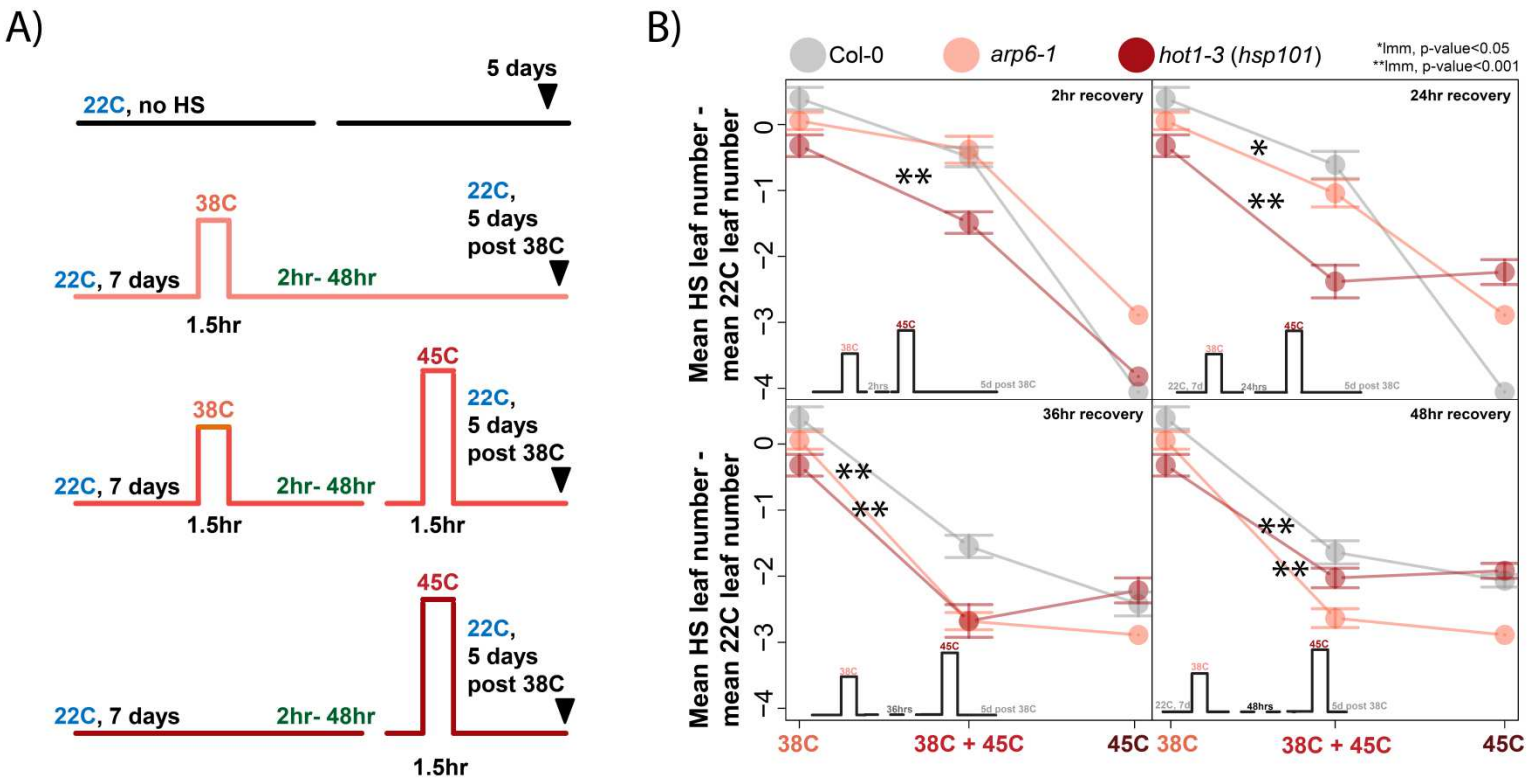

Figure A.2: The H2A.Z deposition mutant, *apr6-1*, displays defects in long-term memory of acquired thermotolerance. (A) Outline of heat shock treatments used for 7-day old seedlings. Plants were treated with various heat treatments and then counted for number of leaves at 5-days post 38C treatment. Plants are exposed to mild 38C heat treatments that are protective against otherwise lethal 45C treatments. What is varied is the amount of recovery time between 38C and 45C treatments (2 – 48 hours). **(B)** X-axis: heat treatments **(A)** applied to different groups of plants. Y-axis: mean leaf number of heat-treated seedlings normalized to mean leaf number of untreated plants. Here, a defect in growth is measured as the output of long term acquired thermotolerance. **2 hour recovery**: *arp6-1* and wild-type (Col-0) maintain acquired thermotolerance, while the *hsp101* mutant, *hot1-3*, displays decreased growth after exposure to 38C+45C. **24 hour recovery**: wild-type maintains acquired thermotolerance, while *arp6-1* is modestly sensitive to subsequent heat treatments. *hot1-3* is the most sensitive to 38C+45C treatments. **36 hour recovery**: wild-type still maintains acquired thermotolerance and is somewhat resistant to subsequent heat treatments. Both *hot1-3* and *arp6-1* do not maintain memory of prior hear treatments. **48 hour recovery**: wild-type still has some memory of previous heat treatments while *arp6-1* and *hot1-3* have not maintained acquired thermotolerance. N=144 seedlings per genotype/treatment. Error bars represent 95% confidence intervals. Linear mixed modeling (LMM) testing for interaction between genotype and treatment, random effects set as individuals within a replicate. *p<0.05, **p<0.001.

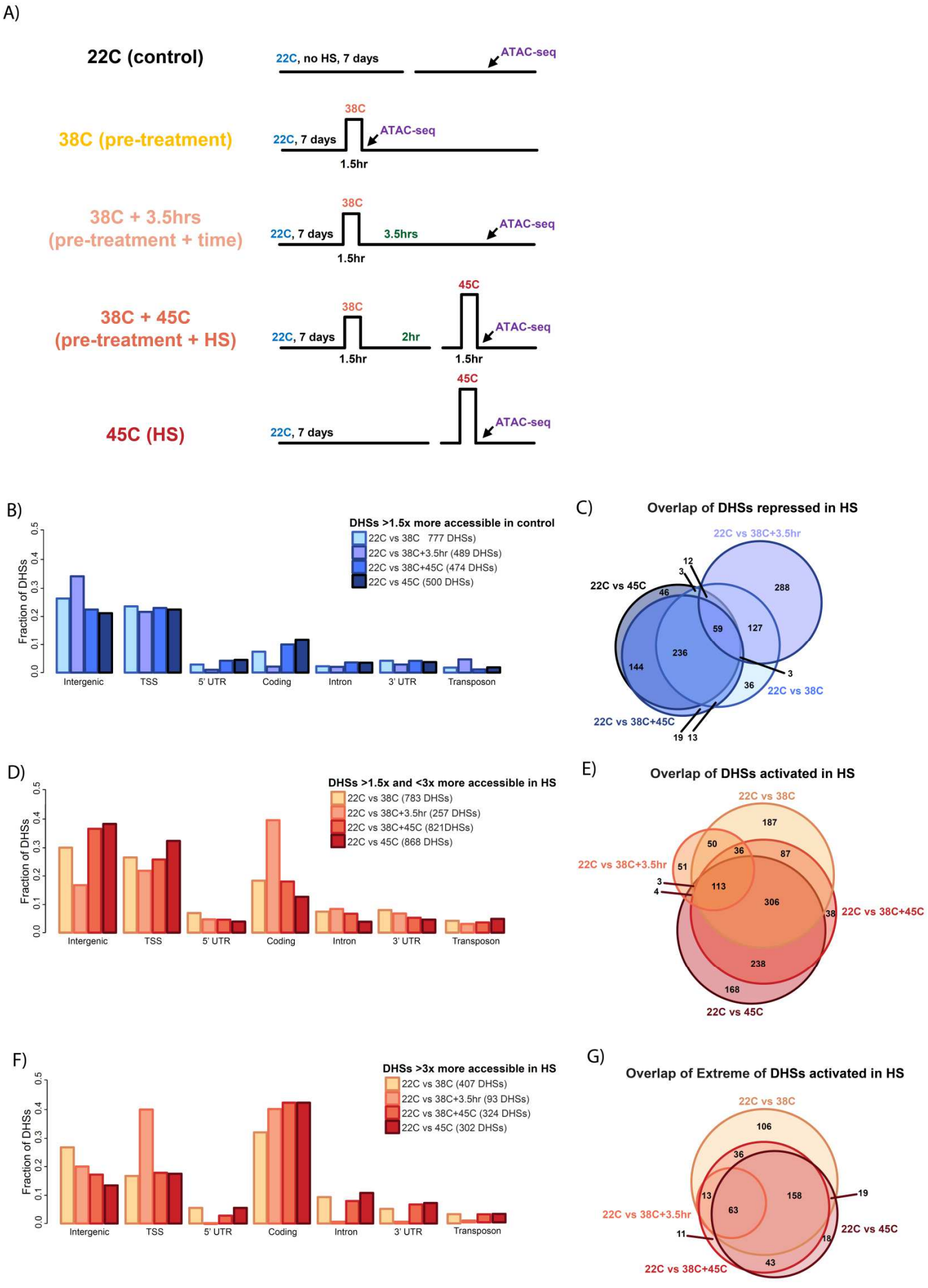
A)
22C (control)
22C, no HS, 7 days
ATAC-seq
38C (pre-treatment)
38C
22C, 7 days
ATAC-seq
1.5hr
38C + 3.5hrs
(pre-treatment + time)
38C
22C, 7 days
3.5hrs
ATAC-seq
1.5hr
38C + 45C
(pre-treatment + HS)
38C
45C
22C, 7 days
2hr
ATAC-seq
1.5hr
1.5hr
45C (HS)
45C
22C, 7 days
ATAC-seq
B)
DHSs >1.5x more accessible in control
22C vs 38C 777 DHSs)
22C vs 38C+3.5hr (489 DHSs)
22C vs 38C+45C (474 DHSs)
22C vs 45C (500 DHSs)
Fraction of DHSs
0.0
0.1
0.2
0.3
0.4
0.5
Intergenic
TSS
5' UTR
Coding
Intron
3' UTR
Transposon
C)
Overlap of DHSs repressed in HS
22C vs 38C+3.5hr
22C vs 45C
22C vs 38C
22C vs 38C+45C
12
3
46
288
59
127
236
144
3
36
19
13
D)
DHSs >1.5x and <3x more accessible in HS
22C vs 38C (783 DHSs)
22C vs 38C+3.5hr (257 DHSs)
22C vs 38C+45C (821DHSs)
22C vs 45C (868 DHSs)
Fraction of DHSs
0.0
0.1
0.2
0.3
0.4
0.5
Intergenic
TSS
5' UTR
Coding
Intron
3' UTR
Transposon
E)
Overlap of DHSs activated in HS
22C vs 38C
22C vs 38C+3.5hr
22C vs 38C+45C
22C vs 45C
187
50
36
87
51
3
4
113
306
38
238
168
F)
DHSs >3x more accessible in HS
22C vs 38C (407 DHSs)
22C vs 38C+3.5hr (93 DHSs)
22C vs 38C+45C (324 DHSs)
22C vs 45C (302 DHSs)
Fraction of DHSs
0.0
0.1
0.2
0.3
0.4
0.5
Intergenic
TSS
5' UTR
Coding
Intron
3' UTR
Transposon
G)
Overlap of Extreme of DHSs activated in HS
22C vs 38C
22C vs 38C+3.5hr
22C vs 45C
22C vs 38C+45C
106
36
13
63
158
19
11
18
43

Figure A.3: Genomic distribution of differential ATAC hypersensitive sites (DHS) are similar across heat treatments. (A) Outline of heat shock treatments used for 7-day old seedlings followed by ATAC-seq[338,397-399]. We used DESeq2[400] on cut-counts within unionDHSs[338] derived from all five time points. We used groupings such that each uDHS is assigned a p-value reporting how likely we would see what we see given that all time points are the same. Here, a p-value of $\leq$1.0E-10 was used. To make the list of pairwise differential DHSs (dDHSs), we took only the uDHSs that had both (1) the low p-value and (2) had abs(log2foldchange) $\geq$1. **(B)** Distribution of dDHSs that are less accessible in heat treatments relative to control treatment. Here, we see an enrichment of dDHSs in intergenic and transcription start site (TSS) regions, similar to published results[345]. **(C)** Overlap of dDHSs in **(D).** Distribution of dDHSs that are activated, or more are more accessible, in heat treatments relative to control. We observe an enrichment of activated dDHSs in intergenic, TSS, and coding regions. **(E)** Overlap of dDHSs in **(D). (F)** Distribution of extreme heat activated dDHSs relative control conditions. We observe here an enrichment of extreme activated dDHSs in coding regions for heat treated samples. **(G)** Overlap of dDHSs in **(F).**

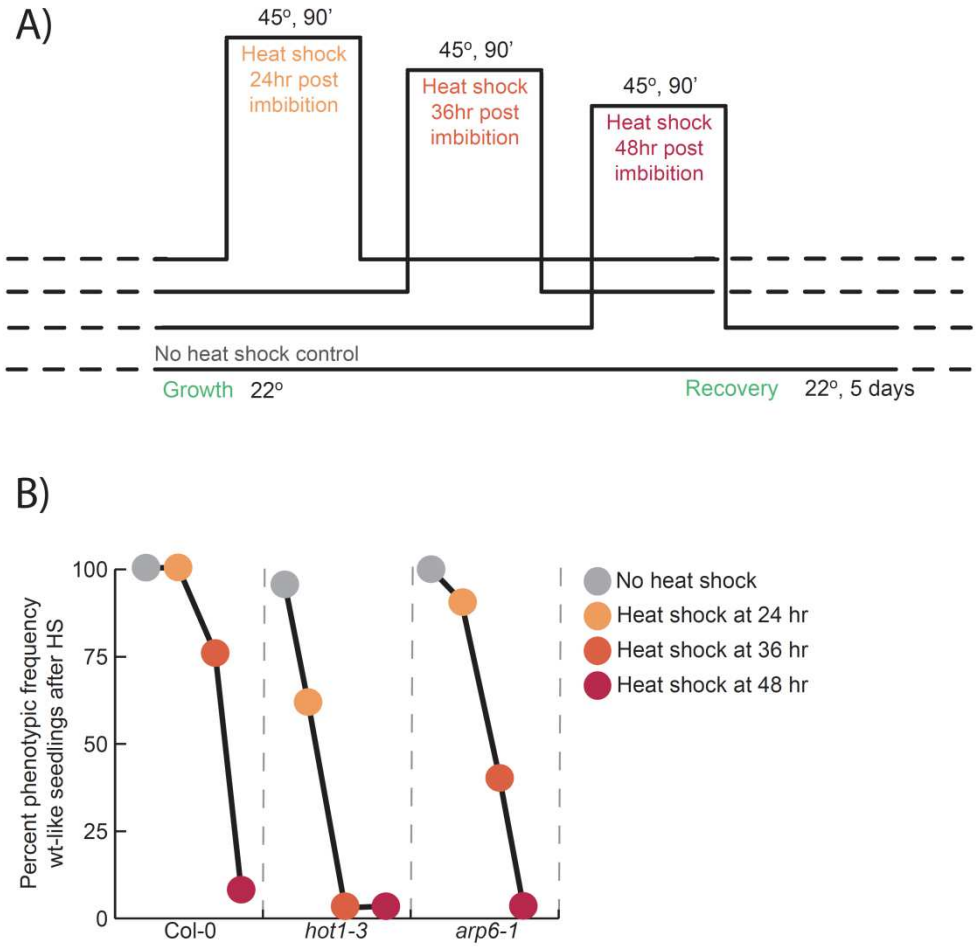

Figure A.4: The H2A.Z deposition mutant, *apr6-1*, displays defects in basal thermotolerance. (A) Outline of heat shock treatments used for germinating seeds. Seeds germinated on 1% sucrose plates at 22°C for 24 hours, 36 hours, or 48 hours were exposed to 45C for 90 minutes (HS). After heat treatment, seedlings were allowed to grow for 5 days at 22C. Seedlings were scored for wild-type-like appearance (*i.e.* green cotyledons, healthy roots, little anthocyanin accumulation, *etc*.). **(B)** Percent phenotypic frequency of wild-type-like seedlings after heat treatments. Col-0 (wild-type) has moderate basal thermotolernace until 48 hours after being plated. *hot1-3* displays weak basal thermotolerance. *arp6-1* shows intermediate basal thermotolerance. Assays based on Queitsch *et al.,* 2000[49]. *n*=72 seedlings per genotype/treatment.

References

1. Felix, M.A. & Wagner, A. Robustness and evolution: concepts, insights and challenges from a developmental model system. *Heredity (Edinb)* **100**, 132-40 (2008).
2. Lachowiec, J., Queitsch, C. & Kliebenstein, D.J. Molecular mechanisms governing differential robustness of development and environmental responses in plants. *Ann Bot* **117**, 795-809 (2016).
3. Bergman, A. & Siegal, M.L. Evolutionary capacitance as a general feature of complex gene networks. *Nature* **424**, 549-52 (2003).
4. Ciliberti, S., Martin, O.C. & Wagner, A. Innovation and robustness in complex regulatory gene networks. *Proc Natl Acad Sci U S A* **104**, 13591-6 (2007).
5. de Visser, J.A. *et al.* Perspective: Evolution and detection of genetic robustness. *Evolution Int J Org Evolution* **57**, 1959-72 (2003).
6. Jarosz, D.F., Taipale, M. & Lindquist, S. Protein homeostasis and the phenotypic manifestation of genetic diversity: principles and mechanisms. *Annu Rev Genet* **44**, 189-216 (2010).
7. Leclerc, R.D. Survival of the sparsest: robust gene networks are parsimonious. *Mol Syst Biol* **4**, 213 (2008).
8. Lehner, B. Selection to minimise noise in living systems and its implications for the evolution of gene expression. *Mol Syst Biol* **4**, 170 (2008).
9. Levy, S.F. & Siegal, M.L. Network hubs buffer environmental variation in Saccharomyces cerevisiae. *PLoS Biol* **6**, e264 (2008).
10. Li, X., Cassidy, J.J., Reinke, C.A., Fischboeck, S. & Carthew, R.W. A microRNA imparts robustness against environmental fluctuation during development. *Cell* **137**, 273-82 (2009).
11. Manu *et al.* Canalization of gene expression and domain shifts in the Drosophila blastoderm by dynamical attractors. *PLoS Comput Biol* **5**, e1000303 (2009).
12. Masel, J. & Siegal, M.L. Robustness: mechanisms and consequences. *Trends Genet* **25**, 395-403 (2009).
13. Raser, J.M. & O'Shea, E.K. Noise in gene expression: origins, consequences, and control. *Science* **309**, 2010-3 (2005).
14. Wagner, A. Robustness against mutations in genetic networks of yeast. *Nat Genet* **24**, 355-61 (2000).
15. Wagner, A. Gene duplications, robustness and evolutionary innovations. *Bioessays* **30**, 367-73 (2008).
16. Salathia, N. & Queitsch, C. Molecular mechanisms of canalization: Hsp90 and beyond. *J Biosci* **32**, 457-63 (2007).
17. Sangster, T.A., Lindquist, S. & Queitsch, C. Under cover: causes, effects and implications of Hsp90-mediated genetic capacitance. *Bioessays* **26**, 348-62 (2004).
18. Rutherford, S., Hirate, Y. & Swalla, B.J. The Hsp90 capacitor, developmental remodeling, and evolution: the robustness of gene networks and the curious evolvability of metamorphosis. *Crit Rev Biochem Mol Biol* **42**, 355-72 (2007).
19. Baggs, J.E. *et al.* Network features of the mammalian circadian clock. *PLoS Biol* **7**, e52 (2009).
20. Whitacre, J.M. Biological robustness: paradigms, mechanisms, and systems principles. *Frontiers in genetics* **3**, 67 (2012).
21. Gibson, G. *et al.* Canalization in evolutionary genetics: a stabilizing theory? *BioEssays* **22**, 372-380 (2017).
22. Debat, V. & David, P. Mapping phenotypes: canalization, plasticity and developmental stability. *Trends in Ecology & Evolution* **16**, 555-561 (2001).

23. Dworkin, G.G. & Ian. Uncovering cryptic genetic variation. *Nature Reviews Genetics* **5**, 681 (2004).
24. Wagner, A. Circuit topology and the evolution of robustness in two-gene circadian oscillators. (2005).
25. Hornstein, E. & Shomron, N. Canalization of development by microRNAs. *Nat Genet* **38 Suppl**, S20-4 (2006).
26. Flatt, T. The evolutionary genetics of canalization. *Q Rev Biol* **80**, 287-316 (2005).
27. Wagner, A. Circuit topology and the evolution of robustness in two-gene circadian oscillators. *Proc Natl Acad Sci U S A* **102**, 11775-80 (2005).
28. Burga, A., Casanueva, M.O. & Lehner, B. Predicting mutation outcome from early stochastic variation in genetic interaction partners. *Nature* **480**, 250-3 (2011).
29. Jarosz, D.F. & Lindquist, S. Hsp90 and environmental stress transform the adaptive value of natural genetic variation. *Science* **330**, 1820-4 (2010).
30. Lehner, B., Crombie, C., Tischler, J., Fortunato, A. & Fraser, A.G. Systematic mapping of genetic interactions in Caenorhabditis elegans identifies common modifiers of diverse signaling pathways. *Nat Genet* **38**, 896-903 (2006).
31. Queitsch, C., Sangster, T.A. & Lindquist, S.L. Hsp90 as a capacitor of phenotypic variation. *Nature* **417**, 618-24 (2002).
32. Rutherford, S.L. & Lindquist, S.L. Hsp90 as a capacitor for morphological evolution. *Nature* **396**, 336-342 (1998).
33. Yeyati, P.L., Bancewicz, R.M., Maule, J. & van Heyningen, V. Hsp90 selectively modulates phenotype in vertebrate development. *PLoS Genet* **3**, e43 (2007).
34. Cohen, D. Optimizing reproduction in a randomly varying environment. *J Theor Biol* **12**, 119-29 (1966).
35. Lenski, R.E., Barrick, J.E. & Ofria, C. Balancing robustness and evolvability. *PLoS Biol* **4**, e428 (2006).
36. Waddington, C.H. Genetic Assimilation of an Acquired Character. *Evolution* **7**, 118-126 (1953).
37. Ledon-Rettig, C.C., Pfennig, D.W. & Crespi, E.J. Diet and hormonal manipulation reveal cryptic genetic variation: implications for the evolution of novel feeding strategies. *Proc Biol Sci* **277**, 3569-78 (2010).
38. Suzuki, Y. & Nijhout, H.F. Evolution of a polyphenism by genetic accommodation. *Science* **311**, 650-2 (2006).
39. Milton, C.C., Ulane, C.M. & Rutherford, S. Control of canalization and evolvability by Hsp90. *PLoS One* **1**, e75 (2006).
40. Queitsch, C., Sangster, T.A. & Lindquist, S. Hsp90 as a capacitor of phenotypic variation. *Nature* **417**, 618-24 (2002).
41. Cowen, L.E. & Lindquist, S. Hsp90 potentiates the rapid evolution of new traits: drug resistance in diverse fungi. *Science* **309**, 2185-9 (2005).
42. Casanueva, M.O., Burga, A. & Lehner, B. Fitness trade-offs and environmentally induced mutation buffering in isogenic C. elegans. *Science* **335**, 82-5 (2012).
43. Rohner, N. *et al.* Cryptic variation in morphological evolution: HSP90 as a capacitor for loss of eyes in cavefish. *Science* **342**, 1372-5 (2013).
44. Karras, G.I. *et al.* HSP90 Shapes the Consequences of Human Genetic Variation. *Cell* **168**, 856-866 e12 (2017).
45. Gorre, M.E., Ellwood-Yen, K., Chiosis, G., Rosen, N. & Sawyers, C.L. BCR-ABL point mutants isolated from patients with imatinib mesylate-resistant chronic myeloid leukemia remain sensitive to inhibitors of the BCR-ABL chaperone heat shock protein 90. *Blood* **100**, 3041-4 (2002).

46. Nimmanapalli, R. *et al.* Molecular characterization and sensitivity of STI-571 (imatinib mesylate, Gleevec)-resistant, Bcr-Abl-positive, human acute leukemia cells to SRC kinase inhibitor PD180970 and 17-allylamino-17-demethoxygeldanamycin. *Cancer Res* **62**, 5761-9 (2002).
47. PaxDb: Protein Abundance Database. (2017).
48. Borkovich, K.A., Farrelly, F.W., Finkelstein, D.B., Taulien, J. & Lindquist, S. hsp82 is an essential protein that is required in higher concentrations for growth of cells at higher temperatures. *Mol Cell Biol* **9**, 3919-30 (1989).
49. Queitsch, C., Hong, S.W., Vierling, E. & Lindquist, S. Heat shock protein 101 plays a crucial role in thermotolerance in Arabidopsis. *Plant Cell* **12**, 479-92 (2000).
50. Zhao, R. *et al.* Navigating the Chaperone Network: An Integrative Map of Physical and Genetic Interactions Mediated by the Hsp90 Chaperone. *Cell* **120**, 715-727 (2005).
51. Taipale, M. *et al.* A quantitative chaperone interaction network reveals the architecture of cellular protein homeostasis pathways. *Cell* **158**, 434-448 (2014).
52. Taipale, M., Jarosz, D.F. & Lindquist, S. HSP90 at the hub of protein homeostasis: emerging mechanistic insights. *Nat Rev Mol Cell Biol* **11**, 515-28 (2010).
53. Sangster, T.A. & Queitsch, C. The HSP90 chaperone complex, an emerging force in plant development and phenotypic plasticity. *Curr Opin Plant Biol* **8**, 86-92 (2005).
54. Biebl, F.H.S., Johannes, B. & Maximilian, M. The HSP90 chaperone machinery. *Nature Reviews Molecular Cell Biology* **18**, 345 (2017).
55. Schopf, F.H., Biebl, M.M. & Buchner, J. The HSP90 chaperone machinery. *Nat Rev Mol Cell Biol* **18**, 345-360 (2017).
56. Krukenberg, K.A., Street, T.O., Lavery, L.A. & Agard, D.A. Conformational dynamics of the molecular chaperone Hsp90. *Q Rev Biophys* **44**, 229-55 (2011).
57. Meyer, P. *et al.* Structural basis for recruitment of the ATPase activator Aha1 to the Hsp90 chaperone machinery. *EMBO J* **23**, 1402-10 (2004).
58. Meyer, P. *et al.* Structural and functional analysis of the middle segment of hsp90: implications for ATP hydrolysis and client protein and cochaperone interactions. *Mol Cell* **11**, 647-58 (2003).
59. Sato, S., Fujita, N. & Tsuruo, T. Modulation of Akt kinase activity by binding to Hsp90. *Proc Natl Acad Sci U S A* **97**, 10832-7 (2000).
60. Karagoz, G.E. *et al.* Hsp90-Tau complex reveals molecular basis for specificity in chaperone action. *Cell* **156**, 963-74 (2014).
61. Vaughan, C.K. *et al.* Structure of an Hsp90-Cdc37-Cdk4 complex. *Mol Cell* **23**, 697-707 (2006).
62. Street, T.O., Lavery, L.A. & Agard, D.A. Substrate binding drives large-scale conformational changes in the Hsp90 molecular chaperone. *Mol Cell* **42**, 96-105 (2011).
63. Hugel, C.R., Johannes, B., Martin, H., Moritz, M. & Thorsten. The large conformational changes of Hsp90 are only weakly coupled to ATP hydrolysis. *Nature Structural and Molecular Biology* **16**, 281 (2009).
64. Hugel, B.H., Florian, K., Martin, Z., Philipp, W. & Thorsten. Multidomain structure and correlated dynamics determined by self-consistent FRET networks. *Nature Methods* **14**, 174 (2016).
65. Cintron, N.S. & Toft, D. Defining the requirements for Hsp40 and Hsp70 in the Hsp90 chaperone pathway. *J Biol Chem* **281**, 26235-44 (2006).
66. Pearl, L.H. Hsp90 and Cdc37 – a chaperone cancer conspiracy. *Current Opinion in Genetics & Development* **15**, 55-61 (2005).
67. Verba, K.A. & Agard, D.A. How Hsp90 and Cdc37 Lubricate Kinase Molecular Switches. *Trends Biochem Sci* **42**, 799-811 (2017).
68. Cutforth, T. & Rubin, G.M. Mutations in Hsp83 and cdc37 impair signaling by the sevenless receptor tyrosine kinase in Drosophila. *Cell* **77**, 1027-36 (1994).

69. Stepanova, L., Leng, X., Parker, S.B. & Harper, J.W. Mammalian p50Cdc37 is a protein kinase-targeting subunit of Hsp90 that binds and stabilizes Cdk4. *Genes Dev* **10**, 1491-502 (1996).
70. Vaughan, C.K. *et al.* Hsp90-dependent activation of protein kinases is regulated by chaperone-targeted dephosphorylation of Cdc37. *Mol Cell* **31**, 886-95 (2008).
71. Smith, D.L.R. *et al.* Functional Specificity of Co-Chaperone Interactions with Hsp90 Client Proteins. *http://dx.doi.org/10.1080/10409230490892513* (2010).
72. Earley, K.W. & Poethig, R.S. Binding of the cyclophilin 40 ortholog SQUINT to Hsp90 protein is required for SQUINT function in Arabidopsis. *J Biol Chem* **286**, 38184-9 (2011).
73. Breiman, A. Plant Hsp90 and its Co-Chaperones. *Current Protein & Peptide Science* **15**, 232-244 (2017).
74. Zuehlke, A. & Johnson, J.L. Hsp90 and co-chaperones twist the functions of diverse client proteins. *Biopolymers* **93**, 211-7 (2010).
75. Salminen, A., Ojala, J., Kaarniranta, K., Hiltunen, M. & Soininen, H. Hsp90 regulates tau pathology through co-chaperone complexes in Alzheimer's disease. *Prog Neurobiol* **93**, 99-110 (2011).
76. Fan, A.C. & Young, J.C. Function of cytosolic chaperones in Tom70-mediated mitochondrial import. *Protein Pept Lett* **18**, 122-31 (2011).
77. Zhang, X.C., Millet, Y.A., Cheng, Z., Bush, J. & Ausubel, F.M. Jasmonate signalling in Arabidopsis involves SGT1b-HSP70-HSP90 chaperone complexes. *Nat Plants* **1**(2015).
78. Edkins, A.L. CHIP: a co-chaperone for degradation by the proteasome. *Subcell Biochem* **78**, 219-42 (2015).
79. Calderwood, S.K. Cdc37 as a co-chaperone to Hsp90. *Subcell Biochem* **78**, 103-12 (2015).
80. Baindur-Hudson, S., Edkins, A.L. & Blatch, G.L. Hsp70/Hsp90 organising protein (hop): beyond interactions with chaperones and prion proteins. *Subcell Biochem* **78**, 69-90 (2015).
81. Guy, N.C., Garcia, Y.A., Sivils, J.C., Galigniana, M.D. & Cox, M.B. Functions of the Hsp90-binding FKBP immunophilins. *Subcell Biochem* **78**, 35-68 (2015).
82. Karam, J.A., Parikh, R.Y., Nayak, D., Rosenkranz, D. & Gangaraju, V.K. Co-chaperone Hsp70/Hsp90-organizing protein (Hop) is required for transposon silencing and Piwi-interacting RNA (piRNA) biogenesis. *J Biol Chem* **292**, 6039-6046 (2017).
83. Eichler, E.E. *et al.* Missing heritability and strategies for finding the underlying causes of complex disease. *Nat Rev Genet* **11**, 446-50 (2010).
84. Gibson, G. Rare and common variants: twenty arguments. *Nat Rev Genet* **13**, 135-45 (2012).
85. Manolio, T.A. *et al.* Finding the missing heritability of complex diseases. *Nature* **461**, 747-53 (2009).
86. Queitsch, C., Carlson, K.D. & Girirajan, S. Lessons from model organisms: phenotypic robustness and missing heritability in complex disease. *PLoS Genet* **8**, e1003041 (2012).
87. Golubov, A. *et al.* Microsatellite instability in Arabidopsis increases with plant development. *Plant Physiol* **154**, 1415-27 (2010).
88. van Leeuwen, J. *et al.* Exploring genetic suppression interactions on a global scale. (2016).
89. Costanzo, M. *et al.* A global genetic interaction network maps a wiring diagram of cellular function. *Science* **353**(2016).
90. Whitesell, L., Mimnaugh, E.G., De Costa, B., Myers, C.E. & Neckers, L.M. Inhibition of heat shock protein HSP90-pp60v-src heteroprotein complex formation by benzoquinone ansamycins: essential role for stress proteins in oncogenic transformation. *Proc Natl Acad Sci U S A* **91**, 8324-8328 (1994).
91. Xu, Y. & Lindquist, S. Heat-shock protein hsp9O governs the activity of pp6Ovsrc kinase. *PNAS* **90**, 7074-7078 (1993).

92. Chen, B. & Wagner, A. Hsp90 is important for fecundity, longevity, and buffering of cryptic deleterious variation in wild fly populations. *BMC Evol Biol* **12**, 25 (2012).
93. Sgro, C.M., Wegener, B. & Hoffmann, A.A. A naturally occurring variant of Hsp90 that is associated with decanalization. *Proc Biol Sci* **277**, 2049-57 (2010).
94. Lachowiec, J. *et al.* The protein chaperone HSP90 can facilitate the divergence of gene duplicates. *Genetics* **193**, 1269-77 (2013).
95. Lachowiec, J., Lemus, T., Borenstein, E. & Queitsch, C. Hsp90 promotes kinase evolution. *Mol Biol Evol* **32**, 91-9 (2015).
96. Press, M.O. *et al.* Genome-scale co-evolutionary inference identifies functions and clients of bacterial Hsp90. *PLoS Genet* **9**, e1003631 (2013).
97. Jarosz, D.F. & Lindquist, S. Hsp90 and Environmental Stress Transform the Adaptive Value of Natural Genetic Variation. *Science* (2010).
98. Sangster, T.A. *et al.* HSP90-buffered genetic variation is common in Arabidopsis thaliana. *Proc Natl Acad Sci U S A* **105**, 2969-74 (2008).
99. Sangster, T.A. *et al.* HSP90 affects the expression of genetic variation and developmental stability in quantitative traits. *Proc Natl Acad Sci U S A* **105**, 2963-8 (2008).
100. Queitsch, C., Sangster, T.A. & Lindquist, S. Hsp90 as a capacitor of phenotypic variation. *Nature* (2002).
101. Rutherford, S.L. & Lindquist, S. Hsp90 as a capacitor for morphological evolution. *Nature* (1998).
102. Dorrity, M.W., Cuperus, J.T., Carlisle, J.A., Fields, S. & Queitsch, C. Trait specificity mediated by alternative DNA-binding preferences of a single transcription factor in yeast. *BiorXiv* DOI: 10.1101/117911 (2017).
103. Whitesell, L. & Lindquist, S.L. HSP90 and the chaperoning of cancer. *Nat Rev Cancer* **5**, 761-72 (2005).
104. Perfect, J.R. Cryptococcus neoformans: the yeast that likes it hot. *FEMS Yeast Res* **6**, 463-8 (2006).
105. Johnson, A. The biology of mating in Candida albicans. *Nat Rev Microbiol* **1**, 106-16 (2003).
106. Dong, H. & Courchesne, W. A novel quantitative mating assay for the fungal pathogen Cryptococcus neoformans provides insight into signalling pathways responding to nutrients and temperature. *Microbiology* **144 (Pt 6)**, 1691-7 (1998).
107. Shapiro, R.S. & Cowen, L.E. Thermal control of microbial development and virulence: molecular mechanisms of microbial temperature sensing. *MBio* **3**(2012).
108. Hummel, B. *et al.* The evolutionary capacitor HSP90 buffers the regulatory effects of mammalian endogenous retroviruses. *Nat Struct Mol Biol* **24**, 234-242 (2017).
109. Xu, Y., Singer, A., M. & Lindquist, S. Maturation of the tyrosine kinase c-src as a kinase and as a substrate depends on the molecular chaperone Hsp90. *PNAS* **96**, 109-114 (1999).
110. Neckers, L. Heat shock protein 90: the cancer chaperone. *J Biosci* **32**, 517-30 (2007).
111. Nimmanapalli, R. *et al.* Molecular Characterization and Sensitivity of STI-571 (Imatinib Mesylate, Gleevec)- resistant, Bcr-Abl-positive, Human Acute Leukemia Cells to SRC Kinase Inhibitor PD180970 and 17-Allylamino-17-demethoxygeldanamycin. *Cancer Res* **62**, 5761-9 (2016).
112. Cowen, L.E. & Lindquist, S. Hsp90 Potentiates the Rapid Evolution of New Traits: Drug Resistance in Diverse Fungi. *Science* **309**, 2185-9(2005).
113. Pratt, W.B. The role of heat shock proteins in regulating the function, folding, and trafficking of the glucocorticoid receptor. *J Biol Chem* **268**, 21455-8 (1993).
114. Voellmy, R. On mechanisms that control heat shock transcription factor activity in metazoan cells. *Cell Stress Chaperones* **9**, 122-33 (2004).

115. Voellmy, R. & Boellmann, F. Chaperone regulation of the heat shock protein response. *Adv Exp Med Biol* **594**, 89-99 (2007).
116. Prodromou, C. Mechanisms of Hsp90 regulation. *Biochem J* **473**, 2439-52 (2016).
117. Zeyl, C. & DeVisser, J.A. Estimates of the rate and distribution of fitness effects of spontaneous mutation in Saccharomyces cerevisiae. *Genetics* **157**, 53-61 (2001).
118. Eyre-Walker, A. & Keightley, P.D. The distribution of fitness effects of new mutations. *Nat Rev Genet* **8**, 610-618 (2007).
119. Masel, J. & Trotter, M.V. Robustness and evolvability. *Trends Genet* **26**, 406-14 (2010).
120. Mittelman, D., Sykoudis, K., Hersh, M., Lin, Y. & Wilson, J.H. Hsp90 modulates CAG repeat instability in human cells. *Cell Stress Chaperones* **15**, 753-9 (2010).
121. Dote, H., Burgan, W.E., Camphausen, K. & Tofilon, P.J. Inhibition of hsp90 compromises the DNA damage response to radiation. *Cancer Res* **66**, 9211-20 (2006).
122. Chen, G., Bradford, W.D., Seidel, C.W. & Li, R. Hsp90 stress potentiates rapid cellular adaptation through induction of aneuploidy. *Nature* **482**, 246-50 (2012).
123. Khurana, N., Laskar, S., Bhattacharyya, M.K. & Bhattacharyya, S. Hsp90 induces increased genomic instability toward DNA-damaging agents by tuning down RAD53 transcription. *Mol Biol Cell* **27**, 2463-78 (2016).
124. Specchia, V. *et al.* Hsp90 prevents phenotypic variation by suppressing the mutagenic activity of transposons. *Nature* **463**, 662-5 (2010).
125. Piacentini, L. *et al.* Transposons, environmental changes, and heritable induced phenotypic variability. *Chromosoma* **123**, 345-54 (2014).
126. Gangaraju, V.K. *et al.* Drosophila Piwi functions in Hsp90-mediated suppression of phenotypic variation. *Nat Genet* **43**, 153-8 (2011).
127. Izumi, N. *et al.* Hsp90 facilitates accurate loading of precursor piRNAs into PIWI proteins. *RNA* **19**, 896-901 (2013).
128. Ryan, C.P., Brownlie, J.C. & Whyard, S. Hsp90 and Physiological Stress Are Linked to Autonomous Transposon Mobility and Heritable Genetic Change in Nematodes. *Genome Biol Evol* **8**, 3794-3805 (2016).
129. Xiol, J. *et al.* A role for Fkbp6 and the chaperone machinery in piRNA amplification and transposon silencing. *Mol Cell* **47**, 970-9 (2012).
130. Ichiyanagi, T. *et al.* HSP90alpha plays an important role in piRNA biogenesis and retrotransposon repression in mouse. *Nucleic Acids Res* **42**, 11903-11 (2014).
131. Kozeko, L., Talalaiev, O., Neimash, V. & Povarchuk, V. A protective role of HSP90 chaperone in gamma-irradiated Arabidopsis thaliana seeds. *Life Sci Space Res (Amst)* **6**, 51-8 (2015).
132. Picard, D. Hsp90Int.DB. Vol. 2017 The Hps90 chaperone machine database (2017).
133. Migicovsky, Z. & Kovalchuk, I. Changes to DNA methylation and homologous recombination frequency in the progeny of stressed plants. *Biochem Cell Biol* **91**, 1-5 (2013).
134. Galhardo, R.S., Hastings, P.J. & Rosenberg, S.M. Mutation as a stress response and the regulation of evolvability. *Critical reviews in biochemistry and molecular biology* **42**, 399-435 (2007).
135. Dai, C. & Whitesell, L. HSP90: a rising star on the horizon of anticancer targets. *Future Oncol* **1**, 529-40 (2005).
136. Cullinan, S.B. & Whitesell, L. Heat shock protein 90: a unique chemotherapeutic target. *Semin Oncol* **33**, 457-65 (2006).
137. Rosenberg, S.M. & Queitsch, C. Medicine. Combating evolution to fight disease. *Science* **343**, 1088-9 (2014).
138. Cowen, L.E., Carpenter, A.E., Matangkasombut, O., Fink, G.R. & Lindquist, S.L. Genetic architecture of Hsp90-dependent drug resistance. *Eukaryotic Cell* **5**, 2184-8 (2006).

139. Cowen, L.E. Hsp90 orchestrates stress response signaling governing fungal drug resistance. *PLoS pathogens* **5**, e1000471 (2009).
140. Singh, S.D. *et al.* Hsp90 governs echinocandin resistance in the pathogenic yeast Candida albicans via calcineurin. *PLoS pathogens* **5**, e1000532 (2009).
141. Shapiro, R.S. *et al.* Hsp90 orchestrates temperature-dependent Candida albicans morphogenesis via Ras1-PKA signaling. *Current biology : CB* **19**, 621-9 (2009).
142. Cowen, L.E. *et al.* Harnessing Hsp90 function as a powerful, broadly effective therapeutic strategy for fungal infectious disease. *Proc Natl Acad Sci U S A* **106**, 2818-23 (2009).
143. Garcia-Dorado, A. & Caballero, A. On the average coefficient of dominance of deleterious spontaneous mutations. *Genetics* **155**, 1991-2001 (2000).
144. Agrawal, A.F. & Whitlock, M.C. Inferences about the distribution of dominance drawn from yeast gene knockout data. *Genetics* **187**, 553-66 (2011).
145. Huang, N., Lee, I., Marcotte, E.M. & Hurles, M.E. Characterising and predicting haploinsufficiency in the human genome. *PLoS Genet* **6**, e1001154 (2010).
146. Raynes, Y., Gazzara, M.R. & Sniegowski, P.D. Mutator dynamics in sexual and asexual experimental populations of yeast. *BMC Evol Biol* **11**, 158 (2011).
147. Jarosz, D. & Lindquist, S. Hsp90 and environmental stress transform the adaptive value of natural genetic variation. *Science* **330**, 1820-1824 (2010).
148. Taipale, M., Jarosz, D. & Lindquist, S. HSP90 at the hub of protein homeostasis: emerging mechanistic insights. *Nat Rev Mol Cell Biol* **11**, 515-528 (2010).
149. Taipale, M. *et al.* Quantitative analysis of HSP90-client interactions reveals principles of substrate recognition. *Cell* **150**, 987-1001 (2012).
150. Echeverria, P.C. & Picard, D. A Global View of the Proteome Perturbations by Hsp90 Inhibitors. In: Houry W. (eds) The Molecular Chaperones Interaction Networks in Protein Folding and Degradation. in *Interactomics and Systems Biology*, Vol. 1 (New York, NY, Springer, 2014).
151. Gong, Y. *et al.* An atlas of chaperone-protein interactions in Saccharomyces cerevisiae: implications to protein folding pathways in the cell. *Mol Syst Biol* **5**, 275 (2009).
152. Sangster, T.A. *et al.* Phenotypic diversity and altered environmental plasticity in Arabidopsis thaliana with reduced Hsp90 levels. *PLoS One* **2**, e648 (2007).
153. Takahashi, A., Casais, C., Ichimura, K. & Shirasu, K. HSP90 interacts with RAR1 and SGT1 and is essential for RPS2-mediated disease resistance in Arabidopsis. *Proc Natl Acad Sci U S A* **100**, 11777-82 (2003).
154. Zou, J., Guo, Y., Guettouche, T., Smith, D.F. & Voellmy, R. Repression of heat shock transcription factor HSF1 activation by HSP90 (HSP90 complex) that forms a stress-sensitive complex with HSF1. *Cell* **94**, 471-480 (1998).
155. Li, J. & Buchner, J. Structure, function and regulation of the hsp90 machinery. *Biomed J* **36**, 106-17 (2013).
156. Sangster, T. *et al.* HSP90-buffered genetic variation is common in Arabidopsis thaliana. *Proceedings of the National Academy of Sciences of the United States of America* **105**, 2969-2974 (2008).
157. Burga, A., Casanueva, M.O. & Lehner, B. Predicting mutation outcome from early stochastic variation in genetic interaction partners. *Nature* **480**, 250-253 (2011).
158. Casanueva, M.O., Burga, A. & Lehner, B. Fitness trade-offs and environmentally induced mutation buffering in isogenic C. elegans. *Science* **335**, 82-85 (2012).
159. Queitsch, M.W.D., Josh, T.C., Jolie, A.C., Stanley, F. & Christine. Trait specificity mediated by alternative DNA-binding preferences of a single transcription factor in yeast. *BioRXiv* (2017).
160. Oda, T., Hayano, T., Miyaso, H., Takahashi, N. & Yamashita, T. Hsp90 regulates the Fanconi anemia DNA damage response pathway. *Blood* **109**, 5016-26 (2007).

161. Weigel, D. & Glazebrook, J. *Arabidopsis: A Laboratory Manual*, (CSHL Press, 2002).
162. Sasaki, T., Naumann, U., Forai, P., Matzke, A.J. & Matzke, M. Unusual case of apparent hypermutation in Arabidopsis thaliana. *Genetics* **192**, 1271-80 (2012).
163. Queitsch, C. Thesis (Ph D), University of Chicago, Dept. of Molecular Genetics and Cell Biology, December 2001. (2001).
164. Sangster, T.A. Thesis (Ph D), University of Chicago, Committee on Genetics, August 2007. (2007).
165. Queitsch, C., Sangster, T. & Lindquist, S. Hsp90 as a capacitor of phenotypic variation. *Nature* **417**, 618-624 (2002).
166. Wang, R. *et al.* HSP90 regulates temperature-dependent seedling growth in Arabidopsis by stabilizing the auxin co-receptor F-box protein TIR1. *Nat Commun* **7**, 10269 (2016).
167. Watanabe, E., Mano, S., Hara-Nishimura, I., Nishimura, M. & Yamada, K. HSP90 stabilizes auxin receptor TIR1 and ensures plasticity of auxin responses. *Plant Signal Behav* **12**, e1311439 (2017).
168. Watanabe, E. *et al.* HSP90 Stabilizes Auxin-Responsive Phenotypes by Masking a Mutation in the Auxin Receptor TIR1. *Plant Cell Physiol* **57**, 2245-2254 (2016).
169. Dorrity, M.W., Cuperus, J.T., Carlisle, J.A., Fields, S. & Queitsch, C. (2017).
170. Zurbriggen, M.D., Carrillo, N. & Hajirezaei, M.-R. ROS signaling in the hypersensitive response. *Plant Signaling & Behavior* **5**, 393-396 (2010).
171. Liu, Y., Burch-Smith, T., Schiff, M., Feng, S. & Dinesh-Kumar, S.P. Molecular chaperone Hsp90 associates with resistance protein N and its signaling proteins SGT1 and Rar1 to modulate an innate immune response in plants. *J Biol Chem* **279**, 2101-8 (2004).
172. Lu, R. *et al.* High throughput virus-induced gene silencing implicates heat shock protein 90 in plant disease resistance. *EMBO J* **22**, 5690-5699 (2003).
173. Hubert, D.A. *et al.* Cytosolic HSP90 associates with and modulates the Arabidopsis RPM1 disease resistance protein. *EMBO J* **22**, 5679-5689 (2003).
174. Samakovli, D., Thanou, A., Valmas, C. & Hatzopoulos, P. Hsp90 canalizes developmental perturbation. *Journal of experimental botany* **58**, 3513-3524 (2007).
175. Yeyati, P.L.L., Bancewicz, R.M.M., Maule, J. & Van Heyningen, V. Hsp90 selectively modulates phenotype in vertebrate development. *PLoS Genet* **3**, e43-e43 (2007).
176. Fu, J. *et al.* System-wide molecular evidence for phenotypic buffering in Arabidopsis. *Nat Genet* **41**, 166-7 (2009).
177. Robert-Seilaniantz, A., Grant, M. & Jones, J.D. Hormone crosstalk in plant disease and defense: more than just jasmonate-salicylate antagonism. *Annual review of phytopathology* **49**, 317-343 (2011).
178. Silva-Correia, J., Freitas, S., Tavares, R.M., Lino-Neto, T. & Azevedo, H. Phenotypic analysis of the Arabidopsis heat stress response during germination and early seedling development. *Plant Methods* **10**, 7 (2014).
179. Fahlgren, N., Gehan, M.A. & Baxter, I. Lights, camera, action: high-throughput plant phenotyping is ready for a close-up. *Curr Opin Plant Biol* **24**, 93-99 (2015).
180. Geiler-Samerotte, K.A., Zhu, Y.O., Goulet, B.E., Hall, D.W. & Siegal, M.L. Selection Transforms the Landscape of Genetic Variation Interacting with Hsp90. *PLoS Biol* **14**, e2000465 (2016).
181. Richardson, J.B., Uppendahl, L.D., Traficante, M.K., Levy, S.F. & Siegal, M.L. Histone variant HTZ1 shows extensive epistasis with, but does not increase robustness to, new mutations. *PLoS Genet* **9**, e1003733 (2013).
182. Stasinopoulos, T.C. & Hangarter, R.P. Preventing photochemistry in culture media by long-pass light filters alters growth of cultured tissues. *Plant Physiol* **93**, 1365-9 (1990).
183. Li, H. & Durbin, R. Fast and accurate short read alignment with Burrows-Wheeler Transform. *Bioinformatics* **25**, 1754-60 (2009).

184. Lempe, J., Lachowiec, J., Sullivan, A.M. & Queitsch, C. Molecular mechanisms of robustness in plants. *Curr Opin Plant Biol* **16**, 62-9 (2013).
185. Sunkar, R., Li, Y.F. & Jagadeeswaran, G. Functions of microRNAs in plant stress responses. *Trends Plant Sci* **17**, 196-203 (2012).
186. Li, W.X. *et al.* The Arabidopsis NFYA5 transcription factor is regulated transcriptionally and posttranscriptionally to promote drought resistance. *Plant Cell* **20**, 2238-51 (2008).
187. Bozorov, T.A., Baldwin, I.T. & Kim, S.G. Identification and profiling of miRNAs during herbivory reveals jasmonate-dependent and -independent patterns of accumulation in Nicotiana attenuata. *BMC Plant Biol* **12**, 209 (2012).
188. Pandey, S.P., Shahi, P., Gase, K. & Baldwin, I.T. Herbivory-induced changes in the small-RNA transcriptome and phytohormone signaling in Nicotiana attenuata. *Proc Natl Acad Sci U S A* **105**, 4559-64 (2008).
189. Varallyay, E., Valoczi, A., Agyi, A., Burgyan, J. & Havelda, Z. Plant virus-mediated induction of miR168 is associated with repression of ARGONAUTE1 accumulation. *EMBO J* **29**, 3507-19 (2010).
190. Zhang, B., Xie, D. & Jin, Z. Global analysis of non-coding small RNAs in Arabidopsis in response to jasmonate treatment by deep sequencing technology. *J Integr Plant Biol* **54**, 73-86 (2012).
191. Navarro, L. *et al.* A plant miRNA contributes to antibacterial resistance by repressing auxin signaling. *Science* **312**, 436-9 (2006).
192. Qutob, D. *et al.* Phytotoxicity and innate immune responses induced by Nep1-like proteins. *Plant Cell* **18**, 3721-44 (2006).
193. Boller, T. & Felix, G. A renaissance of elicitors: perception of microbe-associated molecular patterns and danger signals by pattern-recognition receptors. *Annu Rev Plant Biol* **60**, 379-406 (2009).
194. Chisholm, S.T., Coaker, G., Day, B. & Staskawicz, B.J. Host-microbe interactions: shaping the evolution of the plant immune response. *Cell* **124**, 803-14 (2006).
195. Clay, N.K., Adio, A.M., Denoux, C., Jander, G. & Ausubel, F.M. Glucosinolate metabolites required for an Arabidopsis innate immune response. *Science* **323**, 95-101 (2009).
196. Kim, M.G. *et al.* Two Pseudomonas syringae type III effectors inhibit RIN4-regulated basal defense in Arabidopsis. *Cell* **121**, 749-59 (2005).
197. Broekaert, W.F., Delaure, S.L., De Bolle, M.F. & Cammue, B.P. The role of ethylene in host-pathogen interactions. *Annu Rev Phytopathol* **44**, 393-416 (2006).
198. Kim, J.H. *et al.* Trifurcate feed-forward regulation of age-dependent cell death involving miR164 in Arabidopsis. *Science* **323**, 1053-7 (2009).
199. Schommer, C. *et al.* Control of jasmonate biosynthesis and senescence by miR319 targets. *PLoS Biol* **6**, e230 (2008).
200. Koornneef, A. & Pieterse, C.M. Cross talk in defense signaling. *Plant Physiol* **146**, 839-44 (2008).
201. Coll, N.S., Epple, P. & Dangl, J.L. Programmed cell death in the plant immune system. *Cell Death Differ* **18**, 1247-56 (2011).
202. Shirasu, K., Nakajima, H., Rajasekhar, V.K., Dixon, R.A. & Lamb, C. Salicylic acid potentiates an agonist-dependent gain control that amplifies pathogen signals in the activation of defense mechanisms. *Plant Cell* **9**, 261-70 (1997).
203. Balbi, V. & Devoto, A. Jasmonate signalling network in Arabidopsis thaliana: crucial regulatory nodes and new physiological scenarios. *New Phytol* **177**, 301-18 (2008).
204. Gfeller, A., Dubugnon, L., Liechti, R. & Farmer, E.E. Jasmonate biochemical pathway. *Sci Signal* **3**, cm3 (2010).
205. Koo, A.J. & Howe, G.A. The wound hormone jasmonate. *Phytochemistry* **70**, 1571-80 (2009).

206. Memelink, J. Regulation of gene expression by jasmonate hormones. *Phytochemistry* **70**, 1560-70 (2009).
207. Turner, J.G., Ellis, C. & Devoto, A. The Jasmonate Signal Pathway. *The Plant Cell* **14**, S153-S164 (2002).
208. Wasternack, C. Jasmonates: an update on biosynthesis, signal transduction and action in plant stress response, growth and development. *Ann Bot* **100**, 681-97 (2007).
209. Orozco-Cardenas, M.L., Narvaez-Vasquez, J. & Ryan, C.A. Hydrogen peroxide acts as a second messenger for the induction of defense genes in tomato plants in response to wounding, systemin, and methyl jasmonate. *Plant Cell* **13**, 179-91 (2001).
210. Bleecker, A.B. & Kende, H. Ethylene: a gaseous signal molecule in plants. *Annu Rev Cell Dev Biol* **16**, 1-18 (2000).
211. Pre, M. *et al.* The AP2/ERF domain transcription factor ORA59 integrates jasmonic acid and ethylene signals in plant defense. *Plant Physiol* **147**, 1347-57 (2008).
212. Chen, H. ETHYLENE INSENSITIVE3 and ETHYLENE INSENSITIVE3-LIKE1 repress SALICYLIC ACID INDUCTION DEFICIENT2 expression to negatively regulate plant innate immunity in Arabidopsis. *Plant Cell* **21**(2009).
213. Lorenzo, O., Chico, J.M., Sanchez-Serrano, J.J. & Solano, R. JASMONATE-INSENSITIVE1 encodes a MYC transcription factor essential to discriminate between different jasmonate-regulated defense responses in Arabidopsis. *Plant Cell* **16**, 1938-50 (2004).
214. Ballare, C.L. Jasmonate-induced defenses: a tale of intelligence, collaborators and rascals. *Trends Plant Sci* **16**, 249-57 (2011).
215. Anderson, J.P. *et al.* Antagonistic interaction between abscisic acid and jasmonate-ethylene signaling pathways modulates defense gene expression and disease resistance in Arabidopsis. *Plant Cell* **16**, 3460-79 (2004).
216. Song, S. *et al.* Interaction between MYC2 and ETHYLENE INSENSITIVE3 modulates antagonism between jasmonate and ethylene signaling in Arabidopsis. *Plant Cell* **26**, 263-79 (2014).
217. Iki, T. *et al.* In vitro assembly of plant RNA-induced silencing complexes facilitated by molecular chaperone HSP90. *Molecular Cell* **39**, 282-291 (2010).
218. Iwasaki, S. *et al.* Hsc70/Hsp90 chaperone machinery mediates ATP-dependent RISC loading of small RNA duplexes. *Mol Cell* **39**, 292-9 (2010).
219. Johnston, M. HSP90 protein stabilizes unloaded argonaute complexes and microscopic P-bodies in human cells. *Mol Biol Cell* **21**, 1462-9 (2010).
220. Queitsch, C., Carlson, K.D. & Girirajan, S. Lessons from model organisms: phenotypic robustness and missing heritability in complex disease. *PLoS Genet* **8**, e1003041-e1003041 (2012).
221. Sangster, T.A. *et al.* HSP90 affects the expression of genetic variation and developmental stability in quantitative traits. *Proceedings of the National Academy of Sciences of the United States of America* **105**, 2963-2968 (2008).
222. Bohmert, K. *et al.* AGO1 defines a novel locus of Arabidopsis controlling leaf development. *EMBO J* **17**, 170-80 (1998).
223. Morel, J.-B. *et al.* Fertile Hypomorphic ARGONAUTE (ago1) Mutants Impaired in Post-Transcriptional Gene Silencing and Virus Resistance. *The Plant Cell* **14**, 629-639 (2002).
224. Yang, L., Liu, Z., Lu, F., Dong, A. & Huang, H. SERRATE is a novel nuclear regulator in primary microRNA processing in Arabidopsis. *Plant J* **47**, 841-50 (2006).
225. Smith, M.R. *et al.* Cyclophilin 40 is required for microRNA activity in Arabidopsis. *Proc Natl Acad Sci U S A* **106**, 5424-9 (2009).
226. Boutilier, K. Ectopic Expression of BABY BOOM Triggers a Conversion from Vegetative to Embryonic Growth. *The Plant Cell Online* **14**, 1737-1749 (2002).

227. Grigg, S.P., Canales, C., Hay, A. & Tsiantis, M. SERRATE coordinates shoot meristem function and leaf axial patterning in Arabidopsis. *Nature* **437**, 1022-6 (2005).
228. Sugimoto, K., Jiao, Y. & Meyerowitz, E.M. Arabidopsis regeneration from multiple tissues occurs via a root development pathway. *Dev Cell* **18**, 463-71 (2010).
229. van Doorn, W.G. *et al.* Morphological classification of plant cell deaths. *Cell Death Differ* **18**, 1241-6 (2011).
230. Mackerness, S.A.H. *et al. Ultraviolet-B-induced stress and changes in gene expression in Arabidopsis thaliana: Role of signalling pathways controlled by jasmonic acid, ethylene and reactive oxygen species*, 1413-1423 (1999).
231. Mazza, C.A., Zavala, J., Scopel, A.L. & Ballare, C.L. Perception of solar UVB radiation by phytophagous insects: behavioral responses and ecosystem implications. *Proc Natl Acad Sci U S A* **96**, 980-5 (1999).
232. Feys, B., Benedetti, C.E., Penfold, C.N. & Turner, J.G. Arabidopsis Mutants Selected for Resistance to the Phytotoxin Coronatine Are Male Sterile, Insensitive to Methyl Jasmonate, and Resistant to a Bacterial Pathogen. *Plant Cell* **6**, 751-759 (1994).
233. Boter, M., Ruiz-Rivero, O., Abdeen, A. & Prat, S. Conserved MYC transcription factors play a key role in jasmonate signaling both in tomato and Arabidopsis. *Genes Dev* **18**, 1577-91 (2004).
234. Mur, L.A., Kenton, P., Atzorn, R., Miersch, O. & Wasternack, C. The outcomes of concentration-specific interactions between salicylate and jasmonate signaling include synergy, antagonism, and oxidative stress leading to cell death. *Plant Physiol* **140**, 249-62 (2006).
235. van Loon, L.C., Rep, M. & Pieterse, C.M. Significance of inducible defense-related proteins in infected plants. *Annu Rev Phytopathol* **44**, 135-62 (2006).
236. Ruiz-Ferrer, V. & Voinnet, O. Roles of plant small RNAs in biotic stress responses. *Annu Rev Plant Biol* **60**, 485-510 (2009).
237. Voinnet, O. Origin, biogenesis, and activity of plant microRNAs. *Cell* **136**, 669-87 (2009).
238. Zhou, X., Wang, G. & Zhang, W. UV-B responsive microRNA genes in Arabidopsis thaliana. *Mol Syst Biol* **3**, 103 (2007).
239. Mukhtar, M.S., Nishimura, M.T. & Dangl, J. NPR1 in Plant Defense: It's Not over 'til It's Turned over. *Cell* **137**, 804-6 (2009).
240. Yi, H. & Richards, E.J. A cluster of disease resistance genes in Arabidopsis is coordinately regulated by transcriptional activation and RNA silencing. *Plant Cell* **19**, 2929-39 (2007).
241. Falk, A. *et al.* EDS1, an essential component of R gene-mediated disease resistance in Arabidopsis has homology to eukaryotic lipases. *Proc Natl Acad Sci U S A* **96**, 3292-7 (1999).
242. Rustérucci, C., Aviv, D.H., Holt, B.F., Dangl, J.L. & Parker, J.E. The disease resistance signaling components EDS1 and PAD4 are essential regulators of the cell death pathway controlled by LSD1 in Arabidopsis. *Plant Cell* **13**, 2211-2224 (2001).
243. Danisman, S. *et al.* Arabidopsis class I and class II TCP transcription factors regulate jasmonic acid metabolism and leaf development antagonistically. *Plant Physiol* **159**, 1511-23 (2012).
244. Guranowski, A., Miersch, O., Staswick, P.E., Suza, W. & Wasternack, C. Substrate specificity and products of side-reactions catalyzed by jasmonate:amino acid synthetase (JAR1). *FEBS letters* **6**, 815-820 (2007).
245. Alonso, J.M. EIN2, a Bifunctional Transducer of Ethylene and Stress Responses in Arabidopsis. *Science* **284**, 2148-2152 (1999).
246. Nakano, T., Suzuki, K., Fujimura, T. & Shinshi, H. Genome-wide analysis of the ERF gene family in Arabidopsis and rice. *Plant Physiol* **140**, 411-432 (2006).
247. Lorenzo, O., Piqueras, R., Sánchez-Serrano, J.J. & Solano, R. ETHYLENE RESPONSE FACTOR1 integrates signals from ethylene and jasmonate pathways in plant defense. *Plant Cell* **15**, 165-178 (2003).

248. Berrocal-Lobo, M., Molina, A. & Solano, R. Constitutive expression of ETHYLENE-RESPONSE-FACTOR1 in Arabidopsis confers resistance to several necrotrophic fungi. *Plant J* **29**, 23-32 (2002).
249. Verhage, A. *et al.* Rewiring of the Jasmonate Signaling Pathway in Arabidopsis during Insect Herbivory. *Front Plant Sci* **2**(2011).
250. Genoud, T. *et al.* The protein phosphatase 7 regulates phytochrome signaling in Arabidopsis. *PLoS One* **3**, e2699 (2008).
251. Yan, J. *et al.* The Arabidopsis CORONATINE INSENSITIVE1 protein is a jasmonate receptor. *Plant Cell* **21**, 2220-36 (2009).
252. Lempe, J., Lachowiec, J., Sullivan, A.M. & Queitsch, C. Molecular mechanisms of robustness in plants. *Curr Opin Plant Biol* **16**, 62-69 (2012).
253. Kurihara, Y. *et al.* Transcriptome analyses revealed diverse expression changes in ago1 and hyl1 Arabidopsis mutants. *Plant Cell Physiol* **50**, 1715-20 (2009).
254. Zhang, X., Cal, A.J. & Borevitz, J.O. Genetic architecture of regulatory variation in Arabidopsis thaliana. *Genome research* **21**, 725-33 (2011).
255. Zhang, X. *et al.* Cucumber mosaic virus-encoded 2b suppressor inhibits Arabidopsis Argonaute1 cleavage activity to counter plant defense. *Genes Dev* **20**, 3255-68 (2006).
256. Chiu, M.H., Chen, I.H., Baulcombe, D.C. & Tsai, C.H. The silencing suppressor P25 of Potato virus X interacts with Argonaute1 and mediates its degradation through the proteasome pathway. *Mol Plant Pathol* **11**, 641-9 (2010).
257. Chapman, E.J., Prokhnevsky, A.I., Gopinath, K., Dolja, V.V. & Carrington, J.C. Viral RNA silencing suppressors inhibit the microRNA pathway at an intermediate step. *Genes Dev* **18**, 1179-86 (2004).
258. Lakatos, L. *et al.* Small RNA binding is a common strategy to suppress RNA silencing by several viral suppressors. *Embo j* **25**, 2768-80 (2006).
259. Giner, A., Lakatos, L., Garcia-Chapa, M., Lopez-Moya, J.J. & Burgyan, J. Viral protein inhibits RISC activity by argonaute binding through conserved WG/GW motifs. *PLoS Pathog* **6**, e1000996 (2010).
260. Azevedo, J. *et al.* Argonaute quenching and global changes in Dicer homeostasis caused by a pathogen-encoded GW repeat protein. *Genes Dev* **24**, 904-15 (2010).
261. Iwakawa, H.O. & Tomari, Y. Molecular insights into microRNA-mediated translational repression in plants. *Mol Cell* **54**, 591-601 (2013).
262. Rhoades, M.W. *et al.* Prediction of plant miRNA targets. *Cell* **110**, 513-520 (2002).
263. Bari, R., Datt Pant, B., Stitt, M. & Scheible, W.R. PHO2, microRNA399, and PHR1 define a phosphate-signaling pathway in plants. *Plant Physiol* **141**, 988-99 (2006).
264. Aukerman, M.J. & Sakai, H. Regulation of flowering time and floral organ identity by a MicroRNA and its APETALA2-like target genes. *Plant Cell* **15**, 2730-2741 (2003).
265. Brodersen, P. *et al.* Widespread translational inhibition by plant miRNAs and siRNAs. *Science* **320**, 1185-90 (2008).
266. Stief, A. *et al.* Arabidopsis miR156 Regulates Tolerance to Recurring Environmental Stress through SPL Transcription Factors. *Plant Cell* **26**, 1792-1807 (2014).
267. Gandikota, M. *et al.* The miRNA156/157 recognition element in the 3' UTR of the Arabidopsis SBP box gene SPL3 prevents early flowering by translational inhibition in seedlings. *Plant J* **49**, 683-693 (2007).
268. Voinnet, O. Post-transcriptional RNA silencing in plant-microbe interactions: a touch of robustness and versatility. *Curr Opin Plant Biol* **11**, 464-70 (2008).
269. Sunkar, R., Chinnusamy, V., Zhu, J. & Zhu, J.K. Small RNAs as big players in plant abiotic stress responses and nutrient deprivation. *Trends Plant Sci* **12**, 301-309 (2007).

270. Ballare, C.L., Scopel, A.L., Stapleton, A.E. & Yanovsky, M.J. Solar Ultraviolet-B Radiation Affects Seedling Emergence, DNA Integrity, Plant Morphology, Growth Rate, and Attractiveness to Herbivore Insects in Datura ferox. *Plant Physiol* **112**, 161-170 (1996).
271. Demkura, P.V., Abdala, G., Baldwin, I.T. & Ballare, C.L. Jasmonate-dependent and -independent pathways mediate specific effects of solar ultraviolet B radiation on leaf phenolics and antiherbivore defense. *Plant Physiol* **152**, 1084-95 (2010).
272. Hubert, D.A. *et al.* Cytosolic HSP90 associates with and modulates the Arabidopsis RPM1 disease resistance protein. *EMBO J* **22**, 5679-89 (2003).
273. Rutherford, S.L. & Lindquist, S. Hsp90 as a capacitor for morphological evolution. *Nature* **396**, 336-342 (1998).
274. Queitsch, C., Sangster, T.A. & Lindquist, S. Hsp90 as a capacitor of phenotypic variation. *Nature* **417**, 618-624 (2002).
275. Lempe, J., Lachowiec, J., Sullivan, A.M. & Queitsch, C. Molecular mechanisms of robustness in plants. *Current Opinion in Plant Biology* **16**, 62-69 (2013).
276. Gutiérrez, J. & Maere, S. Modeling the evolution of molecular systems from a mechanistic perspective. *Trends in plant science* **19**, 292-303 (2014).
277. Masel, J. & Siegal, M.L. Robustness: mechanisms and consequences. *Trends in Genetics* **25**, 395-403 (2009).
278. Whitacre, J.M. Biological robustness: paradigms, mechanisms, and systems principles. *Frontiers in genetics* **3**, 67-67 (2012).
279. Axtell, M.J. Classification and comparison of small RNAs from plants. *Annu Rev Plant Biol* **64**, 137-59 (2013).
280. Bologna, N.G. & Voinnet, O. The Diversity, Biogenesis, and Activities of Endogenous Silencing Small RNAs in Arabidopsis. *Annual Review of Plant Biology* **65**, 473-503 (2014).
281. Reis, R.S., Hart-Smith, G., Eamens, A.L., Wilkins, M.R. & Waterhouse, P.M. Gene regulation by translational inhibition is determined by Dicer partnering proteins. *Nature Plants* **1** 14027 (2015).
282. Hilgers, V., Bushati, N. & Cohen, S.M. Drosophila microRNAs 263a/b Confer Robustness during Development by Protecting Nascent Sense Organs from Apoptosis. *PLoS Biol* **8**, e1000396 (2010).
283. Cassidy, J.J. *et al.* miR-9a minimizes the phenotypic impact of genomic diversity by buffering a transcription factor. *Cell* **155**, 1556-67 (2013).
284. Wang, Y., Mercier, R., Hobman, T.C. & LaPointe, P. Regulation of RNA interference by Hsp90 is an evolutionarily conserved process. *Biochim Biophys Acta* **1833**, 2673-81 (2013).
285. Miyoshi, T., Takeuchi, A., Siomi, H. & Siomi, M.C. A direct role for Hsp90 in pre-RISC formation in Drosophila. *Nat Struct Mol Biol* **17**, 1024-1026 (2010).
286. Iwasaki, S. *et al.* Hsc70/Hsp90 Chaperone Machinery Mediates ATP-Dependent RISC Loading of Small RNA Duplexes. *Molecular Cell* **39**, 292-299 (2010).
287. Johnston, M., Geoffroy, M.C., Sobala, A., Hay, R. & Hutvagner, G. HSP90 protein stabilizes unloaded argonaute complexes and microscopic P-bodies in human cells. *Mol Biol Cell* **21**, 1462-9 (2010).
288. Woehrer, S.L. *et al.* A Tetrahymena Hsp90 co-chaperone promotes siRNA loading by ATP-dependent and ATP-independent mechanisms. *Embo j* **34**, 559-77 (2015).
289. Iki, T. *et al.* In vitro assembly of plant RNA-induced silencing complexes facilitated by molecular chaperone HSP90. *Mol Cell* **39**, 282-91 (2010).
290. Koumproglou, R. *et al.* STAIRS: a new genetic resource for functional genomic studies of Arabidopsis. *The Plant Journal* **31**, 355-364 (2002).

291. Lempe, J. *et al.* Diversity of Flowering Responses in Wild <italic>Arabidopsis thaliana</italic> Strains. *PLoS Genet* **1**, e6 (2005).
292. Salomé, P.A. *et al.* Genetic Architecture of Flowering-Time Variation in Arabidopsis thaliana. *Genetics* **188**, 421-433 (2011).
293. Doyle, M.R. *et al.* HUA2 is required for the expression of floral repressors in Arabidopsis thaliana. *Plant J* **41**, 376-85 (2005).
294. Sangster, T.A. *et al.* HSP90 affects the expression of genetic variation and developmental stability in quantitative traits. *Proceedings of the National Academy of Sciences* **105**, 2963-2968 (2008).
295. Sangster, T.A. *et al.* HSP90-buffered genetic variation is common in Arabidopsis thaliana. *Proceedings of the National Academy of Sciences* **105**, 2969-2974 (2008).
296. Pouteau, S. *et al.* Extensive phenotypic variation in early flowering mutants of Arabidopsis. *Plant Physiol* **135**, 201-11 (2004).
297. Takahashi, M. & Morikawa, H. Nitrogen dioxide accelerates flowering without changing the number of leaves at flowering in Arabidopsis thaliana. *Plant Signaling & Behavior* **9**, e970433 (2014).
298. Michaels, S.D., He, Y., Scortecci, K.C. & Amasino, R.M. Attenuation of FLOWERING LOCUS C activity as a mechanism for the evolution of summer-annual flowering behavior in Arabidopsis. *Proceedings of the National Academy of Sciences of the United States of America* **100**, 10102-10107 (2003).
299. Liu, J., He, Y., Amasino, R. & Chen, X. siRNAs targeting an intronic transposon in the regulation of natural flowering behavior in Arabidopsis. *Genes & Development* **18**, 2873-2878 (2004).
300. Song, Y.H., Ito, S. & Imaizumi, T. Flowering time regulation: photoperiod- and temperature-sensing in leaves. *Trends Plant Sci* **18**, 575-83 (2013).
301. Song, Y.H., Shim, J.S., Kinmonth-Schultz, H.A. & Imaizumi, T. Photoperiodic Flowering: Time Measurement Mechanisms in Leaves. *Annual Review of Plant Biology* (2014).
302. Andres, F. & Coupland, G. The genetic basis of flowering responses to seasonal cues. *Nat Rev Genet* **13**, 627-639 (2012).
303. Spanudakis, E. & Jackson, S. The role of microRNAs in the control of flowering time. *J Exp Bot* **65**, 365-80 (2014).
304. Cao, J. *et al.* Whole-genome sequencing of multiple Arabidopsis thaliana populations. *Nat Genet* **43**, 956-963 (2011).
305. Schneeberger, K. & Weigel, D. Fast-forward genetics enabled by new sequencing technologies. *Trends Plant Sci* **16**, 282-8 (2011).
306. Chen, X. & Meyerowitz, E.M. HUA1 and HUA2 Are Two Members of the Floral Homeotic AGAMOUS Pathway. *Molecular Cell* **3**, 349-360 (1999).
307. Sunkar, R. & Zhu, J.K. Novel and stress-regulated microRNAs and other small RNAs from Arabidopsis. *Plant Cell* **16**, 2001-19 (2004).
308. Mason, G.A., Lemus, T. & Queitsch, C. The Mechanistic Underpinnings of an ago1-Mediated, Environmentally Dependent, and Stochastic Phenotype. *Plant Physiol* **170**, 2420-31 (2016).
309. Mendez-Vigo, B. *et al.* Environmental and genetic interactions reveal FLOWERING LOCUS C as a modulator of the natural variation for the plasticity of flowering in Arabidopsis. *Plant Cell Environ* **39**, 282-94 (2016).
310. Ilk, N., Ding, J., Ihnatowicz, A., Koornneef, M. & Reymond, M. Natural variation for anthocyanin accumulation under high-light and low-temperature stress is attributable to the ENHANCER OF AG-4 2 (HUA2) locus in combination with PRODUCTION OF ANTHOCYANIN PIGMENT1 (PAP1) and PAP2. *New Phytol* **206**, 422-35 (2015).

311. Park, W., Li, J., Song, R., Messing, J. & Chen, X. CARPEL FACTORY, a Dicer Homolog, and HEN1, a Novel Protein, Act in microRNA Metabolism in Arabidopsis thaliana. *Current Biology* **12**, 1484-1495 (2002).
312. Chen, X., Liu, J., Cheng, Y. & Jia, D. HEN1 functions pleiotropically in Arabidopsis development and acts in C function in the flower. *Development* **129**, 1085-94 (2002).
313. Sieber, P., Wellmer, F., Gheyselinck, J., Riechmann, J.L. & Meyerowitz, E.M. Redundancy and specialization among plant microRNAs: role of the MIR164 family in developmental robustness. *Development* **134**, 1051-1060 (2007).
314. Posadas, D.M. & Carthew, R.W. MicroRNAs and their roles in developmental canalization. *Curr Opin Genet Dev* **27**, 1-6 (2014).
315. Siegal, M.L. & Leu, J.-Y. On the Nature and Evolutionary Impact of Phenotypic Robustness Mechanisms. *Annual Review of Ecology, Evolution, and Systematics* **45**, 495-517 (2014).
316. de Meaux, J., Hu, J.-Y., Tartler, U. & Goebel, U. Structurally different alleles of the ath-MIR824 microRNA precursor are maintained at high frequency in Arabidopsis thaliana. *Proceedings of the National Academy of Sciences of the United States of America* **105**, 8994-8999 (2008).
317. Ehrenreich, I.M. & Purugganan, M.D. Sequence Variation of MicroRNAs and Their Binding Sites in Arabidopsis. *Plant Physiology* **146**, 1974-1982 (2008).
318. Schneeberger, K. *et al.* SHOREmap: simultaneous mapping and mutation identification by deep sequencing. *Nat Methods* **6**, 550-1 (2009).
319. Morel, J.-B. *et al.* Fertile Hypomorphic ARGONAUTE (ago1) Mutants Impaired in Post-Transcriptional Gene Silencing and Virus Resistance. *The Plant Cell* **14**, 629-639 (2002).
320. James, G.V. *et al.* User guide for mapping-by-sequencing in Arabidopsis. *Genome Biol* **14**, R61 (2013).
321. Waddington, C.H. Canalization of development and the inheritance of acquired characters. *Nature* **150**, 563-565 (1942).
322. Félix, M.-A. & Barkoulas, M. Pervasive robustness in biological systems. *Nature reviews. Genetics* **16**, 483-96 (2015).
323. Hall, M.C., Dworkin, I., Ungerer, M.C. & Purugganan, M. Genetics of microenvironmental canalization in Arabidopsis thaliana. *Proc Natl Acad Sci U S A* **104**, 13717-13722 (2007).
324. Ansel, J. *et al.* Cell-to-cell stochastic variation in gene expression is a complex genetic trait. *PLoS genetics* **4**, e1000049-e1000049 (2008).
325. Rinott, R., Jaimovich, A. & Friedman, N. Exploring transcription regulation through cell-to-cell variability. *Proceedings of the National Academy of Sciences of the United States of America* **108**, 6329-34 (2011).
326. Jimenez-Gomez, J.M., Corwin, J.A., Joseph, B., Maloof, J.N. & Kliebenstein, D.J. Genomic analysis of QTLs and genes altering natural variation in stochastic noise. *PLoS Genet* **7**, e1002295 (2011).
327. Metzger, B.P.H., Yuan, D.C., Gruber, J.D., Duveau, F. & Wittkopp, P.J. Selection on noise constrains variation in a eukaryotic promoter. *Nature* **521**, 344-347 (2015).
328. Ayroles, J.F. *et al.* Behavioral idiosyncrasy reveals genetic control of phenotypic variability. *Proceedings of the National Academy of Sciences of the United States of America* **112**, 6706-11 (2015).
329. DeLuna, A., Springer, M., Kirschner, M.W. & Kishony, R. Need-based up-regulation of protein levels in response to deletion of their duplicate genes. *PLoS biology* **8**, e1000347-e1000347 (2010).
330. DeLuna, A. *et al.* Exposing the fitness contribution of duplicated genes. *Nat Genet* **40**, 676-681 (2008).
331. Swarbreck, D. *et al.* The Arabidopsis Information Resource (TAIR): gene structure and function annotation. *Nucleic Acids Research* **36**, D1009-D1014 (2008).

332. Simillion, C., Vandepoele, K., Van Montagu, M.C.E., Zabeau, M. & Van de Peer, Y. The hidden duplication past of Arabidopsis thaliana. *Proceedings of the National Academy of Sciences* **99**, 13627-13632 (2002).
333. Bowers, J.E., Chapman, B.A., Rong, J. & Paterson, A.H. Unravelling angiosperm genome evolution by phylogenetic analysis of chromosomal duplication events. *Nature* **422**, 433-438 (2003).
334. The Arabidopsis, I. Analysis of the genome sequence of the flowering plant Arabidopsis thaliana. *Nature* **408**, 796-796 (2000).
335. Franco-Zorrilla, J.M. *et al.* DNA-binding specificities of plant transcription factors and their potential to define target genes. *Proceedings of the National Academy of Sciences of the United States of America* **111**, 2367-72 (2014).
336. Phillips, T. & Hoopes, L. Transcription Factors and Transcriptional Control. Vol. 1 119-119 (2008).
337. Wang, Z.-Y., Bai, M.-Y., Oh, E. & Zhu, J.-Y. Brassinosteroid signaling network and regulation of photomorphogenesis. *Annual review of genetics* **46**, 701-24 (2012).
338. Sullivan, A.M. *et al.* Mapping and dynamics of regulatory DNA and transcription factor networks in A. thaliana. *Cell Rep* **8**, 2015-2030 (2014).
339. Lachowiec, J., Queitsch, C. & Kliebenstein, D.J. Molecular mechanisms governing differential robustness of development and environmental responses in plants. *Annals of botany* **117**, 795-809 (2015).
340. Chan, S.S.-K. & Kyba, M. What is a Master Regulator? *Journal of stem cell research & therapy* **3**(2013).
341. Li, B. *et al.* Promoter-based integration in plant defense regulation. *Plant physiology* **166**, 1803-20 (2014).
342. Wang *et al.* Nuclear-localized BZR1 mediates brassinosteroid-induced growth and feedback suppression of brassinosteroid biosynthesis. *Developmental cell* **2**, 505-513 (2002).
343. Blanc, G., Hokamp, K. & Wolfe, K.H. A Recent Polyploidy Superimposed on Older Large-Scale Duplications in the Arabidopsis Genome. *Genome Research* **13**, 137-144 (2003).
344. Zhao, J. *et al.* Two putative BIN2 substrates are nuclear components of brassinosteroid signaling. *Plant physiology* **130**, 1221-1229 (2002).
345. Yin *et al.* BES1 accumulates in the nucleus in response to brassinosteroids to regulate gene expression and promote stem elongation. *Cell* **109**, 181-191 (2002).
346. Clouse, S.D. Brassinosteroids. *The Arabidopsis book / American Society of Plant Biologists* **9**, e0151-e0151 (2002).
347. Gampala, S.S. *et al.* An Essential Role for 14-3-3 Proteins in Brassinosteroid Signal Transduction in Arabidopsis. *Developmental cell* **13**, 177-189 (2007).
348. Tang, W. *et al.* PP2A activates brassinosteroid-responsive gene expression and plant growth by dephosphorylating BZR1. *Nature cell biology* **13**, 124-131 (2011).
349. Yin *et al.* A new class of transcription factors mediates brassinosteroid-regulated gene expression in Arabidopsis. *Cell* **120**, 249-259 (2005).
350. He *et al.* BZR1 is a transcriptional repressor with dual roles in brassinosteroid homeostasis and growth responses. *Science* **307**, 1634-1638 (2005).
351. Sun *et al.* Integration of brassinosteroid signal transduction with the transcription network for plant growth regulation in Arabidopsis. *Developmental cell* **19**, 765-777 (2010).
352. Yu, X. *et al.* A brassinosteroid transcriptional network revealed by genome-wide identification of BESI target genes in Arabidopsis thaliana. *The Plant Journal* **65**, 634-646 (2011).
353. Ye, H., Li, L., Guo, H. & Yin, Y. MYBL2 is a substrate of GSK3-like kinase BIN2 and acts as a corepressor of BES1 in brassinosteroid signaling pathway in Arabidopsis. *Proceedings of the National Academy of Sciences* **109**, 20142-20147 (2012).

354. Li, Ye, H., Guo & Yin. Arabidopsis IWS1 interacts with transcription factor BES1 and is involved in plant steroid hormone brassinosteroid regulated gene expression. *Proceedings of the National Academy of Sciences of the United States of America* **107**, 3918-23 (2010).
355. Yu, X., Li, L.L., Guo, M., Chory, J. & Yin. Modulation of brassinosteroid-regulated gene expression by Jumonji domain-containing proteins ELF6 and REF6 in Arabidopsis. *Proceedings of the National Academy of Sciences of the United States of America* **105**, 7618-23 (2008).
356. Shigeta, T. *et al.* Molecular evidence of the involvement of heat shock protein 90 in brassinosteroid signaling in Arabidopsis T87 cultured cells. *Plant cell reports* **33**, 499-510 (2013).
357. Rozhon, W., Mayerhofer, J., Petutschnig, E., Fujioka, S. & Jonak, C. ASKθ, a group-III Arabidopsis GSK3, functions in the brassinosteroid signalling pathway. *The Plant Journal* **62**, 215-223 (2010).
358. Krizek, B.A. Making bigger plants: key regulators of final organ size. *Current opinion in plant biology* **12**, 17-22 (2009).
359. Queitsch, J.L., Mason, G.A., Karla, S. & Christine. Redundancy, feedback, and robustness in the Arabidopsis thaliana BZR/BEH gene family. (2016).
360. Levy, S.F. & Siegal, M.L. Network hubs buffer environmental variation in Saccharomyces cerevisiae. *PLoS biology* **6**, e264-e264 (2008).
361. Wang, X., Weigel, D. & Smith, L.M. Transposon variants and their effects on gene expression in Arabidopsis. *PLoS genetics* **9**, e1003255-e1003255 (2013).
362. Jeong, Y.J., Corvalán, C., Kwon, S.I. & Choe, S. Analysis of anti-BZR1 antibody reveals the roles BES1 in maintaining the BZR1 levels in Arabidopsis. *Journal of Plant Biology* **58**, 87-95 (2015).
363. Sangster, T.A., Lindquist, S.L. & Queitsch, C. Under cover: causes, effects and implications of Hsp90-mediated genetic capacitance. *BioEssays : news and reviews in molecular, cellular and developmental biology* **26**, 348-362 (2004).
364. Lorrain, S. Lesion mimic mutants: keys for deciphering cell death and defense pathways in plants? *Trends in Plant Science* **8**, 263-271 (2003).
365. Lachowiec, J., Lemus, T., Borenstein, E. & Queitsch, C. Hsp90 promotes kinase evolution. *Molecular biology and evolution* **32**, 91-9 (2015).
366. Wagner, A. Genetic redundancy caused by gene duplications and its evolution in networks of transcriptional regulators. *Biological cybernetics* **74**, 557-567 (1996).
367. Ordas, B., Malvar, R.A. & Hill, W.G. Genetic variation and quantitative trait loci associated with developmental stability and the environmental correlation between traits in maize. *Genet Res (Camb)* **90**, 385-395 (2008).
368. Eisenberg, E. & Levanon, E.Y. Preferential attachment in the protein network evolution. *Physical review letters* **91**, 138701-138701 (2003).
369. Kunin, V., Pereira-Leal, J.B. & Ouzounis, C.A. Functional evolution of the yeast protein interaction network. *Molecular biology and evolution* **21**, 1171-6 (2004).
370. Saeed, R. & Deane, C.M. Protein protein interactions, evolutionary rate, abundance and age. *BMC bioinformatics* **7**, 128-128 (2006).
371. Oh, E. *et al.* Cell elongation is regulated through a central circuit of interacting transcription factors in the Arabidopsis hypocotyl. *eLife* **3**, e03031-e03031 (2014).
372. Hornstein, E. & Shomron, N. Canalization of development by microRNAs. *Nature genetics* **38**, S20-S24 (2006).
373. Ebert, M.S. & Sharp, P.A. Roles for microRNAs in conferring robustness to biological processes. *Cell* **149**, 515-24 (2012).
374. Cassidy, J.J. *et al.* miR-9a minimizes the phenotypic impact of genomic diversity by buffering a transcription factor. *Cell* **155**, 1556-1567 (2013).
375. Xu, Y. Heat-Shock Protein hsp90 Governs the Activity of pp60v-src Kinase. *Proceedings of the National Academy of Sciences* **90**, 7074-7078 (1993).

376. Shukla, L.I., Chinnusamy, V. & Sunkar, R. The role of microRNAs and other endogenous small RNAs in plant stress responses. *Biochim Biophys Acta* **1779**, 743-8 (2008).
377. Kim, J.H. *et al.* Trifurcate feed-forward regulation of age-dependent cell death involving miR164 in Arabidopsis. *Science* **322**, 1053-1057 (2009).
378. Silva-Navas, J. *et al.* Flavonols Mediate Root Phototropism and Growth through Regulation of Proliferation-to-Differentiation Transition. *Plant Cell* **28**, 1372-87 (2016).
379. Joo, J.H., Bae, Y.S. & Lee, J.S. Role of auxin-induced reactive oxygen species in root gravitropism. *Plant Physiol* **126**, 1055-1060 (2001).
380. Silva-Navas, J. *et al.* D-Root: a system for cultivating plants with the roots in darkness or under different light conditions. *Plant J* **84**, 244-55 (2015).
381. Preston, J.C. & Hileman, L.C. Functional Evolution in the Plant SQUAMOSA-PROMOTER BINDING PROTEIN-LIKE (SPL) Gene Family. *Frontiers in Plant Science* **4**, 80 (2013).
382. Poethig, R.S. Chapter Five - Vegetative Phase Change and Shoot Maturation in Plants. in *Current Topics in Developmental Biology*, Vol. Volume 105 (eds. Ann, E.R. & Michael, B.O.C.) 125-152 (Academic Press, 2013).
383. Wang, J.-W., Schwab, R., Czech, B., Mica, E. & Weigel, D. Dual Effects of miR156-Targeted SPL Genes and CYP78A5/KLUH on Plastochron Length and Organ Size in Arabidopsis thaliana. *The Plant Cell Online* **20**, 1231-1243 (2008).
384. Yamaguchi, A. *et al.* The MicroRNA-Regulated SBP-Box Transcription Factor SPL3 Is a Direct Upstream Activator of LEAFY, FRUITFULL, and APETALA1. *Developmental Cell* **17**, 268-278 (2009).
385. Ryu, H., Cho, H., Bae, W. & Hwang, I. Control of early seedling development by BES1/TPL/HDA19-mediated epigenetic regulation of ABI3. *Nat Commun* **5**(2014).
386. Yang, X., Bai, Y., Shang, L., Xin, R. & Tang, W. The antagonistic regulation of abscisic acid-inhibited root growth by brassinosteroids is partially mediated via direct suppression of ABSCISIC ACID INSENSITIVE 5 expression by BRASSINAZOLE RESISTANT 1. *Plant Cell Environ* **39**, 1994-2003 (2016).
387. Lopez-Molina, L., Mongrand, S., McLachlin, D.T., Chait, B.T. & Chua, N.H. ABI5 acts downstream of ABI3 to execute an ABA-dependent growth arrest during germination. *Plant J* **32**, 317-28 (2002).
388. Skubacz, A., Daszkowska-Golec, A. & Szarejko, I. The Role and Regulation of ABI5 (ABA-Insensitive 5) in Plant Development, Abiotic Stress Responses and Phytohormone Crosstalk. *Front Plant Sci* **7**(2016).
389. Nolan, T., Chen, J. & Yin, Y. Cross-talk of Brassinosteroid signaling in controlling growth and stress responses. *Biochem J* **474**, 2641-2661 (2017).
390. Coleman-Derr, D. & Zilberman, D. Deposition of histone variant H2A.Z within gene bodies regulates responsive genes. *PLoS Genet* **8**, e1002988 (2012).
391. Kumar, S.V. & Wigge, P.A. H2A.Z-containing nucleosomes mediate the thermosensory response in Arabidopsis. *Cell* **140**, 136-47 (2010).
392. March-Diaz, R. *et al.* Histone H2A.Z and homologues of components of the SWR1 complex are required to control immunity in Arabidopsis. *Plant J* **53**, 475-87 (2008).
393. March-Diaz, R. & Reyes, J.C. The beauty of being a variant: H2A.Z and the SWR1 complex in plants. *Mol Plant* **2**, 565-77 (2009).
394. Sura, W. *et al.* Dual Role of the Histone Variant H2A.Z in Transcriptional Regulation of Stress-Response Genes. *Plant Cell* **29**, 791-807 (2017).
395. Zilberman, D., Coleman-Derr, D., Ballinger, T. & Henikoff, S. Histone H2A.Z and DNA methylation are mutually antagonistic chromatin marks. *Nature* **456**, 125-9 (2008).

396. Cortijo, S. *et al.* Transcriptional Regulation of the Ambient Temperature Response by H2A.Z Nucleosomes and HSF1 Transcription Factors in Arabidopsis. *Mol Plant* **10**, 1258-1273 (2017).
397. Bajic, M., Maher, K.A. & Deal, R.B. Identification of Open Chromatin Regions in Plant Genomes Using ATAC-Seq. *Methods Mol Biol* **1675**, 183-201 (2018).
398. Deal, R.B. & Henikoff, S. The INTACT method for cell type-specific gene expression and chromatin profiling in Arabidopsis thaliana. *Nat Protoc* **6**, 56-68 (2011).
399. Maher, K.A. *et al.* Profiling of accessible chromatin regions across multiple plant species and cell types reveals common gene regulatory principles and new control modules. *Plant Cell* (2017).
400. DESeq2. (2017).